Reports of the

U.S. ~ U.S.S.R. WEDDELL POLYNYA EXPEDITION

October - November

1981

Volume 8
Collected Reprints

U.S. Army Cold Regions Research and Engineering Laboratory
Special Report 86-6
1986

Reports of the U.S.-U.S.S.R. Weddell Polynya Expedition, October-November 1981:

Volume 1--Introduction. B.A. Huber and A.L. Gordon, Lamont-Doherty Geological Observatory, Technical Report LDGO-83-2, 1983.

Volume 2--Hydrographic Data. B.A. Huber, J. Jennings, C.-T. Chen, J. Marra, S. Rennie, P. Mele and A. Gordon, Lamont-Doherty Geological Observatory, LDGO-83-1, 1983.

Volume 3--Biology. J. Stepien, J. Marra, L. Burckle and J. Morley, Lamont-Doherty Geological Observatory, August 1983.

Volume 4--Physical, Chemical and Biological Properties of Ice Cores. U.S. Army Cold Regions Research and Engineering Laboratory, Internal Report 965, 1983.

Volume 5--Sea Ice Observations. S.F. Ackley and S.J. Smith, U.S. Army Cold Regions Research and Engineering Laboratory, Special Report 83-2, 1983.

Volume 6--Upper-Air Data. E.L Andreas, U.S. Army Cold Regions Research and Engineering Laboratory, Special Report 83-13, 1983.

Volume 7--Surface-Level Meteorological Data. U.S. Army Cold Regions Research and Engineering Laboratory, Special Report 83-14, 1983.

Unclassified

SECURITY CLASSIFICATION OF THIS PAGE *(When Data Entered)*

REPORT DOCUMENTATION PAGE		READ INSTRUCTIONS BEFORE COMPLETING FORM
1. REPORT NUMBER Special Report 86-6	2. GOVT ACCESSION NO.	3. RECIPIENT'S CATALOG NUMBER
4. TITLE *(and Subtitle)* REPORTS OF THE U.S.-U.S.S.R. WEDDELL POLYNYA EXPEDITION, OCTOBER-NOVEMBER 1981 VOLUME 8: COLLECTED REPRINTS		5. TYPE OF REPORT & PERIOD COVERED 6. PERFORMING ORG. REPORT NUMBER
7. AUTHOR*(s)* The WEPOLEX Group (Stephen F. Ackley and Donna R. Murphy, Editors)		8. CONTRACT OR GRANT NUMBER*(s)*
9. PERFORMING ORGANIZATION NAME AND ADDRESS U.S. Army Cold Regions Research and Engineering Laboratory Hanover, New Hampshire 03755-1290		10. PROGRAM ELEMENT, PROJECT, TASK AREA & WORK UNIT NUMBERS
11. CONTROLLING OFFICE NAME AND ADDRESS U.S. Army Cold Regions Research and Engineering Laboratory Hanover, New Hampshire 03755-1290		12. REPORT DATE March 1986 13. NUMBER OF PAGES 163
14. MONITORING AGENCY NAME & ADDRESS*(if different from Controlling Office)*		15. SECURITY CLASS. *(of this report)* Unclassified 15a. DECLASSIFICATION/DOWNGRADING SCHEDULE

16. DISTRIBUTION STATEMENT *(of this Report)*

Approved for public release; distribution unlimited.

17. DISTRIBUTION STATEMENT *(of the abstract entered in Block 20, if different from Report)*

18. SUPPLEMENTARY NOTES

19. KEY WORDS *(Continue on reverse side if necessary and identify by block number)*

Atmospheric sciences
Chemical oceanography
Marine biology
Physical oceanography
Weddell polynya

20. ABSTRACT *(Continue on reverse side if necessary and identify by block number)*

The papers assembled here represent the eighth volume of the collection summarizing the results of the 1981 joint Weddell Polynya Expedition (WEPOLEX). As indicated by the papers, the expedition was a multidisciplinary effort with research components in physical oceanography, chemical oceanography, marine biology, atmospheric sciences and sea ice studies.

DD FORM 1 JAN 73 1473 EDITION OF 1 NOV 65 IS OBSOLETE

Unclassified

SECURITY CLASSIFICATION OF THIS PAGE *(When Data Entered)*

PREFACE

The papers assembled here represent the eighth volume of the collection summarizing the results of the 1981 joint Weddell Polynya Expedition (WEPOLEX). As indicated by the papers, the expedition was a multidisciplinary effort with research components in physical oceanography, chemical oceanography, marine biology, atmospheric sciences and sea ice studies. General background on the expedition and its participants is given in the two articles in the *Introduction* section.

It was decided to publish this collected reprint volume since the first seven reports of this series were primarily data reports and cruise logs of the various components. The analyses of the data are given in the papers in this report. As shown here the reprints, 25 articles, represent a fairly broad range of scientific and general interest literature, with publications in *Journal of Geophysical Research, Antarctic Journal of the U.S., Nature, Marine Ecology--Progress Series, Monthly Weather Review, Micropaleontology, EOS* and *Ocean Engineering.* It was felt therefore that a single collection of the published journal articles, commonly linked by the data collected on the Weddell Polynya Expedition, would be, at least, a convenience to those who participated in the program and possibly of value to others who can save a little time in cross-referencing the articles without having to obtain journals either unfamiliar or unavailable to them.

All the participants in the program are indebted to Arnold Gordon of Lamont-Doherty Geological Observatory and E.I. Sarukhanyan of Arctic and Antarctic Research Institute, who provided the continuous care and feeding necessary for the expedition to take place. It is a major tribute to their character that the expedition took place despite generally rising international tensions and deteriorating cooperation between the two countries.

Support to the program was provided by several agencies; the primary U.S. support was from the Division of Polar Programs, National Science Foundation. Specific grants are acknowledged in the individual articles reprinted here. The editors gratefully acknowledge the support of the U.S. Army Cold Regions Research and Engineering Laboratory in preparing this report.

CONTENTS

SECTION 1: INTRODUCTION

American and Soviet Expedition into the Southern Ocean Sea Ice in October and November 1981

A. L. Gordon and E. I. Sarukhanyan

At the end of the austral winter, the Southern Ocean sea ice covers over 20 million square kilometers of ocean, an area larger than Antarctica. In November the ice begins to melt rapidly, retreating to only 20% of winter value by February. The basis of our understanding of the complex Southern Ocean is data obtained during the ice-free period; yet, it is in the ice-covered state, where the data base is essentially zero, that many significant events are believed to take place. Direct observations within the ice cover are limited to ships inadvertently locked in the ice, notably the Weddell Sea experience of the *Deutschland* in 1912, to coastal observations at Antarctic stations, and to a few year-long bottom-moored current meter deployments below the winter ice: in total, a very small data set that is restricted to a few types of measurements. It is likely that the extensive winter ice cover surrounding Antarctica represents the largest segment of the world ocean without a fundamental data set.

In recent years, satellite-based remote sensing of winter ice conditions has been particularly useful, but cloud cover restricts viewing of the sea surface, and interpretation of the data is hindered without ground-based data. However, satellite data have revealed a feature of particular interest in the region near the Greenwich Meridian and 65°S. Here, in the winters of 1974–1976, a 0.2–0.3 million square kilometer region, which usually is covered by sea ice, had little or no ice cover [*Carsey*, 1980]. Oceanographic observations in the austral summer of 1977 provided indirect evidence that this ice-free region or polynya is associated with deep-ocean convection. The convective process transfers deep-water heat into the surface layer, thus inhibiting ice formation, and carries surface water to abyssal depths that cools and ventilates the deep ocean [*Gordon*, 1978].

Fig. 1. Scientific group and officers aboard the *Mikhail Somov* for the US-USSR Weddell Polynya Expedition. The authors of this article are seated on either side of the *Somov* captain (third from the right).

Reprinted with permission.

To obtain the first comprenensive data set within the Southern Ocean sea ice during the period of maximum ice extent when the accumulative effects of winter are present, and to provide an opportunity to study an active polynya event, should one develop, a joint American and Soviet expedition was organized. This expedition, called the US-USSR Weddell Polynya Expedition, was carried out during October and November 1981 aboard the Soviet research vessel *Mikhail Somov.* Scientists from several laboratories in the United States and from the Arctic and Antarctic Research Institute in Leningrad participated in the inter-disciplinary expedition. The scientific team, equally divided between 26 Americans and Soviets, was integrated into a single scientific program under the supervision of the head of the expedition, E. I. Sarukhanyan, the National Coordinator of the USSR POLEX-South program, and A. L. Gordon, the head of the U.S. scientific party.

The science program was composed of the following components: (1) physical oceanography studies of the thermohaline stratification below the sea ice, current meter observations from the ship, and thermal structure of the upper ocean during transit between station sites; (2) chemistry of the water column and sea ice, including oxygen, nutrients, carbonate system parameters, and silicate particulates; (3) biology within the water column and sea ice, including sampling for zooplankton, chlorophyll *a* distributions, diatoms, and primary productivity; (4) sea ice samples and observations for study of the physical characteristics of the ice and morphology of the ice cover and to provide samples for the chemical and biological programs; and (5) atmospheric boundary layer study by profile methods, spectral characteristics of turbulence, upper air soundings, and underway meteorological observations.

The *Somov* left Montevideo on October 9, 1981, entering the northern fringe of the ice on October 20 near 56½°S and 5°E. The strategy was to penetrate as far south into the interior of the sea ice and obtain a comprehensive data set from the ice edge zone to the point of maximum penetration. Should the satellite information received aboard the ship indicate the development of an open ocean polynya, the *Somov* would attempt entry. While a small area of lower ice concentration (70% cover) did develop for a period in late October in the vicinity of 65°S between 0° to 5°E, it was replaced by full cover by the end of October. There was no clear indication of a polynya structure in 1981. Hence, to maximize station time, the southernmost penetration of *So-*

mov was marked at 62½°S on November 3, some 300 nm south of the ice edge at that time. The *Somov* left the ice on November 14 after obtaining an extensive inter-disciplinary data set in the interior and edge zones of the Southern Ocean sea ice.

The data represent a significant and unparalleled set of observations, which will form the basis of numerous scientific studies and of planning for other attempts to enter the sea ice edge and interior zones. It also may be noted that while a fully developed polynya was not entered, the data do provide some insight into a possible initiation of a polynya cycle. This and many other interesting, often unexpected, observations in each discipline will be developed in 1982 and 1983 as the *Somov* data set is studied. Results will be presented at joint U.S. and USSR meetings and in the scientific literature. The accomplishments of the US-USSR Weddell Polynya Expedition demonstrate the benefits of international American-Soviet efforts for the scientific study of the earth.

Acknowledgments

Comment from ALG: The US-USSR Weddell Polynya Expedition went very well. The Americans and Soviets worked side by side in the cold, snow, and wind, overcoming a variety of obstacles, to obtain an extensive array of high quality data. I congratulate all of the science group and gratefully acknowledge the crew of the *Mikhail Somov* for their active help and hospitality in both the preparation period and during the Expedition itself.

Participating scientists from the United States represented Lamont-Doherty Geological Observatory (physical, chemical, and biological oceanography); Oregon State University (chemical oceanography); Cold Regions Research and Engineering Laboratory (sea ice and atmospheric study).

References

Carsey, F., Microwave observations of the Southern Ocean, *Mon. Weather Rev., 108,* 2032–2044, 1980.

Gordon, A., Deep Antarctic convection near Maud Rise, *J. Phys. Oceanogr., 8,* 600–612, 1978.

A. L. Gordon is the associate editor for the Oceanography Report and is with the Lamont-Doherty Geological Observatory of Columbia University, Palisades, New York.

E. I. Sarukhanyan is with the Arctic and Antarctic Research Institute, Leningrad, USSR.

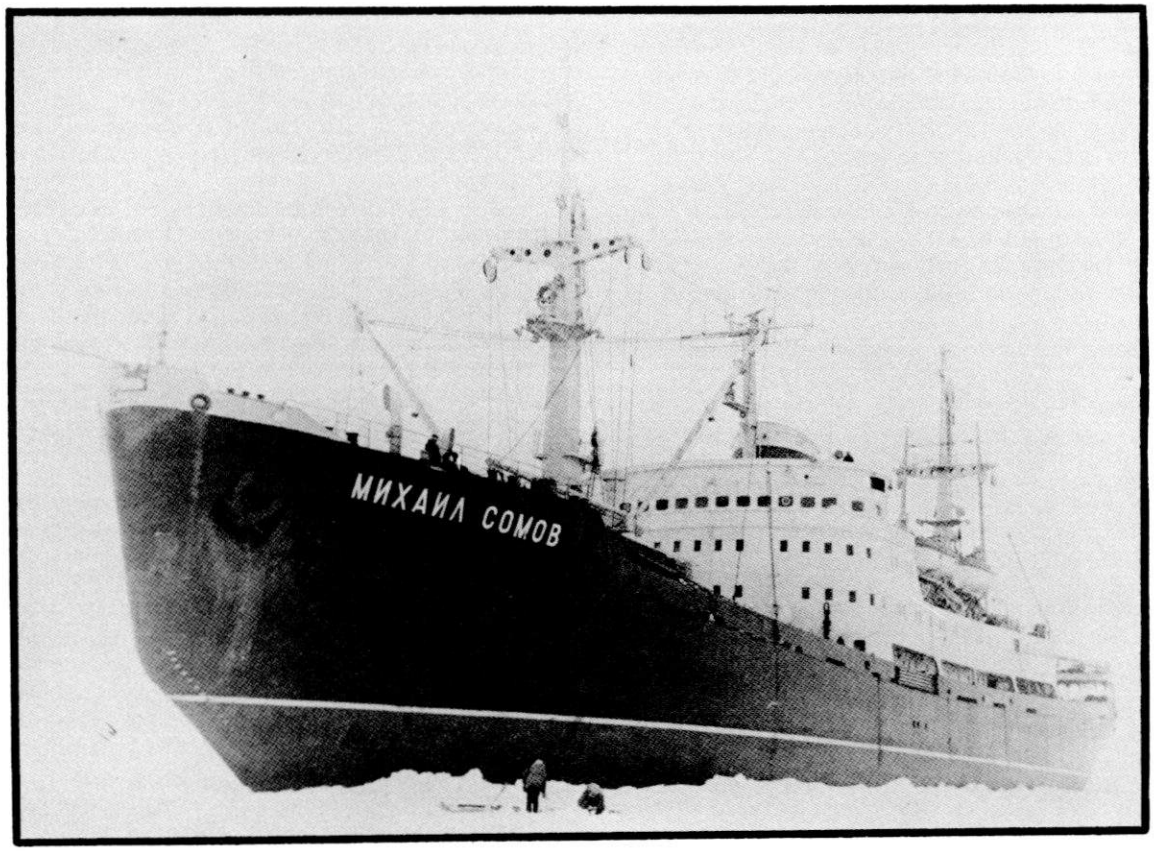

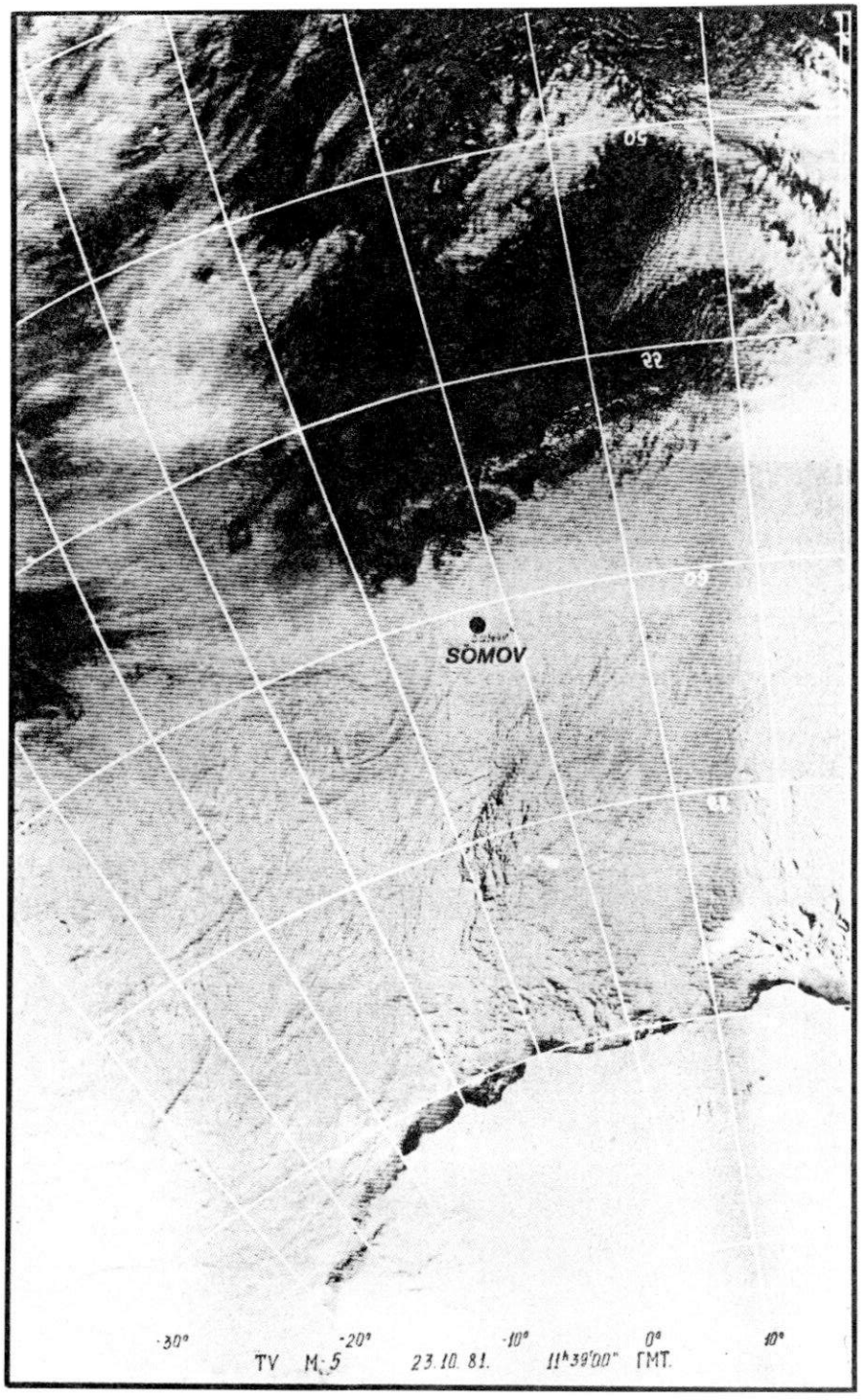
70
65
60
55
SOMOV
-30°
-20°
-10°
0°
10°
TV M-5
23.10.81.
11h39'00" GMT.

The U.S.-U.S.S.R. Weddell Polynya expedition

ARNOLD L. GORDON

Lamont-Doherty Geological Observatory
of Columbia University
Palisades, New York 10964

From 9 October to 25 November 1981 a unique joint U.S.-U.S.S.R. oceanographic field effort, the U.S.-U.S.S.R. Weddell Polynya expedition (WEPOLEX-81), was carried out within the southern ocean sea ice (Gordon and Sarukhanyan 1982). The objectives of WEPOLEX-81 were to obtain the first comprehensive, interdisciplinary data set well before the end of winter seasonal sea ice cover and to study an active, open-ocean polynya.

The need for winter information in all of the oceanographic, sea ice, and atmospheric sciences within the southern ocean seasonal sea ice cover has long been recognized. However, the logistical difficulties of obtaining such a data set are formidable. To begin the task of fulfilling this important requirement, WEPOLEX plans were developed under the U.S.-U.S.S.R. Governmental Bilateral Agreement for Cooperation in World Ocean Studies.

The Soviet ship *Mikhail Somov* (length 133 meters, beam 18.8 meters), of the Arctic and Antarctic Research Institute of Leningrad, was used for the work. The expedition head was E. I. Sarukhanyan, the U.S.S.R. national coordinator for POLEX (Polar Experiment)-South. The U.S. component was led by the deputy chief scientist, A. L. Gordon. Each national group had 13 members, who were integrated into a single scientific team within each of the participating disciplines.

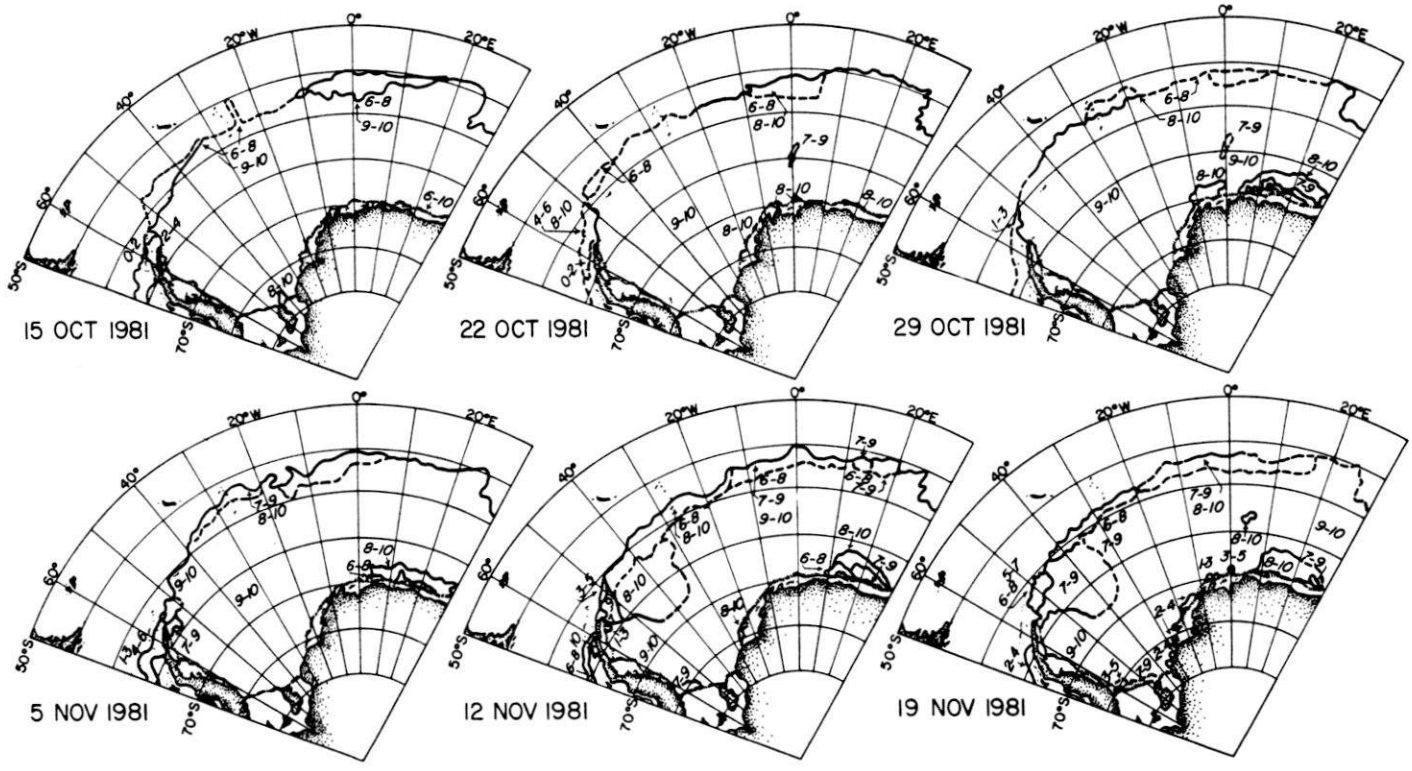

Figure 1. Extent and concentration of sea ice during the U.S.–U.S.S.R. Weddell Polynya expedition, October–November 1981, taken from U.S. Navy-National Oceanic and Atmospheric Adminstration Joint Ice Center maps.

Reprinted with permission.

After leaving Leningrad, the *Somov* stopped at Helsinki, Finland, on 9 September to pick up three members of the U.S. team and the U.S. equipment. With the aid of the Soviets, they undertook the difficult task of setting up the scientific apparatus and laboratory spaces for the expedition. The U.S. team provided most of the apparatus used during the cruise, including 7,000 meters of conducting cable for the conductivity-temperature-depth (CTD) work. During the transit from Helsinki, the cable was spooled onto the *Somov*'s winch, the CTD and computer equipment was installed and tested, and motor-generator sets were installed for converting 15 kilowatts of 50 hertz ship's power to 60 hertz power. During this time the ship's crew worked diligently to finish the routine maintenance tasks and modifications to the lab spaces that had not been completed in Leningrad because of *Somov*'s early departure.

The rest of the U.S. scientists boarded the *Somov* in Montevideo and headed for the ice on 9 October 1981. The ice edge near 5°E was reached at 56½°S on 20 October. The Greenwich meridian region was chosen for penetration into the ice because we believed we would encounter thinner ice with fewer pressure ridges there than further west and because the Weddell polynya, which formed in the 1974–76 period (Carsey 1980), occurred near 65°S and the Greenwich meridian.

Ice conditions during October and November 1981 were relatively heavy, with no well-developed, open-ocean polynya (figures 1 and 2). There were many leads—areas of reduced concentration—within the ice fields, which aided penetration into the ice interior. One of these leads, which was persistent, occurred near 65°S and the Greenwich meridian in approximately the same area that the Weddell polynya was observed in the mid-1970's. We were interested in this feature, but time requirements and the lack of a clear polynya signal made penetration farther south than our southernmost point of 62½°S counterproductive. The expedition track and station positions are shown in figure 3. The table (page 98) lists the Soviet and U.S. participants.

The articles that follow in this section describe the scientific components of WEPOLEX-81. Joint meetings of the U.S. and U.S.S.R. participants are planned for 1982 in the United States and for 1983 in the Soviet Union. A consolidated data report of scientific results will be prepared and distributed in 1983, and the scientific results will be published.

I wish to thank the participants of the U.S. and U.S.S.R. scientific teams and the *Somov* crew and officers, whose dedication led to the collection of an extensive array of high-quality data in a unique, previously unknown environment.

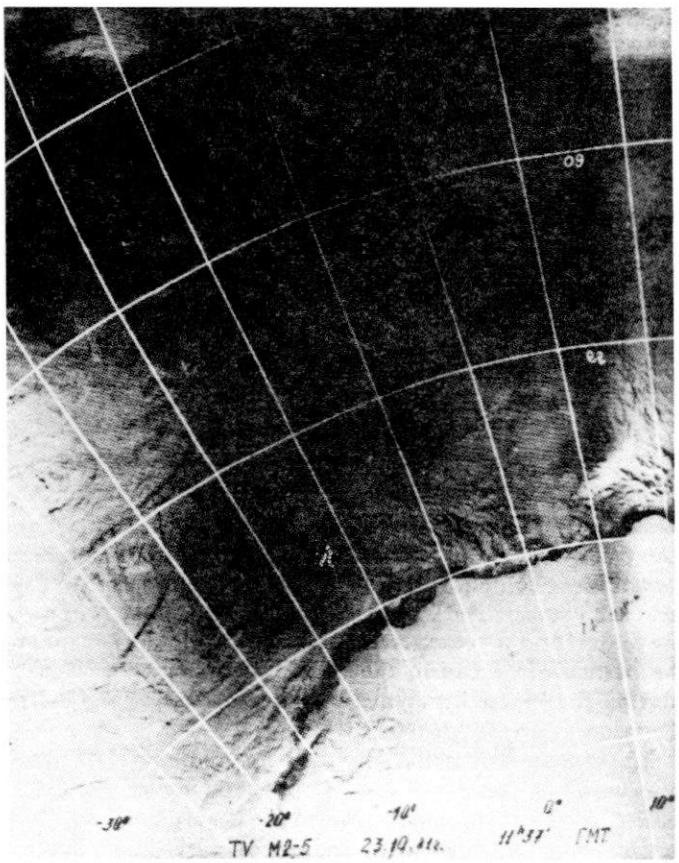

Figure 2. Satellite image transmitted from the Soviet Meteor satellite on 23 October 1981.

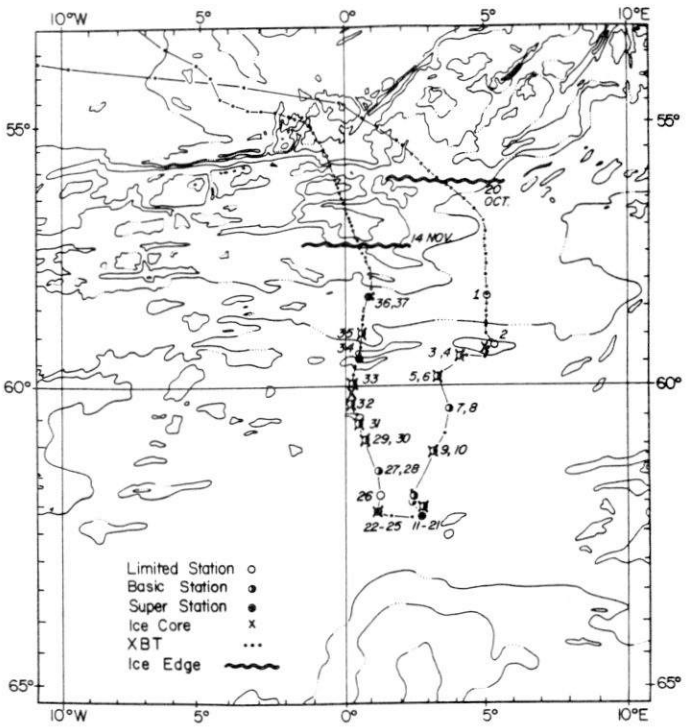

Figure 3. *Somov* track and observation sites during the U.S.-U.S.S.R. Weddell Polynya expedition. The limited stations included conductivity-temperature-depth (CTD) hydrographic stations. The basic stations included CTD and water column biology observation and atmospheric boundary layer observations. The super stations included all water column components. En route the thermal structure of the upper few hundred meters was observed with an expendable bathythermography system, surface chemistry was determined from water samples, and meteorological balloons were launched.

U.S. and Soviet participants in WEPOLEX-81

Chief—E. I. Sarukhanyan
Deputy Chief—A. L. Gordon
Captain of *Somov*—F. A. Pesyakov

Discipline	U.S. personnel	U.S.S.R. personnel
Physical oceanography	Bruce Huber, Head, LDGO[a] David Woodroffe, LDGO Walter Richter, SIO[c] Jan Szelag, URI[d]	Ivan Chuguy, Head[b] Nikolai Antipov Nikolai Bagriantsev Vladimir Romanov
Chemistry	Arthur Chen (carbonate system), OSU[e] Joe Jennings (nutrients and silicon), OSU Gerry Metcalf (oxygen, carbonate system, and radon), WHOI[f]	Victor Haritonov Vladimir Feodorov
Biology	Jeanne Stepien (zooplankton), LDGO David Boardman (chlorophyll, primary productivity), LDGO Diane Clarke (diatoms), LDGO	Valyeri M. Zhuravlev (zooplankton)
Sea ice	Stephen Ackley, USACRREL[g]	Boris Sustenov Alexandre Samoshkin
Meteorology	Ed Andreas, USACRREL	Alexandre Makshtas Ed Lysakov
Velocity of sound in the ocean		Peter Bogarodski

[a]LDGO = Lamont-Doherty Geological Observatory.
[b]All Soviet personnel were from the Arctic and Antarctic Research Institute, Leningrad, except Valyeri M. Zhuravlev, who was from the NVIRO, Moscow.
[c]SIO = Scripps Institution of Oceanography.
[d]URI = University of Rhode Island.
[e]OSU = Oregon State University.
[f]WHOI = Woods Hole Oceanographic Institution.
[g]USACRREL = U.S. Army Cold Regions Research and Engineering Laboratory.

References

Carsey, F. 1980. Microwave observations of the southern ocean. *Monthly Weather Review*, 108, 2032–2044.

Gordon, A. L., and Sarukhanyan, E. I. 1982. American and Soviet expedition into the southern ocean sea ice in October and November 1981. *EOS, Transactions of the American Geophysical Union*, 63(1), 2.

SECTION 2: PHYSICAL AND CHEMICAL OCEANOGRAPHY

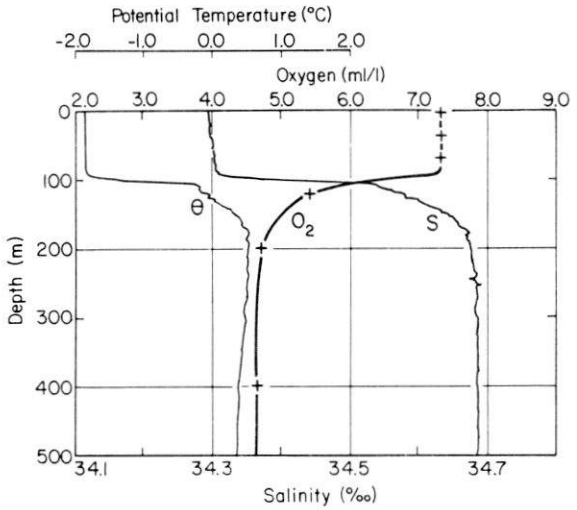

Fig. 1. Potential temperature, salinity, and oxygen stratification at *Somov* station 22 at 62 12'S, 1 05'E on November 5, 1981. The thermohaline data are derived from the CTD system. The oxygen data are from titration of water samples obtained from a rosette system. There was a 100% ice cover with few leads [*Ackley and Smith*, 1982]. The hydrographic data are reported by *Huber et al.* [1983].

mixes with the saline WDW that is diffused into the mixed layer during the spring melting period (as discussed below).

3. Mixed Layer Oxygen

The oxygen content of the entire mixed layer below the sea ice averages 7.40 (with a ±0.1 ml/l distribution about the mean) or 86% of saturation (Figure 2). This is about 1.1 ml/l below the full saturation value and is similar to the oxygen levels of the summer period temperature minimum (*Gordon and Molinelli* [1982], see temperature-oxygen relation for the vertical sections, plates 109 and 195). The WDW saturation levels are seasonally invariant near 57% to 60% of full oxygen saturation.

The origin of the mixed-layer oxygen undersaturation is likely due to entrainment of oxygen-poor WDW by the winter mixed layer. The oxygen content can be used to determine the amount of entrained WDW if we assume: (1) oxygen exchange between ocean and atmosphere is effectively blocked by the presence of a more or less complete (greater than 90%) snow and sea ice cover, (2) the net biological production and utilization of oxygen below the sea ice is zero, and (3) the mixed layer immediately prior to the ice cover is at the freezing point and at full oxygen saturation of 8.54 ml/l. Support for these assumptions is offered below.

1. The sea ice collected in the study region is dominated by frazil ice structure [*Ackley et al.*, 1983] with few brine channels. Thus the gas permeability is expected to be low [*Weiss et al.*, 1979; *Chen*, 1982]. The depletion in oxygen is probably not due to rapid oxidation of organic matter after the pack ice is formed because the surface water oxygen consumption rate is not large enough to generate a 14% oxygen undersaturation within a period of months [*Packard et al.*, 1971; *Skopintsev*, 1976; *Knauer et al.*, 1979].

2. The bacterial and biological activities are also low at the time of observation [*Marra et al.*, 1982], suggesting a low rate of oxygen production and consumption. The oxygen concentration in the remnant winter water at GEOSECS station 89 (60 01'S, 0 01'E, January 22, 1973; *Bainbridge* [1981]), which is less than 35 km from *Somov* station 33, is only 0.02 ml/l lower than our measured value, while the temperature and salinity are only 0.01°C and 0.07 ‰ higher, respectively. The excellent agreement in oxygen concentration collected in different seasons again suggests a low rate of oxygen production and consumption. Additionally, *Somov* oxygen, *p*H, calcium, alkalinity, total CO_2, nitrate, phosphate, and silica concentrations and the GEOSECS station 89 oxygen, alkalinity, total CO_2, nutrients, and ^{13}C values (*Chen* [1982]; also, see data listings of *Huber et al.* [1983]) all correlate linearly with salinity from surface down to the WDW core, which again indicates that the distribution of these chemical properties in the upper water column below the ice is predominantly controlled by conservative mixing processes with little production or utilization of chemicals [*Weiss et al.*, 1979; *Edmond et al.*, 1979; *Minas*, 1980].

3. The assumption regarding the mixed layer prior to the ice cover period is straightforward, since oxygen equilibrium is expected during the cooling period prior to the ice cover formation. Possibly some entrainment might occur before ice formation, and the resulting water does not equilibrate; however, this is reflected in the total entrainment determined below.

4. Rates of Deep to Surface Water Heat Flux

The potential temperature versus oxygen relationships for all *Somov* data points (Figure 3*a*) can be used to determine the ratio of WDW to the surface water characteristic of the period immediately prior to winter ice formation. A one-part WDW (0.5°C and 4.50 ml/l) to three parts surface water (−1.87°C and 8.54 ml/l) blend is required to produce the observed

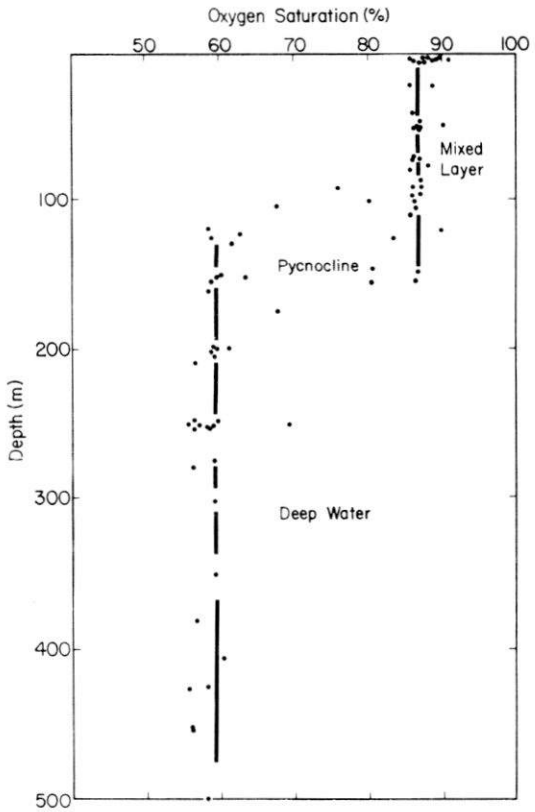

Fig. 2. Oxygen saturation from all rosette samples obtained by *Somov*. The saturation is determined by using the equation given in the *UNESCO International Oceanographic Tables* [1973].

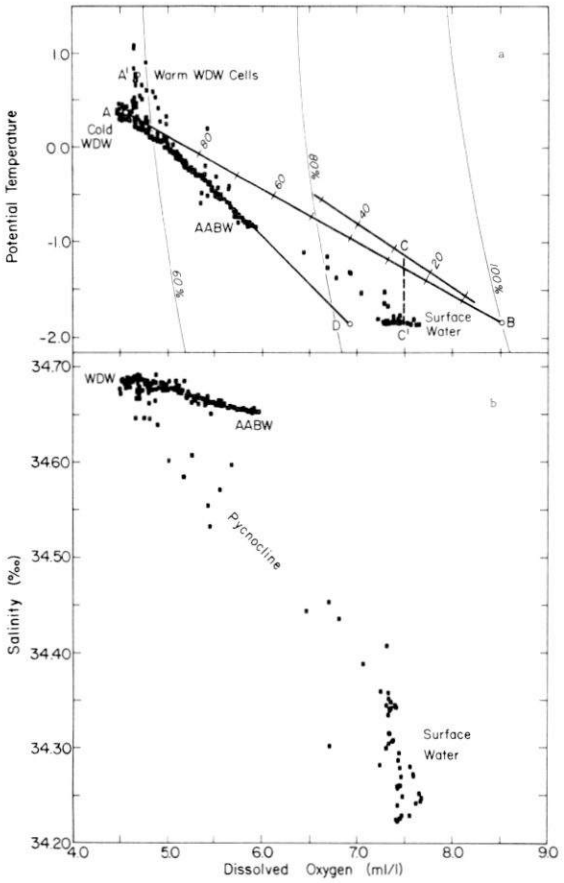

Fig. 3. Potential temperature versus oxygen content (*a*) and salinity versus oxygen content (*b*) from all rosette samples obtained by *Somov*. WDW is Weddell Deep Water and AABW is Antarctic Bottom Water. The two linear mixing lines AB and A'B are marked with percent of A water type (WDW) relative to B water type. Point D is the freezing temperature extension of the line fit to the temperature-oxygen trend of deep and bottom water colder than 0°C.

mixed-layer oxygen of 7.4 ml/l (line AB on Figure 3*a*). However, the temperature of this mixture would be 0.63°C above the freezing point. For the average mixed-layer thickness of 108 m the heat accompanying the upward transfer of WDW is 6.66×10^3 cal/cm^2 (2.78×10^8 J/m^2). If the warm WDW cells [*Gordon and Huber*, this issue] are responsible for the regionally depressed mixed-layer oxygen, the heat transfer is slightly increased (see line A'B on Figure 3*a*) to 7.93×10^3 cal/cm^2 (3.31×10^8 J/m^2). Thus the average heat flux during the 5-month ice-covered period [*Gordon and Huber*, this issue] is 20 to 25 W/m^2. If the vertical heat transfer across the pycnocline is taken as zero for the 7-month ice-free period, the average annual heat flux is 9 to 11 W/m^2.

While entrainment of WDW would cease with the onset of the seasonal pycnocline, some diffusive heat flux is expected during the ice-free part of the year. A vertical mixing coefficient K_z of 0.1 cm^2/s would accomplish a cross-pycnocline heat flux during the 7-month ice-free period of 1 W/m^2; a K_z of unity yields 10 W/m^2. Therefore, the total deep to surface water heat flux (ice cover plus ice free periods) may be in the range of 9–16 W/m^2. A value of 12 W/m^2 is suggested for a working value, reflecting a K_z of 0.5 cm^2/s.

How realistic is the winter period entrainment value and heat flux? For an annual steady state the rate of winter entrainment must balance the annual Ekman-induced upwelling of the pycnocline. The above calculation suggests an effective WDW entrainment of 27 m into the mixed layer during the winter-ice-covered period. This agrees quite well with the annual average upwelling rate of 1×10^{-4} cm/s (31 m/yr) determined from Ekman pumping calculations by using a climatically averaged wind field for the region of the *Somov* data [*Gordon et al.*, 1977].

The annual average heat flux from WDW to the mixed layer of 9–16 W/m^2 is somewhat below the annual ocean-to-atmosphere heat flux calculated from meteorological parameters. *Zillman* [1972] calculates a heat loss of 18 W/m^2 at 60°S south of Australia (Zillman's Figure 3); while *Gordon* [1981] finds 31 W/m^2 average for the 60°–70°S circumpolar belt. However, it is noted that the *Somov* results pertain to the 59°–62°S region and would be expected to be lower than the 60°–70°S average but somewhat above the Zillman value because the Weddell pycnocline is weaker than the circumpolar average [*Martinson et al.*, 1981]. In view of the uncertainty in the diffusive heat flux determined during the ice-free period and the difference in the type of calculation, agreement is reasonably good.

5. Rate of Deep to Surface Water Salt Flux

The salt introduction to the surface water mixed layer by the effective entrainment of 27 m of WDW during the five winter ice cover months requires freshwater input of 34 cm to reduce the WDW salinity (34.680‰) to the annual mean surface water salinity (34.250‰, representing a 7:5 blend of the 34.224‰ average summer salinity from *Islas Orcadas* data with 34.287‰ winter salinity from the *Somov* data). During the ice-free period, salt diffusion across the pycnocline would place additional requirements for compensating freshwater input. Using K_z of 0.1 and 1.0 cm^2/s introduces 0.078 to 0.78 gm of salt per centimeter squared, respectively, into the surface water over 7 months, requiring a freshwater input of 2.3 to 23 cm to produce the annual mean surface water salinity.

Thus the annual freshwater input required to balance the total WDW salt flux into the surface layer is 36 to 57 cm/yr. A value of 46 cm/yr would correspond to the 12 W/m^2 best guess (K_z of 0.5 cm^2/s).

Estimates of annual freshwater flux into the 60°–70°S belt by excess precipitation over evaporation and continental runoff (glacial ice meltwater) are as high as 40 cm/yr [*Gordon*, 1981]. However, the mean snow cover on the sea ice was only 20 cm [*Ackley et al.*, 1982], which translates to only 2–6 cm of water, thus a value of 40 cm/yr may be an overestimate. Additional freshwater input could be derived if there is a net advection of sea ice into the region.

Support for this suggestion is derived by considering the approximate salinity balance for the five ice-covered months. A 1:3 mix of WDW to the surface water just prior to the ice cover would result in an end-of-winter salinity of 34.338‰. To reduce the salinity to the observed average of 34.287‰ requires 20 cm of sea ice (with a salinity of 5‰, *Ackley et al.*, [1982]). A meteoric source of water is unlikely during the winter since the snow on the ice is not available for release into the ocean until the spring melt.

Melting would be encouraged by the heat flux discussed above; the mixed-layer temperature slightly above freezing may be a direct evidence of this process. Sea ice melting of 20 cm requires about 20% of the winter heat flux, the rest would be lost to the atmosphere in leads and thin ice. It is probable

that much of the ice melting occurs in October, when the ocean heat flux into the atmosphere is reduced from the winter maximum [*Gordon*, 1981], but the entrainment of WDW (which is due primarily to ice movement relative to the ocean; *Gordon and Huber* [this issue]) continues. The dynamic-thermodyanmic model of *Hibler and Ackley* [1983, Figure 8] suggests a net ice advection within the *Somov* region of +10 cm of accumulation in the south to 25 cm of net melting in the north. The above calculations favor the net melting value. Net melting has the effect of transporting freshwater into the area, even in the presence of Ekman divergences.

Assuming there is no heat conduction through the sea ice and that leads make up 5% of the area, the average winter heat loss in the leads amounts to about 350 W/m^2. This value is similar to estimates for Arctic Ocean heat loss within leads [*Maykut*, 1978]. It is noted that leads, though effective in removing heat, and perhaps freshwater, by evaporation, would not be effective in enhancing oxygen exchange or freshwater input by precipitation.

5. Discussion

The potential temperature-oxygen scatter (Figure 3*a*) shows that for all conservative linear mixtures of WDW end members with a freezing point, surface water end members require the surface water to have oxygen saturation as low or lower than that observed from *Somov*. Conservative behavior for oxygen in the Southern Ocean is suggested by *Weiss et al.* [1979] and *Edmond et al.* [1979], so it is not likely this relationship is due to in situ oxygen consumption. Deep water colder than 0°C possesses a slightly steeper slope, indicating that the Antarctic bottom water (AABW) requires a freezing point surface water component with oxygen of 6.8 ml/l or 80% saturation (point D, Figure 3*a*), suggesting that a 35% contribution from WDW might be more appropriate for regions further poleward of the *Somov* region.

The salinity-oxygen (S/O_2) distribution (Figure 3*b*) shows that the mixed-layer points have a negative slope such that the mixed-layer water with higher salinity has slightly lower oxygen. This relation is expected from the WDW origin of the reduced mixed-layer oxygen.

Calculations of the oxygen consumption rate have frequently been made with the use of the measured apparent oxygen utilization (AOU) value and the estimated age of the water [*Jenkins*, 1980]. A hidden assumption in the calculation is that the AOU is near zero when the water was last at the surface. Obviously, this assumption needs to be modified for AABW or any water that has a component of the winter Antarctic surface water. Similarly, caution must be exercised when one calculates the age of water or the oceanic circulation rates by using AOU and the independently estimated oxygen consumption rate.

Acknowledgments. Funding for the US-USSR Weddell Polynya Expedition was received from the Division of Polar Programs of the National Science Foundation, grant DPP 80-05765 for the physical oceanography, and from the Department of Energy for the geochemistry support of Chen 81 EV 10611. Comments from Hsien Wang Ou, Bruce Huber, and John Marra are appreciated. Lamont-Doherty Geological Observatory contribution 3549.

References

Ackley, S. F., and S. J. Smith, Reports of the US-USSR Weddell Polynya Expedition of October–November 1981: Vol. 5, Sea Ice Conditions, *SR 83-2*, U.S. Army Corps Eng. Cold Reg. Res. Eng. Lab., Hanover, N. H., 1983.

Ackley, S. F., D. B. Clarke, and S. J. Smith, *Reports of the Weddell Polynya Expedition of October–November 1981*: vol. 4, *Physical, Chemical and Biological Properties of Ice Cores*, U.S. Army Corps Eng. Cold Reg. Res. Eng. Lab., Hanover, N. H., 1983.

Bainbridge, A. E., *GEOSECS Atlantic Expedition*, v. 1, *Hydrographic Data 1972–1973*, 121 pp., National Science Foundation, Washington, D.C., 1981.

Chen, C. T. A., On the distribution of anthropogenic CO_2 in the Atlantic and Southern oceans, *Deep-Sea Res.*, *29*, 563, 1982.

Edmond, J. M., S. S. Jacobs, A. L. Gordon, A. W. Mantyla, and R. F. Weiss, Water column anomalies in dissolved silica over opaline pelagic sediments and the origin of the deep silica maximum, *J. Geophys. Res.*, *84*, 7809–7826, 1979.

Gordon, A. L., Seasonality of Southern Ocean sea ice, *J. Geophys. Res.*, *86*, 4193–4197, 1981.

Gordon, A. L., The US-USSR Weddell Polynya Expedition, *Antarct. J. U.S.*, *17*, 1982.

Gordon, A. L., and B. A. Huber, Thermohaline stratification below the Southern Ocean sea ice, *J. Geophys. Res.*, this issue.

Gordon, A. L., and E. M. Molinelli, *Southern Ocean Atlas: Thermohaline Chemical Distributions and the Atlas Data Set*, 11 pp., 233 plates, Columbia University Press, New York, 1982.

Gordon, A. L., and E. I. Sarukhanyan, American and Soviet Expedition into the Southern Ocean sea ice in October and November 1981, *EOS Trans. AGU*, *63*, 2, 1982.

Gordon, A. L., H. W. Taylor, and D. T. Georgi, Antarctic oceanographic zonation, in *Polar Oceans*, edited by E. Dunbar, pp. 45–76, Arctic Institute of North America, 1977.

Hibler, III, W. D., and S. F. Ackley, Numerical simulation of the Weddell sea pack ice, *J. Geophys. Res.*, *88*, 2873–2887, 1983.

Huber, B., S. Rennie, D. Georgi, S. Jacobs, and A. Gordon, ARA *Islas Orcadas* Data Reports, Cruise 12, *Ref. CU-2-81-TR2*, Lamont-Doherty Geol. Observ., Palisades, N.Y., 1981.

Huber, B. A., J. Jennings, C.-T. Chen, J. Marra, S. Rennie, P. Mele, and A. Gordon, Reports of the US-USSR Weddell Polynya Expedition, vol. 2, Hydrographic data, 115 pp., *L-DGO-83-1*, U.S. Army Corps Eng. Cold Reg. Res. Lab., Hanover, N.H., 1983.

Jenkins, W. J., Tritium and ^{3}He in the Sargasso Sea, *J. Mar. Res.*, *38*, 533–569, 1980.

Knauer, G. A., J. H. Martin, and K. W. Bruland, Fluxes of particulate carbon, nitrogen, and phosphorus in the upper water column of the northeast Pacific, *Deep-Sea Res.*, *26A*, 97–108, 1979.

Marra, J., L. H. Burckle, and H. W. Ducklow, Sea ice and water column plankton distributions in the Weddell Sea in late winter, *Antarct. J. U.S.*, *17*(5), 111–112, 1982.

Martinson, D. G., P. D. Killworth, and A. L. Gordon, A convective model for the Weddell Polynya, *J. Phys. Oceanogr.*, *11*, 466–488, 1981.

Maykut, G. A., Energy exchange over young sea ice in the Central Arctic, *J. Geophys. Res.*, *83*, 3646–3658, 1978.

Minas, H. J., Production Primaire et Secondaire, Colloque Franco-Sovietique, *Publ. 10*, pp. 21–36, CNEXO (Actes du Colloque), Paris, 1980.

Packard, T. T., M. L. Healy, and F. A. Richards, Vertical distribution of the activity of the respiratory electron transport system in marine plankton, *Limnol. Oceanogr.*, *16*, 60–70, 1971.

Skopintsev, B. A., Oxygen consumption in the deep waters of the ocean, *Oceanology*, *15*, 556–561, 1976.

Toole, J. M., Sea ice, winter convection, and the temperature minimum layer in the Southern Ocean, *J. Geophys. Res.*, *86*, 8037–8047, 1981.

UNESCO, *International Oceanographic Tables*, vol. 2, 141 pp., Paris, 1973.

Weiss, R. F., H. G. Ostlund, and H. Craig, Geochemical studies of the Weddell Sea, *Deep-Sea Res.*, *26*, 1093–1120, 1979.

Zillman, J. W., Solar radiation and sea-air interaction south of Australia, in *Antarctic Oceanology I, The Australian-New Zealand Sector*, vol. 19, edited by D. E. Hayes, pp. 11–40, AGU, Washington, D.C., 1972.

C. T. A. Chen, Oregon State University, Corvallis, OR 97331.

A. L. Gordon and W. G. Metcalf, Lamont-Doherty Geological Observatory of Columbia University, Palisades, NY 10964.

(Received April 28, 1983;
revised August 25, 1983;
accepted September 8, 1983.)

JOURNAL OF GEOPHYSICAL RESEARCH, VOL. 89, NO. C1, PAGES 641–648, JANUARY 20, 1984

Thermohaline Stratification Below the Southern Ocean Sea Ice

ARNOLD L. GORDON AND BRUCE A. HUBER

Lamont-Doherty Geological Observatory

The end of winter stratification within the cold cyclonic trough of the Weddell gyre near 60°S between 5°E and the Greenwich meridian is resolved with the *Mikhail Somov* data set. The temperature maximum of the Weddell Deep Water (WDW) is, for the most part, less than 0.5°C, but warmer cells of WDW are found. These warm WDW cells have temperature, salinity, and oxygen properties similar to the WDW characteristic of the Weddell gyre inflow, which is situated to the southeast of the *Mikhail Somov* study region. The warm WDW cells are accompanied by domes in the pycnocline of 40 m amplitude over the surrounding pycnocline, while deeper isopycnals are depressed. Anticyclonic shear below the 27.83 σ-θ isopycnal within the warm WDW cells is compensated by the cyclonic shear associated with the pycnocline dome. The pycnocline domes are exposed to about 50% greater entrainment by the turbulently active winter mixed layer, relative to the regional entrainment rate. This entrainment can significantly erode the warm cells in a single winter season, introducing excess heat and salt into the mixed layer. While the heat is lost to the atmosphere, the excess salt is not necessarily compensated by increased fresh water introduction. It is hypothesized that the warm WDW cells within the Weddell gyre trough are derived from instability within the frontal zone which extends from Maud Rise to the northeast, separating the Weddell warm regime from the cold regime. Greater than normal injection of warm WDW cells into the Weddell gyre trough would increase the surface salinity, which would tend to destabilize the pycnocline, increasing the probability of deep convection and polynya events.

1. INTRODUCTION

During October and November 1981 the joint U.S.-U.S.S.R. Weddell Polynya Expedition was carried out within the Southern Ocean sea ice, aboard the Soviet ship *Mikhail Somov* of the Arctic-Antarctic Research Institute of Leningrad [*Gordon and Sarukhanyan*, 1982; *Gordon*, 1982]. The objectives of the expedition were to obtain a comprehensive interdisciplinary data set near the Greenwich meridian (0°E), well within the seasonal sea ice zone and to investigate an active open ocean polynya. A polynya developed near 65°S and 0°E in the 1974–1976 winters [*Carsey*, 1980]; however, no polynya developed in 1981. The observations extend across the ice edge zone into the interior pack about 590 km from the mean position of the outer fringes of sea ice during the expedition.

The *Mikhail Somov* hydrographic data set resolves the thermohaline stratification during the transition phase from waxing to waning of the Southern Ocean sea ice cover. Sea ice covers the region near 60°S between 0° and 5°E in June, reaching a maximum northward extent during September and October. The region becomes ice free in mid-December (Antarctic Ice Charts, Navy-NOAA Joint Ice Center, Naval Polar Oceans Center, Suitland, Maryland). In 1981 the ice edge overtook the region between June 18 and 25, remained near 56°S from the end of July to early November, and retreated from the region during the third week of December. The *Mikhail Somov* data set reveals the cumulative effects of the 1981 austral winter and thus depicts the end of winter stratification, although the expedition took place in the austral spring.

The positions of the CTD-O_2/Rosette hydrographic stations and the expendable bathythermograph (XBT) observations [*Huber et al.*, 1983], as well as ice core sites [*Ackley et al.*, 1982] and the ice edge position at the time of entry and exit from the pack ice are given as Figure 1.

2. OCEANOGRAPHIC SETTING

Most of the *Mikhail Somov* hydrographic stations fall within the trough of the cyclonic Weddell gyre [*Deacon*, 1976, 1979; *Gordon et al.*, 1981; *Gordon and Molinelli*, 1982, plates 231–233]. This region is characterized by a relatively cold (less than 0.5°C) Weddell Deep Water (WDW) and is here designated as the Weddell cold regime (Figure 2). The northern stations fall within the eastward flowing limb of the Weddell gyre, with stations 36 and 37 positioned north of the northern boundary of the Weddell gyre. The boundary is marked by a slight increase in baroclinicity and a transition into deep water far too warm (well in excess of 1°C at the temperature maximum; Figure 3) to have participated in the upstream segment of the Weddell gyre. This warmer deep water is called Circumpolar Deep Water (CDW).

South of the *Mikhail Somov* data set, historical (summer) data reveal the westward flowing limb of the Weddell gyre, with warmer WDW (temperature maximum of up to 1.1°C), here designated the Weddell warm regime. The warmer WDW is derived from the main mass of CDW in the vicinity of 20°–30°E [*Deacon*, 1979]. It appears as a wedge of warm WDW with its apex near Maud Rise (Figure 2). A rather abrupt transition to the Weddell cold regime occurs to the west of Maud Rise (Figure 4) and extends to the northeast from Maud Rise. The transition from cold to warm regimes occurs within a distance of 100 km (e.g., between *Islas Orcadas* stations 95 and 96; Figure 5). The increase in WDW temperature of over 0.4°C is accompanied by a decrease in depth of the temperature maximum from 425 m to 240 m and shallowing of the pycnocline by approximately 50 m. An *Islas Orcadas* section along 20°E (Figure 6) shows a similar transition occuring between stations 75 and 76.

Thus, there is a relatively sharp transition from warm to cold regime coinciding with southwest flow within the Weddell gyre (Figure 2). It is marked by the 0.6° to 0.8°C isotherms of the temperature maximum, extending from 58°S 20°E to 63°S 2°E. The historical data set suggests that this is a climatic feature (e.g., see 350 m temperature section plate 23 of *Gordon and Molinelli* [1982]).

The primary advective path of warm WDW into the western hemisphere occurs south of Maud Rise, over the continental slope where a relatively strong westward current exists (Figure 2) [*Tchernia*, 1977; *Foster and Carmack*, 1976]. Outside the boundary currents the Weddell gyre is sluggish with

Paper number 3C1642.
0148-0227/84/003C-1642$05.00

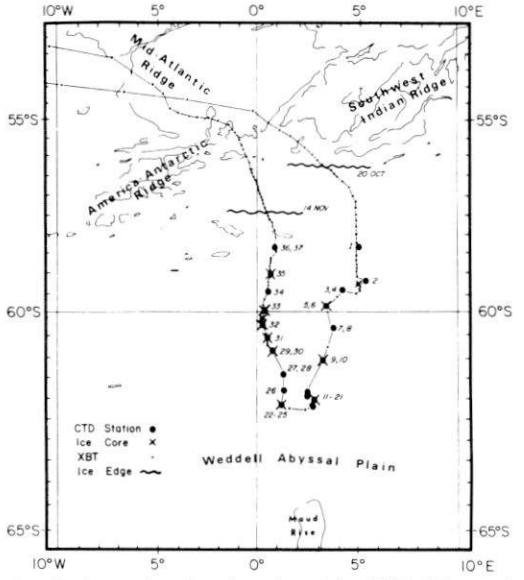

Fig. 1. Cruise track and station sites of the *Mikhail Somov* during the U.S.-U.S.S.R. Weddell Polynya Expedition, October–November 1981.

characteristic velocity of only 1 cm/s [*Gordon et al.*, 1981].

The hydrographic data along the two north-south sections obtained by *Mikhail Somov* (Figures 3 and 7) reveal three structures associated with lateral variations of WDW temperature and pycnocline depth. These structures are (1) the warmer deep water observed at CTD stations 36 and 37 and by the series of expendable bathythermograph (XBT) observations north of the *Mikhail Somov* hydrographic station grid (Figure 8); (2) very cold WDW at station 35; and (3) isolated cells of warm WDW within the Weddell cold regime (above 0.6°C at the temperature maximum).

The warm feature from 57°40′S to 58°40′S on the 0° XBT section (lower panel of Figure 8) is apparently an eddy of CDW. The CDW characteristics within the eddy as revealed at CTD station 36 and 37 extend to 1100 m before yielding to a local oxygen minimum with WDW characteristics [*Huber et al.*, 1983]. The primary transition from Weddell gyre to Circumpolar Deep Water (CDW) occurs near 56°45′S on both XBT sections.

The anomalously cold WDW observed at station 35 (temperature maximum of only 0.19°C at 600 m) and at XBT 103, 109, and 113 surrounds the CDW eddy. This cold deep water is probably an eastward extension of the Weddell-Scotia confluence [*Patterson and Sievers*, 1980].

3. Warm WDW Cells

The warm WDW cells have not previously been observed within the Weddell cold regime, though the historical data set is too sparse to exclude the possibility of their existence during the summer.

The warm cells are represented in temperature-salinity (θ/S) space (Figure 9) as nearly isohaline extensions above the cold WDW. The WDW of the Weddell warm regime and CDW just north of the Weddell gyre have the same nearly isohaline θ/S form above 0.4°C [*Huber et al.*, 1983; *Gordon and Molinelli*, 1982]. This indicates, as expected, that the source of the warm WDW cells is the deep water surrounding the Weddell cold regime. The warm cells appear within or to the south of a trough in dynamic topography as determined from the *Mikhail Somov* data and have characteristics similar to the WDW of the Weddell warm regime found east of Maud Rise.

The *Mikhail Somov* potential temperature-oxygen (θ/O_2) points (Figure 10) within the warm cells follow the θ/O_2 trend of both the South Atlantic CDW and Weddell warm regime. Oxygen levels within the cells are higher than those within the cold WDW temperature maximum. While it is possible that the warm cells are spawned at the Weddell gyre-CDW front, it is probable that the source is the Weddell warm regime which is closer to the observed warm cells. The warm cells represent a transfer of properties across the transitional zone separating the Weddell cold from the warm deep water regimes.

The other major characteristic of the warm cells is doming of the pycnocline above the cells (Figures 7 and 11). Within the warm cells, where the potential temperature maximum (θ-max) is above 0.5°C, the top of the pycnocline (marked by the depth at which the density increases by more than 0.01 sigma-θ units in 10 m) occurs at an average depth of 74 m. At sites of the cold WDW (θ-max of less than 0.5°C) more typical of the region, the top of the pycnocline occurs at 114 m.

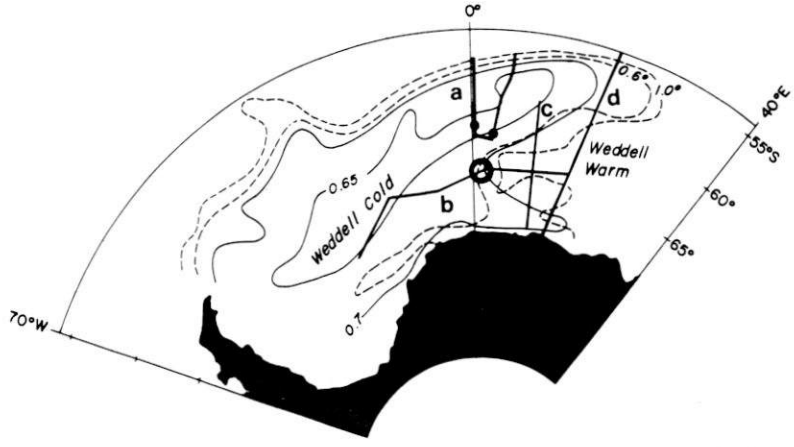

Fig. 2. Schematic of the Weddell gyre. Dashed lines show the isotherms 0.6° and 1.0°C within the oxygen minimum core layer [*Gordon and Molinelli*, 1982, plate 206) which is coincident with the temperature maximum core layer within the Weddell gyre. Solid lines show the 0/2500 dbar isopleths 0.65 and 0.70 dynamic meters [*Gordon and Molinelli*, 1982, plate 230). The *Mikhail Somov* sections (line a) and schematic representation of the warm WDW cells (solid circles) appear north of Maud Rise (large open circle near 65°S and the Greenwich meridian).

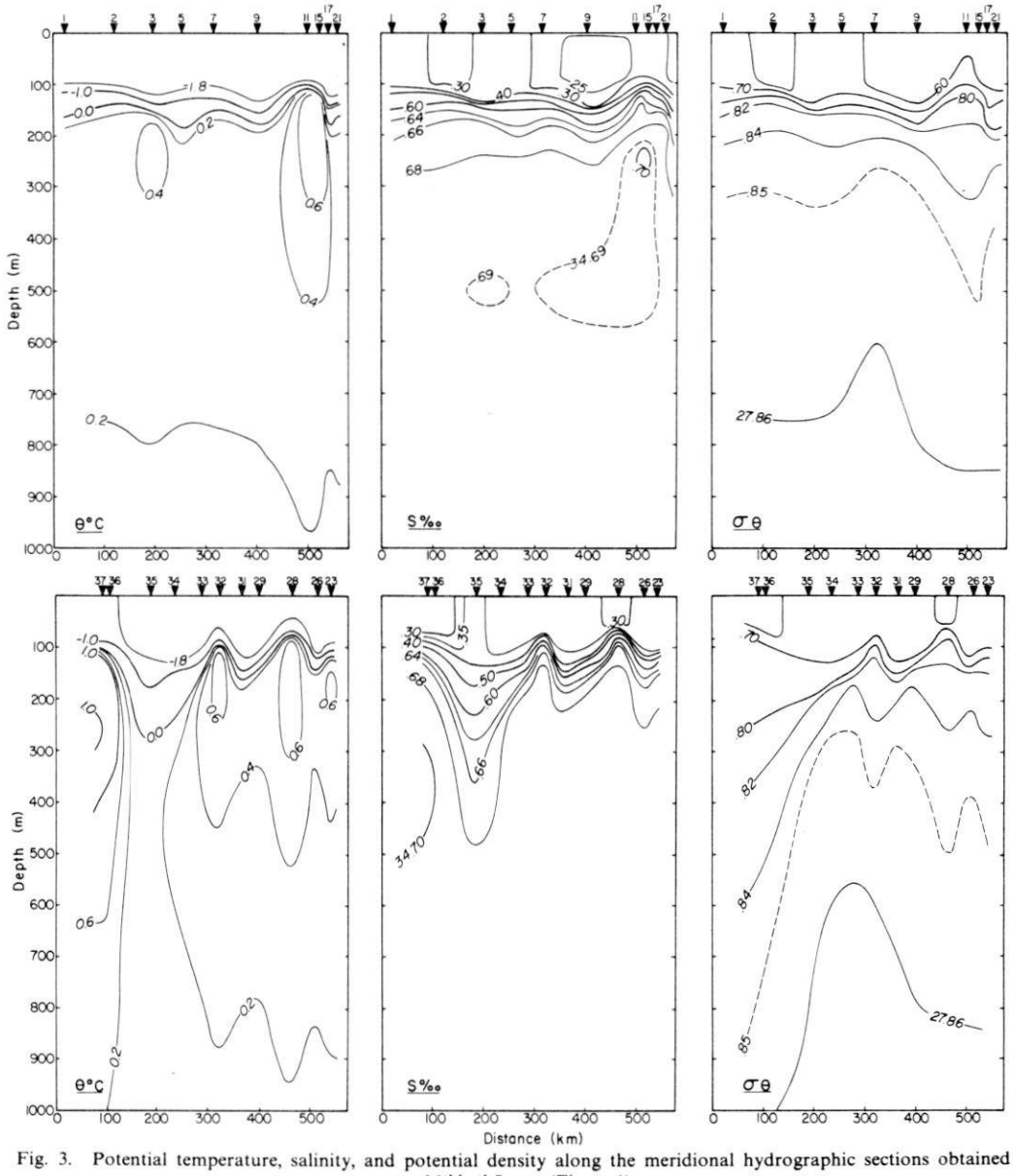

Fig. 3. Potential temperature, salinity, and potential density along the meridional hydrographic sections obtained by *Mikhail Somov* (Figure 1).

Similarly, the depth of the 0°C isotherm increases by about 50 m as the θ-max temperature is reduced from 0.7° to 0.4°C. The same relation is found in the regional *Islas Orcadas* data set.

The warm WDW cells (represented by station 28 and 32) contain an excess of 20.5 Kcal/cm^2 of heat (49 Joules/m^2) and 2.3 gm/cm^2 (23 kg/m^2) of salt relative to the Weddell cold regime water column (represented by stations 31 and 33) above 500 m (Figure 11).

The isopycnal interval 27.82 to 27.83 near 200 m, which coincides with the θ-max, is nearly horizontal, while deeper isopycnals dip below the warm cells (Figure 7). This induces anticyclonic geostrophic shear below 27.83 and cyclonic shear above 27.82. The baroclicity is not great. A maximum geostrophic velocity of only 0.5 cm/s relative to 1900 decibars (dbar) occurs in the 27.82 to 27.83 sigma-θ interval. A secondary velocity maximum of the same magnitude but of opposite sign occurs at the sea surface. The geostrophic velocity at 1900 dbar relative to 5000 dbar (*Mikhail Somov* station pair 29–32) is 0.4 cm/s in the same sense as the θ-max velocity maximum; thus the surface current relative to 5000 dbar is close to zero. Hence, the pycnocline dome effectively compensates the baroclinicity of the rest of the water column. This situation is similar to, though substantially less energetic than, the pycnocline eddies observed in the Arctic [*Newton et al.*, 1974; *Manley*, 1981]. The shear reversal within the upper layer of the Arctic is believed to be induced by secondary Ekman circulation in the ocean boundary layer below the sea ice cover [*Manley*, 1981].

The secondary Ekman circulation associated with the warm WDW cell is extremely weak, inducing a maximum pycnocline upwelling of 10^{-5} to 10^{-6} cm/s. This assumes a circular form of the warm cells, a drag coefficient at the sea ice-water interface of 5×10^{-3} [*Langleben*, 1982; *Andreas*, 1983], and a tangential anticyclonic velocity within the cell of 0.5 to

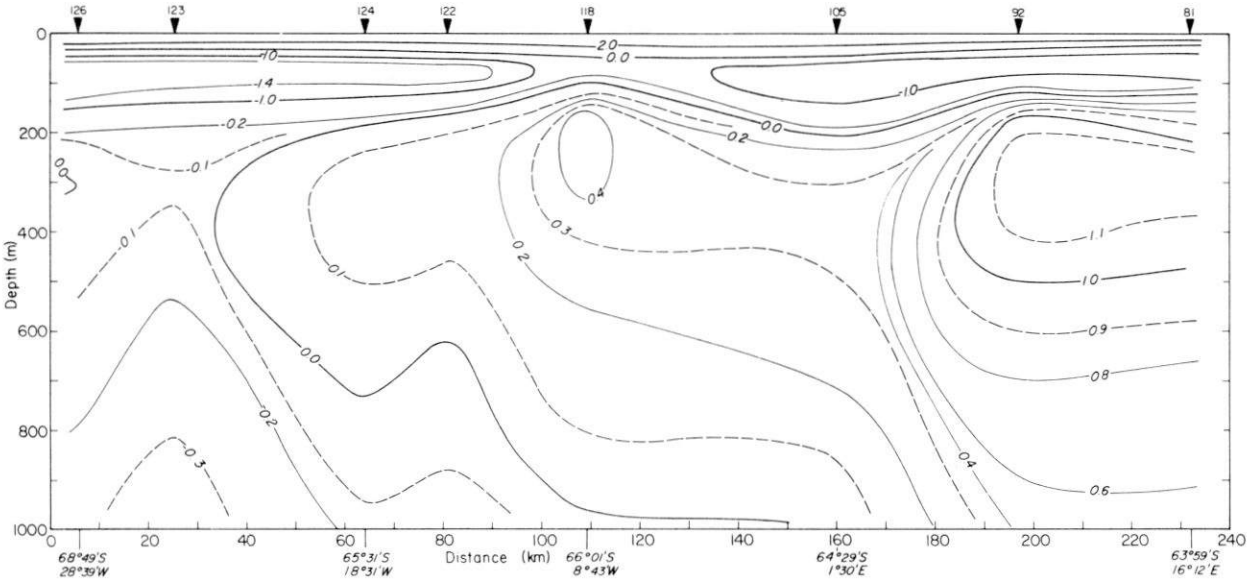

Fig. 4. East-west potential temperature section (line b of Figure 2) from *Islas Orcadas* cruise 12 [*Huber et al.*, 1981].

1.0 cm/s as determined from the geostrophic velocity relative to 1900 and 5000 dbar, respectively. During the ice-covered period this would induce a pycnocline dome of only a meter or two, not the 40 m pycnocline relief observed. It is more likely that the shallow pycnocline associated with a warm WDW cell is a characteristic transferred into the region from the Weddell warm regime.

4. Entrainment of the Warm WDW Cells

The pycnocline dome of the warm cells is exposed to more intense entrainment by mixed layer turbulence than is the surrounding deeper pycnocline. Within the warm cells the pycnocline intensity is stronger (Figure 11), which may be taken as evidence for enhanced entrainment [*Phillips*, 1977]. *Niiler and Kraus* [1977], in a review of one-dimensional mixed layer models, offer the following equation for mixed layer deepening rate, W_E (cm s^{-1}) in a two layer system:

$$W_E = \frac{2m\ \rho U_*^{\ 3}}{h\ g\Delta\rho} - \frac{n\rho B_0}{g\Delta\rho} \tag{1}$$

where U_* is the friction velocity defined by $U_* = (C_d U^2)^{1/2}$, ρ is the water density, C_d is the drag coefficient at the ice-water

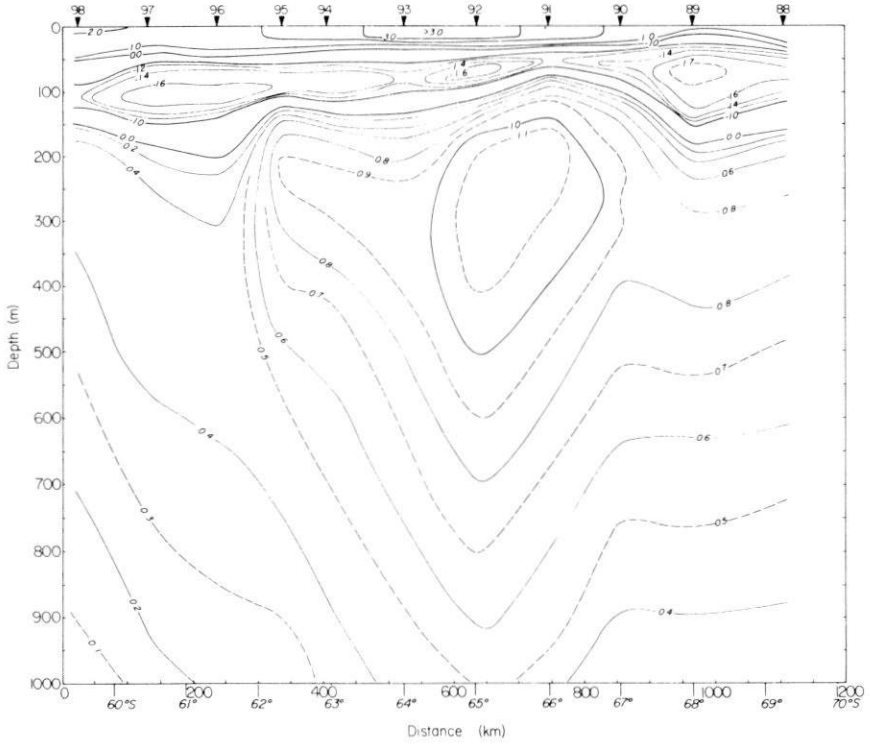

Fig. 5. Potential temperature section along 10°E (line c of Figure 2) from *Islas Orcadas* cruise 12 [*Huber et al.*, 1981].

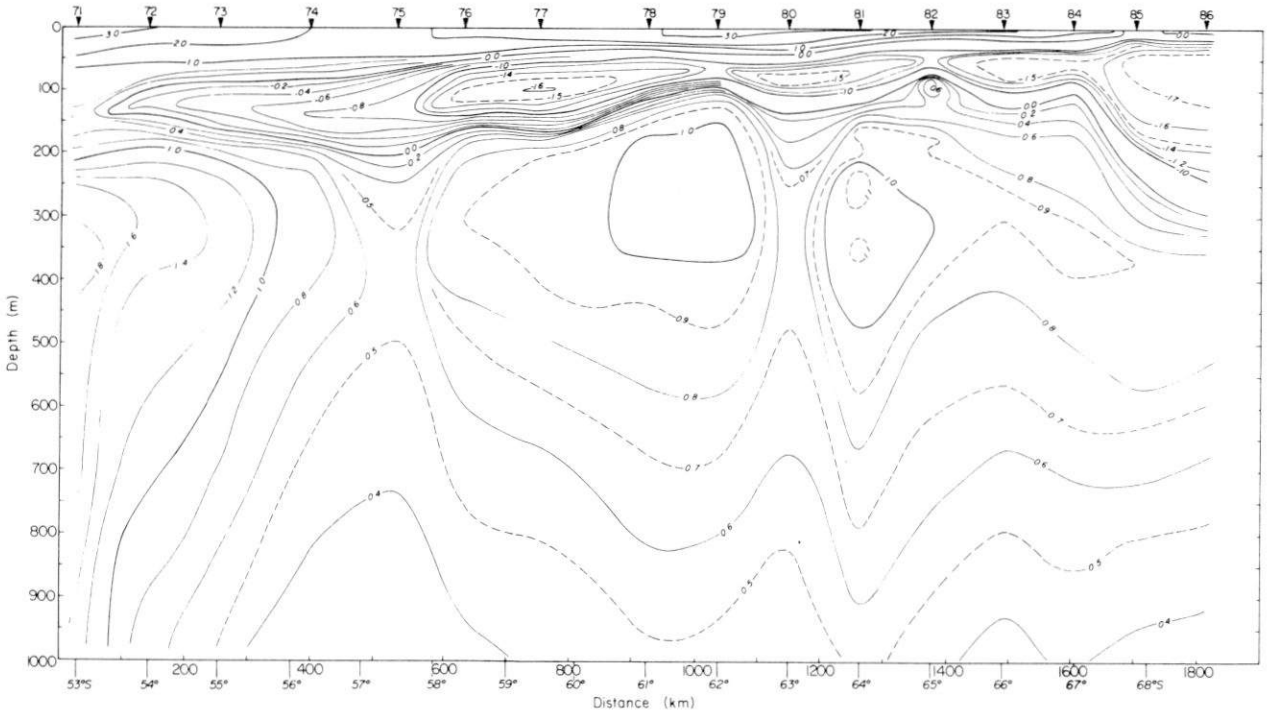

Fig. 6. Potential temperature section along 20°E (line d of Figure 2) from *Islas Orcadas* cruise 12 [*Huber et al.*, 1981].

interface (a value of 5×10^{-3} is used [*Langleben*, 1982; *Andreas*, 1983]); U is the magnitude of the ocean current relative to the ice; h is the mixed layer thickness, taken as 74 m for the warm cells and 114 m for regional value; $\Delta\rho$ is the density difference across the pycnocline, taken as 0.2 σ-θ units; B_0 is the buoyancy flux into the ocean (at the ice-ocean interface $B_0 = g[\beta SF]$ where β is the expansion coefficient for salinity, S is the salinity of the mixed layer, F is the freshwater input to the ocean); g is the acceleration of gravity. The coefficients m and n are proportionality factors. The value of m is taken as 1.25, given by *Kato and Phillips* [1969] though a range of 0.9–2.8 has been suggested [*Cushman-Roisin*, 1981]. The factor n is proportional to the loss of convective energy to dissipation and ranges from 0 to 1 (approaching zero as the mixed layer deepens).

A maximum negative B_0 value would occur if all the observed 75 cm of sea ice [*Ackley et al.*, 1982] were formed locally. Using $n = 0.036$ (*Farmer* [1975] for frozen lakes mixed layer) the entrainment induced by the second term on the right of equation (1) is 2.8×10^{-5} cm s^{-1}. It is likely that much of the sea ice is transported into the region, rather than formed locally (by the end of winter there may be net melting [*Gordon et al.*, 1983]); thus, this represents a maximum value.

From the first term on the right of equation (1) and the relief of the pycnocline over the warm cells the entrainment rate at the pycnocline dome is expected to be 1.54 times larger

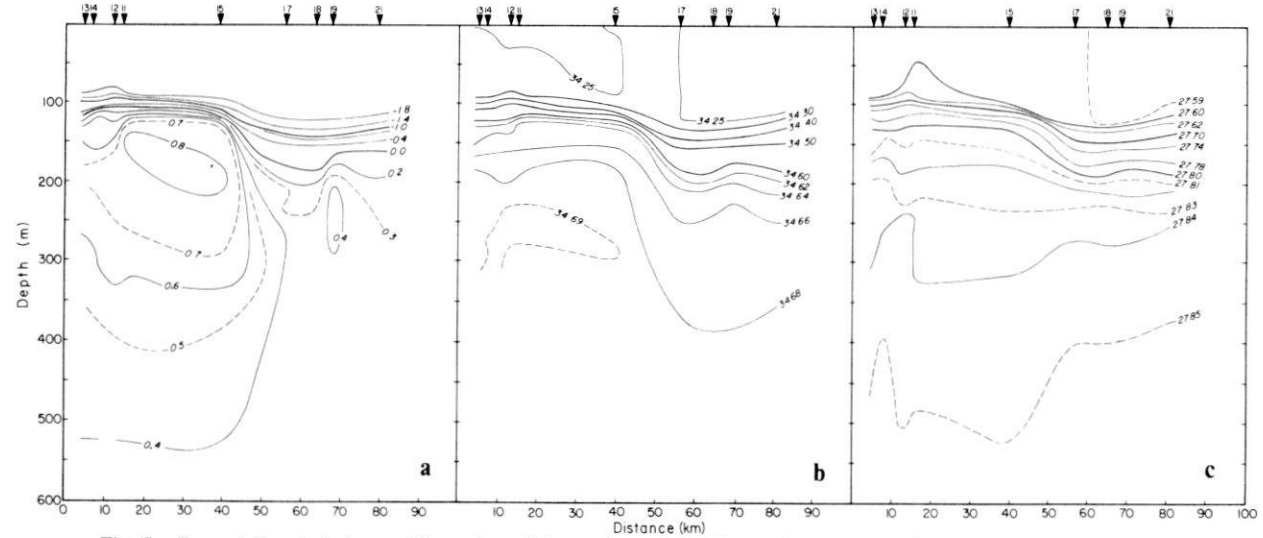

Fig. 7. Expanded scale hydrographic section of the stations within the southeast corner of the *Mikhail Somov* station array (Figure 1).

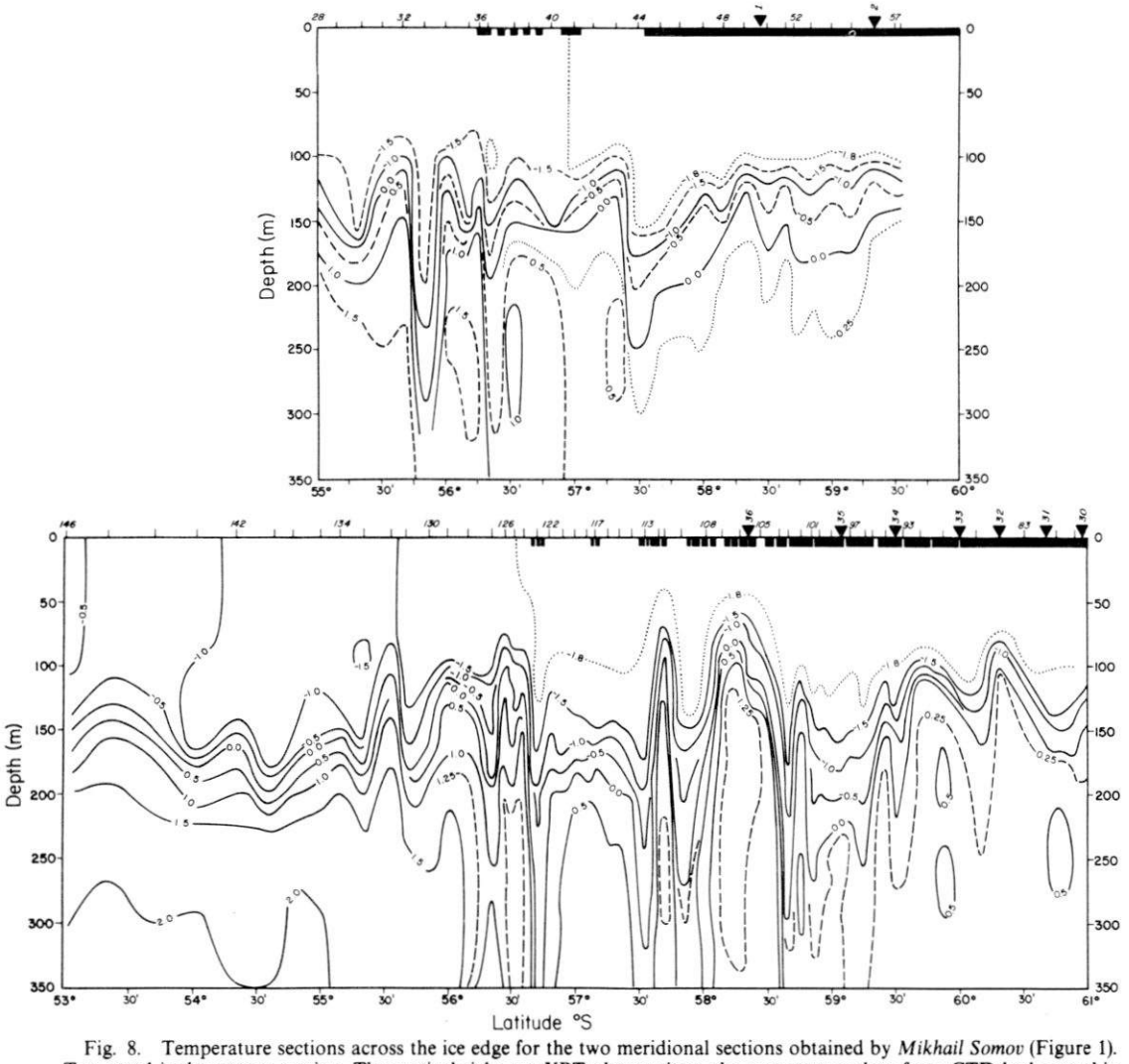

Fig. 8. Temperature sections across the ice edge for the two meridional sections obtained by *Mikhail Somov* (Figure 1). Top panel is the eastern section. The vertical ticks are XBT observations, the temperature data from CTD hydrographic stations are marked by triangles. The approximate sea ice cover is denoted by the thick solid line along the sea surface [see *Ackley and Smith*, 1982].

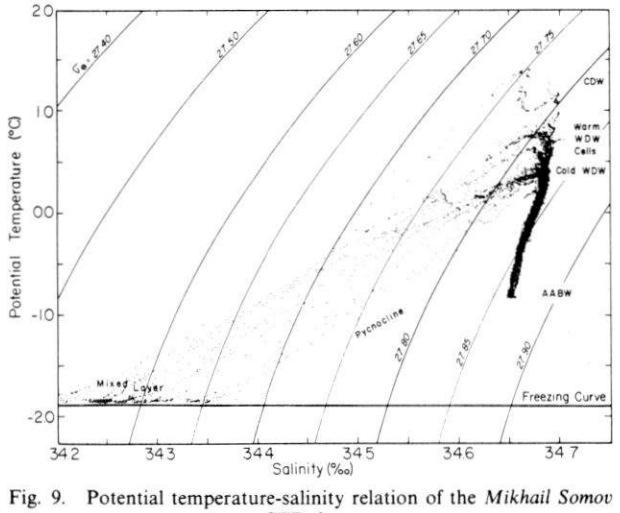

Fig. 9. Potential temperature-salinity relation of the *Mikhail Somov* CTD data.

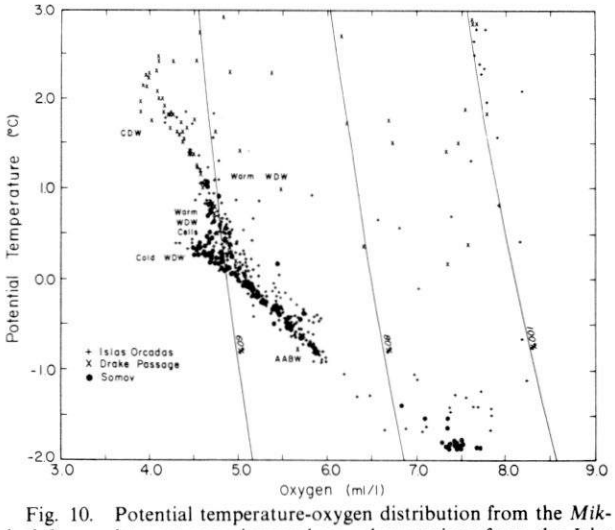

Fig. 10. Potential temperature-oxygen distribution from the *Mikhail Somov* data set, superimposed on select stations from the *Islas Orcadas* cruise 12 and Drake Passage station from FDRAKE-75 data [*Nowlin et al.*, 1977].

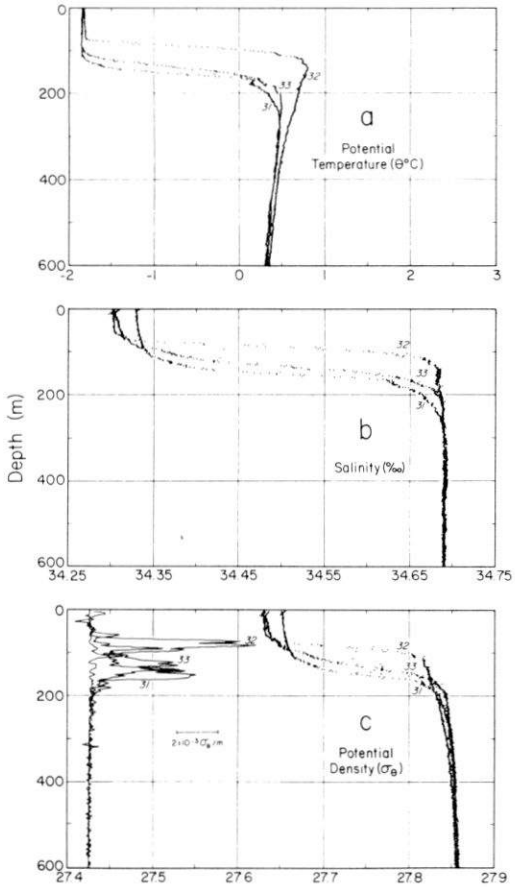

Fig. 11. (*a*) Potential temperature, (*b*) salinity, and (*c*) potential density and vertical gradient of density of three *Mikhail Somov* hydrographic stations across a warm WDW cell (see Figures 1 and 3). The scale bar for density gradient represents a value of 2×10^{-3} σ_θ units per meter.

than the regional rate. Using a value for U of 17 cm/s, based on a 6 hour Soviet current meter record at 60 m [*Huber et al.*, 1983], an estimate of the entrainment rate at the dome is 32.1×10^{-4} cm/s (82 m/month) versus 20.1×10^{-4} cm/s (54 m/month) for the regional deeper pycnocline value.

However, this U value is most likely not representative. In addition, the relative ocean-ice motion at a depth of 1 m, within the logarithmic boundary layer, would be the appropriate value to use with C_d values [*Langleben*, 1982]. Such a value would be significantly less than U at 60 m. For example, calculating U from the winter entrainment rate determined from *Mikhail Somov* oxygen data [*Gordon et al.*, this issue] yields a value of 8 cm/s.

A reasonable conclusion of the entrainment estimates is that the 40 m pycnocline domes of the warm WDW cells would be expected to be significantly attenuated within a single ice-covered season, introducing much of their heat and salt anomaly into the mixed layer. Warm cells that survive the winter would be subject to much less intense entrainment during the summer, when the density difference across the seasonal pycnocline increases to greater than 0.5 σ-θ units.

5. Discussion

As the warm cells are entrained, injecting excess heat and salt into the mixed layer, some impact on mixed layer characteristics is expected. The average mixed layer temperature and salinity observed from *Mikhail Somov* was −1.844°C and 34.287‰, respectively, which is 0.035°C above the freezing point (Figure 9). Pre- and post-cruise calibration of the CTD and independent calibration of the reversing thermometers [*Huber et al.*, 1983] support the significance of the above-freezing mixed layer temperature, which is believed a product of the upward flux of deep water heat. The excess heat would either be lost to the atmosphere in leads and thin ice or be used in the melting of sea ice [*Gordon*, 1981; *Gordon et al.*, this issue]. Presumably, local sea ice production occurs only when the atmosphere removes heat faster than deep water heat is entrained into the mixed layer.

The excess salt introduced to the mixed layer initially may be diluted with sea ice melt, but since all the sea ice melts regionally each spring anyway, the excess salt of the warm WDW cells must ultimately be compensated by an increase in atmospheric water and glacier melt or by net convergence of sea ice. If the salinity anomaly of the warm WDW cells is introduced into the overlying mixed layer within 1 year, then a 67 cm increase in the yearly fresh water input is required locally to produce the mean annual surface water salinity of 34.25‰ [*Gordon et al.*, this issue]. This would more than double the normal annual fresh water input of 45 cm [*Gordon*, 1981].

Naturally, the area over which extra fresh water is required to maintain static stability depends on the degree to which the salinity anomaly spreads laterally within the mixed layer. It may spread rapidly into the entire regional mixed layer, in which case the required extra fresh water demand is not significant, though this ultimately depends on the number of warm cells. It is more likely that the excess salt introduced into the mixed layer is confined to the cell scale of tens of kilometers. Thus the local requirement for fresh water is large and may not be met. In this situation, the warm cell might convert to a convective chimney [*Gordon*, 1978; *Killworth*, 1979]. This interesting possibility deserves further attention.

What relation might the warm WDW cells have to the polynya? The normal route of warm WDW into the Weddell cold regime seems to be by way of a westward flow over the continental slope [*Foster and Carmack*, 1976]. Instability of the frontal zone from Maud Rise to the northeast would inject warm WDW directly into the axial trough of the Weddell cold regime (to the 0.65 dy m isopleth; Figure 2) where it would be advected directly into the deep ocean west of Maud Rise, thus transfering salt into the central region or "hub" of the Weddell gyre. An increase in the transfer of warm WDW cells into the central region of the gyre would increase the salinity of the surface water and decrease the pycnocline stability, unless an increase in fresh water flux accompanies the deep water transfer. This is unlikely since these two processes are not coupled. The decrease of pycnocline stability increases the probability of convective events and the initiation of an open ocean polynya.

What would induce instability and generation of warm WDW cells? An increase in the curl of the wind stress would spin-up the Weddell gyre [*Gordon et al.*, 1981] which would draw more warm saline CDW into the gyre thus increasing the frontal zone intensity between the Weddell warm and cold regimes. Perhaps this would make the front more prone to instability, increasing warm WDW cell generation.

6. Conclusion

Instability of the frontal zone separating relatively warm deep water of the Weddell gyre inflow from colder deep water

of the Weddell gyre outflow injects WDW cells into cyclonic trough of the Weddell gyre. The excess heat and salt of these cells eventually (of the order of 1 year) enters the surface water. Any increase in the injection rate of these cells, perhaps due to spinup of the Weddell gyre, would force more heat and salt into the central region or hub of the Weddell gyre, which ultimately would enter the surface layer. The excess heat would be lost to the atmosphere, but the excess salt would accumulate unless a commensurate increase in fresh water input occurs, which is unlikely. Thus greater production of warm WDW cells would tend to lower the pycnocline stability making the central region of the Weddell gyre more susceptible to complete pycnocline break down and polynya occurrence.

Acknowledgments. The funding for the U.S.-U.S.S.R. Weddell Polynya Expedition was provided by the Division of Polar Programs of the National Science Foundation. The physical oceanography research is supported by grant DPP 80-05765. Lamont-Doherty Geological Observatory contribution number 3555. Discussions with Hsien Wang Ou were particularly useful. We thank S. S. Jacobs for review of the manuscript.

REFERENCES

Ackley, S. F., and S. J. Smith, Reports of the US-USSR Weddell Polynya Expeditions, Sea Ice Observations, vol. 5, *CRREL Spec. Rep. 83-2*, U.S. Army Corps of Eng., Hanover, N. H., 1983.

Ackley, S. F., D. B. Clarke, and S. J. Smith, Weddell Polynya Expedition preliminary data report: Physical, chemical and biological properties of ice cores, technical note, U.S. Army Cold Regions Res. and Eng. Lab., Hanover, N. H., 1982.

Andreas, E. L., Comment on "Water drag coefficient of first-year sea ice" by M. P. Langleben, *J. Geophys. Res., 88*, 779–780, 1983.

Carsey, F. D., Microwave observation of the Weddell Polynya, *Mon. Weather Rev., 108*, 2032–2044, 1980.

Cushman-Roisin, B., Deepening of the wind-mixed layer: A model of the vertical structure, *Tellus, 33*, 564–582, 1981.

Deacon, G. E. R., The cyclonic circulation in the Weddell Sea, *Deep Sea Res., 23*, 125–126, 1976.

Deacon, G. E. R., The Weddell Gyre, *Deep Sea Res., 26A*, 981–995, 1979.

Farmer, D. M., Penetrative convection in the absence of mean shear, *Q. J. R. Meteorol. Soc., 101*, 869–891, 1975.

Foster, T. D., and E. C. Carmack, Temperature and salinty structure in the Weddell Sea, *J. Phys. Oceanogr., 6*, 36–44, 1976.

Gordon, A. L., Deep Antarctic convection west of Maud Rise, *J. Phys. Oceanogr., 8*, 600–612, 1978.

Gordon, A. L., Seasonality of Southern Ocean sea ice, *J. Geophys. Res., 85*, 4193–4197, 1981.

Gordon, A. L., The US-USSR Weddell Polynya Expedition, *Antarctic J., 17*, 96–98, 1982.

Gordon, A. L., and E. M. Molinelli, *Southern Ocean Atlas: Thermohaline-Chemical Distributions and the Atlas Data Set*, Columbia University Press, New York, 1982.

Gordon, A. L., and E. I. Sarukhanyan, American and Soviet Expedition into the Southern Ocean sea ice in October and November 1981, *Eos Trans. AGU, 63*, 2, 1982.

Gordon, A. L., D. G. Martinson, and H. W. Taylor, The wind-driven circulation in the Weddell-Enderby Basin, *Deep Sea Res., 28A*, 151–163, 1981.

Gordon, A. L., C. T. A. Chen, and W. G. Metcalf, Winter mixed layer entrainment of Weddell Deep Water, *J. Geophys. Res.*, this issue.

Huber, B., S. Rennie, D. Georgi, S. Jacobs, and A. Gordon, *Ara Islas Orcadas* Data Report, Cruise 12, *Ref. CU-2-81-TR2*, Lamont-Doherty Geol. Observ., Palisades, New York, 1981.

Huber, B. A., J. Jennings, C.-T. Chen, J. Marra, S. Rennie, P. Mele, and A. Gordon, Reports of the US-USSR Weddell Polynya Expedition, Hydrographic data, vol. 2, *L-DGO-83-1*, Lamont-Doherty Geol. Observ., Palisades, New York, 1983.

Kato, H., and O. M. Phillips, On the penetration of a turbulent layer into stratified fluid, *J. Fluid Mech., 37*, 643–655, 1969.

Killworth, P. D., On "chimney" formations in the ocean, *J. Phys. Oceanogr., 9*, 531–554, 1979.

Langleben, M. P., Water drag coefficient of first-year sea ice, *J. Geophys. Res., 87*, 573–578, 1982.

Manley, T. O., Eddies of the western Arctic Ocean: Their characteristics and importance to the energy, heat and salt balance, *CU-1-81, Tech. Rep. 1*, Lamont-Doherty Geol. Obs., Palisades, New York, 1981.

Newton, J. L., K. Aagaard, and L. K. Coachman, Baroclinic eddies in the Arctic Ocean, *Deep Sea Res., 21*, 707–719, 1974.

Niiler, P. P., and E. B. Kraus, One-dimensional models of the upper ocean, in *Modelling and Prediction of the Upper Layers of the Ocean*, edited by E. B. Kraus, pp. 143–172, Pergamon, New York, 1977.

Nowlin, W. D. Jr., T. Whitworth III, L. I. Gordon, and G. C. Anderson, Oceanographic station data collected aboard R/V *Melville* during FDRAKE 75, *Ref. 77-2-D*, Texas A&M Res. Foundation, College Station, 1977.

Patterson, S. L., and H. A. Sievers, The Weddell-Scotia confluence, *J. Phys. Oceanogr., 10*, 1584–1610, 1980.

Phillips, O. M., Entrainment in *Modelling and Prediction of the Upper Layers of the Ocean*, edited by E. B. Kraus, pp. 92–101, Pergamon, New York, 1977.

Tchernia, P., Etude de la Derive Antarctique Est-Ouest au Moyen d'Ice-bergs Suivio par le Satellite Eole, in *Polar Oceans*, edited by M. J. Dunbar, Arctic Institute of North America, Montreal, Quebec, 1977.

A. L. Gordon and B. A. Huber, Lamont-Doherty Geological Observatory, Columbia University, Palisades, NY 10964.

(Received April 28, 1983;
revised October 6, 1983;
accepted October 6, 1983.)

Physical oceanography during WEPOLEX–81

ARNOLD L. GORDON *and* BRUCE A. HUBER

Lamont-Doherty Geological Observatory
of Columbia University
Palisades, New York 10964

The physical oceanographic objective of the U.S.-U.S.S.R. Weddell Polynya expedition (WEPOLEX–81) was to resolve the vertical and horizontal scales of the thermohaline stratification of the water column below the sea ice and, if possible, within the Weddell polynya. The low vertical stability of the southern ocean water column permits significant vertical fluxes of heat and salt (Gordon 1981). These fluxes strongly influence the sea ice budget and water mass conversion, and they are believed to be particularly active in the winter. Water mass conversion during the Weddell polynya period 1974–76 was significant (Gordon in press).

The Neil Brown conductivity-temperature-depth (CTD) meter was used in a number of ways: (1) to obtain vertical profiles to varied depths, (2) to obtain repeated profiles at a single site ("yo-yo" stations), and (3) to make time series observations at specific depths (see table; also see figure 3 in Gordon, *Antarctic Journal*, this issue). At the CTD time series sites, current meters (Soviet instruments) were used to obtain current shear information. A 12-bottle, 1.7-liter rosette sampler accompanying the CTD meter provided water samples for CTD calibration and for oxygen, nutrient, and biological study. The oxygen determinations were carried out by Gerry Metcalf. Observations by expendable bathythermograph (XBT) were made between CTD hydrographic stations (see figure 3 in Gordon, *Antarctic Journal*, this issue) to define better the horizontal scales within the thermal structure along the ship track. Surface water samples were obtained for determination of a variety of physical and biological parameters.

Several environmentally induced equipment problems deserve mention. The CTD meter was stowed on deck between stations and thus was exposed to temperatures well below the freezing point of seawater. To ensure good conductivity read-

Summary of conductivity-temperature-depth (CTD) stations by type and station number[a]

Water depth				Time series observations	
Shallow (≤ 1,000 m)	Intermediate (2,000–3,000 m)	Deep (>3,000 m)	Yo-Yo (No. of casts)	(duration)	(stratification feature)
1 (220 m)	2, 3, 5, 7, 13, 21, 22, 31, 36 (2,000 m)	17 (5,225 m)	4 (2)	12 (1.4 hr)	pycnocline
26 (1,000 m)		23 (5,425 m)	6 (8)	14 (4.6 hr)	T-max[b]
27 (1,000 m)		28 (5,200 m)	8 (6)	19 (13 hr)[c]	T-max
		29 (5,300 m)	10 (6)	25 (11.8 hr)[d]	T-max
		30 (4,200 m)	12 (4)		
	9, 11, 15, 33, 34, 35 (3,000 m)	32 (5,250 m)	14 (3)		
		37 (4,300 m)	16 (6)		
			18 (10)		
			19 (1)		
			20 (3)		
			24 (6)		
			25 (4)		

[a]Stations 1, 2, and 17–37 have CTD oxygen sensor data.

[b]T-max = Temperature maximum.

[c]19—Soviet current meters deployed for 12 hours.

[d]25—Soviet current meters deployed for 9 hours.

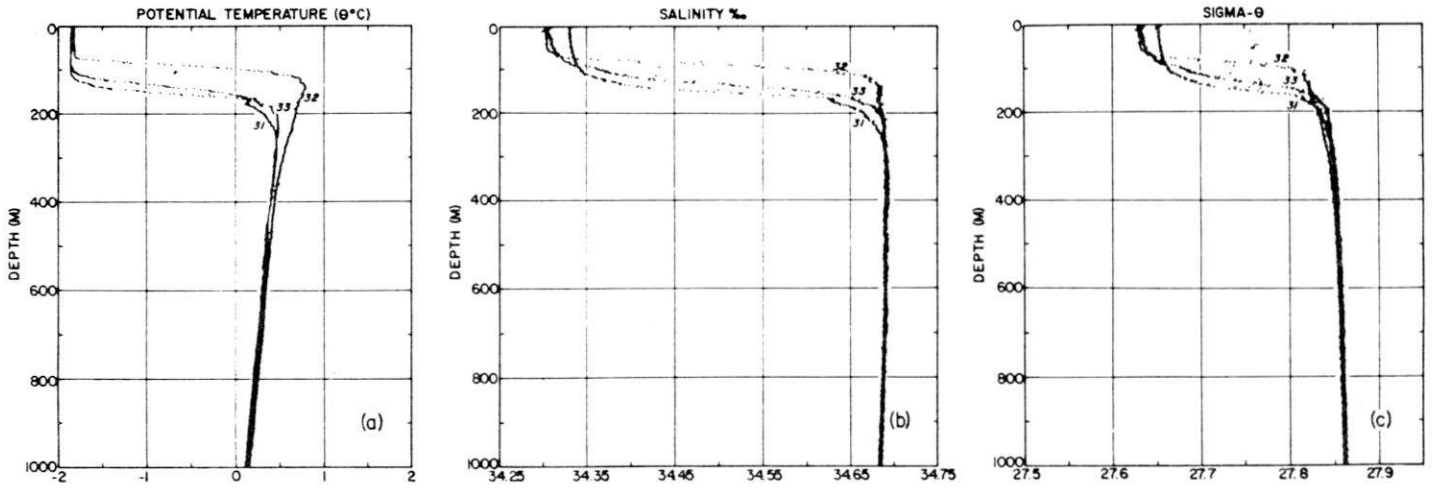

Figure 1. Potential temperature, salinity, and density (SIGMA-θ) at three neighboring conductivity-temperature-depth stations. Station 32 is within a pycnocline dome, while stations 31 and 33 are within the more "normal" stratification regime.

ings, the instrument had to be lowered to the temperature maximum layer to thaw out and then returned to the surface to begin each cast. The oxygen sensor failed at station 3, apparently because of freezing of the moisture in the Teflon membrane, resulting in its rupture. The sensor was not replaced until station 17, after which it performed well. Near-surface salinity samples did not agree well with CTD salinities, but deeper samples did, with a standard deviation of approximately 0.002. The large scatter in the surface samples may have been caused by ice crystal formation in the Niskin bottles during the short time the bottles were on deck before the samples were drawn. Finally, the cold air temperatures affected the underwater connectors used in the CTD wiring harness. We found that the rubber connectors had to be prewarmed before assembly on deck to ensure watertight mating.

The *Somov* data provide the first modern information concerning the actual end-of-winter condition of the sea-ice-covered water column of the southern ocean. The data set is situated in what can be defined, according to data for the summer, as the Weddell Sea outflow of the cyclonic Weddell Gyre. This water is colder and fresher than the inflow found farther to the east and southeast. Although the *Somov* hydrographic data support this view, two interesting and new aspects of the stratification were found: the mixed layer is significantly deficient in oxygen, and the pycnocline has what can be called bumps, or domes, which are composed of relatively warm water more characteristic of the Weddell Gyre inflow.

The oxygen saturation level of the mixed layer (average thickness of 130 meters) was 85–88 percent. Since the ice shields the water from light and gas exchange (Chen, *Antarctic Journal*, this issue) and the water column biomass is quite low, the oxygen undersaturation may result from an admixture of oxygen-deficient Weddell deep water and surface water saturated with oxygen at the beginning of the ice-cover period. Using oxygen as a conservative parameter during the ice-cover period (about 5 months), it has been determined that the amount of deep water required to account for the undersaturation is 40 meters. Presumably this deep water enters the mixed layer by a combination of wind-induced Ekman upwelling, entrainment, and diffusion. This information provides the basis for estimation of the vertical flux of heat (30 watts per square meter during the 5 ice-cover months), salinity, and chemical parameters into the surface layer.

The pycnocline domes (figure 1) (page 99) are particularly curious features. The depth of the mixed layer over the domes is nearly half what it is elsewhere. The domes seem to have a lateral dimension of about 20 kilometers. Three occurrences were noted (stations 13, 27, and 32), though limited maneuverability of the ship in the ice precluded a full survey. As figure 1 shows, the deep water is significantly warmer below the pycnocline dome. The pycnocline domes may be entrained into the mixed layer more rapidly than is the case in a normal pycnocline situation. Mixed-layer temperatures at all stations were .02° to .05°C warmer than the calculated freezing point of seawater at the observed salinities (Doherty and Kester 1974). The temperature elevation over the freezing point at the pycnocline domes was .06° to .07°C. The relatively warm mixed-layer temperature above the domes may be evidence of the enhanced vertical flux.

The thermal structure and surface parameter traces along the return track from 61°S to 53°S (figure 2) reveal the varied stratification and surface water conditions across the transition from the ice interior to the open ocean. The transition region, or ice edge zone, is associated with increased vertical relief of isotherms and variation in the surface nutrients. As Stepien (*Antarctic Journal*, this issue) points out, water column biomass is increased in the ice edge zone relative to the interior of the pack ice. The ice edge zone is marked by smaller ice floes than are characteristic of the interior, as well as by noticeable swell propagation (Ackley, Smith, and Clarke, *Antarctic Journal*, this issue).

We are pleased to acknowledge the Soviet members of the physical oceanography team: Ivan Chuguy, Nikolai Bagriantsev, Nikolai Antipov, and Vladimir Romanov.

This work was supported by National Science Foundation grant DPP 80–05765.

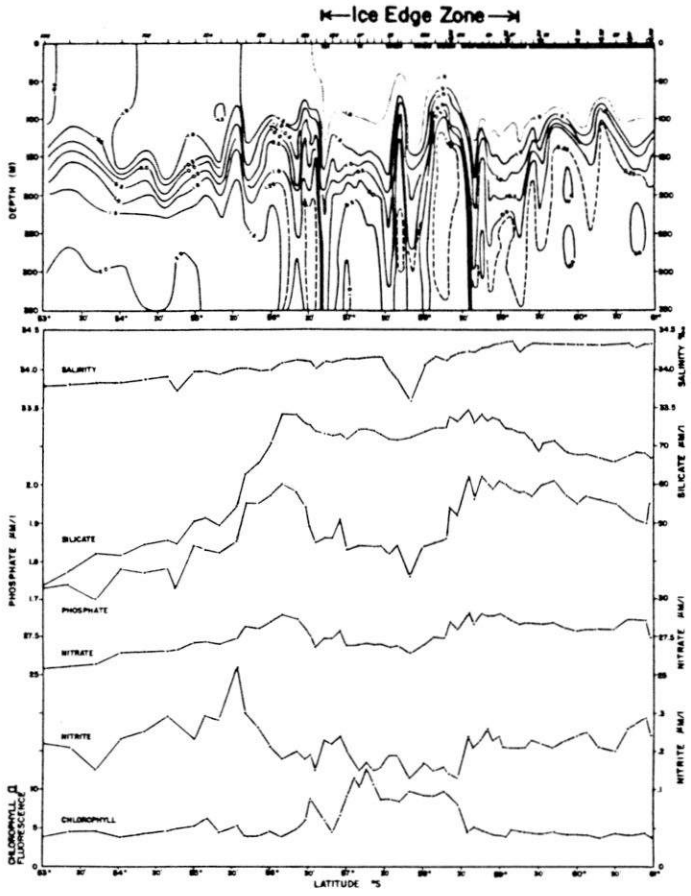

Figure 2. Thermal structure for the upper 350 meters approximately along the Greenwich meridian from 61° to 53°S. Expendable bathythermograph observations 81 to 146 are indicated as vertical tick marks, and the conductivity-temperature-depth thermal data are indicated by triangles. The thick horizontal bar along the sea surface denotes the sea ice cover. Meridional traces of various surface water parameters are given. Salinity was determined by AutoSal, nutrients by Auto Analyzer (see Jennings, Nelson, and Gordon, *Antarctic Journal*, this issue), and fluorescence by Turner Fluorometer (determination by D. Boardman). μ/l = micromoles per liter.

References

Ackley, S. F., Smith, S. J., and Clarke, D. B. 1982. Observations of pack ice properties in the Weddell Sea. *Antarctic Journal of the U.S.*, 17(5).

Chen, C.-T. A. 1982. Carbonate chemistry during WEPOLEX-81. *Antarctic Journal of the U.S.*, 17(5).

Gordon, A. L. 1981. Seasonality of southern ocean sea ice. *Journal of Geophysical Research*, 86(C5), 4193–4197.

Gordon, A. L. 1982. The U.S.-U.S.S.R. Weddell Polynya Expedition. *Antarctic Journal of the U.S.*, 17(5).

Gordon, A. L. In press. Weddell deep water variability. *Journal of Marine Research*.

Stepien, J. C. 1982. Zooplankton in the Weddell Sea, October–November 1981. *Antarctic Journal of the U.S.*, 17(5).

Nutrient chemistry program during WEPOLEX–81

JOE JENNINGS, DAVID NELSON, *and* LOUIS I. GORDON

School of Oceanography
Oregon State University
Corvallis, Oregon 97331

The nutrient chemistry program of the U.S.-U.S.S.R. Weddell Polynya expedition (WEPOLEX–81) was designed to study the distribution and cycling of nutrients in the Weddell Sea under late winter/early spring conditions and to obtain the first data on particulate silica distributions and production/dissolution rates in the Weddell waters. An Auto Analyzer was used to determine nitrate, nitrite, phosphate, and silicate concentrations both in the water column and in samples from ice cores. In addition, samples collected and filtered at five hydrographic stations will be analyzed for biogenous and total particulate silicon in the laboratory at Oregon State University.

The vertical distribution of dissolved nutrients in the water column is similar to that of temperature and salinity: a very homogenous surface mixed layer some 60–110 meters thick overlying sharp gradients as concentrations increase to those of the Warm Deep Water. (See Carmack and Foster 1975 for water mass definitions.) Phosphate and nitrate concentrations decrease from a slight maximum in the Warm Deep Water at 400–800 meters ($\geq$ 2.3 micromolar and $\leq$ 33 micromolar, respectively) to Weddell Sea bottom water values of approximately 2.2 micromolar and 31.5 micromolar, respectively. The silicate maximum (approximately 129 micromolar) is broad and lies below 1,000 meters, slightly deeper than the 0°C potential temperature isotherm. The silicate concentrations decrease gradually through the Weddell Sea Bottom Water until the −.5°C isotherm at approximately 3,000 meters, below which concentrations decrease more rapidly to near bottom minima of 117–120 micromolar.

Because ice conditions restricted the *Somov* to a relatively small sector within the Weddell Gyre, it is necessary to examine the data in context with data from other cruises in the same area to discern regional oceanographic features and temporal trends. Most of the recent historical nutrient data in the eastern Weddell Sea were collected during 1977 and 1978 *Islas Orcadas* cruises, and the overall oceanographic regime during the WEPOLEX cruise appears similar to that presented by Gordon (1980) on the basis of those cruises. Stations 3, 5, and 30–35 appear to be characteristic of the eastern extent or outflow of the Weddell Gyre, with the northernmost and southernmost stations exhibiting Gordon's "warm-saline" signal indicative of the influence of the circumpolar current. Surface nutrient concentrations are highest in the northernmost stations, decreasing somewhat in the Gyre proper. The increase in surface concentrations to the south of the central Weddell Gyre evident in the *Islas Orcadas* data was not observed, probably because ice conditions precluded *Somov's* reaching the vicinity of the Maud Rise.

A comparison was made of data from WEPOLEX and from the Geochemical Ocean Sections Study (GEOSECS), or using GEOSECS Atlantic station 89, which was at 60°S 0°E in January 1973. Disregarding the surface waters, in which seasonal changes should be most manifest, the agreement is very good. Silicate and phosphate values are in close agreement. Phosphate and nitrate values in the Warm Deep Water are higher at the GEOSECS station, but they become closer with increasing depth.

Winter water at GEOSECS station 89 and wintertime surface water at WEPOLEX station 35

Station	Pressure (decibels)	Potential temperature (°C)	Salinity (‰)	Silicate concentration (micromolar)	Phosphate concentration (micromolar)	Nitrate concentration (micromolar)
GEOSECS 89 22 Jan 73	75	− 1.830	34.383	75.7	2.03	29.4
WEPOLEX 35 21 Nov 82	entire surface mixed layer	− 1.858	34.358	75.7	2.04	29.3

Reprinted with permission.

One preliminary finding concerning the distinct subsurface T_{min} (temperature minimum) layer, which Carmack and Foster (1975) call Winter Water, emerged from the comparison of WEPOLEX and GEOSECS data. Although Winter Water has long been thought to be a relic of the winter surface waters underlying the seasonal pack ice (Foster and Middleton 1979), the lack of actual winter data has precluded establishing this definitely. The table shows that, at the core of the Winter Water present at GEOSECS station 89, the nutrient concentrations as well as the temperature and salinity are almost identical to those found in the surface mixed layer (under the ice) at WEPOLEX station 35. Thus, our winter data set tends strongly to confirm that the local mixed layer in winter is the source of the appropriately named Winter Water.

The enthusiastic assistance of all of the Soviet scientists, ship's officers, and crew members—particularly the Soviet chemical technicians V. Fedorov and V. Hazitonov—contributed greatly to the success of the chemical programs.

This research was supported by National Science Foundation grant DPP 80–07620.

References

Carmack, E. C., and Foster, T. D. 1975. On the flow of water out of the Weddell Sea. *Deep-Sea Research*, 22, 711–724.

Foster, T. D., and Middleton, J. H. 1979. Variability in the bottom water of the Weddell Sea. *Deep-Sea Research*, 26A, 743–762.

Gordon, A. L. 1980. Circumpolar water masses. *Antarctic Journal of the U.S.*, 15(5), 89–90.

Carbonate chemistry during WEPOLEX-81

CHEN-TUNG ARTHUR CHEN

School of Oceanography
Oregon State University
Corvallis, Oregon 97331

As part of the U.S.-U.S.S.R. Weddell Polynya expedition (WEPOLEX-81), my Soviet counterparts and I measured acidity and alkalinity of seawater samples on board the ship. Library seawater samples were collected for later measurements of total carbon dioxide (CO_2) and partial pressures of CO_2 (by T. Takahashi at Lamont-Doherty Geological Observatory) and for density and calcium (at Oregon State University). Some melted ice samples also were collected for measurements (at Oregon State University) of conductivity, chlorinity, density, calcium, and alkalinity. The objectives are (1) to use the calcium and carbonate data as water tracers, (2) to estimate the effect of pack ice on air-sea exchange of gases and on calcium and carbon cycles, (3) to quantify the CO_2 flux between atmosphere and the polar water, (4) to estimate the penetration depth of the fossil fuel CO_2, and (5) to quantify the error in densities calculated from the seawater equation of state.

Preliminary analysis indicates that acidity is useful in identifying the source of waters. For instance, a large portion of the water near the broad S_{max} (salinity maximum) layer at station 34 (see figure 3 of Gordon, *Antarctic Journal*, this issue) seems to come from modified North Atlantic deep water (NADW). By the time NADW signal is incorporated into the Weddell Gyre from the circumpolar ocean, it is characterized by low acidity and high apparent oxygen utilization (see figure 1). In contrast, the warmer, saltier S_{max} layer at station 36, which represents circumpolar water just north of the Weddell Gyre, has a broad maximum acidity within the S_{max} layer from approximately 250 to 1,000 meters and lower apparent oxygen utilization than that observed in the S_{max} at station 34 (figure 1). This suggests that not as much decomposition of organic material has occurred in the circumpolar S_{max} water at station 36 as has occurred within the Weddell Gyre, represented by station 34.

Preliminary shipboard data indicate that the pack ice effectively blocks the air-sea exchange of oxygen and CO_2. Consequently, the homogeneous surface layer, which has approximately 30 percent deep water, is not in equilibrium with the atmosphere and contains less fossil fuel CO_2 than expected. Most of the winter surface water (identified as WW in figure 2) eventually is exposed to the atmosphere as the ice melts, and exchanges of gases with the atmosphere occur rapidly. Some of the surface water may flow southward beneath the ice toward the continental margin and thus undergo no air-sea gas ex-

Reprinted with permission.

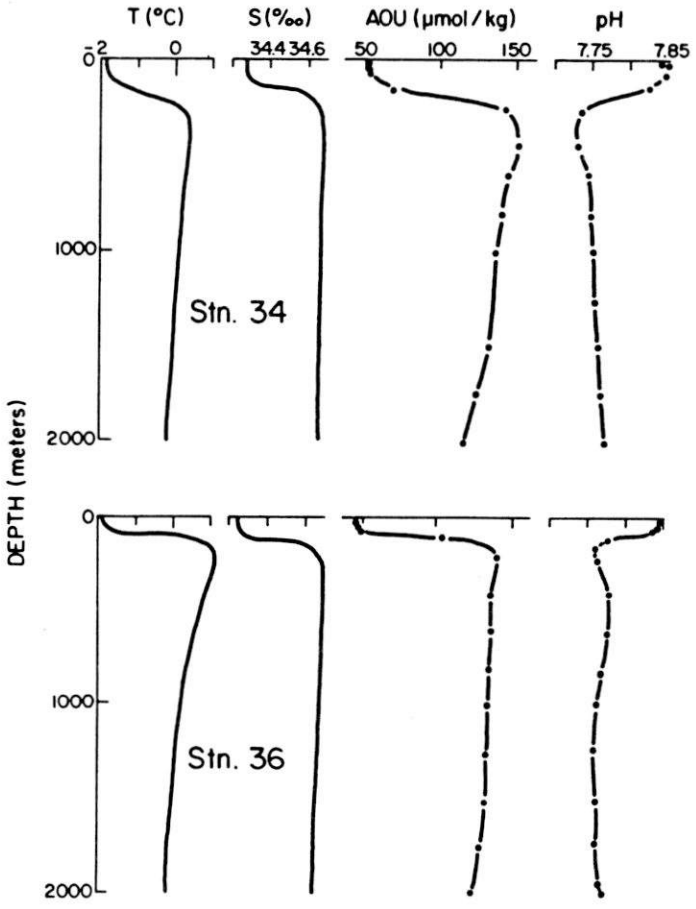

Figure 1. The vertical distributions of temperature (T), salinity (S), apparent oxygen utilization (AOU), and acidity (pH) at WEPOLEX stations 34 (59°30'S 0°30'E; 12 November 1981) and 36 (58°21'S 0°46'E; 13 November 1981). μmol/kg = micromoles per kilogram.

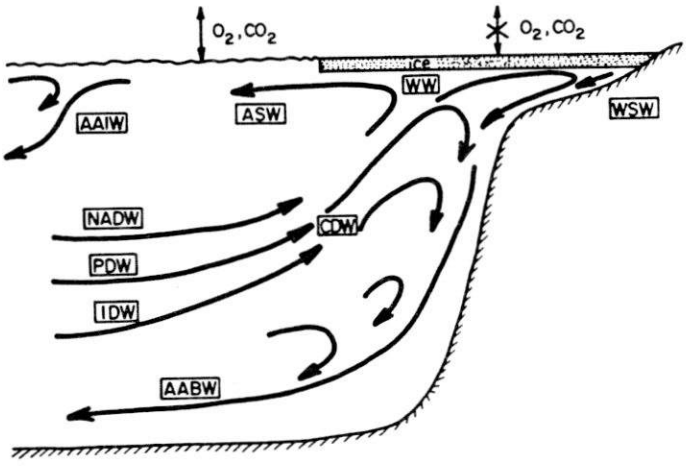

Figure 2. A schematic diagram showing the water masses in the southern ocean. The pack ice blocks the air-sea exchange of gases. AAIW = antarctic intermediate water; ASW = antarctic surface water; WW = winter surface water; WSW = western shelf water; NADW = North Atlantic deep water; CDW = circumpolar deep water; PDW = Pacific deep water; IDW = Indian deep water; AABW = antarctic bottom water.

change. There it mixes with western shelf water (WSW) and circumpolar deep water (CDW) to form antarctic bottom water (AABW) (Foster and Carmack 1976; Weiss, Ostlund, and Craig 1979). Since the circumpolar deep water was formed before the industrial revolution and the winter surface water is also deficient in the excess CO_2, the newly formed antarctic bottom water has little or no fossil fuel CO_2 (Chen 1982).

Laboratory analyses of library samples currently are being performed. Complete data interpretation and reports should be available by the summer of 1983.

I was assisted in the shipboard operations by V. Fedorov and V. Hazitonov of the Arctic and Antarctic Research Institute, U.S.S.R.; G. Metcalf and D. Woodroffe of the Lamont-Doherty Geological Observatory; the expedition chief, E. Sarukhanyan; U.S. chief scientist A. L. Gordon; and the *Somov's* captain and crew. This work was supported by Department of Energy grant 81 EV 10611 and by National Science Foundation grant OCE 80-18770.

References

Chen, C.-T. 1982. On the distribution of anthropogenic CO_2 in the Atlantic and southern oceans. *Deep-Sea Research*, 29, 563–580.

Foster, T. D., and Carmack, E. C. 1976. Frontal zone mixing and antarctic bottom water formation in the southern Weddell Sea. *Deep-Sea Research*, 23, 301–317.

Gordon, A. L. 1982. The U.S.-U.S.S.R. Weddell Polynya Expedition. *Antarctic Journal of the U.S.*, 17(5).

Weiss, R. F., Ostlund, H. G., and Craig, H. 1979. Geochemical studies of the Weddell Sea. *Deep-Sea Research*, 26, 1093–1120.

Carbon dioxide partial pressure in surface waters of the southern ocean

TARO TAKAHASHI *and* DAVID CHIPMAN

Lamont-Doherty Geological Observatory
of Columbia University
Palisades, New York 10964

Measurements of the partial pressure of carbon dioxide (CO_2) in surface waters were carried out during the U.S.-U.S.S.R. Weddell Polynya expedition (WEPOLEX-81) (Gordon, *Antarctic Journal*, this issue). The direction of the net transfer of CO_2 between the atmosphere and the oceans via gas exchange may be characterized in terms of the CO_2 partial pressures (pCO_2) in the surface ocean water and in the overlying atmosphere. If the pCO_2 in the atmosphere is greater than that in the surface water, the net CO_2 flux should be from air to sea, and thus the ocean acts as a CO_2 sink. If the partial pressures are equal, there should be no net transfer flux of CO_2 across the air-sea interface. Because seawater exerts a large temperature effect on pCO_2 (i.e., 4.3 percent per degree Centigrade when alkalinity and total CO_2 concentration in seawater are constant), the warm, low-latitude ocean waters are believed to have a greater pCO_2 than the atmosphere, and thus to act as a source of CO_2; the cold, high-latitude waters have a low pCO_2 and hence act as a CO_2 sink.

In the equatorial oceans, the observed pCO_2 values in surface water are much greater than anticipated for high temperatures (Broecker et al. 1979). This anomaly has been attributed to the upwelling of colder and CO_2-rich subsurface waters (Broecker et al. in press). In contrast, in the high-latitude northern oceans, including the Norwegian-Greenland Sea, the observed pCO_2 values are as low as one-half of the atmospheric value of about 340 microatmospheres, and these low values can be entirely accounted for by the low temperatures. The results of the Geochemical Ocean Sections Study (GEOSECS) expeditions during the austral summers of 1972, 1974, and 1978 (Broecker et al. 1979; Takahashi and Azevedo 1982) indicate that the surface water pCO_2 values in the southern ocean are not as low as those in the northern oceans but are nearly the same as those in the atmosphere, although the temperatures are as low as those in the northern oceans. Since the vertical mixing of ocean water is enhanced during the cold winter months, the CO_2 concentration in surface water in the southern ocean might be increased due to mixing with CO_2-rich subsurface waters, and hence the effect of cooling on the CO_2 partial pressure of seawater may be compensated by an increase in the total CO_2 concentration. Therefore, we hypothesized that the pCO_2 in the southern ocean surface water might not be reduced even during the period of a maximum cooling, and thus the ocean would not become a strong CO_2 sink.

The ship's track and the pCO_2 data obtained during the expedition are shown in figures 1 and 2. The pCO_2 contour lines in

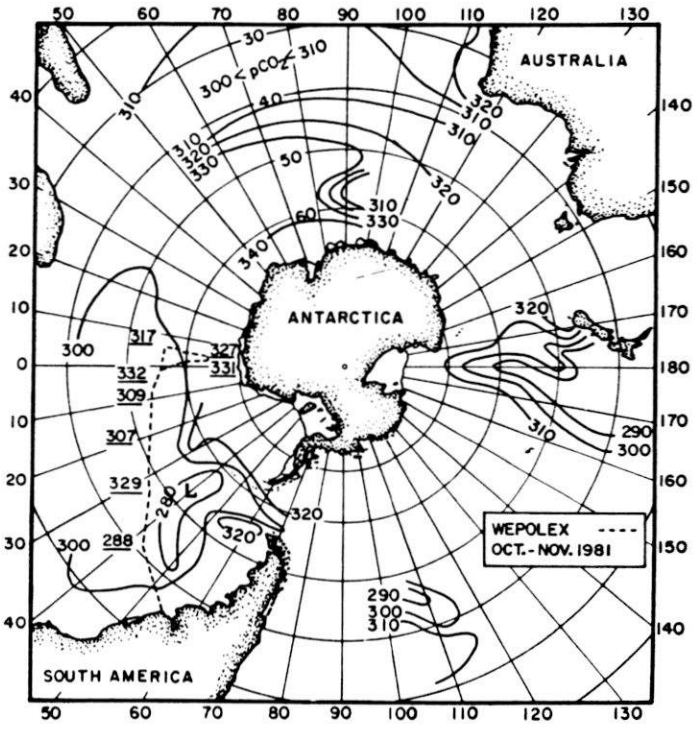

Figure 1. Distribution of partial pressure of CO_2 (pCO_2; expressed in 10^{-6} atmospheres) in surface waters of the southern ocean observed during the GEOSECS Atlantic expedition in January 1973, the GEOSECS Pacific expedition in February–March 1974, and the GEOSECS Indian Ocean expedition in February 1978. The ship's track and the pCO_2 data obtained during the WEPOLEX expedition in October–November 1981 also are indicated. The GEOSECS data are for the austral summer, and the WEPOLEX data are for the austral spring.

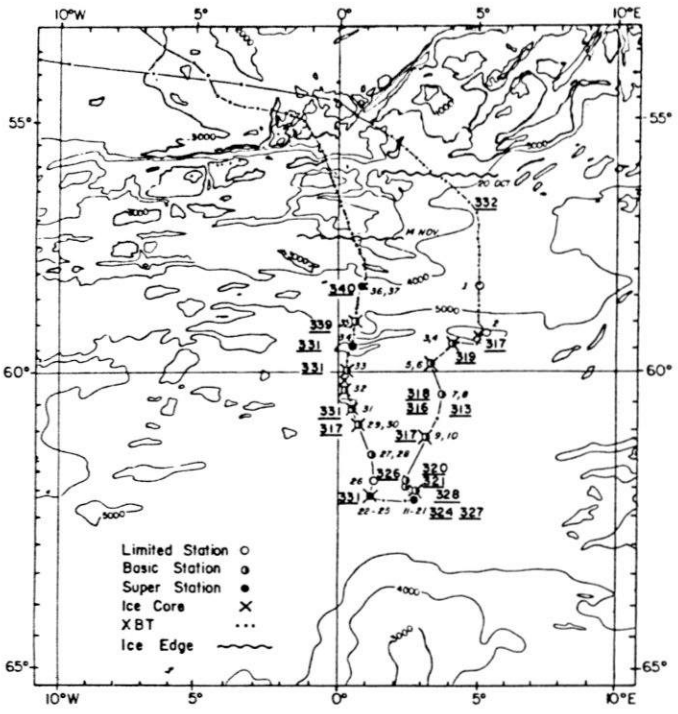

Figure 2. Ship's track and the partial pressure of CO_2 (pCO_2; expressed in 10^{-6} atmospheres) in surface waters observed during the WEPOLEX expedition in October–November 1981 on board the USSR *Somov*. The pCO_2 values are underlined; the station numbers are not. These measurements are the first observational data for surface water pCO_2 obtained in the ice-covered oceanic area during the austral spring.

figure 1 are based on the data obtained by Takahashi and associates during GEOSECS expeditions in the austral summers of 1973, 1974, and 1978. The values obtained during the present expedition (underlined in figures 1 and 2) in the austral spring of 1981 are similar to those of the previous expeditions and range from 307 to 340 microatmospheres. Atmospheric CO_2 measurements obtained during this expedition show that the partial pressure of CO_2 in the atmosphere is 341 (± 1.4) microatmospheres (assuming a mean barometric pressure of 1.000 atmosphere). Thus, the observed pCO_2 in surface water is slightly less than or nearly equal to the atmospheric pCO_2, although the temperature of water is generally −1.9°C. Accordingly, the surface water of the southern ocean appears to be nearly in equilibrium or slightly undersaturated with atmospheric CO_2 during the austral spring. Furthermore, the austral summer data of the GEOSECS expeditions indicate that the southern ocean waters are not far from equilibrium with atmospheric CO_2, as shown in figure 1, although there are some local variations. Therefore, we conclude that the southern ocean surface waters are nearly in equilibrium with the atmospheric CO_2 throughout the year and are neither a strong sink nor a source of CO_2. However, because of the absence of a large polynya area, which may be caused by a deep, vertical, convective chimney in ocean water, we did not have a chance to observe the significance of polynya in the CO_2 exchange between the atmosphere and oceans.

Our observations reveal a significant difference between the CO_2 chemistry of the southern ocean and that of the northern high-latitude oceans, including the Norwegian-Greenland Sea. The pCO_2 observed during the summers of 1979 and 1981 in surface waters of the Norwegian-Greenland Sea average about 230 microatmospheres at the mean temperature of 6.0°C; values as low as 160 microatmospheres at −0.1°C have been observed along the edges of ice fields. The mean pCO_2 value is about 70 percent of the atmospheric pCO_2 of 330 to 340 microatmospheres, indicating that the northern water is a strong sink for CO_2. These low pCO_2 values in surface water have not been observed in the southern ocean.

The warm North Atlantic surface water, which is nearly in equilibrium with the atmospheric CO_2, cools rapidly (in a time scale of weeks) as it flows northward into and through the Norwegian-Greenland basin and farther into the ice-covered Arctic Basin. Since the residence time of the surface water in the Norwegian-Greenland basin is expected to be short, while the time scale for CO_2 uptake by the surface water is of an order of a year or longer, the water does not have enough time to absorb significant amounts of CO_2 from the atmosphere. Furthermore, during the summer months, the vertical mixing between the surface and deep waters is expected to be at a minimum and the photosynthetic utilization of carbon in surface water is expected to be at a maximum. These factors contribute to lowering of pCO_2 in the surface water in the northern oceans.

In the antarctic circumpolar region, however, the water flows around the antarctic continent, driven by the westerly wind and unimpeded by major topographic barriers. The exchange rate of the surface water between the circumpolar water and the warm surface waters of the Atlantic, Pacific, and Indian Oceans generally is slow because they are separated by the Antarctic Convergence Zone. No coherent southward flow of the warm surface waters across the convergence zone into the circumpolar region exists. Thus, the residence time of circumpolar surface water is much longer than that in the Norwegian-Greenland Sea, and, accordingly, the southern ocean circumpolar surface water tends to be close to equilibrium with the atmospheric CO_2. Enhanced vertical mixing, which brings CO_2-rich deep water to the surface, and a minimum photosynthetic utilization of CO_2 during the austral winter tend to increase the pCO_2 on the surface water.

This work has been supported by U.S. Department of Energy grant DE-AC02-81ER60000.

References

Broecker, W. S., Takahashi, T., Quay, P., Bos, D., Chipman, D., and Stuiver, M. In press. Carbon dioxide and radiocarbon budgets in the equatorial Pacific Ocean and the equatorial upwelling rate. *Journal of Geophysical Research*.

Broecker, W. S., Takahashi, T., Simpson, H. J., and Peng, T.-H. 1979. Fate of fossil fuel carbon dioxide and the global carbon budget. *Science*, 206, 409–418.

Gordon, A. L. 1982. The U.S.-U.S.S.R. Weddell Polynya Expedition. *Antarctic Journal of the U.S.*, 17(5).

Takahashi, T., and Azevedo, A. E. G. 1982. The oceans as a CO_2 reservoir. In R. A. Beck and J. R. Hummel (Eds.), *Interpretation of climate and photochemical models, ozone and temperature measurements*. New York: American Institute of Physics.

The Weddell Gyre

ARNOLD L. GORDON

Lamont-Doherty Geological Observatory
of Columbia University
Palisades, New York 10964

The Weddell Gyre is the largest, best formed subpolar gyre of the southern ocean. With its lesser cousins north-northeast of the Ross Sea and east of the Kerguelen Plateau, it carries heat and salt diffused by eddies across the Antarctic Circumpolar current to the continental margins of Antarctica. During this transfer, significant heat loss to the atmosphere occurs. The low degree of baroclinicity and weak lateral gradients make it difficult to resolve the gyre characteristics, yet some progress has been made. However, our view of the Weddell Gyre is based on austral summer data, with the exception of a few year-round current meter moorings, and the *Deutschland* winter data of Brennecke (1921). During the winter, the Weddell Gyre region is ice covered. The very weak regional pycnocline leads us to suspect significant vertical exchange of cold surface water with warm-saline deep water.

The U.S.-U.S.S.R. Weddell Polynya Expedition of 1981 (Gordon 1982; Gordon and Sarukhanyan 1982) aboard the Soviet ship *Somov* obtained an array of *in situ* conductivity-temperature-depth-oxygen (CTD-O^2) sensors/rosette hydrographic stations, in conjunction with biological, chemical, sea-ice, and atmospheric data (see pages 96–114, 1982 review issue of *Antarctic Journal of the U.S.*). Analyses of the hydrographic data lead to two studies: Gordon, Chen, and Metcalf (in press) and Gordon and Huber (in press). In these studies the characteristics of the ocean below the sea-ice cover are described.

The *Somov* data are within the cyclonic trough of the Weddell Gyre, in which the deep water is relatively cold, less than 0.5°C. However, cells composed of warmer deep water were observed. These warm cells have temperature, salinity, and oxygen properties similar to the Weddell deep water (WDW) characteristics of the Weddell Gyre inflow, which is situated to the southeast of the *Somov* study region. The warm WDW cells are accompanied by domes in the pycnocline of 40-meter amplitude over the surrounding pycnocline, while deeper isopycnals are depressed. The pycnolcine domes are exposed to about 50 percent greater entrainment by the turbulently active winter mixed layer, relative to the regional entrainment rate. It is hypothesized that the warm WDW cells within the Weddell Gyre trough are derived from instability within the frontal zone, which extends from Maud Rise to the northeast separating the Weddell warm regime from the cold regime. Greater than normal injection of warm WDW cells into the Weddell Gyre trough would increase the surface salinity, which would tend to destabilize the pycnocline, increasing the probability of deep convection and polynya events.

The *Somov* data also reveal that the surface mixed layer below the sea-ice cover is undersaturated in oxyen by as much as 1.1 milliliters per liter. This deficit is believed to be a consequence of oxgygen-poor (4.5 milliliters/liter) WDW entrainment by the winter mixed layer. Assuming effective cut off of ocean-atmosphere oxygen exchange by the nearly complete snow- and sea-ice cover with no net impact of oxygen content due to biological factors, a mixing ratio of 1 to 3 for WDW to beginning-of-winter surface water is required to explain the end-of-winter mixed-layer oxygen content. Using this entrainment rate and the assumption that vertical exchange in the non-ice-covered period is only diffusive, a mean annual heat flux of 15 watts per square meter is determined with an annual fresh water demand of 46 centimeters per year.

This work is supported by DPP 80–05765.

References

Brennecke, W. 1921. Die ozeanographischen Arbeiten der deutschen antarktischen Expedition 1911–1912. *Archiv der Deutschen Seewarte*, 39(1), 1–216, and 14 maps.

Gordon, A. L. 1982. the U.S.-U.S.S.R. Weddell Polynya expedition. *Antarctic Journal of the U.S.*, 17(5), 96–98.

Gordon, A. L., C. T. A. Chen, and W. G. Metcalf. In press. Winter mixed layer entrainment of Weddell Deep Water. *Journal of Geophysical Research.*

Gordon, A. L., and B. A. Huber. In press. Thermohaline stratification below the Southern Ocean sea ice. *Journal of Geophysical Research.*

Gordon, A. L., and E. I. Sarukhanyan. 1982. American and Soviet expedition into the Southern Ocean sea ice in October and November 1981. *The Oceanography Report, EOS*, 63(1), 2.

Nutrient depletion indicates high primary productivity in the Weddell Sea

Joe C. Jennings Jr, Louis I. Gordon & David M. Nelson

College of Oceanography, Oregon State University, Corvallis, Oregon 97331, USA

The Southern Ocean, and in particular the Weddell Sea, have long been considered areas of high biological productivity[1], but recent isotopic measurements of primary productivity have not confirmed this view[2,3]. Because the large zooplankton and marine mammal populations of the Southern Ocean depend ultimately on phytoplankton as the base of the food web, accurate knowledge of primary productivity is essential to our understanding of the Antarctic ecosystem. Oceanographic data collected aboard the Soviet icebreaker *Mikhail Somov* have allowed us to derive a new productivity estimate, based on the seasonal depletion of nitrate, phosphate and silicic acid in the surface layer. From these depletions and data on the elemental composition of Southern Ocean phytoplankton, we estimate average primary productivity in the Weddell Sea in the springtime to be 220–420 mg C m^{-2} day^{-1}. Our most conservative estimate is 1.5–4 times higher than recently reported measurements of productivity in the open ocean areas of the Southern Ocean[2–5]. Our estimates are inherently averages over time and space, including the effects of brief, intense spring blooms of phytoplankton which may occur near the receding ice edge[6–8]. Studies of primary productivity based on isotope uptake experiments, particularly in the austral summer, may fail to account for the significance of such blooms.

In October and November 1981, the joint US–Soviet Weddell Polynya Expedition aboard *Mikhail Somov* penetrated several hundred kilometres into the seasonal pack ice covering the eastern Weddell Sea, roughly along the Greenwich meridian. Preliminary results, including a description of the hydrographic regime and sea ice conditions, have been reported elsewhere[9–12]. The sub-ice surface waters comprised a very homogeneous mixed layer some 60–110 m thick in which dissolved nutrient concentrations were highest at the northernmost stations, decreasing slightly in the Weddell gyre proper. Because ice conditions restricted *Somov* to a relatively small sector of the northeastern Weddell gyre, it was necessary to examine the data set in the context of data from other cruises in the same area. Comparison of the nutrient data with austral summer data from GEOSECS and *Islas Orcadas* revealed that the austral summer data exhibited evidence of marked surface layer nutrient depletions. It was also apparent that virtually unaltered remnants of winter surface waters were present at several of the austral summer stations[12]. The existence of this unaltered winter water[13] (WW) at GEOSECS station 89, near the *Somov* track, with nutrient concentrations very similar to those in the winter surface layer, led us to derive an estimate of phytoplankton productivity from the net depletion of nutrients in the overlying surface waters.

Several assumptions are implicit in this approach to the estimation of seasonal nutrient depletion: (1) the separate summer and winter data sets (that is, different cruises) are quantitatively compatible; (2) little or no vertical or lateral mixing takes place to alter nutrient concentrations in either the surface layer or

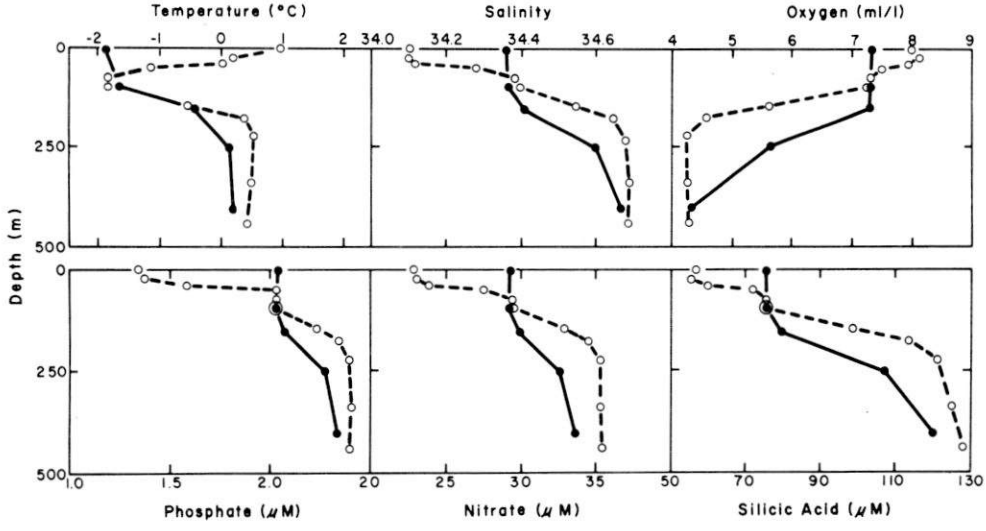

Fig. 1 Hydrographic properties at *Somov* station 35 at 59° 30′ S 0° 30′ E (solid lines) and GEOSECS station 89 at 60° 1.5′ S 0° 1.5′ E (dashed lines). The remnant winter water at the GEOSECS station is at 75–100 m.

Table 1 Winter water at GEOSECS 89 and wintertime surface water at WEPOLEX 35

Station	Pressure (db)	Potential temperature (°C)	Salinity (‰)	Silicate (μM)	Phosphate (μM)	Nitrate (μM)
GEOSECS 89	1	0.965	34.103	56.9	1.34	22.9
22 January 73	75	−1.830	34.383	75.7	2.03	29.4
60° 01′ S/0° 01′ E						
WEPOLEX 35	Entire	−1.858	34.358	75.7	2.04	29.3
12 November 81	surface					
59° 05′ S/0° 40′ E	mixed layer					

the WW layer beneath it; (3) a realistic time frame can be assigned over which the depletion of nutrients occurs; (4) vertical homogeneity in the surface layer under the ice is characteristic of late winter conditions in all years.

The hydrographic data used here were collected on the GEOSECS Atlantic cruise in 1972–73, *Islas Orcadas* cruise 12 in 1977 and the *Somov* cruise in 1981. The nutrient data from the GEOSECS and *Somov* cruises were obtained using the same automated techniques[14]; on *Islas Orcadas* manual techniques were used[15]. Intercomparisons of the nutrient chemical data on deep potential temperature and density surfaces confirm the comparability of the GEOSECS and *Somov* data, but the *Islas Orcadas* data appear to be systematically lower in dissolved silicic acid and higher in phosphate. In our calculations, we have used the *Islas Orcadas* data solely to illustrate the spatial extent of the nutrient depletion. Table 1 presents the temperature, salinity and dissolved nutrient data (phosphate, nitrate and silicic acid) we used.

Table 1 and Fig. 1 illustrate the evidence for stating that minimal vertical diffusion has occurred to alter the dissolved nutrient concentrations in either the surface layer or the WW. The *Somov* data show the temperature of the entire surface mixed layer beneath the ice to be almost at the freezing point. It is underlain by warmer, more saline water and would be heated from above by insolation as the ice recedes; thus, any substantial vertical mixing across the WW layer would cause an increase in its temperature. No such increase was observed (Fig. 1). Instead, a cold lens of remnant WW exists in the Weddell Sea. This was first noted half a century ago[16] but very few chemical observations have been available until recently. For the depletion calculations discussed here, we have used only the GEOSECS station at which the WW properties were demonstrably identical to those in the wintertime mixed layer (Fig. 1).

Generally, horizontal advection and mixing could also modify nutrient concentrations in surface waters above the remnant WW layer, but in the Weddell gyre lateral transport would do little to alter the apparent depletion of the surface waters relative to the underlying WW. There is a high degree of lateral homogeneity in the Weddell Sea, particularly in the zonal direction in which the major circulation occurs[16]. Additionally, circulation within the gyre is quite weak[9,17], and vertical shear between the surface and WW is not sufficient for the surface waters observed in the austral summer to have originated very far away from the underlying WW.

Dilution of the surface layer by melt water from the receding ice pack (mean thickness = 1 m) would cause an apparent depletion of nutrients in the surface layer. Adding 1 m of melt water to a surface layer 40 m thick (that is, a dilution of 2.5%) would account for ~7% of the observed nutrient depletion. Some of the *Islas Orcadas* stations we examined had surface salinities which were diluted by as much as 5% relative to the WW, which could account for 15–20% of the apparent nutrient depletion. At the austral summer GEOSECS station used in our calculations, the surface salinity is within 1% of the salinity of the WW layer, indicating that dilution effects were negligible.

The assignment of a time frame during which the observed nutrient depletion took place is somewhat problematical. The timing of the retreat of the pack ice is highly variable from year to year, usually beginning in mid-November[18,19]. November 1972 had the greatest extent of pack ice for the decade 1966–76[19], and it is thus unlikely that the GEOSECS station location was ice free until late November or early December. (The November ice extent data are the best indication of maximum annual ice extent available for the pre-microwave satellite era[19].) The GEOSECS observations were made during January 1973; therefore, we have assigned a 60–90 day time frame to the observed nutrient depletion.

The annual cooling of the surface layer at the onset of the austral winter results in the formation of a homogeneous surface layer before ice formation[16]. The *Somov* data indicate that this layer remains homogeneous in all properties throughout the winter; therefore little or no primary production occurs below the ice to alter the nutrient concentrations. Observations of very low levels of chlorophyll *a* and extremely limited light penetration of the pack ice during the *Somov* cruise[20] support the conclusion that primary productivity under the ice pack is minimal. Thus, the homogeneity of nutrient concentrations in the surface mixed layer at the end of austral winter can be assumed to be typical.

Figure 2 illustrates the spatial extent of the summer/winter contrast in dissolved silicic acid and phosphate concentrations in the eastern Weddell Sea. Because we believe the *Islas Orcadas* nutrient data to be systematically offset from the *Somov* data, we have used only the GEOSECS data to quantify the observed nutrient depletion. Taking the seasonal depletion to be the difference between the observed nutrient concentration and the WW nutrient concentration, the vertically integrated depletions at GEOSECS station 89 are 850 mmol m^{-2}, 27 mmol m^{-2} and 300 mmol m^{-2} for silicic acid, phosphate and nitrate, respectively. The average rates of depletion over the 60 and 90 day time frames assigned are shown in Table 2.

Our average nutrient depletion rates can be compared with experimentally determined rates of nitrogen and silicon assimilation by Antarctic phytoplankton. On recent cruises in the Scotia Sea[4,7], vertically integrated nitrate uptake rates were 0.74–2.41 mmol m^{-2} day^{-1} for those stations which were not in close proximity to a land mass. (An 18-h day has been used to convert from reported hourly rates.) Our most conservative estimate of the average daily nitrate depletion (Table 2) is 2.5–4 times the mean rate for these Scotia Sea stations. Similarly, for stations south of 60° S in the Pacific sector of the Southern Ocean, net production of biogenic silica in the euphotic zone was 2.5–4.5 mmol Si m^{-2} day^{-1} (ref. 21), compared with our calculated silicic acid depletion rates of 9.4–14.2 mmol m^{-2} day^{-1}. There-

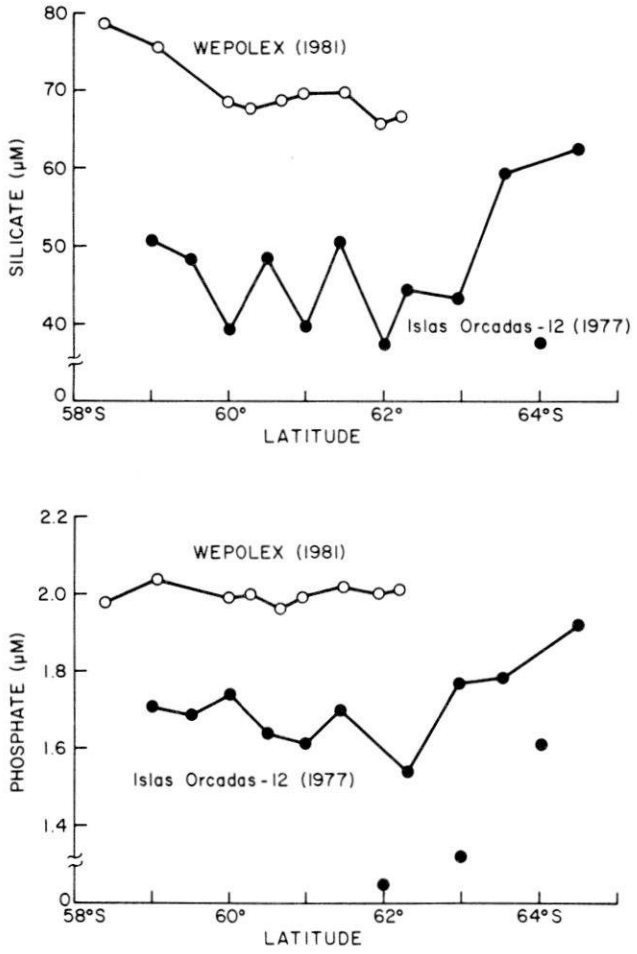

Fig. 2 Meridional distribution of dissolved silicic acid and phosphate in surface waters of the eastern Weddell Sea. *Islas Orcadas* data from summer 1977 are contrasted with *Somov* data from winter 1981 to illustrate the north–south extent of the apparent seasonal depletion.

fore, the seasonal average depletion rates of both nitrate and silicic acid exceed by a factor of 1.5–5 the few available directly measured rates in the Southern Ocean.

The estimation of primary productivity from nutrient depletion requires knowledge of the stoichiometry of nutrient assimilation and carbon fixation by phytoplankton. The average composition of marine phytoplankton is often taken to be C/N/P = 106/16/1 (ref. 22), but lower C/N and C/P ratios have been reported for Southern Ocean phytoplankton[23]. Similarly, C/Si ratios for diatoms in the Southern Ocean are apparently lower than those for most marine diatoms[23]. We have used C/N/P = 62/11/1 and C/Si = 2.5 as representative of Antarctic phytoplankton[23]. Our estimates of average primary productivity are shown in Table 2. They range from ~220 mg C m^{-2} day^{-1} to 420 mg C m^{-2} day^{-1}.

Our lowest estimates of average primary productivity are based on phosphate and nitrate depletion occurring over a 90-day period. Because particulate nitrogen and phosphorus are remineralized more rapidly than is biogenic silica, they are more likely to be recycled within the euphotic zone. One aspect of this recycling is that some nitrogen is returned to the euphotic zone as ammonium by zooplankton excretion and microbial regeneration (see, for example, ref. 4). This ammonium is utilized preferentially by phytoplankton[4], so our nitrate-based estimate of primary productivity is inherently an underestimate. The estimate of primary productivity from nitrate depletion is considered to be that fraction of the total which is available for net transport up the food chain[4,7]. Available data on ammonium and nitrate uptake by Southern Ocean phytoplankton suggest that ammonium utilization supports 40–70% of the total productivity[4,7], so our estimate of nitrate utilization probably accounts for no more than half of the total. As only direct measurements of biogenic silica dissolution made in the Southern Ocean indicate that about one-third of the assimilated silicic acid dissolves in the upper 100 m[21], our silicic acid-based calculation may well be low by that amount. If our nitrate- and silicic acid-based primary productivity estimates are increased accordingly, they agree within 10%.

Table 2 Primary productivity estimated from nutrient depletion

Nutrient	Observed depletion (mmol m^{-2})	Depletion rate (mmol m^{-2} day^{-1}) 90-day interval	60-day interval	Estimated primary production (mg C m^{-2} day^{-1})
Silicic acid	850	9.5	14.2	282–426
Phosphate	27	0.30	0.45	223–335
Nitrate	300	3.4	5.1	223–335

We believe that our calculations are conservative ones, resulting in estimates of primary productivity that are probably low, yet are 1.5–5 times higher than recent isotopic productivity measurements in the Southern Ocean[2,3,5,24]. Intense phytoplankton blooms have been reported near the edge of the receding seasonal ice pack which could easily account for much of the discrepancy between our calculated rates and those measured isotopically. Primary productivity in these blooms often exceeded 1 g C m^{-2} day^{-1} (refs 6–8, 24). As its seasonal ice cover recedes, most of the Weddell Sea surface is an ice edge zone for some period of the austral spring. A brief (10–15 day) bloom during which productivity was in excess of 1 g C m^{-2} day^{-1}, followed by a longer period of much lower productivity (closer to the ~0.1 g C m^{-2} day^{-1} values of the recent literature[2,3,5,24]), would result in seasonal average rates similar to those we derive. The contribution of such blooms is inherently included in our calculations, but may be missed by discrete measurements which are remote from the ice edge.

We gratefully acknowledge the support of this work by the Division of Polar Programs of the US NSF (DPP80-107620 and DPP82-03529) and by the Arctic and Antarctic Institute of the USSR. We thank A. L. Gordon, leader of the US component of the Weddell Polynya Experiment, for his help; the scientists, officers and crew of *Somov* and our American colleagues for their support; and M. Sparrow and J. Ahern for technical support in our laboratories at Oregon State University.

Received 26 September 1983; accepted 2 February 1984.

1. Hart, T. J. *Discovery Rep.* **8,** 3–268 (1934).
2. Holm-Hansen, O., El-Sayed, S. Z., Franceschini, G. A. & Cuchel, R. L. in *Proc. 3rd SCAR Symp. Antarctic Biology*, 11–50 (Smithsonian Institution, Washington DC, 1977).
3. El-Sayed, S. Z. & Turner, J. T. in *Polar Oceans* (ed. Dunbar, M. J.) 463–503 (Arctic Institute of North America, Calgary, Alberta, 1977).
4. Glibert, P. M., Biggs, D. C. & McCarthy, J. J. *Deep-Sea Res.* **29,** 837–850 (1982).
5. Slawyk, G. *Aust. J. mar. Freshwat. Res.* **30,** 431–448 (1977).
6. El-Sayed, S. Z. in *Biology of the Antarctic Seas* Vol. 4 (eds Land, G. & Wallen, I.) 301–312 (American Geophysical Union, Washington DC, 1971).
7. Olson, R. J. *Limnol. Oceanogr.* **25,** 1064–1074 (1980).
8. Smith, W. O. & Nelson, D. M. in *Proc. 4th Symp. Antarctic Biology* (Elsevier, New York, in the press).
9. Gordon, A. L. & Huber, B. A. *J. geophys. Res.* **89** (C1), 641–648 (1984).
10. Gordon, A. L., Chen, C. T. A. & Metcalf, W. G. *J. geophys. Res.* **89** (C1), 637–640 (1984).

11. Clarke, D. B. & Askley, S. F. *J. geophys. Res.* (in the press).
12. Jennings, J. C. Jr, Nelson, D. M. & Gordon, L. I. *Antarct. J. U.S.* **8,** 101 (1982).
13. Carmack, E. C. & Foster, T. D. *Deep-Sea Res.* **22,** 711–724 (1975).
14. Bainbridge, A. E. *Geosecs Atlantic Expedition* Vol. 1 (National Science Foundation, Washington DC, 1981).
15. Huber, B. A., Rennie, S. E., Georgi, D. T., Jacobs, S. S. & Gordon, A. L. *Islas Orcadas Reports, Cruise 12, Jan–Feb 1977,* Tech. Rep. CU-2-81-TR2 (Lamont-Doherty Geological Observatory, Columbia University, Palisades, 1981).
16. Mosby, H. *Scientific Results of the Norwegian Antarctic Expeditions, 1927–1928,* Vol. 1(11) (Det Norske Videnskaps-Academi I, Oslo, 1934).
17. Gordon, A. L., Martinson, D. G. & Taylor, H. W. *Deep-Sea Res.* **28A,** 151–163 (1981).
18. Gordon, A. L. *J. geophys. Res.* **86,** 493–4197 (1981).
19. Ackley, S. F. *Int. Ass. hydrol. Sci.* **131,** 129–159 (1981).
20. Marra, J. & Boardman, D. C. *Mar. Ecol.-Prog. Ser.* (submitted).
21. Nelson, D. M. & Gordon, L. I. *Geochim. cosmochim. Acta* **46,** 491–501 (1982).
22. Redfield, A. C., Ketchum, B. H. & Richards, F. A. in *The Sea, Ideas and Observations* Vol. 2, 26–77 (Interscience, New York, 1963).
23. Copin-Montegut, C. & Copin-Montegut, G. *Deep-Sea Res.* **25,** 911–931 (1978).
24. El-Sayed, S. Z. & Taguchi, S. *Deep-Sea Res.* **28A,** 1017–1032 (1981).

SECTION 3: BIOLOGY

Zooplankton in the Weddell Sea, October–November 1981

JEANNE C. STEPIEN

Lamont-Doherty Geological Observatory
of Columbia University
Palisades, New York 10964

Zooplankton was collected beneath the pack ice of the Weddell Sea and at the ice edge during the Weddell Polynya expedition (WEPOLEX-81) (Gordon, *Antarctic Journal*, this issue). The Soviet research vessel *Mikhail Somov* entered the ice in mid-October near 56.5°S 5°E and penetrated as far south as 62.5° before leaving the ice in mid-November at approximately 58°S. To characterize the Weddell Sea zooplankton community, with special emphasis on the distribution, abundance, biomass, feeding habits, and reproductive state of krill, macrozooplankton was collected beneath the ice and at the ice edge. Paired 500-micrometer and 1,000-micrometer mesh, 0.75-meter nets were fished routinely from 0–200 meters and 0–500 meters and occasioally from 0–1000 meters. Ice conditions limited the sampling to vertical hauls. Krill also were collected for feeding studies using the gut fluorescence method (Mackas and Bohrer 1976) and microscopic examination aboard ship.

The results show several striking differences between the pack ice and ice edge (see figure 2 of Gordon and Huber, *Antarctic Journal*, this issue) in October–November in terms of species of krill and total zooplankton abundance and biomass. *Euphausia superba*, the dominant species of antarctic krill, was observed at the ice edge in both mid-October and mid-November, although not in swarm concentrations. With the exception of a few isolated juveniles, however, this species was not collected or observed within the pack ice, where *Thysanoessa macrura* was the dominant species at all stations. There was a dramatic difference in total zooplankton biomass and abundance between the pack ice and ice edge (Figure 1). Biomass in the upper 200 meters and 500 meters increased from means of 1.2 and 1.0 milligrams per cubic meter beneath the ice to 2.9 and 4.5 milligrams per cubic meter at the ice edge; total abundance in the upper 200 meters and 500 meters increased from 3 and 5 per cubic meter beneath the ice to 25 and 42 per cubic meter at the ice edge. Biomass and abundance figures at the ice edge actually should be higher, because the vertical tows did not adequately sample the *E. superba* population observed. The increases in zooplankton abundance and biomass at the ice edge parallel the increase in chlorophyll *a* and photosynthesis reported by Marra, Burckle, and Ducklow (*Antarctic Journal*, this issue).

T. macrura was present throughout the pack ice, reaching a maximum abundance of 9 per cubic meter in the upper 200 meters and accounting on average for 32 percent and 27 percent

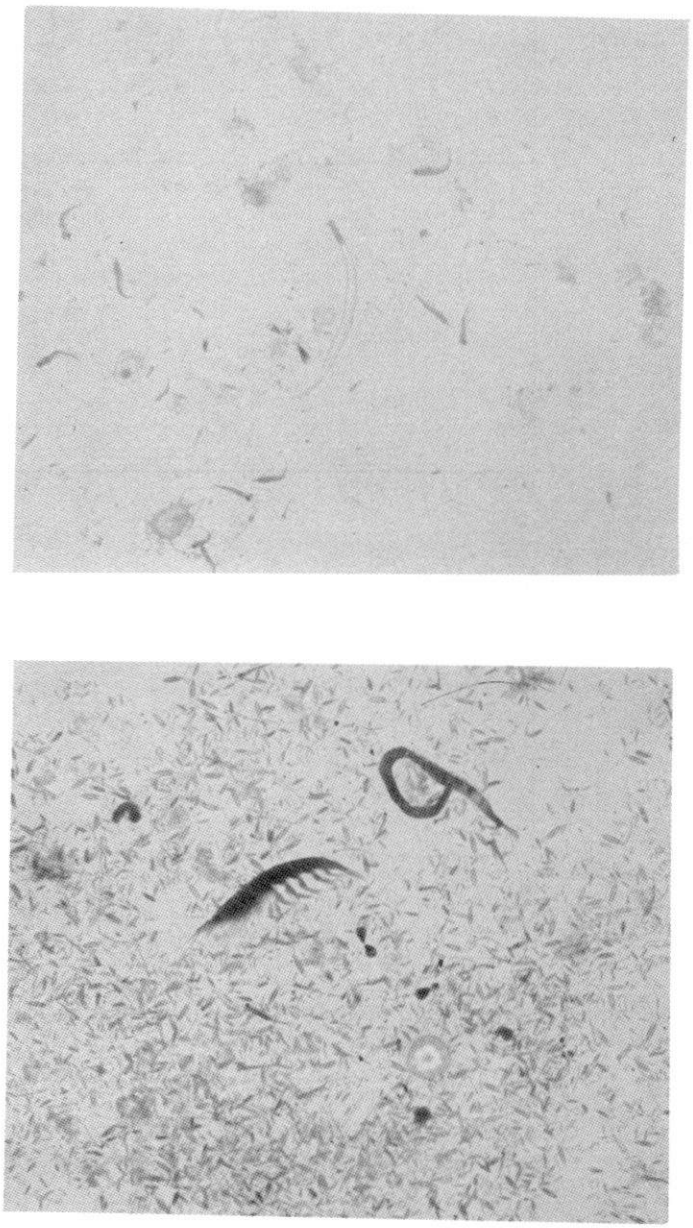

Figure 1. Silhouette photographs (Ortner et al. 1979) of typical zooplankton samples taken within the pack ice (top panel) and at the ice edge (bottom panel). Both samples were collected with a 500-micrometer mesh net hauled vertically from 0 to 200 meters. Photographs show one half of the original sample.

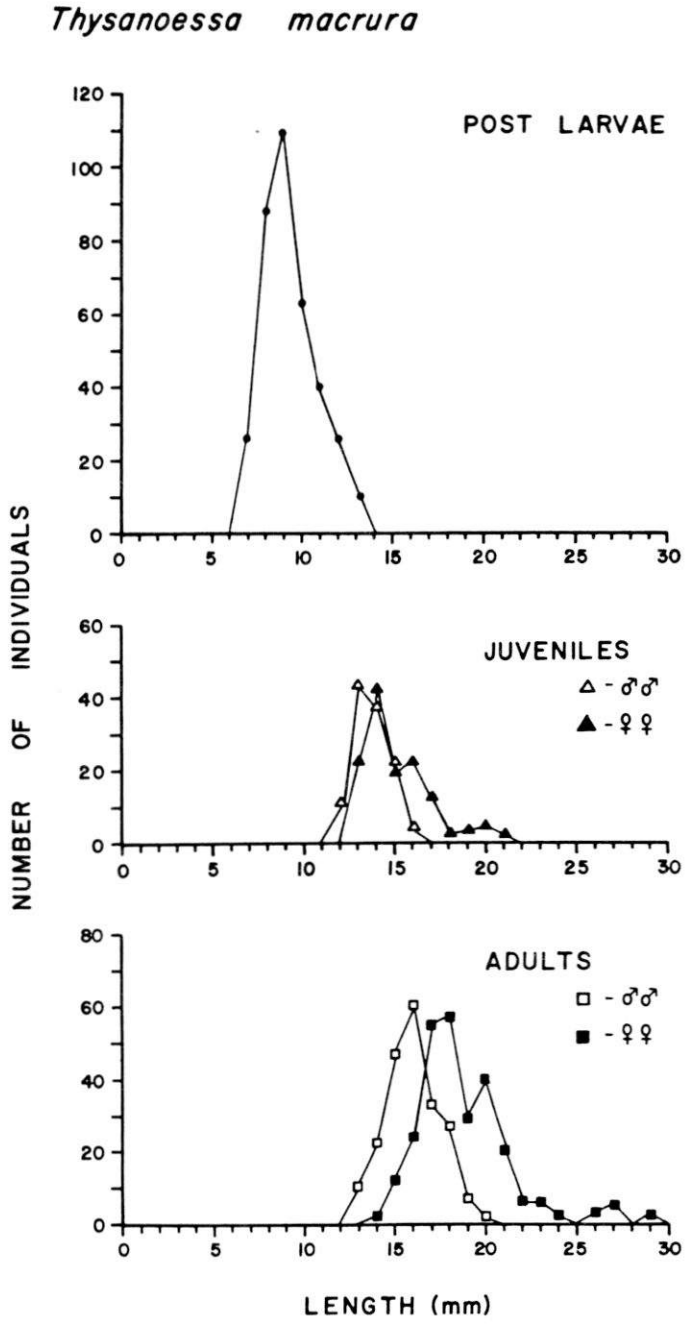

Figure 2. Total length of *T. macrura* post-larvae, juveniles, and adults collected within the pack ice.

of total biomass in the upper 200 meters and 500 meters, respectively. Since all of the hydrographic stations during WEPOLEX were within the ice (figure 3 of Gordon, *Antarctic Journal*, this issue), it was possible to collect many specimens of *T. macrura*. Total length and stage of sexual maturity were determined for more than 1,000 individuals (figure 2). The *T. macrura* population sampled consisted of three groups: post-larvae (secondary sexual characteristics not visible), juveniles (immature males and females and females with spermatophores), and adults (mature males and females with ripening gonads). The developmental stage of the ovaries of the ripening adult females suggests that spawning had not begun. Females spawn at stage IV, yet all females examined were in stage II or III (Roger 1974). It is known that under the proper conditions the ovaries can mature to stage IV within a week (Zhuravlev, personal communication). Chlorophyll levels beneath the ice were low (0.1 microgram per liter) (see Marra, Burckle, and Ducklow, *Antarctic Journal*, this issue), and gut fluorescence measurements and visual examination of stomach contents indicated that *T. macrura* were not feeding. Perhaps the springtime retreat of the ice, which brings increased productivity in the formerly ice-covered water column, triggers the maturation of the ovaries to stage IV, thus initiating spawning by *T. macrura* in the Weddell Sea. Such a spawning response is possible since *T. macrura* is known to spawn in the Scotia Sea in spring (Makarov 1979).

D. Boardman, D. Clarke, and V. Zhuravlev assisted in the collection of samples. V. Zhuravlev measured *T. macrura* and determined stages of maturity, and C. Newcomer provided technical assistance. This research was supported by National Science Foundation grant DPP 80-08011.

References

Gordon, A. L. 1982. The U.S.-U.S.S.R. Weddell Polynya Expedition. *Antarctic Journal of the U.S.*, 17(5).

Mackas, D., and Bohrer, R. 1976. Fluorescence analysis of zooplankton gut contents and an investigation of diel feeding patterns. *Journal of Experimental Marine Biology and Ecology*, 25, 77–85.

Makarov, R. R. 1979. Larval distribution and reproductive ecology of *Thysanoessa macrura* (Crustacea: Euphausiacea) in the Scotia Sea. *Marine Biology*, 52, 377–386.

Ortner, P. B., Cummings, S. R., Aftring, R. P., and Edgerton, H. E. 1979. Silhouette photography of oceanic zooplankton. *Nature*, 277, 50–51.

Roger, C. 1974. Les euphausiacés du Pacifique équatorial et sud tropical. Zoogéographie, écologie, biologie et situation trophique. *Memoires ORSTROM*, No. 71.

Zhuravlev, V. Personal communication, 1981.

Sea ice and water column plankton distributions in the Weddell Sea in late winter

JOHN MARRA, LLOYD H. BURCKLE, *and* HUGH W. DUCKLOW

Lamont-Doherty Geological Observatory
of Columbia University
Palisades, New York 10964

During the joint U.S.-U.S.S.R. Weddell Polynya expedition (WEPOLEX-81) (see Gordon, *Antarctic Journal*, we measured chlorophyll *a*, phytoplankton photosynthesis parameters, diatom distributions, and bacterial densities, in both the sea ice and the water column. Our investigations were part of a larger effort to obtain a comprehensive set of oceanographic data for wintertime conditions in the Weddell Sea. The measurements were carried out aboard the Soviet ship *Mikhail Somov. Somov* entered the pack ice at approximately 57°S 4°E on 20 October 1981 and proceeded south about 300 nautical miles (550 kilometers) into the pack ice before returning to the ice edge 24 days later.

Water column distributions. We collected water samples by bucket and, at discrete levels throughout the upper water column, using Niskin samplers attached to the conductivity-temperature-depth (CTD) rosette. Chlorophyll *a* concentrations (analyzed fluorometrically) were very low beneath the pack ice and increased by a factor of 2 at the ice edge (figure 1). According to the thermohaline distribution, the water column may have been more stable at the ice edge than beneath the pack ice. Diatom populations at the ice edge station were dominated by *Corethron hystrix* and *Chaetoceros sp.* Beneath the pack ice, a variety of species was found, including *Nitzschia closterium, N. curta,* and *Tropidoneis vanheurckii.*

The pack ice and ice edge populations differed most strikingly in their photosynthetic characteristics. Surface samples collected from each locale were incubated aboard ship in fluorescent light incubators under a range of light intensities (3–1,000 microEinsteins per square meter per second) and at near-ambient temperatures. Photosynthetic carbon fixation (as carbon-14 uptake) was plotted against the light intensity of incubation. For stations in the pack ice, maximal photosynthesis (normalized to chlorophyll *a*), or P^B_{max}, averaged 1.5 (standard error, ± 1) and the initial slope of the photosynthesis-light intensity relationship (α) averaged 0.014 (standard error, ± 0.010). No significant photoinhibition was observed. At the ice edge, P^B_{max} and α increased fourfold. Since the only environmental parameter that changed significantly between the pack ice stations and the ice edge was ice cover, the higher P^B_{max} and α values at the ice edge may represent an adaptation to higher light intensities in the water column resulting from lower cellular chlorophyll *a* contents.

Sea ice communities. The late winter pack ice contained an active community of microorganisms. Ice cores, obtained with the Cold Regions Research and Engineering Laboratory ice augur (Clarke and Ackley, *Antarctic Journal,* this issue) and sectioned and analyzed aboard ship, showed chlorophyll *a* concentrations that were an order of magnitude greater than those beneath the ice, typically ranging from 0.5 to 3 micrograms per liter. The diatom community was similar to that in the water column. In the top portion of the ice column, the flora was

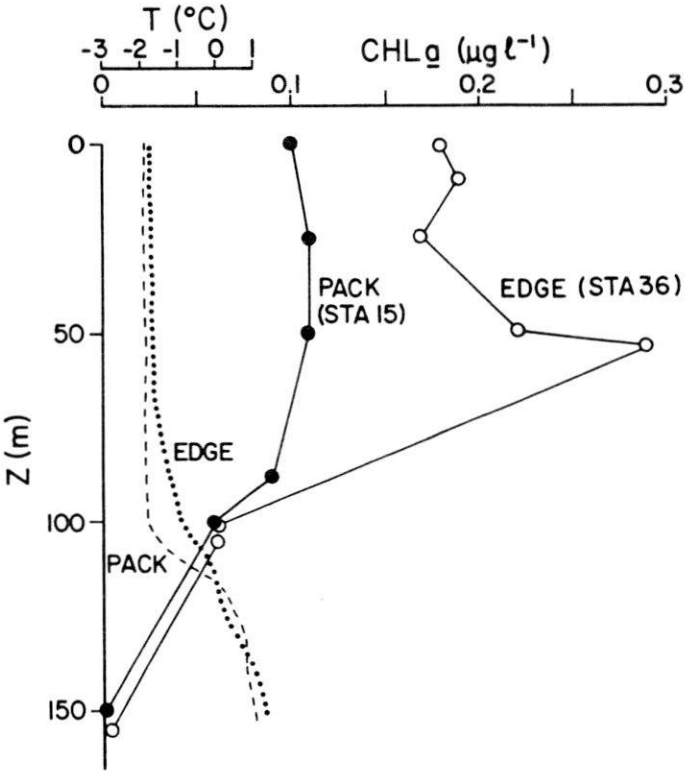

Figure 1. Vertical distribution of chlorophyll *a* (CHL *a*), in micrograms per liter, and temperature (T) for a station in the ice edge zone (station 36) and a station within the pack ice (station 15). Z = depth in meters.

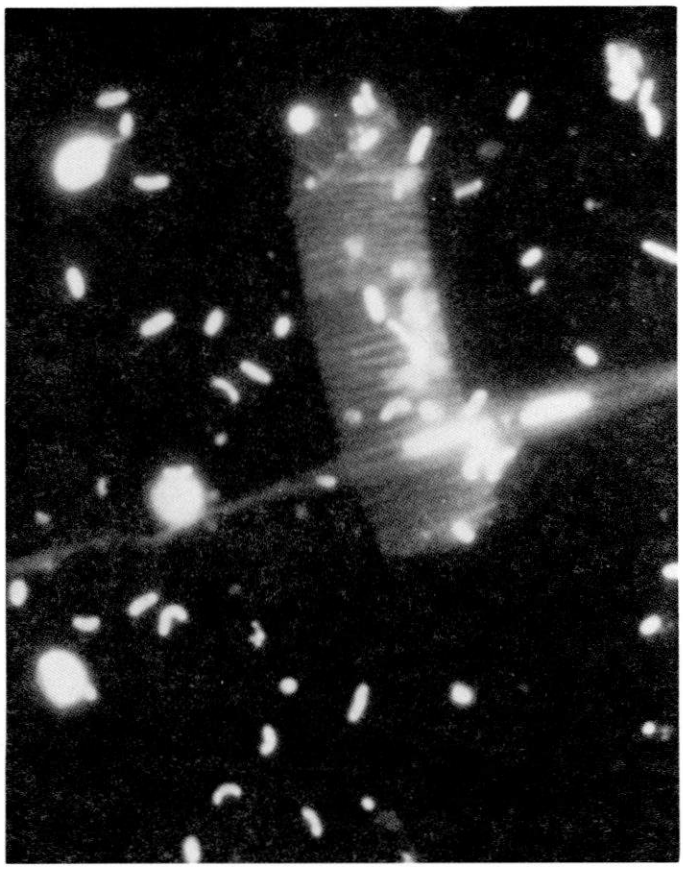

Figure 2. Epifluorescent photomicrographs of the heterotrophic community components in the ice column. The bacteria are about 1.0 micrometer long. Note also the unidentified flagellates, which number approximately 10^7 per liter, and the *Fragilaria sp.* and the *N. closterium* cells.

dominated by *N. closterium* or *T. vanheurckii*. There were relatively few diatom cell fragments. The middle and lower portions of the ice column had a more diverse assemblage (e.g., *N. closterium*, *N. curta*, *N. turgiduloides*, and *T. vanheurckii*), and the ratio of whole cells to cell fragments was low, about 1.

Bacteria in the ice were enriched relative to the water below. Within the ice, and at the depth of the chlorophyll maximum, bacterial density was approximately 10^9 cells per liter, while in the water below density was approximately 10^8 cells per liter. However, the cell counts mask large differences in cell sizes between the populations (figure 2). Using a carbon conversion factor based on cell volume, the bacteria in the ice would represent about 700 milligrams of carbon per cubic meter, while the bacteria in the water column would represent only 0.7 milligram per cubic meter.

While most of the diatoms may be incorporated into the ice during ice formation, the further growth of *N. closterium* and *T. vanheurckii* is indicated by their numerical dominance and by their occurrence in regions where the ratio of whole cells to fragments is high. Also, the large, abundant, and morphologically distinct bacteria found within the ice implies an active, heterotrophic community. If true, this is to our knowledge the first example of both active algal and bacterial growth within the pack ice of the Weddell Sea.

D. Boardman and D. Clarke performed the at-sea collections. We thank S. F. Ackley for providing the ice core samples and for comments on the manuscript. This research was supported by National Science Foundation grant DPP 80-08011.

References

Clarke, D., and Ackley, S. F. 1982. Physical, chemical, and biological properties of winter sea ice in the Weddell Sea. *Antarctic Journal of the U.S.*, 17(5).

Gordon, A. L. 1982. The U.S.-U.S.S.R. Weddell Polynya Expedition. *Antarctic Journal of the U.S.*, 17(5).

Vol. 19: 197–205, 1984 | MARINE ECOLOGY – PROGRESS SERIES
Mar. Ecol. Prog. Ser. | Published October 10

Late winter chlorophyll *a* distributions in the Weddell Sea

John Marra and David C. Boardman

Lamont-Doherty Geological Observatory of Columbia University, Palisades, New York 10964, USA

ABSTRACT: As part of the Weddell Polynya Expedition to the Weddell Sea (in the vicinity of 2° E/60° S) during October, and November, 1981, we report measurements of chlorophyll *a* and phytoplankton photosynthesis. Chlorophyll *a* measurements were made in 3 different environments: beneath the pack ice, in pack ice cores, and in the water volumn in the ice edge zone (IEZ, defined as 6/10's–1/10 ice cover). Photosynthesis measurements were made on samples from beneath the pack ice and from a station at the IEZ. Chlorophyll *a* values in the mixed layer beneath the pack ice average 12 mg m^{-2}. Within the IEZ (at 6/10's coverage) water column chlorophyll *a* doubles. Compared to values beneath the pack ice, the IEZ is characterized by a localized ten-fold increase in surface chlorophyll *a* (1 to 2 mg m^{-3}). Photosynthesis parameters likewise increase at the ice edge, and a rate of primary production of 300 to 400 mg m^{-2} d^{-1} is estimated for this region. Significant amounts of chlorophyll *a* are found near the base of the pack ice column, and evidence is presented which suggests an active biological community living within the pack ice. Overall, the data are consistent with the idea that phytoplankton distributions are regulated by the availability of light. Furthermore, the data indicate the importance of the IEZ to primary production in the Southern Ocean.

INTRODUCTION

The seasonal dynamics of the production ecology of the surface waters surrounding Antarctica are distinguished by uniformly low temperatures south of the Antarctic Convergence (e.g. Gordon and Molinelli, 1982), extremes of solar irradiance, and substantial variability in sea ice. However, ideas concerning controlling factors of production have come largely from observations made in the austral summer. There are few data sets from winter (Hart, 1942; Burkholder and Burkholder, 1967), or from months of maximum ice extent, and discussion continues as to the relative importance of such factors as temperature, nutrients and irradiance to the dynamics of productivity in the Southern Ocean (e.g. Holm-Hansen et al., 1977; El-Sayed, 1978). The search for major environmental influence is important for deriving estimates of production as well as for being able to predict seasonal and areal variability. Also, because logistical support is difficult and expensive in the Southern Ocean, there are potential benefits in being able to predict rates of production from more easily measured, and perhaps remotely sensed, environmental factors.

Unlike most of the world's oceans, nutrients are abundant in Antarctic Surface Water (AASW) (Gordon and Molinelli, 1982). Nutrient levels seldom drop below 1 μg-at PO_4-P l^{-1}, 10 μg-at NO_3-N l^{-1} and 20 μg-at Si $(OH)_4$-Si l^{-1} anywhere south of the Antarctic convergence. While significant nutrient variability exists, nutrient levels are well above thresholds where growth of phytoplankton might be considered nutrient-limited (e.g. Eppley et al., 1969; Walsh, 1971). Biggs (1978) reports low ammonium concentrations in the AASW, in spite of high concentrations of other nutrients, and possibly high turnover rates for this substrate. Whether these low concentrations affect rates of production is not clear. Ammonium is nearly always the preferred nitrogen source for phytoplankton in a wide variety of environments and under a wide range of physico-chemical conditions (e.g. McCarthy et al., 1977). The same is true of the Antarctic, at least in austral summer (Glibert et al., 1982), even though concentrations of ammonium are 1 to 2 orders of magnitude lower than nitrate. Olson's (1980) winter data from the Scotia Sea shows equal preference for nitrate and ammonia. It seems, therefore, that what has to be explained is the non-depletion of nitrate. It is possible that light or temperature limitation makes ammonium uptake more favorable energetically (Bates, 1976;

0171-8630/84/0019/0197/$ 02.50

Slawyk, 1979; Syrett, 1981) to the extent that nitrate cannot be fully utilized.

Low temperatures are the probable cause of the uniformly low assimilation numbers characteristic for Antarctic waters (Eppley, 1972). Neori and Holm-Hansen (1982) have clearly shown a temperature effect, suggesting that Antarctic phytoplankton are at least facultative psychrophiles. Bunt (1968) has also reported experimental evidence showing a temperature influence on photosynthesis in Southern Ocean phytoplankton. While temperature probably limits physiological rates, Walsh (1971) has found temperature to be of minor importance in explaining variations in phytoplankton standing stock on transects with water temperature ranging from 6 to −1 °C.

Light intensity, by virtue of its strong annual and areal variability, seems more likely than either nutrients or temperature to regulate primary production and the relative distribution of standing stocks in the Antarctic on a seasonal basis. The data of Hart (1942) show large increases in standing stock in summer relative to data collected in winter. The large variability in ice cover must also be considered. Ice cover ranges from a maximum in September and October of 20 million km^2 to 3 million km^2 in February (MacKintosh, 1972). The presence of ice inhibits air/sea exchanges and wind-induced mixing, and also markedly diminishes solar irradiance available for photosynthesis to the water column below. The formation of ice destabilizes the surface layer via the input of brine and consequent convective mixing. Conversely, the seasonal deterioration of the ice pack may stabilize, as well as provide seed populations for, the water column. For within-season studies, however, light intensity regulation is more difficult to demonstrate (Walsh, 1971), and there can be large spatial variations in primary production during the summer months (El-Sayed, 1970; El-Sayed and Weber, 1982). Large spatial variations could be due to hydrographic features or phenomena which increase the availability of light to phytoplankton, but oftentimes in the past, station-spacing on Antarctic expeditions was simply not adequate to isolate these.

During October and November, 1981, a joint US-USSR oceanographic program, The Weddell Polynya Expedition, was undertaken, one of the primary objectives of which was to obtain a comprehensive data set on winter or early spring conditions in the Southern Ocean. The Expedition was carried out aboard the Soviet ship 'Mikhail Somov' (length: 133 m, beam: 18.8 m) of the Arctic and Antarctic Research Institute of Leningrad. We made measurements of photosynthesis and chlorophyll *a* on water column samples and measured distributions of chlorophyll *a* in pack ice from mid-October to mid-November, 1981, that is during months of near-maximum ice extent. We present evidence consistent with the idea that the distribution and production of phytoplankton is regulated by the availability of light.

METHODS

The horizontal variability of chlorophyll *a* was measured by *in vivo* fluorescence in water continuously pumped from 4 m depth through a Turner Designs Model 10 fluorometer. Conductivity and temperature were measured simultaneously. Details of the system, its operation, calibration and the data reduction can be found in Marra et al. (1982a). This system was operated continuously after R.V. 'Mikhail Somov' entered the pack ice, however, fluorescence values are uniformly low and data featureless. We found no evidence that algae from sea ice were contaminating the signal. The vertical distribution of chlorophyll *a* was determined on samples from Niskin bottles in the upper 100 to 150 m of the water column. Chlorophyll *a* was also determined at various depths in pack ice cores, obtained with a CRREL ice-augur and sectioned while still frozen aboard ship (Clarke and Ackley, 1984). Standard chlorophyll *a* analyses were immediately performed on melts of the section (Holm-Hansen et al., 1965).

During one foray onto the pack ice to collect ice cores, measurements of light attenuation through the ice were made using a Lambda Instruments underwater quantum sensor. For measurements on the ship, this sensor agreed well with a radiometer mounted on the mast of R.V. 'Mikhail Somov' assuming that photosynthetically active irradiance (as measured by the quantum sensor) is 43 % of the total (downward) irradiance measured by the radiometer (Withrow and Withrow, 1956). Irradiance values from the R.V. 'Mikhail Somov' radiometer were recorded daily and are here reported in units of ly d^{-1}.

Rates of photosynthesis were determined by incubating duplicate near-surface (3 to 10 m depth) seawater samples in the presence of $NaH^{14}CO_3$ (5 μCi). All samples were taken between 0900 and 1100 h to minimize variability which might be caused by diel changes in photosynthesis parameters. Samples were collected at Stations 19, 21, 22, 34 and 36, and also at several locales between stations to ensure the proper time of collection. The samples were incubated under a range of light intensities in a fluorescent light incubator for 3 to 6 h. Temperatures in the incubator were kept at 1 to 2 °C above *in situ* by means of a refrigerated circulating bath. According to the data of Neori and Holm-Hansen (1982), this small temperature difference should not result in bias. The incubations were terminated by filtering the samples onto Millipore HA mem-

brane filters, which were then placed in glass scintillation vials with 10 ml of a toluene-based, water-compatible fluor (Bakerfluor). Upon return to the laboratory, the samples were counted on a Beckman LS100 liquid scintillation counter equipped with automatic external standardization. Photosynthesis *vs.* irradiance (P^b *vs.* I) data were fitted to the equation

$$P^b = P^b\max \cdot \tanh(\alpha I/P^b\max) - R \quad (1)$$

of Jassby and Platt (1976) by the non-linear regression techniques described in Malone and Neale (1981). Here, $P^b\max$ = light saturated rate of photosynthesis normalized to chlorophyll *a* concentration; α = initial slope of the curve; R = computed photosynthetic (respiration) rate at zero irradiance. Average errors in α and $P^b\max$ were typically 10 and 30 % of the reported values, respectively.

RESULTS

Fig. 1 shows the cruise track of R.V. 'Mikhail Somov' and station positions (CTD/rosette casts, ice cores, and expendable bathythermograph observations) during the cruise. The ship entered the ice on 20 October, 1981, and departed on 14 November, 25 d later. The positions of the nominal ice edges (3/10's coverage) are shown at these times in Fig. 1. The fact that the ice edge defined this way is further south on 14 November than on 20 October as much represents variability in the position of the ice edge as it does a net reduction in the pack ice cover over the period of the cruise. The nominal ice edge itself occurs in a mixed zone of open water and variably sized floes (Ackley and Smith, 1983), indicative of a dynamic region of general ice decay and even some new ice formation. We have defined the ice edge zone (Fig. 2) as lying between 1/10–6/10's ice cover.

Fig. 2, from Gordon and Huber (1982), illustrates the oceanographic setting for the biological measurements. It also shows surface parameter traces collected while the ship was underway and transiting the ice edge zone (IEZ). The stations in the IEZ show mesoscale features of Circumpolar Deep Water (CDW; e.g. Station 36) which are not apparent either to the north or south. Surface water temperatures in and south of the IEZ never vary more than a few hundredths of a degree above −1.8 °C, the surface freezing temperature. North of the ice edge zone, surface water temperatures gradually warm. Mixed layer depths vary from about 60 to 120 m. There is approximately a 2-fold increase in chlorophyll *a* fluorescence localized to the IEZ. Concurrent with this are negative anomalies in surface salinity and in nutrient concentrations. The surface chlorophyll *a* distributions derived from these

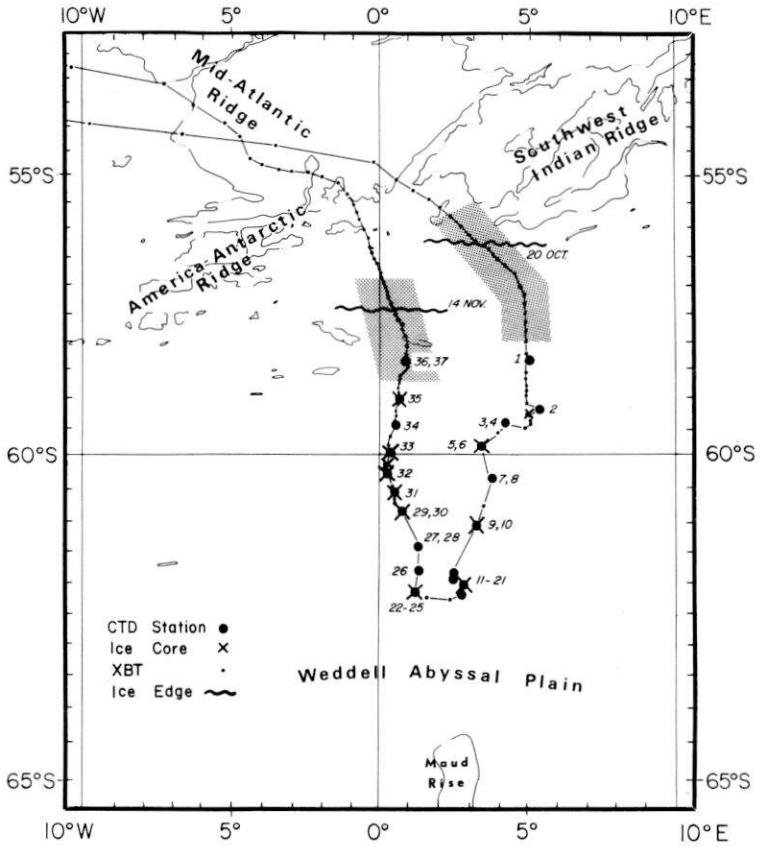

Fig. 1. Bathymetric map showing cruise track and station positions during the Weddell Polynya Expedition. The line defining the ice edge corresponds to about 3/10's ice coverage, and the shaded area defines the ice edge zone (IEZ). R.V. 'Mikhail Somov' entered the ice on 20 Oct, 1981, and departed 25 d later on 14 Nov

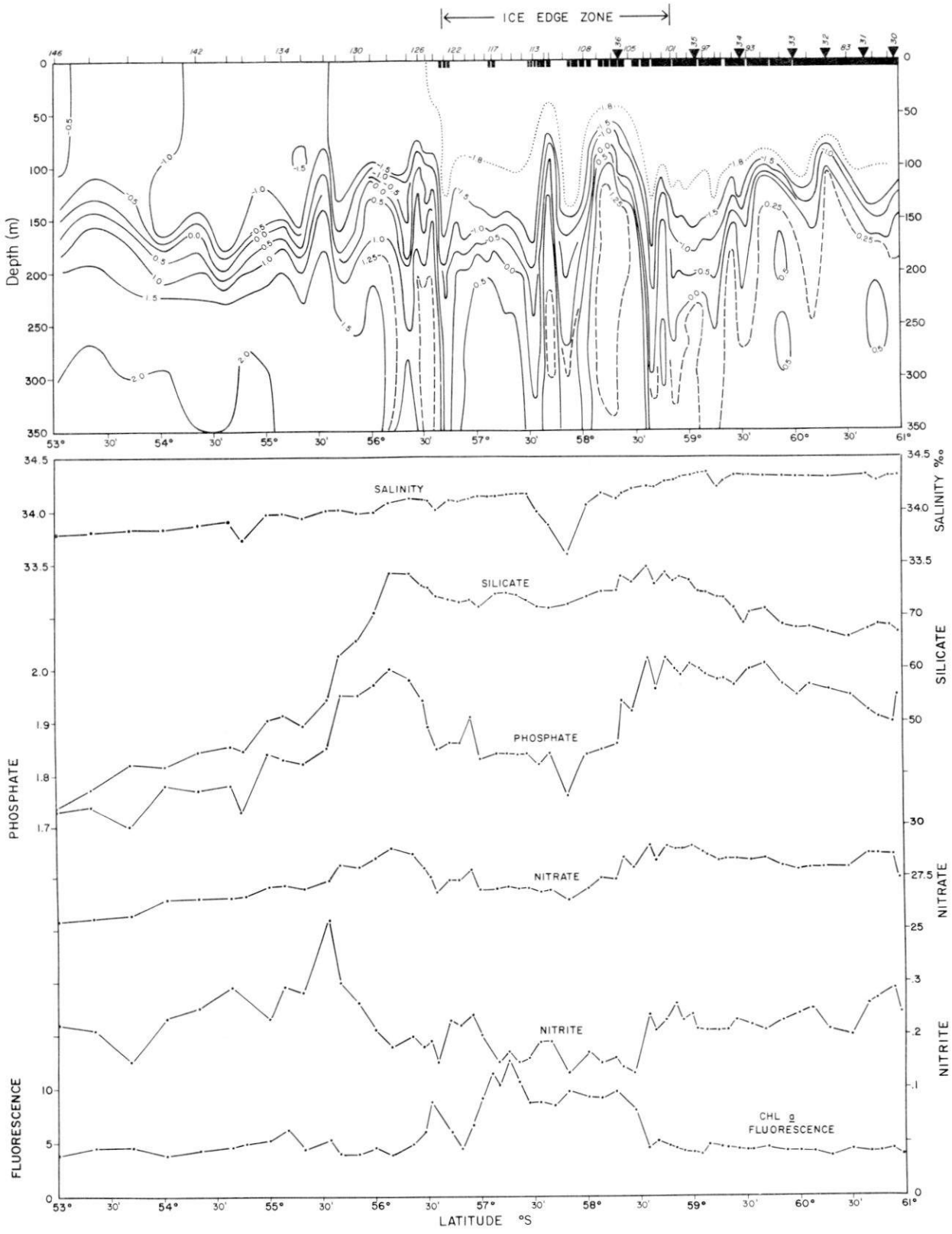

Fig. 2. Adapted from Gordon and Huber (1982). Depth *vs.* distance transect through the IEZ, approximately along the Greenwich Meridian. CTD stations (30 to 36) and positions of expendable bathythermograph launches (80 to 146) are indicated across the top, as is relative ice cover (thick solid line). Contours of temperature are given in °C. Salinity values were determined on an Autosal; nutrient values are courtesy of J. Jennings and were determined by Autoanalyser. Chlorophyll *a* fluorescence is in relative units. These values were sampled from the continuous fluorescence and temperature record

fluorescence values are discussed in more detail below.

Fig. 3 compares water column distributions of chlorophyll *a* for a station in the pack ice field and Station 36 in the IEZ (Fig. 1 and 2). Table 1 compares various environmental and biological variables for the pack ice and Station 36. The distribution of chlorophyll *a* in the water column beneath the pack ice (Station 15) shown in Fig. 3 is typical for all stations occupied in

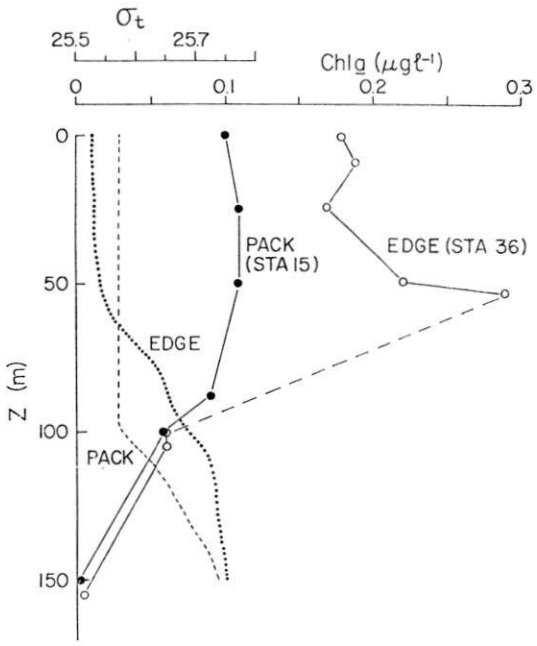

Fig. 3. Comparison of depth profiles of chlorophyll *a* and sigma-t (σ_t) between a station in the pack ice (STA 15) and in the IEZ (STA 36)

that area. Concentrations are low and uniform down to the pycnocline, and then decrease to near zero. The decrease in chlorophyll always occurred at the same depth as the pycnocline. Integrated chlorophyll *a* above the pycnocline (n = 17) averages 11.7 (SD = ± 2.67) mg m^{-2}. At Station 36, in the IEZ, water column chlorophyll *a* doubles to 21.9 mg m^{-2}. This increase is associated with a much shallower isopycnal layer and of course, less ice cover. Thus the increase in phytoplankton biomass, as indicated by chlorophyll *a*, may be due to an increase in the availability of light for growth through an increase in stratification and a reduction in ice cover.

This feature in the data is borne out by some biological characteristics of the populations as well (Table 1). The P^b *vs.* I curve parameters (Equation 1, P^b max and α), increase dramatically in the sample from Station 36; the approximately 2.5x difference in P^bmax for the ice edge station is significant at $P < 0.05$ (Fig. 4). The populations beneath the pack ice, although the

Table 1. Comparison of environmental and biological variables between stations occupied in the pack ice (mean ± S.D.) and the station at the ice edge zone, Station 36 (58° 21.9′ S / 00° 49.2′ W). Number of observations (n) in parentheses where means of observations are reported

Variables	Pack ice	Station 36
Sea surface temperature (°C)	−1.81	−1.78
Surface irradiance (1y d^{-1})	115±19 (n=8)	94
Nitrate-nitrogen (μg-at l^{-1})	28.4	29.1
Ice cover (tenths)	9–10	6
Euphotic zone depth (1% I_o) (m)	2	~ 70
Chlorophyll *a* (mg m^{-2})	11.7±2.6 (n=17)	22.0
α [mgC (mg Chl *a*)$^{-1}$ h^{-1} (μEinst m^{-2} s^{-1})$^{-1}$]	0.012±0.009 (n=8)	0.027
P^b_{max} [mgC (mg Chl *a*)$^{-1}$ h^{-1}]	1.34±0.254	3.82

euphotic zone is only a few m deep, exhibit no significant photoinhibition. However, there is a 20 % decrease in photosynthesis at the highest irradiance in the IEZ sample. We have no explanation for this difference in photoinhibitory behavior.

The continuous measurement of chlorophyll *a* fluorescence on the transect exiting the pack ice field (Fig. 2) allows a further evaluation of the increase in biological activity at the ice edge. Station 36 (Fig. 3) occurs at the southern edge of a localized increase in surface chlorophyll *a* within the IEZ. Surface chlorophyll *a* increased about fourfold while the ship drifted to the east on Station 36. Upon getting underway, chlorophyll *a* continued to rise, within 10 km reaching 1 mg m^{-3} (or more) and remained high for

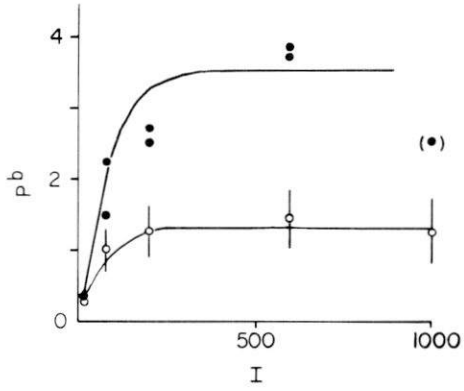

Fig. 4. Comparison of chlorophyll *a*-specific photosynthesis (P^b) *vs.* irradiance (I) curves for samples taken from beneath the pack ice (open symbols) and a sample taken at Station 36, in the IEZ (closed symbols). Open symbols are means (and error bars are standard deviations) of all experiments (n = 7) conducted while in the pack ice. Curves were drawn using parameters derived from Equation (1). P^b has units of mg C (mg Chl*a*)$^{-1}$ m^{-3} h^{-1}, and I has units of μEin m^{-2} s^{-1}

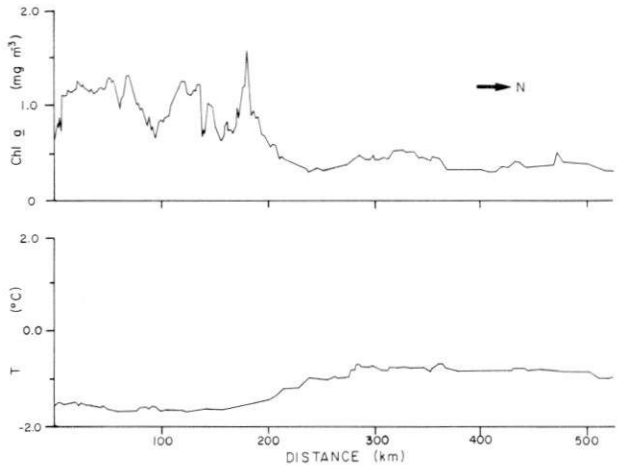

Fig. 5. Near-surface chlorophyll *a* (top) and temperature (bottom) *vs.* distance plots for the transect beginning upon departure of Station 36 (km = 0). Chlorophyll *a* units are mg m^{-3}, temperature units °C. There is a systematic error in the temperature plot of about 0.4 C° due to warming of water as it passes through the ship's pumping system

the next 200 km (Fig. 5). Beyond this, temperature increased gradually by 1 C° and chlorophyll *a* coincidentally decreased by ~ 1.0 mg m^{-3}. There is some spatial variability in chlorophyll *a* in the IEZ (Fig. 5), however, the spectrum of this variability shows no significant peaks relative to the temperature variance spectrum. Therefore, both temperature and chlorophyll *a* have a common source of variability (Denman, 1976).

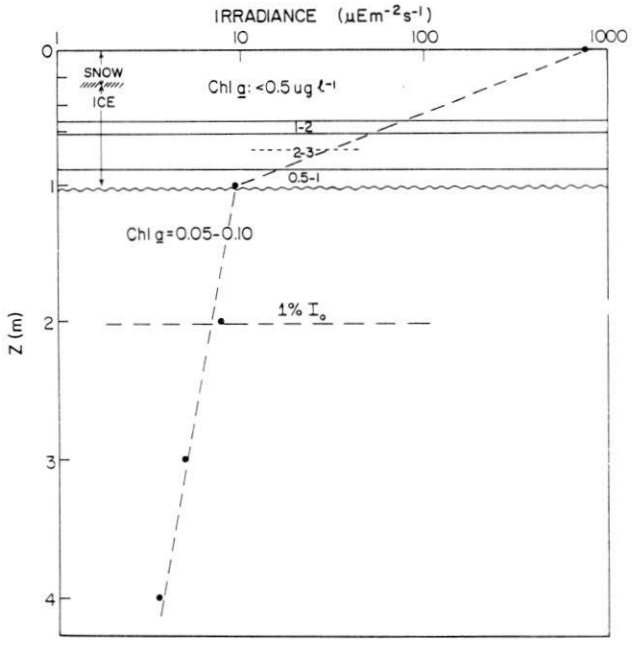

Fig. 6. Generalized schematic of chlorophyll *a* distribution in relation to snow and ice cover, and light attenuation through the ice. Chlorophyll *a* values are approximate; actual values for the cores are presented in Clarke and Ackley (1984)

This source of variability must be a physical process, which does not provide enough persistence to allow spatial variability (due to phytoplankton growth) to develop (Denman et al., 1977; Marra et al., 1982a).

In the area covered by the pack ice, a variable but significant proportion (10 to 30 %) of the biomass of the phytoplankton (as indicated by chlorophyll *a*) is located within the ice column itself. For the Weddell Sea Expedition, Clarke and Ackley (1984) and Burckle (in prep.) treat this complex subject in more detail. In general, chlorophyll *a* concentrations increase in the bottom third of the ice column, much as pictured schematically in Fig. 6. The distribution of chlorophyll *a* correlates positively with the distribution of diatom cells (Clarke and Ackley, 1984). Fig. 6 also shows the attenuation of light through the ice for the one station where we were able to make light measurements. The maximum chlorophyll *a* layer occurs from 1 to 10 % of surface irradiance (assuming exponential decay through the ice). Common species found in the ice include *Nitszchia closterium, N. curta* and *Tropidoneis* sp., all pennates, and presumably able to move within the interstices of ice crystals. The other striking feature about the pack ice is the presence of abundant and apparently active heterotrophic populations of bacteria and microflagellates (Marra et al., 1982b). Bacteria, enumerated by the method of epifluorescence microscopy (Daley and Hobbie, 1975), are very large (1 to 3 μm in length) compared to bacteria found in the water column beneath the ice.

DISCUSSION

In general, the chlorophyll *a* distributions and the photosynthesis parameters suggest that the phytoplankton populations in the Antarctic during the months of maximum ice extent are largely regulated by the availability of light. A similar conclusion was reached by El-Sayed and Taguchi (1981) for the Weddell Sea in summer. The IEZ exhibited greater water column stability, less ice cover, and anywhere from 2 to 10 times the amount of chlorophyll *a* compared to the water column beneath the pack ice (Fig. 2, 3 and 5). Differences in nutrient concentrations were not of a magnitude to suggest that these might regulate distributions, and differences in temperature were negligible (Table 1; Fig. 2). The increase in P^bmax and α (Table 1; Fig. 4) at the ice edge may be interpreted as a physiological response to greater availability of light (Beardall and Morris, 1976; Falkowski, 1980). Although our measurements suggest a euphotic zone (i.e. 1 to 100 % of surface irradiance) extending only 1 to 2 m below the pack ice, and mixed layers to about 100 m, our samples show the populations to have more

typical responses to higher light intensities. There is no severe photoinhibition (cf. Bunt, 1964) and the light intensity at which photosynthesis is maximal is similar to phytoplankton species of temperate and tropical environments (Yentsch and Lee, 1966). Some sea ice diatoms are able to retain viability in darkness (Bunt and Lee, 1972) and other diatom species can remain viable for long periods under extremely low light conditions (Thorne, 1981). At these latitudes (55 to 60° S) there are still about 6 h of daylight at the winter solstice, thus the populations never experience a period of winter darkness. Also, transient leads in the ice would increase the amount of light reaching the under-ice populations and may be a factor in their maintenance.

Significant amounts of chlorophyll *a* are found within the pack ice itself (Fig. 6). This may be part of an active biological community consisting of bacteria, algae and microflagellates that exists in interstices between ice crystals (Marra et al., 1982b). Based on our measurement of light attenuation through the ice at one station, the typical maximum in chlorophyll *a* was found at 1 to 10 % of surface irradiance, which is within the same range of light levels where subsurface chlorophyll maxima are found in stratified water columns (e.g. Cullen and Eppley, 1981).

Much has been written concerning the biological significance of ice edges for all trophic levels (Marr, 1962; Siniff et al., 1970; MacKintosh, 1972; Alexander, 1980; Ainley and Jacobs, 1981; Stirling and Cleator, 1981). It has been hypothesized that the ultimate reason for the importance of ice edges to zooplankton, nekton, mammals, and birds, is the occurrence of enhanced levels of primary production. This has been documented in a few cases (El-Sayed, 1971; Alexander, 1980), but the specific phenomena at ice edges leading to enhanced phytoplankton growth there relative to open water areas are not understood. One possibility is that the algae contained in the pack ice are released upon melting to grow later. This idea is attractive from the standpoint that overwintering in the ice may be part of the seasonal dynamics of Antarctic phytoplankton (Ackley et al., 1979). To our knowledge there is no evidence which would support this idea for the Southern Ocean, although Alexander (1980) found dissimilar populations from sea ice and water column samples in the Bering Sea. Another possibility is that, given the activity of bacteria and heterotrophs in the pack ice (Marra et al., 1982b), the meltwater is suitably 'conditioned' with trace substances and organic chelators (Barber and Ryther, 1969). In support of this hypothesis, Dunbar (1981) reports experiments showing a stimulant effect by melted ice on the growth of laboratory cultures of microalgae. Finally, ice edge blooms may result from purely physical phenomena. Melting pack ice will stabilize the top 5 to 10 m of the surface layer through input of fresh water, and wind-induced mixing may be reduced near the ice edge, contributing to stabilization of the water column.

During the Weddell Polynya Expedition, we observed localized increases in surface chlorophyll *a* an order of magnitude greater than the values found to the south (in the pack ice region) and 4 times greater than values seaward of the IEZ (Fig. 2 and 5). This localized increase in phytoplankton biomass is associated with greater stratification than further south (Fig. 3) and a decrease in surface salinity which lightens the surface layer by 0.6 sigma-t units (Fig. 2). This is evidence, therefore, suggesting ice-melt freshening of the surface layer as the reason for the IEZ phytoplankton increase. The biomass increase we observe did not appear to be derived from the seed populations contained within the ice. We have no preserved samples from this region; however, *Corethron hystrix* Castracane and other chain-forming centrics were captured in the zooplankton nets. *C. hystrix* is commonly found in this area of the Weddell Sea (Hart, 1942). This lack of correspondence in water column and ice algae agrees with the finding of Alexander (1980); but we point out that given inadequate knowledge of the temporal dynamics of the ice edge, the importance of seeding with sea-ice algae to the ice edge bloom would be difficult to establish or to rule out. Certainly, *C. hystrix* and other centrics have been found to be present in sea ice (Hart, 1942; Burkholder and Mandelli, 1965).

It may be significant that neither El-Sayed and Taguchi (1981) nor Glibert et al. (1982) found enhanced concentrations of chlorophyll *a* at the summertime ice edge in the Antarctic. It is possible, therefore, that the enhanced phytoplankton activity may be associated with the seasonally receding ice edge and break-up of the winter ice pack. Furthermore, a reduction of wind-induced mixing at ice edges should occur regardless of season. This lends additional circumstantial support to the idea of melt-water stabilization of the water column near ice-edges as the primary factor leading to enhanced productivity of the IEZ. Smith and Nelson (in press) have come to a similar conclusion regarding the distribution of chlorophyll *a* near a receding ice edge in the Ross Sea. The possibility remains that some chemical agent, melted out of the ice, promotes growth of water column phytoplankton (Dunbar, 1981), but this effect should be secondary to any change in water stratification caused by melting. Then too, any organic chelator (for example) will undergo substantial dilution by the surrounding seawater.

In summary, the evidence suggests that the availability of light modulated through water column stratification, ice cover, and melt-water stabilization controls

the distribution of phytoplankton biomass (as indicated by chlorophyll *a*) in the Weddell Sea in late austral winter. The increase in chlorophyll *a* at the IEZ is associated with shallower mixed layers and reductions in surface salinity, both of which would contribute to greater water column stability. Where the water column is covered by ice, the euphotic zone depth is 1 to 2 m, and a significant portion of the phytoplankton (compared to the water column) is found within the pack ice. Although our evidence is indirect, the populations existing in the ice appear healthy and active (Marra et al., 1982b; Clarke and Ackley, 1984).

Since the euphotic zone beneath the pack ice is so shallow, production rates there are probably close to zero. Using the P^b-I curve data, a calculation similar to that of Burkholder and Burkholder (1967) indicates a rate of primary production at Station 36 of 136 mg m^{-2} d^{-1}, consistent with rates found by others (Volkovinsky, 1964; Burkholder and Mendelli, 1965; Burkholder and Burkholder, 1967; El-Sayed, 1968). The ice edge bloom, evident from the underway sampling system, reaches 1 to 2 mg m^{-3}. If the same P^b-I relation holds there, and allowing for an increase in light attenuation with the higher chlorophyll *a* concentrations (Riley, 1956), rates of production for the ice edge bloom would approach 300 to 400 mg m^{-2} d^{-1}. Both the chlorophyll biomass and the primary production estimate for the ice-edge bloom are higher than other values we have found in the literature for similar latitudes and similar times of the year (Burkholder and Burkholder, 1967; Bolter and Dawson, 1982). Clearly, any new estimates of primary production for the Southern Ocean will have to take into account the biological dynamics at the ice edge zone.

Acknowledgements. This research was supported under grant no. DPP-80-08011 awarded by the National Science Foundation. We thank S. Ackley for supplying the ice core samples from which the chlorophyll analyses were made, A. L. Gordon and B. Huber for the use of hydrographic data, and J. Jennings for use of the surface nutrient data. G. L. Landriau, Jr. performed much of the data reduction. We are grateful to the officers and crew of R.V. 'Mikhail Somov' for assistance in data collection, and express our deep appreciation for their professionalism. Comments by S. Jacobs led to a much improved manuscript. Lamont-Doherty Geological Observatory Contr. No. 3687.

LITERATURE CITED

Ackley, S. F., Buck, K. R., Taguchi, S. (1979). Standing crop of algae in the sea ice of the Weddell Sea region. Deep Sea Res. 26: 269–281

Ackley, S. F., Smith, S. J. (1983). Reports of the U.S.-U.S.S.R. Weddell Polynya Expedition, October-November 1981. Sea ice observations. Vol. 5. Spec. Rep. 83-2 U.S. Army Cold Reg. Res. and Eng. Lab., Hanover, N.H.

Ainley, D. G., Jacobs, S. S. (1981). Sea bird affinities for ocean and ice boundaries in the Antarctic. Deep Sea Res. 28: 1173–1185

Alexander, V. (1980). Interrelationships between the seasonal sea ice zone and biological regimes. Cold Reg. Sci. Technol. 2: 157–178

Barber, R. T., Ryther, J. H. (1969). Organic chelators: factors affecting primary production in the Cromwell Current upwelling. J. exp. mar. Biol. Ecol. 3: 191–199

Bates, S. S. (1976). Effects of light and ammonium on nitrate uptake by two species of estuarine phytoplankton. Limnol. Oceanogr. 21: 212–218

Beardall, J., Morris, I. (1976). The concept of light intensity adaptation in marine phytoplankton: some experiments with *Phaeodactylum tricornutum*. Mar. Biol. 37: 377–387

Biggs, D. C. (1978). Comment on 'non-biogenic fixed nitrogen in Antarctic surface waters'. Nature, Lond. 276: 96–97

Bolter, M., Dawson, R. (1982). Heterotrophic utilisation of biochemical compounds in Antarctic waters. Neth. J. Sea Res. 16: 315–332

Bunt, J. S. (1964). Primary productivity under sea ice in Antarctic waters. I. Concentrations and photosynthetic activities of microalgae in the waters of McMurdo Sound, Antarctica. In: Lee, M. O. (ed.) Biology of the Antarctic Seas (Antarctic Research Series 1). American Geophysical Union, Washington, D.C., p. 13–26

Bunt, J. S. (1968). Some characteristics of microalgae isolated from Antarctic sea ice. In: Llano, G. A., Schmitt, W. L. (ed.) Biology of the Antarctic Seas (Antarctic Research Series II). American Geophysical Union, Washington, D.C., p. 1–14

Bunt, J. S., Lee, C. C. (1972). Seasonal primary production in Antarctic sea ice at McMurdo Sound in 1967. J. mar. Res. 28: 305–320

Burkholder, P. R., Burkholder, L. M. (1967). Primary productivity in surface waters of the South Pacific Ocean. Limnol. Oceanogr. 12: 606–617

Burkholder, P. R., Mandelli, E. F. (1965). Productivity of microalgae in Antarctic sea ice. Science, N.Y. 149: 872–874

Clarke, D. B., Ackley, S. F. (1984). Sea ice structure and biological activity in the Antarctic marginal ice zone. J. geophys. Res. 89: 2087–2095

Cullen, J. J., Eppley, R. W. (1981). Chlorophyll maximum layers of the Southern California Bight and possible mechanisms of their formation and maintenance. Oceanologica Acta 4: 23–32

Daley, R. J., Hobbie, J. E. (1975). Direct counts of aquatic bacteria by a modified epifluorescence technique. Limnol. Oceanogr. 20: 875–882

Denman, K. L. (1976). Covariability of chlorophyll and temperature in the sea. Deep Sea Res. 23: 539–550

Denman, K. L., Okubo, A., Platt, T. (1977). The chlorophyll fluctuation spectrum in the sea. Limnol. Oceanogr. 22: 1033–1038

Dunbar, M. J. (1981). Physical causes and biological significance of polynyas and other open water in sea ice. In: Stirling, I., Cleator, H. (ed.) Polynyas in the Canadian Arctic. Canadian Wildlife Service, Ottawa. Occ. Pap. No. 45

El-Sayed, S. Z. (1968). Primary productivity of the Antarctic and the subantarctic. In: Balech, E., El-Sayed, S. Z., Hasle, G., Neushul, M., Zaneveld, J. S. (ed.) Antarctic map folio series. American Geographical Society, New York (Folio 10)

El-Sayed, S. Z. (1970). On the productivity of the Southern Ocean. In: Holdgate, M. W. (ed.) Antarctic ecology, Vol. 1. Academic Press, New York, p. 119–135

El-Sayed, S. Z. (1971). Observations on phytoplankton bloom in the Weddell Sea. In: Llano, G. A., Wallen, I. E. (ed.) Biology of the Antarctic Seas (Antarctic Research Series IV) Vol. 17. American Geophysical Union, Washington, p. 301–312

El-Sayed, S. Z. (1978). Primary productivity and estimates of potential yields of the Southern Ocean. In: McWhinnie, M. A. (ed.) Polar research. Am. Ass. Adv. Sci., Washington D. C., p. 141–159

El-Sayed, S. Z., Taguchi, S. (1981). Primary production and standing crop of phytoplankton along the ice edge in the Weddell Sea. Deep Sea Res. 28: 1017–1032

El-Sayed, S. Z., Weber, L. H. (1982). Spatial and temporal variations in phytoplankton biomass in the Southwest Atlantic and the Scotia Sea. Polar Biol. 1: 83–90

Eppley, R. W. (1972). Temperature and phytoplankton growth in the sea. Fish. Bull. U.S. 70: 1063–1085

Eppley, R. W., Rogers, J. N., McCarthy, J. J. (1969). Half-saturation constants for the uptake of nitrate and ammonium by marine phytoplankton. Limnol. Oceanogr. 14: 912–920

Falkowski, P. G. (1980). Light-shade adaptation in marine phytoplankton. In: Falkowski, P. G. (ed.) Primary productivity in the sea. Plenum Press, New York, p. 99–119

Glibert, P. M., Biggs, D. C., McCarthy, J. J. (1982). Utilization of ammonium and nitrate during austral summer in the Scotia Sea. Deep Sea Res. 29: 837–850

Gordon, A. L., Molinelli, E. J. (1982). Southern Ocean Atlas: thermohaline and chemical distribution and the Atlas Data Set. Southern Ocean Atlas. Columbia University Press, New York

Gordon, A. L., Huber, B. A. (1982). Physical oceanography during WEPOLEX-81. Ant. J. U.S. 17: 98–100

Hart, T. J. (1942). Phytoplankton periodicity in Antarctic surface waters. 'Discovery' Rep. 21: 261–356

Holm-Hansen, O., Lorenzen, C. J., Holmes, R. W., Strickland, J. D. H. (1965). Fluorometric determination of chlorophyll. J. Cons. perm. int. Explor. Mer 30: 3–15

Holm-Hansen, O., El-Sayed, S. Z., Franceschini, G. A., Cuhel, R. L. (1977). Primary production and the factors controlling phytoplankton growth in the Southern Ocean. In: Llano, G. (ed.) Adaptations within Antarctic ecosystems. Gulf Publ. Co., Houston, p. 11–50

Jassby, A. D., Platt, T. (1976). Mathematical formulation of the relationship between photosynthesis and light for phytoplankton. Limnol. Oceanogr. 21: 540–547

MacKintosh, N. A. (1972). Life cycle of Antarctic krill in relation to ice and water conditions. 'Discovery' Rep. 36: 1–94

Malone, T. C., Neale, P. J. (1981). Parameters of light-dependent photosynthesis for phytoplankton size fractions in temperate estuarine coastal environments. Mar. Biol. 61: 289–297

Marr, J. W. S. (1962). The natural history and geography of the Antarctic krill. 'Discovery' Rep. 32: 33–464

Marra, J., Houghton, R. W., Boardman, D. C., Neale, P. J. (1982a). Variability in surface chlorophyll *a* at a shelf-break front. J. mar. Res. 40: 575–591

Marra, J., Burckle, L. H., Ducklow, H. W. (1982b). Sea ice and water column plankton distributions in the Weddell Sea in late winter. Ant. J. U.S. 17: 111–112

McCarthy, J. J., Taylor, W. R., Taft, J. L. (1977). Nitrogenous nutrition of the plankton in the Chesapeake Bay. I. Nutrient availability and phytoplankton preferences. Limnol. Oceanogr. 22: 996–1011

Neori, A., Holm-Hansen, O. (1982). Effect of temperature on rate of photosynthesis in Antarctic phytoplankton. Polar Biol. 1: 33–38

Olson, R. J. (1980). Nitrate and ammonium uptake in Antarctic waters. Limnol. Oceanogr. 25: 1064–1074

Riley, G. A. (1956). Oceanography of Long Island Sound, 1952–1954. II. Physical Oceanography. Bull. Bingham oceanogr. Coll. 15: 15–46

Siniff, D. B., Cline, D. R., Erickson, A. W. (1970). Population densities of seals in the Weddell Sea, Antarctica, in 1968. In: Holdgate, M. W. (ed.) Antarctic ecology, Vol. 1. Academic Press, London, p. 377–394

Slawyk, G. (1979). ^{13}C and ^{15}N uptake by phytoplankton in the Antarctic upwelling area: results from the Antiprod I Cruise in the Indian Ocean sector. Aust. J. mar. Freshwat. Res. 30: 431–448

Smith, W. O., Jr., Nelson, D. M. (in press). Phytoplankton biomass near a receding ice-edge in the Ross Rea. In: Siegfried, W. (ed.) Proceedings Fourth SCAR Symposium on Antarctic Biology. Springer-Verlag, Berlin

Stirling, I., Cleator, H. (ed.) (1981). Polynyas in the Canadian Arctic. Canadian Wildlife Service, Ottawa. Occ. Pap. No. 45:1–73

Syrett, P. J. (1981). Nitrogen metabolism of microalgae. In: Platt, T. (ed.) Physiological bases of phytoplankton ecology. Can. Bull. Fish. Aquat. Sci. 210: 182–210

Thorne, D. B. (1981). Effects of light intensity and temperature on the respiration, photosynthesis, and cytoplasm structure of a marine diatom *(Amphora coffaeformis).* Ph. D. thesis, Columbia University Teachers College

Volkovinsky, V. V. (1964). Studies of primary production in the waters of the S. Atlantic Ocean. Abstract 2nd International Oceanography Congress. Nauka, Moscow 1966: 386–387

Walsh, J. J. (1971). Relative importance of habitat variables in predicting the distribution of phytoplankton at the ecotone of the Antarctic upwelling ecosystem. Ecol. Monogr. 41: 291–309

Withrow, R. B., Withrow, A. P. (1956). Generation control and measurement of visible and near visible radiant energy. In: Hollaender (ed.) Radiation biology, Vol. 3. McGraw-Hill, New York, p. 125–258

Yentsch, C. S., Lee, R. W. (1966). A study of photosynthetic light reactions, and a new interpretation of sun and shade phytoplankton. J. mar. Res. 24: 319–337

This paper was submitted to the editor; it was accepted for printing on June 11, 1984

Vol. 19: 207–210, 1984 | MARINE ECOLOGY – PROGRESS SERIES Mar. Ecol. Prog. Ser. | Published October 10

Siliceous microfauna in waters beneath Antarctic sea ice

Joseph J. Morley and Jeanne C. Stepien

Lamont-Doherty Geological Observatory of Columbia University, Palisades, New York 10964, USA

ABSTRACT: Plankton tows sampling various water depths beneath Antarctic sea ice recovered a high proportion of the cold water assemblage of Radiolaria present in Recent surface sediments underlying these waters. Of the 3 depth intervals sampled, the highest abundances of polycystine Radiolaria were collected in vertical tows from the upper 100 m. Phaeodarian radiolarians occupy a slightly deeper habitat in ice-covered waters with highest concentrations occurring in tows sampling depths between 100 and 200 m. The water structure at the ship station where the highest numbers of polycystine radiolarians were collected was unique in that it consisted of an entrained warm cell of Weddell Deep Water surrounded by cold Weddell Deep Water.

INTRODUCTION

It has been known for some time that siliceous microfauna are capable of living under sea ice in the Arctic (Hülsemann, 1963; Tibbs, 1967). Until recently, however, very little was known about radiolarian abundance and distribution in ice-covered Antarctic waters. Samples taken during the recently completed Weddell Polynya Expedition permit examination of the late winter/early spring radiolarian population living beneath Antarctic sea ice. As the sampling platform for this joint US-USSR expedition, R/V 'Mikhail Somov' remained within the Antarctic ice field from the last week in October through the second week in November 1981. During this time, various physical, biological and atmospheric measurements were taken along a transect in the Atlantic sector of the Antarctic Ocean which extended nearly 600 km within the sea ice. This report summarizes the radiolarian analyses from plankton-tow samples, comparing faunal abundances with those reported from the open ocean as well as with fauna preserved in the underlying Recent surface sediments.

METHODS

Radiolaria were collected at 14 stations using 75 cm diameter, 64 micron-mesh plankton nets equipped with flow meters and rigged for opening and closing. The nets were vertically towed over 3 depth intervals: 0 to 100 m, 100 to 200 m and 1,000 to 2,000 m. Because of malfunctions in net operation and/or flow meters at several of these stations, this report is limited to describing the radiolarian fauna in tows from only 8 of the 14 stations.

Initial sample preparation consisted of splitting the sample using a plankton splitter into 1/8 to 1/2 portions of the whole, based on the radiolarian density in each sample. After rinsing the split of the total sample through 250 and 63 micron sieves, the residue was placed in 35 % hydrogen peroxide and put in a 60 °C oven for 24 h. This oxidation process removed all organic material from the siliceous skeletons. Hydrochloric acid (37 % solution) was added to dissolve all calcareous organisms. After a final rinsing in distilled water, the entire residue was mounted on glass slides. Complete specimens (> 50 % of skeleton intact) belonging to the 2 major groups of Radiolaria (Phaeodaria and Polycystine) were identified and counted on each slide. Phaeodarian (tripylean) skeletal material differs from that of polycystine radiolarians in that it is composed of a combination of organic substances and silica rather than entirely of amorphous silica. No attempt was made to distinguish between specimens which had been living and those which were dead when collected. Species' counts were converted to number of individuals per cubic m of water filtered by the net (ind m^{-3}).

0171-8630/84/0019/0207/$ 02.50

RESULTS AND DISCUSSION

Station number (CTD), water depth sampled and calculated values (ind m^{-3}) for Polycystines and Phaeodaria for each of the tows are shown in Table 1. Tows taken at Ship Station 36,37 sampled plankton at the sea-ice edge, whereas, the remaining 11 tows sampled plankton at various sites within the Antarctic sea ice (for location of ship (CTD) stations see Fig. 1 in Marra and Boardman, 1984). The number of polycystine Radiolaria in samples collected between 0 and 100 m ranged from 20 to 154 ind m^{-3}. In the nets towed from 100 to 200 m depths, the number of polycystine radiolarians varied between 9 and 69 ind m^{-3}. In the deep tows (1,000 to 2,000 m), polycystine radiolarian abundances of 8 and 18 ind m^{-3} were measured. These values are an order of magnitude lower than those reported for plankton-tow data over similar depth intervals from transects across the equatorial Pacific (Petrushevskaya, 1971; Renz, 1976) and the Gulf Stream off Florida (Casey et al., 1979). However, they are similar to radiolarian abundances calculated in samples collected from the central portion of the North Atlantic subtropical gyre (Casey et al., 1979) and the North Pacific (Kling, 1979).

Examination of the Weddell Polynya Expedition data from ship stations where plankton tows from both 0 to 100 and 100 to 200 m were taken shows that greater numbers of polycystine radiolarians were recovered in tows from the upper 100 m than from the 100 to 200 m interval. Whether living in waters covered by sea ice (this study) or in the open ocean (Petrushevskaya, 1971; Renz, 1976; Casey et al., 1979; Kling, 1979), polycystines occur in highest concentrations in the upper 100 to 150 m of the water column.

The highest number of polycystine radiolarians occurred in a plankton tow which sampled the interval between 0 and 100 m at Ship Station 27,28. Of the 7 ship stations where siliceous plankton were collected beneath the sea ice, this station was the only one to overlie a warm cell of Weddell Deep Water (WDW) within the Weddell cold regime (Fig. 1). As reported by Gordon and Huber (1984), the water in this cell is warmer, saltier, denser and has a higher oxygen content than water from corresponding depths at the other 6 ship stations. The top of the pycnocline is also shallower in this warm cell compared to its position in the surrounding colder WDW. It has been proposed (Gordon and Huber, 1984) that these warm WDW cells are created at the frontal zone separating warmer WDW inflow from colder WDW outflow. Unfortunately, no radiolarian samples were collected at other ship stations where cells of warmer WDW were detected (e.g. Ship Station 32) so we are unable to determine if higher concentrations of polycystine radiolarians were present at these stations as well. Nevertheless, these initial results indicate that polycystine radiolarians inhabit the warmer, saltier, and more oxygenated waters of the warm WDW at higher abundance levels than in the surrounding cold WDW.

The same polycystine radiolarian species were typically present in the 0 to 100 m and 100 to 200 m intervals at all seven ship stations where tows from these specific depths were made. *Spongotrochus glacialis* Popofsky is the most abundant species in samples from the upper 100 m interval and from 100 to 200 m. It is followed in abundance at these levels by *Antarctissa denticulata* Ehrenberg, *Lithelius nautiloides* Popofsky and *Triceraspyris antarctica* Haeckel. All 4 species are present in lower concentrations in tows from 100 to 200 m than from 0 to 100 m. Plankton-tow samples over comparable water-depth intervals beneath the Arctic sea ice also contain *S. glacialis* as the most abundant polycystine radiolarian (Hülsemann, 1963; Tibbs, 1967). In the 2 deep tows (1,000 to 2,000 m) from the Antarctic data set, *Spongurus pylomaticus* Riedel and *S. glacialis* occur in higher concentrations than any other polycystine radiolarians.

With the exception of the ice-edge station (Ship

Table 1. Abundance of phaeodarian and polycystine radiolarians in Weddell Polynya Expedition plankton samples, expressed as numbers of individuals m^{-3} of filtered water

Ship station	Sample depth (m) 0–100		100–200		1000–2000	
	Phaeodaria	Polycystines	Phaeodaria	Polycystines	Phaeodaria	Polycystines
7, 8	33	20	35	9		
9, 10	29	22				
22, 25					4	18
27, 28	41	154				
29, 30	23	99	132	69		
31	24	62	101	24		
34	11	49	21	25		
36, 37	76	108	70	68	6	8

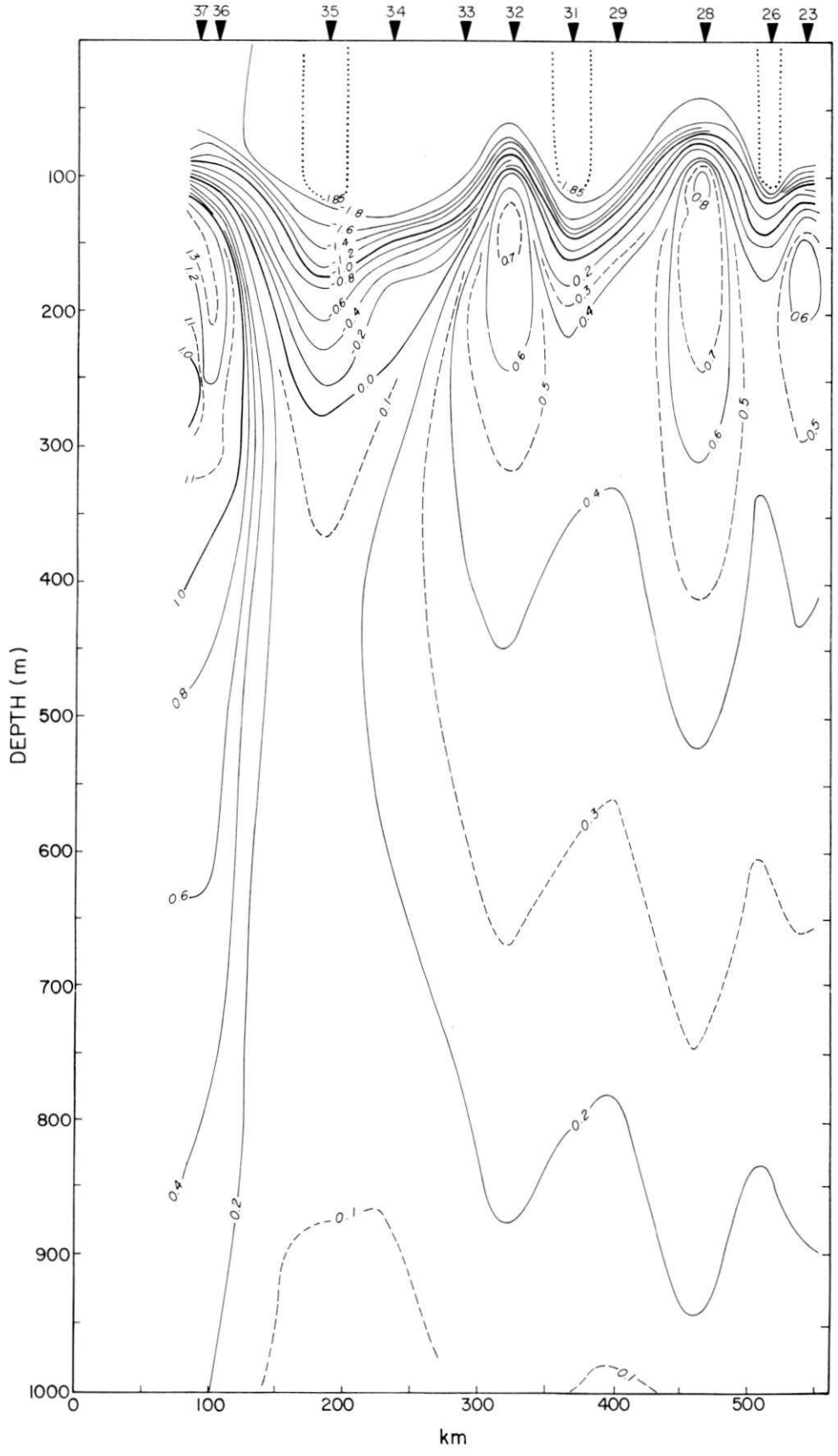

Fig. 1. Potential temperature section compiled from hydrographic stations occupied during exit transect from Antarctic pack ice. Black arrows: location of individual CTD stations along transect

Station 36,37), phaeodarians occur in higher abundances in tows from 100 to 200 m than from 0 to 100 m when comparing results from ship stations where plankton tows from both 0 to 100 m and 100 to 200 m were taken. Examination of individual phaeodarian abundances in the samples taken within the Antarctic sea ice shows that *Challengeron bicorne* Haecker is the most abundant species in tows sampling depths between 0 and 100 m and between 100 and 200 m. In all 3 tows at the ice-edge station, *Protocystis harstoni* Murray occurs in higher concentrations than any other Phaeodaria. Higher concentrations of phaeodarians compared to polycystine radiolarians were encountered in the upper 100 m at the 2 ship stations sampled on the poleward transect (Ship Stations 7,8 and 9,10), whereas, polycystine abundances were higher than phaeodarian radiolarians in tows sampling the upper 100 m at all ship stations on the northward leg of the expedition (Ship Stations 27,28 through 36,37).

We compared the polycystine radiolarian fauna in the Antarctic plankton tows with the fauna in Recent surface-sediment samples from the Atlantic sector of the Antarctic Ocean south of 55° S. Five of the 6 species that dominate the Antarctic radiolarian cold water (polar) assemblage defined by Lozano and Hays (1976) from factor analysis of surface-sediment samples in the Antarctic and subantarctic are also present in the plankton in relatively high abundances. Only 1 of the 7 species that show the greatest affinity for the warm water (subantarctic) assemblage defined by Lozano and Hays, however, was collected in our plankton tows. This indicates that the occurrence of most of the members of the warm water assemblage in Antarctic waters may be limited to times of the year other than late winter or early spring when the water properties are more favorable, or that these species were in such low abundances in the Antarctic waters in October and November that they eluded the plankton nets and consequently were not observed in our samples.

CONCLUSIONS

Although radiolarian abundances in waters beneath Antarctic sea ice are not as high as those from highly productive regions of the open ocean, they are similar to those in less productive waters of the central North Atlantic and North Pacific. The highest concentrations of polycystine radiolarians in the ice-covered Antarctic waters appear to be related to a warm cell of WDW which had been trapped in the surrounding colder WDW. The majority of polycystine species captured in the plankton tows correspond with those which compose the cold water assemblage in the surface sediments underlying the survey area. In the upper 200 m of water beneath Antarctic sea ice, polycystine radiolarians occur in the highest concentrations between 0 and 100 m, whereas, phaeodarian radiolarians are most abundant in the interval between 100 and 200 m.

Acknowledgements. We thank our fellow WEPOLEX members and N. R. Swanberg for critically reviewing this manuscript and offering helpful comments. Data shown in Fig. 1 were provided by A. L. Gordon and B. A. Huber. J. J. M. thanks A. Pesanell for her laboratory assistance. This research was directly supported by National Science Foundation grants DDP80-08011 and OCE79-24563 to Lamont-Doherty Geological Observatory. Lamont-Doherty Geological Observatory of Columbia University Contribution No. 3688.

LITERATURE CITED

Casey, R., Spaw, J. M., Kunze, F., Reynolds, R., Duis, T., McMillen, K., Pratt, D., Anderson, V. (1979). Radiolarian ecology and the development of the radiolarian component in Holocene sediments, Gulf of Mexico and ajdacent seas with potential paleontological applications. Gulf Coast Ass. Geol. Soc. Trans. 29: 228–239

Gordon, A. L., Huber, B. A. (1984). Thermohaline stratification below the Southern Ocean sea ice. J. geophys. Res. 89: 641–648

Hülsemann, K. (1963). Radiolaria in plankton from the Arctic drifting station T-3, including the description of three new species. Arctic Inst. North Am., Tech. Paper 13, p. 1–52

Kling, S. A. (1979). Vertical distribution of polycystine radiolarians in the central North Pacific. Mar. Micropaleontology 4: 295–318

Lozano, J. A., Hays, J. D. (1976). Relationship of radiolarian assemblages to sediment types and physical oceanography in the Atlantic and western Indian Ocean sectors of the Antarctic Ocean. In: Cline, R. M., Hays, J. D. (ed.) Investigation of late Quaternary paleoceanography and paleoclimatology. Mem. geol. Soc. Am. 145: 303–336

Marra, J., Boardman, D. C. (1984). Late winter chlorophyll *a* distributions in the Weddell Sea. Mar. Ecol. Prog. Ser. 19: 197–205

Petrushevskaya, M. G. (1971). Spumellarian and nassellarian radiolaria in the plankton and bottom sediments of the central Pacific. In: Funnell, B. M., Riedel, W. R. (ed.) The micropaleontology of oceans. Cambridge University Press, Cambridge, England, p. 309–318

Renz, G. W. (1976). The distribution and ecology of Radiolaria in the central Pacific plankton and surface sediments. University of California Press, Berkeley, California, p. 1–267

Tibbs, J. F. (1967). On some planktonic Protozoa taken from the track of drift station ARLIS I, 1960–1961. Arctic Inst. North Am. 20: 247–254

This paper was submitted to the editor; it was accepted for printing on June 11, 1984

Antarctic Radiolaria in late winter/early spring Weddell Sea waters

Joseph J. Morley and Jeanne C. Stepien

Lamont-Doherty Geological Observatory of Columbia University, Palisades, New York 10964

ABSTRACT: During the 1981 cruise of the R/V *Mikhail Somov*, we examined the radiolarian population inhabiting Antarctic waters in late winter/early spring (October–November). Samples were collected with plankton tows at stations at the ice edge as well as hundreds of kilometers south of the ice edge. Concentrations of polycystine and phaeodarian Radiolaria in this unique data set are low, with abundances comparable to those reported from some less productive open-ocean regions. Polycystine Radiolaria occur in highest concentrations in the upper 100 m of the water column at the ice edge and beneath the sea ice. At the sea-ice stations, intermediate tows (100–200 m) contain the highest abundances of Phaeodaria. *Spongotrochus glacialis* is the most abundant polycystine present in shallow (0–100 m) and intermediate (100–200 m) tows, with *Spongurus pylomaticus* and *Spongotrochus glacialis* occurring in higher concentrations in deep tows (1000–2000 m) than any other polycystine radiolarian. In all the shallow and intermediate tows taken within the sea ice, the most abundant Phaeodaria present is *Challengeron bicorne*. At the ice edge, *Protocystis harstoni* replaces *C. bicorne* as the most commonly found phaeodarian.

INTRODUCTION

In the Antarctic today, the area covered by sea ice expands from approximately 3×10^6 km^2 in late summer (February) to 20×10^6 km^2 in late winter (September–October) (Zwally et al. 1979). Positioned south of 70°S in summer, the ice edge in the Atlantic sector of the Southern Ocean extends northward during some winters as far as 55°S. Although studies of the phytoplankton and zooplankton living in ice-covered waters near Antarctic field stations have been made (Ferreyra and Tomo 1979; Krebs 1983), few shipboard analyses have been made of the biologic activity beneath the late-winter Antarctic sea ice. One of the objectives of the joint US-USSR Weddell Polynya Expedition was to describe the phytoplankton and zooplankton living in the Antarctic's ice-covered waters as well as in the sea ice during late winter/early spring. The Russian icebreaker *Mikhail Somov*, the sampling platform for the Expedition, entered the ice on 20 October 1981 and proceeded to cut a path extending over 500 km through the sea-ice field. During the 25 days spent within the ice, numerous physical, biological, and atmospheric measurements were made at over 30 ship stations positioned along the south and north transects (text-fig. 1).

METHODS

Radiolaria were collected at 14 stations with ¾ m diameter, 64 μm-mesh plankton nets equipped with General Oceanic flow meters, double release mechanisms and, in some cases, Benthos Time-Depth Recorders. We attempted to sample plankton at three depth intervals: 0–100 m, 100–200 m and 1000–2000 m. Because of limited station time, however, deep (1000–2000 m) tows were made at only a few stations. The nets were lowered to the maximum water depth of the specific interval to be sampled, opened mechanically by a messenger weight, raised vertically to the minimum depth and closed with a second messenger. Ice conditions limited sampling to vertical hauls. In most instances samples from the two shallow depths were taken in series. Because of improper operation of the nets and/or flow meters at some stations, we present the results of analyses of tows taken at only 8 of the 14 stations (table 1).

During ship transit, the samples were preserved in a 5% solution of glutaraldehyde buffered with sodium borate. No tests were conducted to determine the ratio of live to dead specimens at the time of capture. Sample preparation in the laboratory consisted of an initial rinsing of a ⅛ to ½ split of the total sample through a 63-μm sieve. After washing the residue into a petri dish containing a 35% solution of hydrogen peroxide, the sample was placed in an oven at 60°C for a minimum of 24 hr. This portion of the process removed all organic material from the radiolarian tests. The addition of hydrochloric acid (37% solution) dissolved all calcareous organisms. As a final process, the sample was thoroughly washed through a 63-μm sieve and the residue uniformly distributed on glass slides using Canada balsam for a mounting medium. Identification was made of all complete specimens (>50% of skeleton) belonging to the two major groups of Radiolaria (polycystine and phaeodarian). Unlike the tests of polycystine Radiolaria, which consist entirely of amphorous silica, the hollow-tubed phaeodarian skeletons are composed of silica and small amounts of organic matter. To facilitate comparison of specific species counts in the various tows, all tabulations were converted to number of individuals per cubic m of water filtered by the net (ind/m^3).

DISCUSSION

The 14 samples examined in this study are listed in table 1, with date of sample collection, ship-station number, ship location, sea-ice coverage, the depth interval each net sampled, and the number of polycystine and phaeodarian Radiolaria per cubic m of water filtered. Three of the 14 samples were taken at the sea-ice edge (ship station 36,37); the remaining 11 at various stations within the Antarctic sea ice.

The shallow tows (0–100 m), for the most part, sampled a homogenous water layer above the thermocline where temperatures reached near-freezing values (text-fig. 2) and chlorophyll *a* levels were uniformly low (≤0.1 microgram/liter). At the ice-edge station, chlorophyll *a* concentrations reached levels twice as high as those measured at corresponding water depths at stations situated within the sea ice (Marra and Boardman 1984). Samples collected at intermediate depths

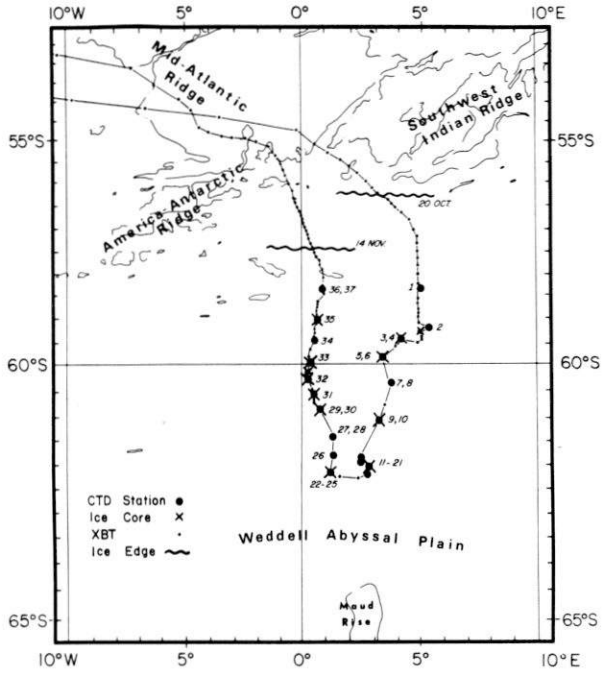

TEXT-FIGURE 1
Cruise track of R/V *Mikhail Somov* during the 1981 US-USSR Weddell Polynya Expedition, showing location of ship stations (CTD), ice coring sites (X) and bathythermograph (XBT) observations. Position of ice edge, corresponding to 3/10's ice coverage, shown at time of entry into and exit from pack ice.

(100–200 m) came from waters characterized by a steep potential temperature gradient, with temperatures averaging 1.5° to 3.0°C warmer than those recorded at shallower depths (text-fig. 2).

The overall radiolarian abundances in the Antarctic tows are lower than those recorded for most open-ocean regions except for the relatively low-productive waters of the central North Atlantic (Casey et al. 1979) and central North Pacific (Kling 1979). In the shallow tows (0–100 m), the number of polycystine Radiolaria ranged from 20 to 154 ind/m³ whereas the number of Phaeodaria varied between 11 and 76 ind/m³. The values for polycystine abundance in the five samples from the intermediate depths (100–200 m) varied between a low of 9 ind/m³ and a high of 69 ind/m³. Phaeodarian abundance in these same intermediate-depth samples ranged from 21 to 132 ind/m³. In the deep tows (1000–2000 m), polycystine and phaeodarian Radiolaria were present at much lower concentrations.

At the five stations where Radiolaria were collected simultaneously from both shallow and intermediate depths (ship stations 7,8; 29,30; 31; 34; 36,37), higher numbers of polycystine Radiolaria were captured in the shallow tows (0–100 m) when compared with their deeper (100–200 m) counterparts. Evidently, the polycystine Radiolaria preferred the homogenous cold waters found in the upper 100 m to the warmer intermediate waters. The highest number of polycystine Radiolaria did not occur in one of the tows taken at the ice edge as one might have expected, but in the shallow tow (0–100 m) made at ship station 27,28. Of the stations within the sea ice where radiolarian samples were collected, this was the only one to sample zooplankton within a warm cell of Weddell Deep Water (WDW). Gordon and Huber (1984) noted that the water in this warm cell is warmer, saltier and denser, and has higher oxygen levels than water from corresponding depths at other stations where radiolarian samples were taken. Although other warm cells of WDW were detected within the more dominant Weddell cold regime (i.e. ship station 32 in text-fig. 2), no radiolarian samples were taken at those stations to confirm this tentative association of increased levels of polycystine Radiolaria with warmer, saltier, more oxygenated waters of the WDW warm cells. Evidence in support of this preliminary conclusion can be drawn from previous analyses of zooplankton in waters beneath Arctic sea ice, where Tibbs (1967) reported finding higher concentrations of Radiolaria associated with temperature maxima within the water column.

TABLE 1
Plankton tow information.

Date Sample Collected (1981)	Ship-Station Number	Ship-Station Location	Sea-Ice Coverage	Water Column Sampled (m)	Polycystine ind/m³	Phaeodaria ind/m³
26 October	7,8	60°26.9'S, 03°37.1'E	10/10's	0–100	20	33
	7,8			100–200	9	35
26 October	9,10	61°10.8'S, 03°06.9'E	10/10's	0–100	22	29
5 November	22,25	62°09.0'S, 01°15.2'E	9/10's	1000–2000	18	4
8 November	27,28	61°30.1'S, 01°07.9'E	9/10's	0–100	154	41
9 November	29,30	60°57.5'S, 00°47.7'E	9/10's	0–100	99	23
	29,30			100–200	69	132
10 November	31	60°40.5'S, 00°30.7'E	9/10's	0–100	62	24
	31			100–200	24	101
12 November	34	59°30.9'S, 00°35.2'E	9/10's	0–100	49	11
	34			100–200	25	21
13 November	36,37	58°22.6'S, 00°52.6'E	8/10's	0–100	108	76
	36,37			100–200	68	70
	36,37	58°27.1'S, 01°08.5'E	8/10's	1000–2000	8	6

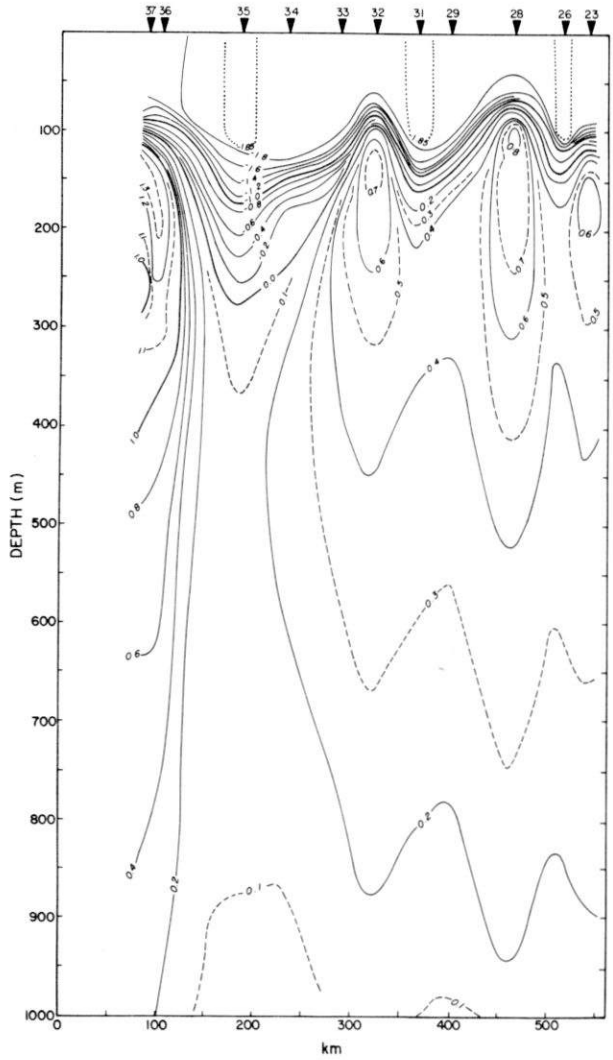

TEXT-FIGURE 2
Potential temperature section compiled from hydrographic measurements taken during exit transect from Antarctic pack ice. Contour interval equals 0.2°C, except for dashed and dotted contours at 0.1° and 0.05°C, respectively. Arrows identify specific ship stations along transect (from Gordon and Huber 1984).

Based on results from analyses of zooplankton captured in the Antarctic tows, Phaeodaria appear to prefer a slightly deeper habitat than polycystine Radiolaria. At the four ship stations where radiolarian samples were collected at both shallow and intermediate water depths beneath the sea ice, phaeodarian concentrations were higher in the intermediate tows (100–200 m) than in their shallow counterparts (0–100 m). Only at the ice-edge station (36,37) were abundances of phaeodarian Radiolaria lower in the sample taken at intermediate water depths than in the shallow-tow sample.

Tables 2 through 4 list the abundances of the most common species of polycystine and phaeodarian Radiolaria in shallow (table 2), intermediate (table 3) and deep (table 4) tows. The ten polycystine Radiolaria listed in these tables comprise 80% (on average) of the total polycystine population in the shallow tows, decreasing to 60% in the deep tows. The Phaeodaria are dominated by only three species which constitute 88% (on average) of the shallow tows and 40% of the deep tows. The diversity in that portion of the samples not specifically identified at the genus/species level was relatively high, with none of the minor species occurring at significant abundance levels.

TABLE 2
Abundance (ind/m³) of the most common species of polycystine and phaeodarian Radiolaria in shallow (0–100 m) tows.

	Ship-Station Number						
	7,8	9,10	27, 28	29, 30	31	34	36, 37
Polycystines							
Spongotrochus glacialis	4	11	44	47	28	34	45
Spongopyle osculosa	0	0	0	0	0	0	0
Spongurus sp.	0	1	0.9	2	0	0.3	2
Spongurus pylomaticus			0.7	0	0	0	
Lithelius nautiloides	3	3	12	10	5	6	7
Lithelius minor	0.5	1	0.9	0.3	0	0	1
Triceraspyris antarctica	4	2	11	2	4	1	3
Cycladophora davisiana	0	0.1	0	0	0	0.1	0
Antarctissa denticulata	1	0.9	14	8	3	4	19
Antarctissa strelkovi	2	0.3	18	1	5	0.4	17
Phaeodarians							
Protocystis harstoni	0	0.6	0.9	0.3	0	0	36
Challengeron bicorne	29	23	26	17	15	8	26
Challengeron swirei	2	3	5	5	5	2	2

Spongotrochus glacialis Popofsky (pl. 1, fig. 6) is the most abundant polycystine in all the shallow (0–100 m) and intermediate (100–200 m) tows. This finding agrees with those

TABLE 3
Abundance (ind/m³) of the most common species of polycystine and phaeodarian Radiolaria in intermediate (100–200 m) tows.

	Ship-Station Number				
	7,8	29,30	31	34	36,37
Polycystines					
Spongotrochus glacialis	3	18	9	12	13
Spongopyle osculosa	0	0	0	0	0.1
Spongurus sp.	0.2	2	0.4	0.4	0.8
Spongurus pylomaticus		0.3	0	0.2	0.1
Lithelius nautiloides	0.7	4	3	3	3
Lithelius minor	0	1	0.4	0.3	0.8
Triceraspyris antarctica	0	11	1	2	2
Cycladophora davisiana	0	0.2	0	0.1	0
Antarctissa denticulata	0.5	6	3	3	11
Antarctissa strelkovi	0.2	0.2	0.1	0.4	3
Phaeodarians					
Protocystis harstoni	0.7	5	0.8	1	37
Challengeron bicorne	26	19	13	7	18
Challengeron swirei	3	4	3	1	3

TABLE 4
Abundance (ind/m³) of the most common species of polycystine and phaeodarian Radiolaria in deep (1000–2000 m) tows.

	Ship-Station Number	
	22,25	36,37
Polycystines		
Spongotrochus glacialis	3	0.9
Spongopyle osculosa	0.2	0.4
Spongurus sp.	0.1	0.3
Spongurus pylomaticus	3	3
Lithelius nautiloides	0.5	0.1
Lithelius minor	1	0.2
Triceraspyris antarctica	0.1	0
Cycladophora davisiana	0.1	0.1
Antarctissa denticulata	0.4	0.5
Antarctissa strelkovi	0.3	0
Phaeodarians		
Protocystis harstoni	0.3	2
Challengeron bicorne	0.9	0.7
Challengeron swirei	0.1	0.1

from Arctic studies (Hulsemann 1963; Tibbs 1967) where *S. glacialis* is the polycystine radiolarian found in the highest concentrations in the upper 400 m of the water column. After *S. glacialis,* the most common polycystines in the shallow tows are: *Lithelius nautiloides* Popofsky (pl. 2, fig. 5), *Antarctissa denticulata* (Ehrenberg) (pl. 2, fig. 7), *Antarctissa strelkovi* Petrushevskaya (pl. 2, fig. 1) and *Triceraspyris antarctica* (Haeckel) (pl. 2, fig. 2). In the intermediate tows, these species also follow *S. glacialis* in abundance except for *A. strelkovi,* which appears to prefer the 0–100-m interval. The concentrations of each of these species were lower in the intermediate tows than in shallow tows. Other polycystine Radiolaria such as *Spongopyle osculosa* Dreyer (pl. 2, fig. 4), *Spongurus* sp. (pl. 1, fig. 7), *Spongurus pylomaticus* Riedel (pl. 2, fig. 8), *Lithelius minor* Jørgensen (pl. 2, fig. 6), *Cycladophora davisiana* Ehrenberg (pl. 2, fig. 3) are also present in some of the shallow and/or intermediate tows.

Challengeron bicorne (Haecker) (pl. 1, fig. 1) dominates the phaeodarian assemblage in the shallow and intermediate tows taken within Antarctic sea ice. At the ice edge, however, *Protocystis harstoni* (Murray) (pl. 1, fig. 5) replaces *C. bicorne* as the most abundant phaeodarian in shallow and intermediate water-depth samples. *Challengeron swirei* (Murray) (pl. 1, fig. 2) was found in all the samples, showing no apparent preference for a specific water depth either at the ice-edge station or within the sea-ice field. *Euphysetta elegans* Bogert (pl. 1, fig. 4) and *Protocystis micropelecus* Haecker (pl. 1, fig. 3) were also present in some of the shallow and intermediate tows but, in all instances, at lower concentrations than *C. bicorne* and *P. harstoni.*

In the one deep-tow sample taken beneath the sea ice (ship station 22,25) *Spongurus pylomaticus* and *Spongotrochus glacialis* dominate the polycystine radiolarian assemblage. *Spongotrochus glacialis* occurs at lower concentrations in the deep tow taken at the ice edge, where *Spongurus pylomaticus* is the most abundant polycystine radiolarian species.

Of the phaeodarian Radiolaria individually identified in the deep tows, *Protocystis micropelecus* is found at higher concentrations than any other Phaeodaria in the sample taken within the sea-ice field. The phaeodarian species present in highest abundances in the deep-tow sample from the ice-edge station is *P. harstoni* followed by *P. micropelecus.*

Since both *Spongotrochus glacialis* and *P. harstoni* comprise major components of the radiolarian population in many of the shallow- and intermediate-tow samples, a large portion of these species found in the deep tows represent individuals that occupied shallower waters while alive and are presently in transit to the sea floor. The presence of *Spongurus pylomaticus* and *P. micropelecus* at much higher abundances in the deep-tow samples than those in shallow and intermediate tows indicates that optimum conditions for these radiolarian species exist at water depths greater than 200 m. Our results support those of Petrushevskaya (1967), who in her examination of existing literature noted that although *S. pylomaticus* had not been identified at that time in any Antarctic plankton-tow samples, it comprised as much as 6% of the total radiolarian fauna in surface sediments from water depths between 1000 and 5000 m compared to only trace levels (less than 0.1%) in sediments from shallow water depths (500–600 m).

CONCLUSIONS

The polycystine and phaeodarian Radiolaria captured in our plankton nets show that Radiolaria occur at low abundance levels through a minimum of the upper 2000 m of the water column in late winter/early spring ice-covered waters of the Antarctic. Identification and tabulation of polycystine and phaeodarian tests from shallow (0–100 m) and intermediate (100–200 m) tows taken within the Antarctic sea-ice field indicate that the highest numbers of polycystine Radiolaria occur in homogenous waters characteristic of the upper 100 m of the water column. Phaeodarian Radiolaria, however, apparently prefer a slightly deeper habitat, with highest abundances recorded in samples collected at water depths between 100 and 200 m.

Highest abundances of polycystine Radiolaria were not encountered at the ice edge, but in a shallow tow (0–100 m), which sampled zooplankton in ice-covered waters characterized by warmer temperatures and higher salinity, and oxygen compared to those of the Weddell Deep Water at the other stations where Radiolaria were collected.

In the shallow (0–100 m) and intermediate (100–200 m) tows, the polycystine Radiolaria present in the highest concentrations is *Spongotrochus glacialis.* The dominant polycystine species in the deep-tow (1000–2000 m) samples were *Spongurus pylomaticus* and *Spongotrochus glacialis.* Of the phaeodarian Radiolaria, *Challengeron bicorne* is the most commonly found species in shallow (0–100 m) and intermediate (100–200 m) tows taken within the sea-ice field, whereas *Protocystis harstoni* occurs in higher concentrations than other Phaeodaria in the three tows (shallow, intermediate, and deep) taken at the ice edge.

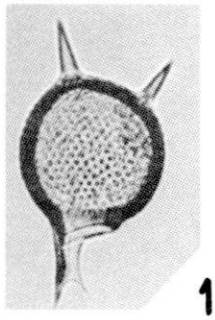

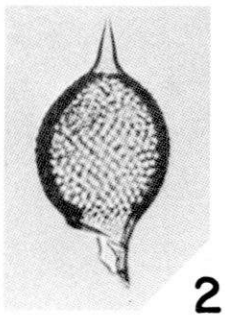

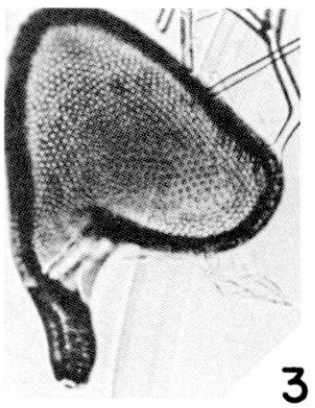

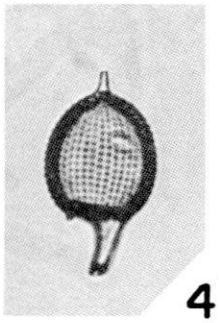

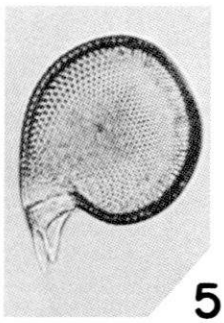

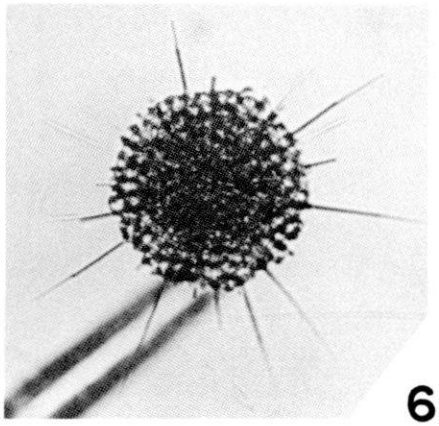

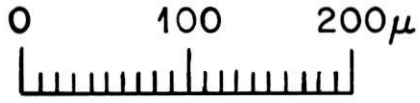

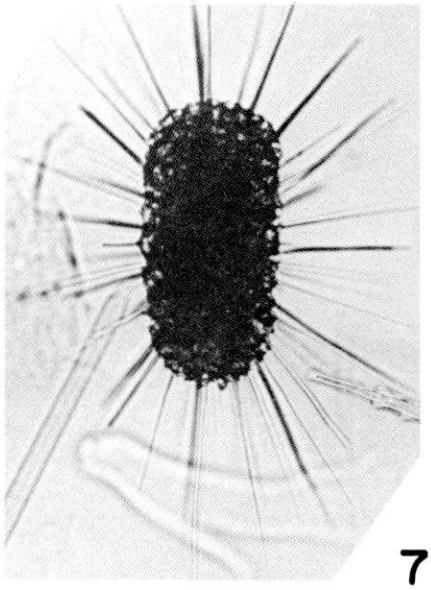

PLATE 1

1 *Challengeron bicorne* (Haecker)
Ship Station 36,37; 100–200 m tow.

2 *Challengeron swirei* (Murray)
Ship Station 36,37; 100–200 m tow.

3 *Protocystis micropelecus* Haecker
Ship Station 36,37; 1000–2000 m tow.

4 *Euphysetta elegans* Borgert
Ship Station 36,37; 1000–2000 m tow.

5 *Protocystis harstoni* (Murray)
Ship Station 36,37; 1000–2000 m tow.

6 *Spongotrochus glacialis* Popofsky
Ship Station 36,37; 1000–2000 m tow.

7 *Spongurus* sp.
Ship Station 36,37; 1000–2000 m tow.


1

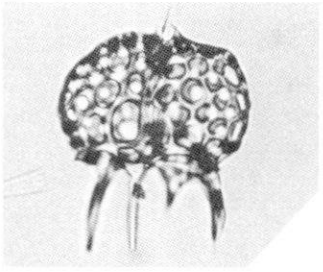
2

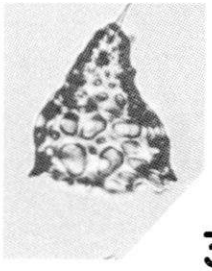
3

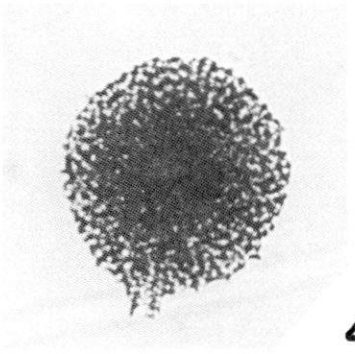
4

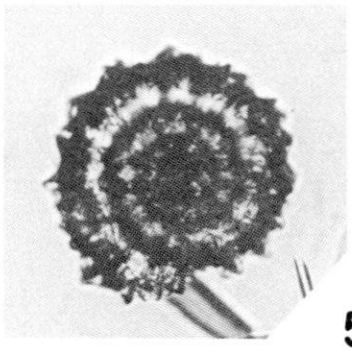
5

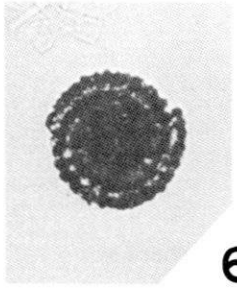
6

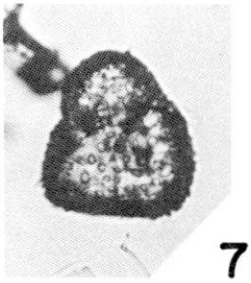
7

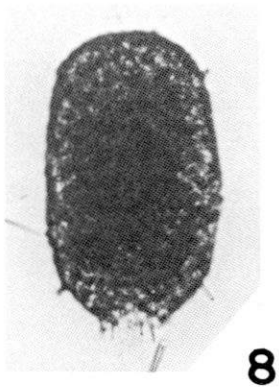
8

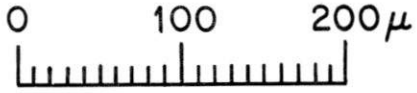

PLATE 2

1 *Antarctissa strelkovi* Petrushevskaya
Ship Station 36,37; 100–200 m tow.

2 *Triceraspyris antarctica* (Haeckel)
Ship Station 36,37; 100–200 m tow.

3 *Cycladophora davisiana* Ehrenberg
Ship Station 36,37; 1000–2000 m tow.

4 *Spongopyle osculosa* Dreyer
Ship Station 36,37; 1000–2000 m tow.

5 *Lithelius nautiloides* Popofsky
Ship Station 36,37; 1000–2000 m tow.

6 *Lithelius minor* Jørgensen
Ship Station 36,37; 100–200 m tow.

7 *Antarctissa denticulata* (Ehrenberg)
Ship Station 36,37; 100–200 m tow.

8 *Spongurus pylomaticus* Riedel
Ship Station 36,37; 1000–2000 m tow.

ACKNOWLEDGMENTS

L. Burckle, J. Marra, K. Takahashi, N. Swanberg and an anonymous reviewer made several helpful comments and suggestions on earlier versions of this manuscript. A. Pesanell assisted with a major portion of the laboratory analyses. Data shown in text-figure 2 were provided by A. Gordon and B. Huber. This research was directly supported by National Science Foundation grants DDP80-08011, OCE 79-24563 and ATM83-18850 to Lamont-Doherty Geological Observatory. This is Lamont-Doherty Geological Observatory of Columbia University Contribution No. 3785.

REFERENCES

CASEY, R., SPAW, J. M., KUNZE, F., REYNOLDS, R., DUIS, T., MCMILLEN, K., PRATT, D., and ANDERSON, V., 1979. Radiolarian ecology and the development of the radiolarian component in Holocene sediments, Gulf of Mexico and adjacent seas with potential paleontological applications. Gulf Coast Assoc. Geol. Soc. Trans., 29:228–239.

FERREYRA, G. A., and TOMO, A. P., 1979. Variación estacional de las diatomeas planctónicas en Puerto Paraíso—I. Instituto Antártico Argentino, Dirección Nacional del Antártico, Contrib. No. 264:149–184 pp.

GORDON, A. L., and HUBER, B. A., 1984. Thermohaline stratification below the Southern Ocean sea ice. Jour. Geophys. Res., 89:641–648.

HULSEMANN, K., 1963. Radiolaria in plankton from the Arctic drifting station T-3, including the description of three new species. Arctic Inst. North America, Tech. Paper 13:1–52.

KLING, S. A., 1979. Vertical distribution of polycystine radiolarians in the central North Pacific. Marine Micropal., 4:295–318.

KREBS, W. N., 1983. Ecology of neritic marine diatoms, Arthur Harbor, Antarctica. Micropaleontology, 29(3):267–297.

MARRA, J., and BOARDMAN, D. C., 1984. Late winter chlorophyll *a* distributions in the Weddell Sea. Marine Ecology-Progress Series, 19:197–205.

PETRUSHEVSKAYA, M. G., 1967. Radiolaria of orders Spumellaria and Nassellaria of the Antarctic region. In: Biological Reports of the Soviet Antarctic Expedition (1955–1958), Volume 3:1–186. Leningrad: Academy of Sciences of the USSR, Zoological Institute. Translated from the Russian in 1968.

TIBBS, J. F., 1967. On some planktonic Protozoa taken from the track of drift station ARLIS I, 1960–1961. Arctic Inst. North America, 20:247–254.

ZWALLY, H. C., PARKINSON, C., CARSEY, F., GLOERSEN, P., CAMPBELL, W. J., and RAMSEIER, R. O., 1979. Antarctic sea ice variations 1973–1975. In: NASA Weather Climate Review, Paper 56:335–340. Washington, D.C.: National Aeronautics and Space Administration.

Manuscript received April 4, 1984.
Revised manuscript accepted November 21, 1984.

SECTION 4: SEA ICE

JOURNAL OF GEOPHYSICAL RESEARCH, VOL. 89, NO. C1, PAGES 662–672, JANUARY 20, 1984

Antarctic Sea Ice Microwave Signatures and Their Correlation With In Situ Ice Observations

J. C. COMISO

Goddard Laboratory for Atmospheric Sciences

S. F. ACKLEY

Cold Regions Research and Engineering Laboratory

A. L. GORDON

Lamont-Doherty Geological Observatory

The general characteristics and microwave radiative properties of sea ice in the Weddell Sea region during the onset of spring are studied by using the NIMBUS 7 Scanning Multichannel Microwave Radiometer (SMMR) and other satellite sensors in conjunction with in situ observations from the *Mikhail Somov*. The position of the ice edge, the gradient of ice concentration, and the width of the Marginal Ice Zone are inferred from the microwave data and are found to be consistent with ship observations especially at 18 GHz. The sensitivities of the various SMMR frequencies to surface and other effects are investigated by using multi-spectral cluster analysis. The results show considerable variability in emissivity, especially at 37 GHz, likely associated with varying degrees of surface wetness. Ice concentrations are derived by using two methods: one that assumes fixed emissivities for consolidated ice and an iterative procedure that accounts for the variable emissivities observed. By using the procedure that allows the emissivities to be variable gives ice concentrations that are more consistent with qualitative field observations.

1. INTRODUCTION

The strong contrast in the microwave emissivities of water and ice, and their day-night almost all-weather capability, make microwave radiometers ideal for monitoring global sea ice cover. The amount of open water within the ice pack in the southern ocean has been determined with about a 15% accuracy by *Zwally et al.* [1983], during 1973–1976, using the one channel NIMBUS 5 Electrically Scanning Microwave Radiometer (ESMR). A substantial improvement in the accuracy of this determination could be made by using the dual polarization Scanning Multichannel Microwave Radiometer (SMMR) on board the more recent NIMBUS 7 satellite because of its potential to better account for the spatial and temporal variations in the physical temperatures of the ice and to distinguish different ice types [*Gloersen and Barath*, 1977]. However, to be able to utilize this sensor to its full capabilities, the microwave signature of sea ice, which is known to vary with age, thickness, salinity, structure, and surface characteristics [*Vant et al.*, 1974; *Ramseier et al.*, 1974], must be better understood.

Generally, simultaneous in situ data on sea ice conditions will enhance the interpretation of satellite imagery especially in the southern ocean. While some experiments, though limited in scale, have been conducted in the Arctic region, hardly any experiment dedicated for this purpose has been undertaken in the southern hemisphere. Fortuitously, ice cover observations from the *Mikhail Somov*, described in *Ackley and Smith* [1982], during the October–November 1981 U.S.-USSR Weddell Polynya Expedition [*Gordon and Sarukhanyan*, 1982], includes in situ observations that could be used to initiate some studies and could help unravel some of the difficulties. On board the ship, daily conditions were recorded by both Soviet and American scientists, including surface temperatures and atmospheric conditions. The observations were made over a period of almost a month (mid-October to mid-November) during a time when the ice cover was undergoing rapid changes. This is also a period when the physical and dielectric properties of the ice are subject to change because of snow cover melt effects, ridging, and infiltration of seawater into the snow/ice interface. These changes in turn affect the radiative properties of the ice and the microwave emissivities, which are defined as the ratio of the radiant flux emitted by a material to that emitted by a blackbody at the same temperature. Thus, the spatial and temporal variation in emissivities are investigated during this period. Furthermore, the overall character of the ice and the gradient in ice concentration at the ice edge are inferred from the microwave data and are compared with observations from the ship. Although this study mainly describes a comparative analysis, other satellite data are also employed to be able to extend the study area and improve the statistics of the data analyzed. Therefore, in addition to specific observations from on board the ship, a more general condition of the ice during this period is presented.

Paper number 3C1471.

2. OBSERVATIONS FROM THE MIKHAIL SOMOV AND SMMR

Ice characteristics recorded during the expedition, by Soviet scientists, are summarized in a graphical form, depicting the position of the ship, ice concentration, ice types, and other parameters [see *Ackley and Smith*, 1982]. These records are compared with independent observations by American scientists, and, in general, there is a very good agreement. Some minor discrepancies have been explained as due to the averaging technique used by the ship's party in representing ice conditions. Some of these observations are also compared with weekly maps derived from satellite data and ship reports by

TABLE 1. First Year Sea Ice Emissivities at SMMR Frequencies

Frequency, GHz	Wavelength, cm	Field of View, km²	ε, Weddell Ice*	ε, Arctic FY Ice†
6.6 H	4.55	148 × 95	0.85 ± 0.02	0.85
V			0.92 ± 0.02	0.93
10.7 H	2.81	91 × 59	0.88 ± 0.02	0.88
V			0.94 ± 0.02	0.94
18.0 H	1.67	55 × 41	0.86 ± 0.02	
V			0.92 ± 0.02	
21.0 H	1.43	46 × 30	0.90 ± 0.04	0.91
V			0.92 ± 0.04	0.95
37.0 H	0.81	27 × 18	0.86 ± 0.02	0.90
V			0.91 ± 0.02	0.94

*This study.
†*Svendsen et al.* [1983].

the Navy-NOAA Joint Ice Center. A discrepancy in the position of and concentration near the ice edge between the Navy-NOAA maps and surface observations from the *Mikhail Somov* has been cited by *Ackley et al.* [1982] and will be evaluated in this paper.

The NIMBUS 7 SMMR was launched in October 1978 and since that time has been delivering useful brightness temperature data. A summary of the basic characteristics of this sensor is given in Table 1. A detailed description of this instrument and potential applications are discussed in *Gloersen and Barath* [1977] and *Njoku et al.* [1980]. Because of power limitations, the sensor operated on an every other day basis only. Also, because of delays in the processing of calibrated SMMR data, only 7 days are available for this study, namely, October 22 and 24, and November 1, 3, 5, 7, and 13, 1981. The orbital data for each of these days are projected to a 293 × 293 polar stereographic grid, with each element having an area of about 30 km by 30 km. Although the resolution varies with frequency, the data from all the channels are projected to the same grid size for convenience in the comparative analysis.

3. Discussion of Results

There are four different but interrelated aspects of this study: (1) sea ice microwave emissivity determinations in the Weddell sea region during spring, (2) ice edge characteristics studies including determination of the 15% ice edge and the width of the marginal ice zone band, (3) surface effects studies emphasizing wetness using multifrequency analysis, and (4) ice concentration determination using various combinations of SMMR channels. A discussion of sources and magnitude of errors is also included.

Sea Ice Microwave Emissivities

The most immediate application of the ship data is in the determination of microwave emissivities of ice at SMMR frequencies along the ship route. The air temperatures were determined on board the ship on a 3-hour interval basis whereas surface ice/snow temperatures were measured on an hourly basis by using a thermistor thrown from the ship to ice floes along the path of the ship. The results of the measurements are shown in Figure 1 and indicate a strong coupling between the surface and the air measurements. In general, the surface temperatures are read as slightly higher than the air temperatures. A few times, surface temperatures are read above the freezing point by as much as 2 K, an impossibility thermodynamically for a snow or ice surface. Some self heating of the thermistor during the reading is the most likely explanation for these phenomena. Core samples of ice taken along the route of the expedition [*Clarke and Ackley*, 1982] indicates that the ice has a mean salinity of 5‰ and, consequently, is optically opaque [*Gloersen and Larabee*, 1981; *Vant et al.*, 1974]. Therefore, much of the observed microwave radiation comes from a thin near isothermal layer of ice at the ice/snow interface. Depth dependent measurements that relate surface temperatures to the ice/snow interface temperatures have been made by R. O. Ramseier (private communications, 1982) for first year ice at Pond Inlet during the same period. A linear fit to the Pond Inlet data is used to derive ice/snow interface temperatures from the in situ surface temperatures. At this time of the year, the adjustment is small (~3 K), and, therefore, the error caused by the application of this fit to obtain the ice/snow interface temperature should be also small. The emissivities, calculated by taking the ratio of the average brightness temperatures (T_B) from SMMR during October 22 and October 24 and the snow/ice temperatures derived from the in situ measurements during the same period are tabulated in Table 1. The SMMR values are the near maximum of a distribution of T_B from an area 150 km × 150 km centered in the ship position to maximize the probability of measuring nearly 100% consolidated ice, within the field of view of the sensor. These emissivities are also compared with previous determinations for first-year ice in the Arctic by *Svendsen et al.*, [1983], and the agreement is good to within 3%. The results are also consistent with emissivities of Arctic first year ice derived from SMMR and THIR data by *Comiso* [1983]. It should be pointed out that the calibration of the SMMR sensor at 21 GHz has greater uncertainty because of complications associated with the greater sensitivity to atmospheric effects at this frequency (T. T. Wilheit, private communication, 1983). This could be the reason why the values at 21 GHz are greater than those at the other frequencies for the horizontal polarization.

Ice Edge Characteristics

To investigate how well the satellite microwave data reproduces the ship data in the marginal ice region, the spatial distribution of radiances along the edge of the ice are generated during the period when the ship first crossed the edge (October 22, 1981) and also when it was leaving the ice pack

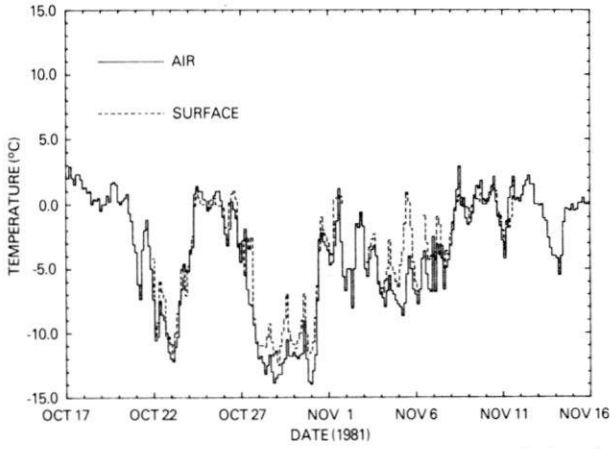

Fig. 1. Observed air and snow surface temperatures during the Weddell Polynya Expedition.

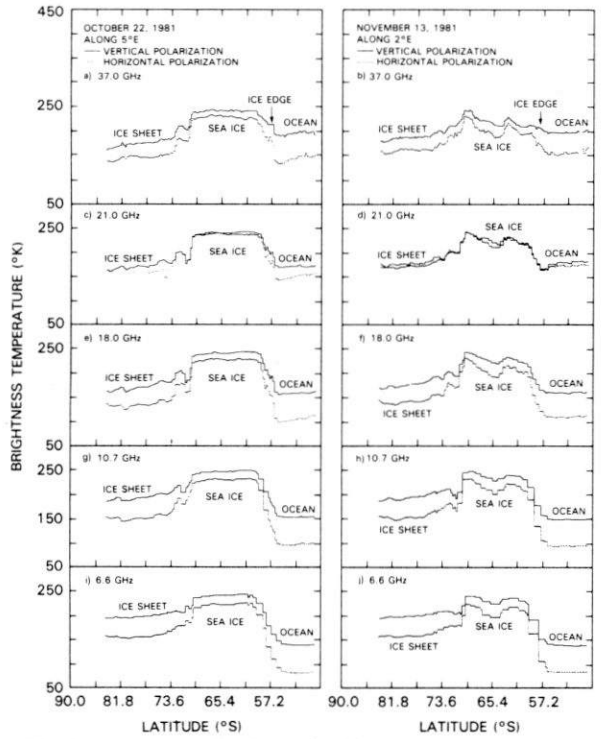

Fig. 2. Spatial distributions of brightness temperatures for all SMMR channels during October 22, 1981, and November 13, 1981, along 5°E and 2°E, respectively, from the South Pole.

(November 13, 1981). Figure 2 shows plots of brightness temperatures for all SMMR channels along 5°E and 2°E for the October 22 and November 13 data, respectively. A schematic diagram of the cruise track and a summary of the ice cover observations made by both U.S. and Russian scientists along the track is shown in Figure 3 [see also *Gordon and Huber*, 1983]. Although the 5°E trajectory is very close to the October ship entry track, at the ice edge the 2°E trajectory is about 1° off the November exit track because of limitations in the orbital coverage of the satellite. A foremost consideration in this study is spatial resolution because in situ observations from the *Mikhail Somov* have indicated considerable variability over a few kilometers. The fields of view of each SMMR channel (given in Table 1) show considerable difference in resolution from one frequency to another. The plots generally show consistency in the position of the ice edge at all channels. The slight shifts in position of the ice edge at the lower frequencies (i.e., 6.6 and 10.7 GHz) are likely caused by the coarser resolution at these frequencies. The distribution at 6.6 GHz is further complicated by an antenna pattern problem which causes measurements at the land/sea boundaries to depend on whether the approach to the boundary is from the land or the sea [*Njoku*, 1980]. However, the lower frequency channels can still be very useful, especially at 10.7 GHz, because the contrast of the brightness temperatures between ocean and ice are strongest in these channels, and surface effects are minimal. Again, possible calibration problems cited earlier is likely the reason for the almost equivalent values for the horizontal and vertical polarizations at 21 GHz (see Figures 2*c* and 2*d*).

A visual examination of the various distributions shows that the 18 GHz channel is best suited for ice edge analysis. Linear regression fits to each brightness temperature distribution at the ice edge were also made, and this channel has the highest slope or the sharpest gradient at the ice edge. Although the resolution is best at 37 GHz, the higher sensitivity to surface and atmospheric effects and the poorer contrast between ice and ocean makes ice edge analysis using this channel subject to considerable error. The width of the marginal ice zone as inferred from the graphs indicates monotonic decreases in the brightness temperatures as the ice edge is approached corresponding to physical changes in ice characteristics. The width of this changing zone (representing the distance for which ice concentration changes from about 10 to 100%), is about 240 km at 18 GHz and 300 km at 37 GHz, with the corresponding gradients at the ice edge being 0.42% ice concentration/km and 0.33% ice concentration/km, respectively. Ship observations, part of which are shown in Figure 3, and qualitative analyses of satellite infrared and visible data show better agreement with the 18 GHz data. The approximate locations where ice concentration increased from 10 to 100%, as inferred from the 18 GHz SMMR data, are indicated by dash lines in Figure 3.

On November 13, 1981, the ability to determine the position of and the gradient at the ice edge has deteriorated in the 37 GHz channels because of surface effects, as will be elaborated in the following discussions. At 18 GHz, however, the edge is still very well defined and can be inferred almost as accurately as the October image. The gradients in ice concentration can also be determined by using this channel if the changes in the emissivity of the ice is accounted for. Again, the ice edge conditions as observed from the *Mikhail Somov*, are approximately consistent with the 18 GHz SMMR data as

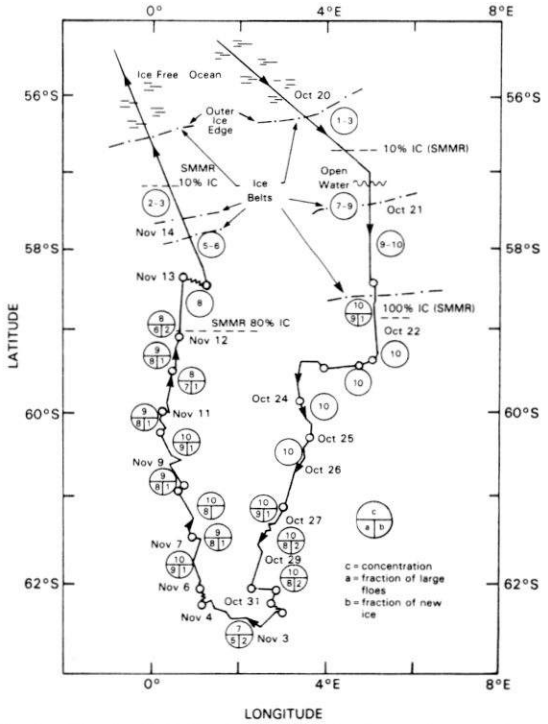

Fig. 3. Track of *Mikhail Somov* and observations of ice concentration (in tenths) made by USSR and U.S. scientists. Boundaries of the ice edge during October 22 and November 13, 1981, inferred from the 18 GHz SMMR brightness temperature data are indicated by dash lines.

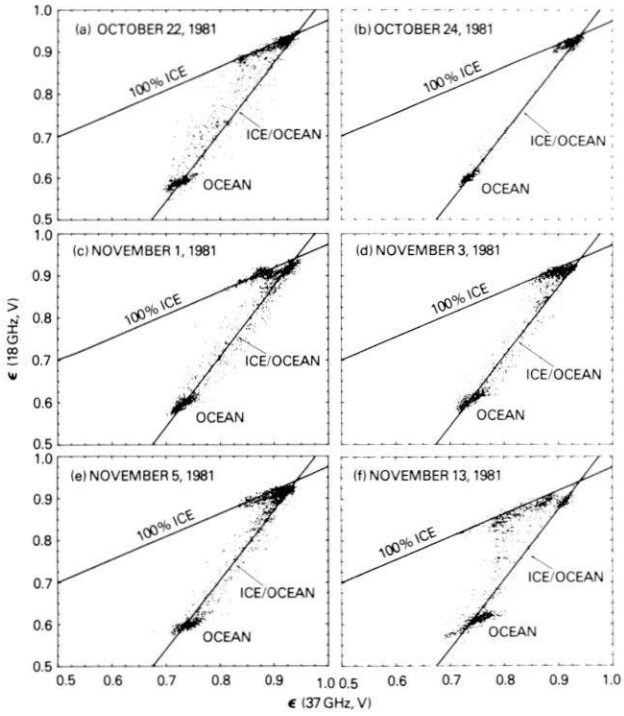

Fig. 4. Multispectral cluster analysis using the emissivities at 18 GHz and 37 GHz, vertical polarization, during October 22 and 24 and November 1, 3, 5, and 13, 1981.

shown in Figure 3. The comparison assumes spatial uniformity in ice distributions because of the indicated 1° longitude difference in location between the ship track and the satellite orbit.

Surface Properties

To study the effects of varying surface properties, cluster analysis in areas in the vicinity of the ship is applied. This analysis utilizes two of the SMMR channels and the thermal channel (11.5 μm) from the Temperature Humidity Infrared Radiometer (THIR), which is also on board the NIMBUS 7 satellite. The use of this technique to study first year and multiyear ice in the Arctic region was described elsewhere [*Comiso*, 1983]. A similar technique using brightness temperatures instead of emissivities and on a limited set of data was also used by *Gudmandsen* [1980]. Since the salinity profiles of sea ice samples collected during the expedition [*Clarke and Ackley*, 1982] show characteristics similar to that of first year ice in the Arctic, the ice in the present study will be assumed to have a similar signature. This assumption has also been used previously [*Zwally et al.*, 1983] for Antarctic sea ice.

To investigate changes in the surface characteristics of the ice, a rectangular area in the polar stereographic map which includes the whole ship route and some ocean areas is examined. The coordinates of the cornerpoints of this area are (52.7°S, 13.6°W), (61.5°S, 18.3°W), (52.6°S, 14.0°E), and (61.4°S, 18.8°E). The two SMMR channels used are normally two different frequencies (e.g., 18 and 37 GHz) of the same polarization, because the penetration depth is frequency dependent. Such analysis could thus show observable depth dependent effects in one channel but not in the other. By plotting the emissivities of points inside the study area for one frequency versus that of another, the higher frequency channel should be more sensitive to surface effects than the other channel. Figure 4 shows such plots at the vertical polarization. Plots were also generated for the horizontal channel, but the results (clustering of points) are very similar and do not provide additional information. To make sure that the effects are not due to errors caused by possible contamination of clouds in the THIR field of view, the brightness temperature at one channel is plotted against that of the other. A comparison of these plots with the emissivity plots showed no basic difference in the clustering of points indicating minimal contamination of the emissivity data by erroneous surface temperatures. Although changes in the amount of atmospheric water vapor could produce similar effects, radiative transfer studies using the actual atmospheric profile obtained by upper air soundings from the *Mikhail Somov* show that such an effect is minimal compared to that caused by changes in the surface properties of the ice cover.

Basically, Figure 4 also summarizes the ice characteristics in the study area during the indicated days. Two lines are drawn in each of the plots and labeled as a 100% ice line and an ice/ocean fraction line, respectively. It is assumed that surface or subsurface effects cause different amount of changes in the emissivity of sea ice for the two different channels. Thus points along the 100% ice line (drawn arbitrarily) are expected to include data from fields of view which are likely to represent 100% or near 100% ice. Data along the ice/ocean fraction line (also drawn arbitrarily) represent fields of view which have partly first year ice with dry snow cover and partly open water. Data points located between the two lines likely represent mixtures of first year ice with wet snow cover, first year ice with dry snow cover, and open water. Although the clustering of points varied from one plot to another, the positions of the lines were kept fixed for ready reference in the study of the variability of the data points. A cluster labeled "ocean" represents points in the ocean area only as has been confirmed by plotting the latitude and longitude of these points and establishing that the locations are outside the ice pack. The variability of the ocean cluster shows sensitivity to the atmospheric water vapor, including wind, and precipitation [*Wilheit*, 1980].

Marked changes from one period to another can be observed from the scatter plots. In October 22 (Figure 4), a considerable amount of surface effects on consolidated ice can be noted as indicated by the degree of scattering of points along the 100% ice line, especially on account of the variations in the 37 GHz emissivities. The stronger sensitivity along the higher frequency channel is an indication that the scatter of points is caused by surface or near surface effects because of shorter penetration depth associated with this frequency. The scatter of emissivity data points along the 100% ice line looks a bit more suppressed on October 24 than on October 22. This phenomenon is likely caused by cooler air temperatures indicated in Figure 1 which would refreeze the wet snow covers. It is assumed that the observed temperatures are representative of the whole study area, an assumption supported by the daily averaged THIR temperatures over the study area which indicated a similar trend. The scatter is enhanced again in November 1, following a warming period, and this effect is basically sustained through November 3 and 5. A dramatic change, however, occurred on November 13. A few days of constant warming immediately before this period apparently caused a more widespread surface melt and thawing as is evident from the substantially higher scatter of points off the 100% ice line. The points are also lower than the 100% ice

line indicating the presence of leads within the areas represented by these points.

The observable correlation of the presence of surface effects with increased temperatures in the region indicates that the effect is likely caused by wetness of the snow cover. Similar effects on microwave radiation have already been reported in the literature [e.g., *Stiles and Ulaby*, 1980; *Hofer and Schanda*, 1978; *Kunzi et al.*, 1982] for wet snow over soil. However, it should be pointed out that the effect depends on the degree of wetness. When the water content is less than about 5%, an increase in brightness temperatures has actually been observed [*Comiso*, 1983; *Zwally and Gloersen*, 1977; *Chang and Gloersen*, 1975]. Further saturation by water, however, causes the emissivities to drop because of increased contribution from water, which has a low emissivity. The amount of scatter seen in the diagram thus could be used as an indication of the saturation. However, care should be exercised in the interpretation of the clustering in this manner because a combination of wet surfaces and dry surfaces would also fall along the 100% ice line.

Factual observations from the *Mikhail Somov* and some surface measurements show confirmation of the hypothesis of wetness as a cause for the scatter in the plots. Two photographs taken from the ship during October 22, 1981, and November 13, 1981, respectively, as shown in Figure 5, indicate the transition of the character of the ice cover between the two periods. In the November 13, 1981, image, an arrow is drawn to indicate where wetness is observed. Several more

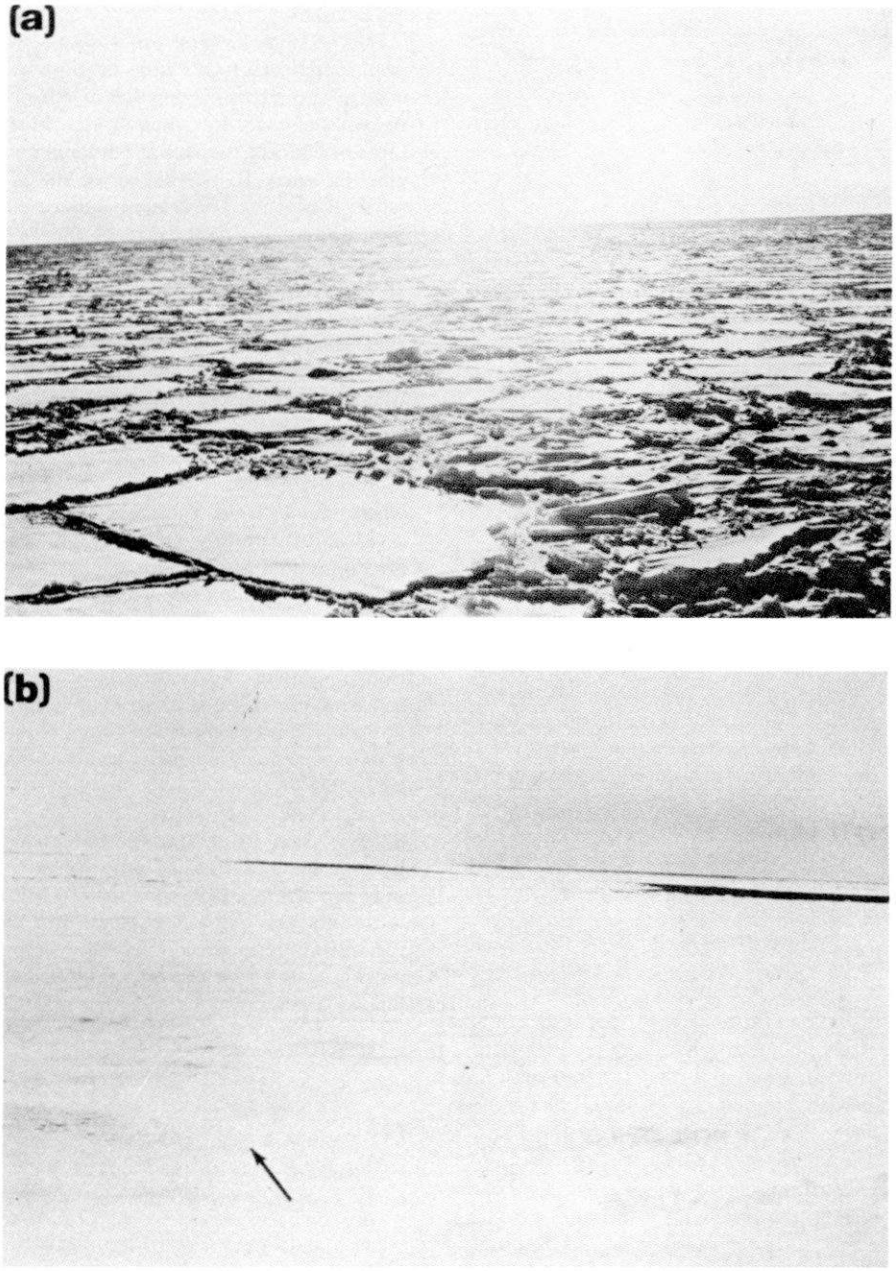

Fig. 5. Photographs of a typical ice conditions on (*a*) October 22, 1981, and (*b*) November 13, 1981. The arrow points to an area with wet snow cover.

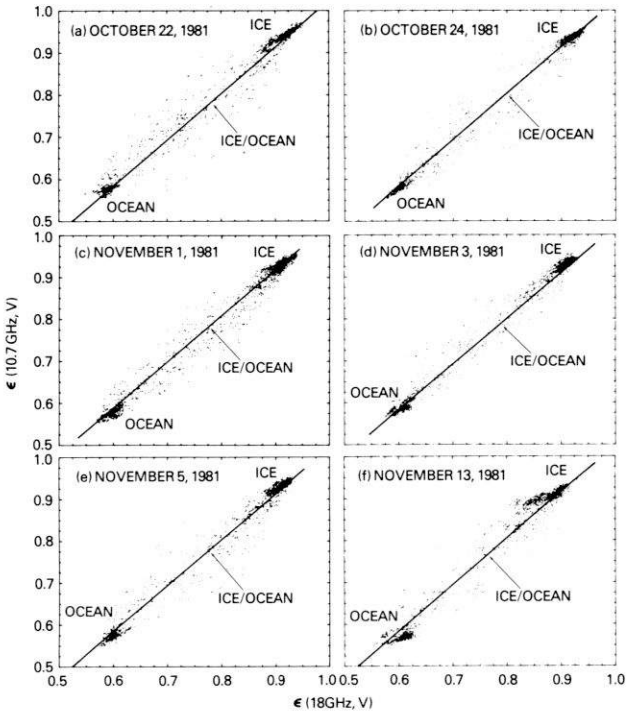

Fig. 6. Multispectral cluster analysis using the emissivities at 10.7 GHz and 18.0 GHz, vertical polarization, during October 22 24 and November 1, 3, 5, and 13, 1981.

examples of photographs of the ice conditions during this period are shown in *Ackley and Smith* [1982]. In some places, other effects such as ridging and infiltration of salt water into the snow ice interface are observed but are relatively localized compared to the snow melt condition on November 13.

To understand further the frequency dependence of this surface effect, emissivities at 10.7 GHz are also plotted against those at 18.0 GHz, and results are shown in Figure 6. A distinctly more compact clustering of points can be readily observed from these plots, again confirming less dependence on the surface properties at lower frequencies. There is, however, more divergence of points again on November 13, 1981, indicating that at this time the wetness has penetrated deep enough to affect even the 18 GHz data. Since the contrast in emissivity between ice and water is higher at 10.7 than at 18 GHz, the less scatter of points in the ice cluster along the lower frequency is also an indication that there is no substantial opening of leads or polynyas in regions represented by data along the 100% ice cluster.

To summarize the results, the distribution of emissivities at the 100% ice line for the various SMMR vertical channels during October 22, 1981, and November 13, 1981, are shown in Figure 7. Contributions from ocean or partly ocean areas are excluded for each channel by imposing a lower limit on the emissivities included in the plot, that is based on a linear functional relationship of the emissivity at this channel with that at another channel below but parallel to the 100% ice line. The well-defined peak at 37 GHz on October 22 likely corresponds to areas with dry snow cover as discussed earlier. The dramatic change in the emissivity distributions from October 22 to November 13 is evident even at 18 GHz, indicating substantially less areas with dry snow cover at the latter date. It is quite clear that the 6.6 GHz has the least variability in emissivity for either day. However, in addition to a relatively poorer resolution, this channel has an additional problem of antenna pattern effects as discussed earlier. Thus, the 10.7 GHz and 18 GHz channels are likely the best SMMR channels to use when surface effects are present. The 21 GHz channel might be of some use, but the high sensitivity of this channel to atmospheric water vapor requires additional considerations. The 37 GHz channel is indeed very sensitive to surface effects and should be used in combination with other frequencies for accurate retrieval of ice information during spring and summer. For comparison, the corresponding distributions at the horizontal polarization are shown in Figure 8. The distribution in these plots are very similar to those at vertical polarization. However, the ice peaks on October 22 are not as well defined especially at 37 and 18 GHz.

Ice Concentration Determination

It is evident from previous discussions that although the best spatial resolution can be obtained from the 37 GHz channels, an error of as much as 20% can be introduced if a unique emissivity for ice is utilized in the retrieval of ice parameters during the spring (and summer) or across the marginal ice zone. To be able to use the 37 GHz channel in the retrieval of ice concentration, surface effects should be taken into account. However, if resolution is not a strong requirement, the use of other channel especially the 10 GHz and the 18 GHz channels should be considered. An additional advantage in the use of these two channels is the almost negligible effect of atmospheric conditions in the polar region. Assuming only one type of ice in the region, the radiative transfer equation for each channel, following *Gloersen and Barath* [1977] and *Comiso and Zwally* [1982], is given by

$$T_B{}^i = C_w(T_w\varepsilon_w{}^i e^{-\tau} + T_{Aw}) + C_I(T_I\varepsilon_I{}^i e^{-\tau} + T_{AI}) + T_S \qquad (1)$$

where (T_w, $\varepsilon_w{}^i$, C_w, and T_{Aw}) and (T_I, $\varepsilon_I{}^i$, C_I, and T_{AI}) are physical temperatures, emissivities at channel i, concentrations (fractions), and atmospheric contribution of water and ice, respectively, τ is the atmospheric transmissivity, and T_S is the contribution from free space which is neglected in this analysis. The effect of atmospheric transmissivity and contributions from upwelling and downwelling radiations from the atmosphere were evaluated in a radiative transfer simulation, similar to *Wilheit* [1980], using actual temperature and humidity profiles taken during the expedition. The net effect is to increase the brightness temperature by about 1 K and therefore is neglected. The factor $T_0{}^i = T_w\varepsilon_w{}^i$ is inferred from the SMMR data by analyzing the brightness temperatures of ocean areas near the ice edge. Since $C_w = 1 - C_I$, there are only two unknowns in equation (1), namely, C_I and T_I. Therefore, only two SMMR channels are required to obtain ice concentration, each representing a simplified version of equation (1). Solving for two equations in two unknowns gives the following relations for temperatures and ice concentrations:

$$T_I = \frac{T_B{}^i T_0{}^j - T_0{}^i T_B{}^j}{\varepsilon_I{}^j(T_B{}^i - T_0{}^i) - \varepsilon_I{}^i(T_B{}^j - T_0{}^j)} \qquad (2)$$

and

$$C_I = \frac{T_B{}^j - T_0{}^j}{\varepsilon_I{}^j T_I - T_0{}^j} \qquad (3)$$

where i and j represent the two SMMR channels used. Essentially, $T_0{}^j$ and $T_0{}^i$ are used as tie points to minimize possible offsets in the calibration of the instrument. It is expected that

the concentration inferred from equation (3) would be identical to that from the other channel, i.e.,

$$C_I = \frac{T_B{}^i - T_0{}^i}{\varepsilon_I{}^i T_I - T_0{}^i} \tag{4}$$

By using 18 and 37 GHz SMMR data, some calculations using equation (2) yielded abnormal values for sea ice physical temperatures (e.g., less than 200 K or greater than 280 K), thereby giving unrealistic ice concentrations when equation (3) is applied. An analysis of the problem indicated that the unrealistic temperatures are caused mainly by the use of one set of values for emissivities in equation (2). However, previous discussions have indicated substantial variability in the emissivity. The physical temperatures derived from equation (2) are only correct if the set of emissivities used correspond to that of the area from which the set of brightness temperatures are observed. Otherwise, some errors are introduced depending on surface characteristics. Thus, this procedure should be used only when the variabilities of the emissivities are adequately accounted for.

One way out of this problem is to use physical temperatures obtained independently, as with the case of the THIR temperatures, and use the same procedure described in *Comiso and Zwally* [1982] with the aid of equations (3) or (4). The ice concentrations derived by using the 18 GHz and the 37 GHz channels separately for the October 22, 1981, and the November 13, 1981, data, are shown in Plates 1*a* to 1*d*. The different gray levels indicate different ice concentrations in steps of 15% as indicated. It is evident that the concentrations inferred from the two channels are not the same. Near the ice edge, at about 5°E and 45°W, the ice concentrations from the 37 GHz on October 22, 1981, show substantially more open water than that from the 18 GHz. Also, the greater than 90% ice areas are substantially more extensive in the 18 GHz than in the 37 GHz images. In November 13, 1981, the difference in the retrievals for ice concentrations between the 18 and the 37 GHz is even more pronounced as shown in Plates 1*b* and 1*d*. Near the 0° longitude between 60°S and 65°S, there is an area which appears to be almost open water in the 37 GHz image but shows more than 50% ice in the 18 GHz. Even the 18 GHz image gives significantly lower concentration than the recorded observations of about 80–90% ice concentration (see Figure 3) of the ice pack during this period. These results show the limitations during this period of a one channel sensor in the determination of ice concentration, especially at 37 GHz.

The more logical procedure, which would account for the

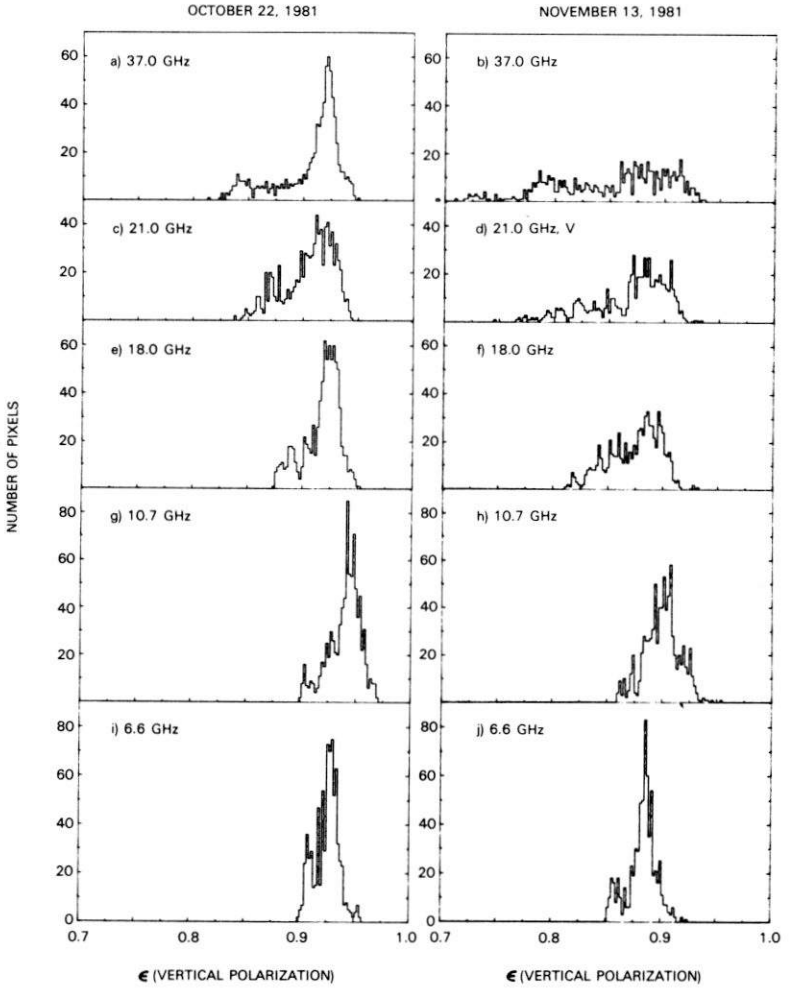

Fig. 7. Histograms of emissivities of 100% or near 100% ice for each SMMR channel at the vertical polarization, using physical temperatures inferred from THIR.

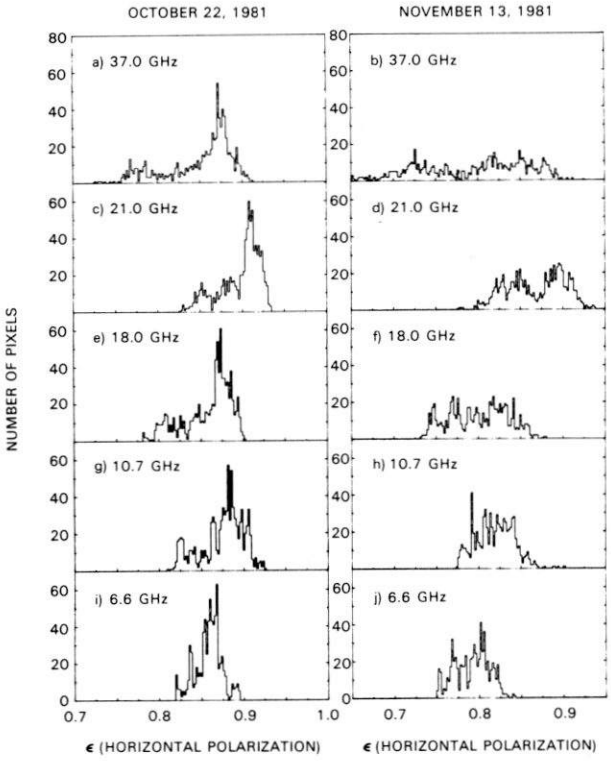

Fig. 8. Histograms of emissivities of 100% or near 100% ice for each SMMR channel at the horizontal polarization using physical temperatures inferred from THIR.

surface effects in each channel, is to allow the emissivities to vary along the 100% ice line until the concentration derived by using equation (3) is consistent with that derived from equation (4). This procedure has an advantage not only in accuracy but also in keeping the resolution relatively close to that of the 37 GHz.

The results of ice concentration determinations are shown in Plates 1*e* and 1*f* for both October 22, 1981, and November 13, 1981, obtained by using an iterative method which searches for the most likely value of emissivities as described above. The iteration started with the highest set of emissivities, and step decreases are performed along the 100% ice line shown in Figure 4 until the concentration from the 18 GHz is consistent with that from the 37 GHz within a limiting accuracy of $\pm 2\%$. If a solution is not possible after this iteration, a second iteration is conducted with the limiting accuracy relaxed from 2 to 4%. Further relaxation to 6 and 8% was implemented after this iteration. Statistically, there was convergence in about 85% of the data after the first iteration. The second, third, and fourth iterations are intended to get the most of the data analyzed with this procedure. Further relaxation of the limiting accuracy for those not surviving the fourth iteration would not be much of an advantage. However, only about 4% of the data did not converge after four iterations, and the 18 GHz channel data, which has lesser sensitivity to surface effects than the 37 GHz, were used to calculate ice concentration for the nonconvergent data points.

It is evident that the results using a combination of the two channels and allowing the emissivity to vary along a hypothetical 100% ice line show less open water within the ice pack than with either channel alone. Although the difference with the 18 GHz result is not substantial in the October 22 data, the spatial resolution is an improvement to that with the 18 GHz alone, because the analysis is done in conjunction with the 37 GHz channel, which has higher resolution. On November 13, 1981, a big improvement in ice concentration values corresponding to the ship observations (see Figure 3) is evident over those obtained from either the 18 or the 37 GHz. Thus, the procedure apparently accounts for the large variability in the emissivities of consolidated ice shown in Figure 4 on November 13.

The general condition of the ice pack during these two days can also be studied by using a higher resolution visual range sensor from a USSR satellite as shown in Figure 9. The images show substantial change in at least the surface characteristics of the ice during the two days. Considerable cloudiness in the area on November 13, 1981, makes it difficult to make a detailed comparison. However, the vicinity of (65°S, 10°W) is cloud free, and the structure of the ice can be studied. Ice concentration is not easy to infer even qualitatively from these images as has been discussed in *Comiso and Zwally* [1982]. Nevertheless, the general condition of the ice can be inferred and shows consistency with interpretations of the SMMR data as previously discussed.

Error Analysis

The evaluation of errors in the measurements of geophysical quantities with the use of satellite sensors is always complicated by various factors that are not easy to quantify. For example, the SMMR sensor data have gone through extensive analysis and simulations before the current calibration was performed, and, yet, the accuracy of the absolute calibration is presently still not well known. Furthermore, the possibility of not having purely vertical and horizontal components of polarization has been suspected, and the direct reflection from the sun during some time of the year and in some areas has been observed to affect one of the reference thermistors used in the calibration [*Gloersen et al.*, 1980]. Moreover, atmospheric effects that are neither spatially uniform nor time independent could at times be a considerable factor, especially at 37 GHz, even though the humidity in the polar regions is generally very low.

However, the overall performance of the instrument has been very good, manifested by the consistency in the measurement of the brightness temperatures of similar surfaces (e.g., ocean). Typical standard deviations for maps averaged over 3 days in ocean areas is about 2.5 K. As has been demonstrated in this study, the lack of an absolute calibration is not an impediment to the ability to extract geophysical parameters from the data. As for an estimate of the accuracy of the absolute calibration, the brightness temperature of ocean areas near the polar region where the humidity is low has been compared with results from a theoretical radiative transfer model, similar to that used by *Wilheit* [1980], and there was agreement within a few degrees as has been noted [*Comiso*, 1983], with the largest deviation occuring at 21 GHz. At this frequency, in addition to possible problems with calibration as indicated earlier, the model results are not very reliable because of the existence of a water vapor line at 22 GHz.

The error associated with the use of THIR temperature data has been evaluated in *Comiso* [1983]. A direct comparison of some THIR temperatures with in situ measurements has indicated agreement within a few degrees, although the THIR values tend to be consistently lower when compared with *Mik-*

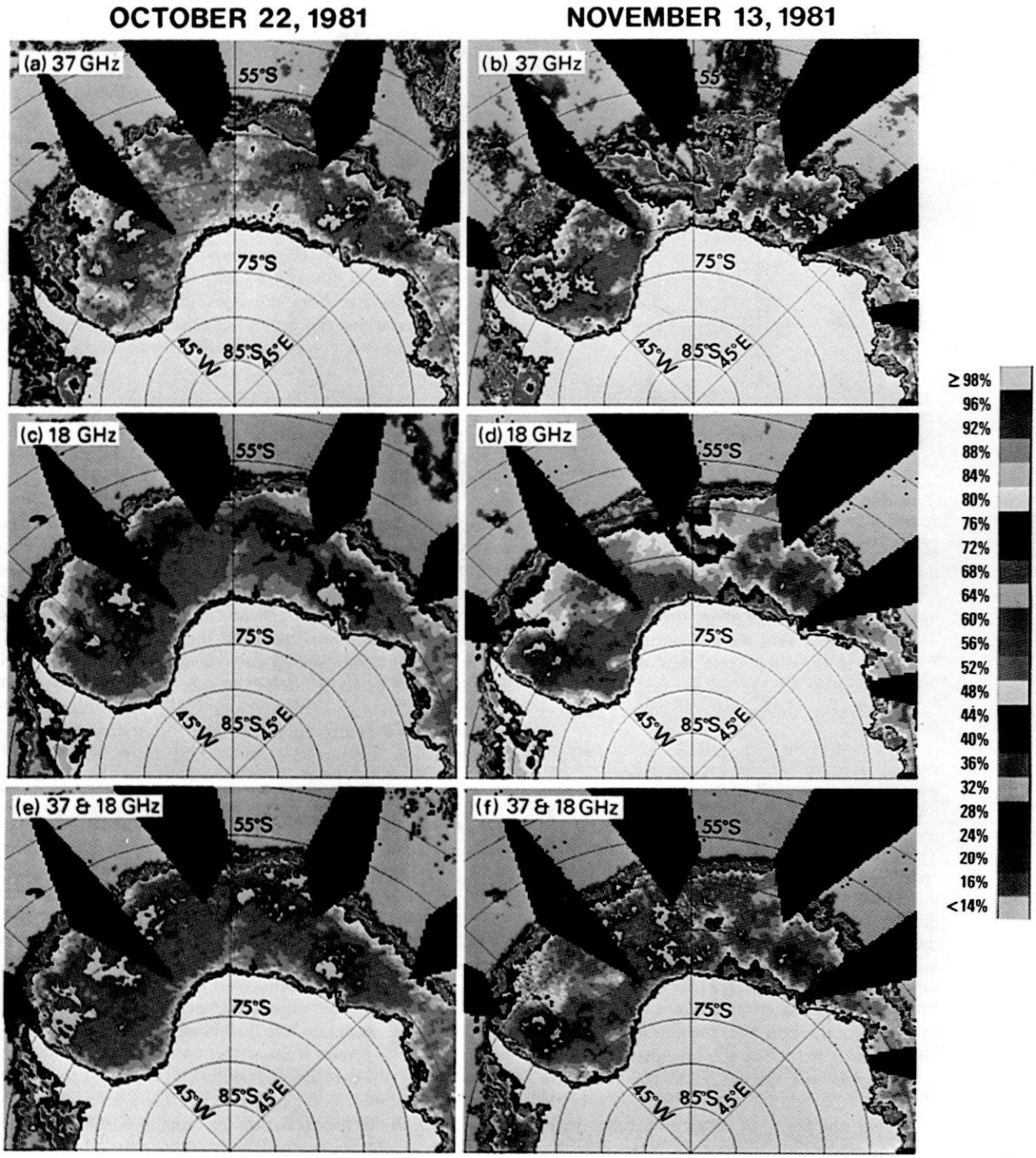

Plate 1. Ice concentrations inferred from SMMR for the October 22, 1981, and November 13, 1981, data using fixed emissivities Plates 1*a*–1*d* and variable emissivities Plates 1*e*–1*f*.

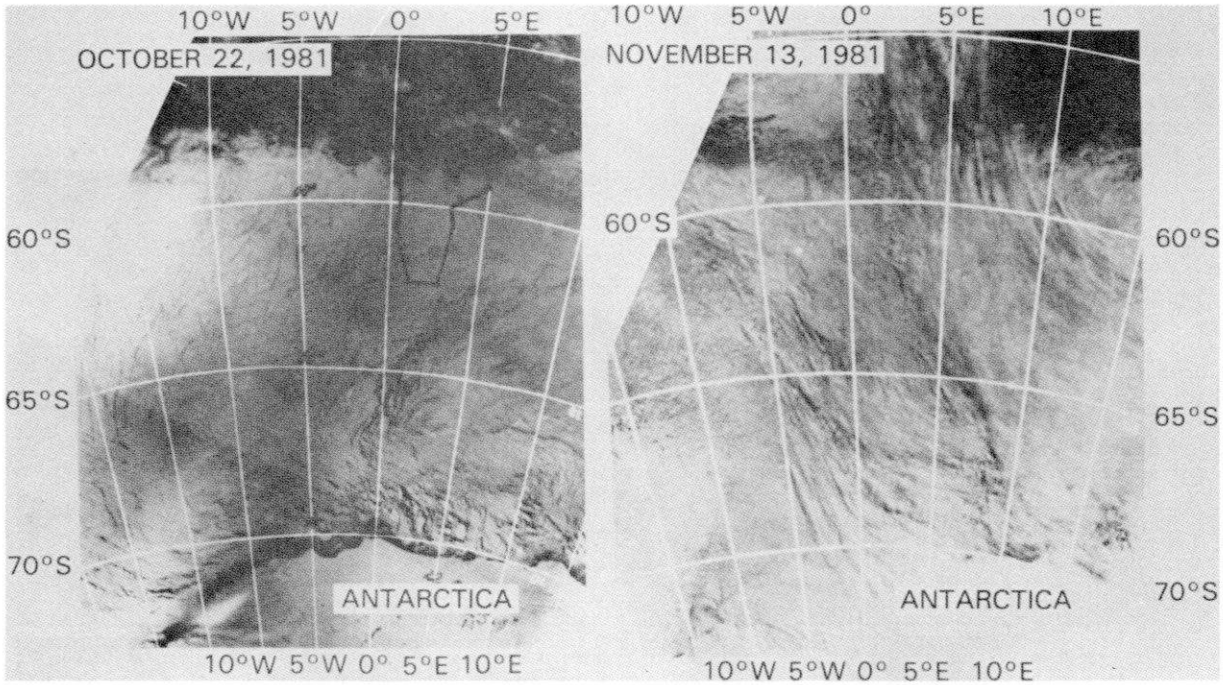

Fig. 9. Ice conditions from a USSR visual range sensor during (*a*) October 22, 1981, and (*b*) November 13, 1981.

hail Somov observations. Moreover, the errors in a study such as of the spatial variability of emissivities, which is statistical in nature, should not be affected by an offset in the measurement of physical temperature. Also, scatter plots using brightness temperatures show good agreement in the clustering of data points with those using emissivities (Figures 4 and 6) in which the THIR data are used. This indicates minimal contributions of possible abnormal physical temperature values inferred from the THIR data, especially in cloud covered regions.

The errors in the surface temperatures observed from the ship are assumed minimal because the thermistors were constantly recalibrated. However, observed ice values were at times greater than 2 K above freezing indicating that sometimes the real surface temperatures were not being measured. This partly explains why THIR values are generally lower. An error of about 2 K is therefore assumed as the uncertainty in the surface temperature measurement. When this error is combined with estimated uncertainty in the relative calibration of the SMMR data of less than 3 K (T. T. Wilheit, private communications, 1982) and other effects, the error in emissivity is calculated and given in Table 1. The larger errors for the emissivities at 21 GHz are due mainly to the aforementioned uncertainties in observed brightness temperatures at this frequency.

In the ice edge analysis the error in using T_B instead of inferred ice concentration is expected to be small, because, generally, there is no substantial variability in the physical temperature in the marginal ice zone. However, in the November 13 distribution of T_B, even the 18 GHz is subject to errors because of surface effects pointed out previously.

As for ice concentration, the main source of error is the use of the THIR temperature data, which is subject to uncertainties in heavily cloud-covered regions. However, statistical analysis of the THIR temperature data shows that this is not expected to affect more than 10% of the study areas. Also, there is consistency in the clustering of points in both the brightness temperature and emissivity scatter plots. Furthermore, any offset in the absolute value of the measurement is subject only to minimal error because the emissivity plots (Figures 4 and 6) are used as tie points in the analysis. There is, however, an uncertainty associated with the scatter of data points of consolidated ice about the 100% ice line. This causes an error in the determination of ice concentration of about 2–4%. The errors in the in situ observations of ice concentration in the near-consolidated ice regions are expected to be very small. In the marginal ice zone, although the percentage ice cover is relatively harder to infer from a ship, the observed width of the marginal ice region should have an error less than the size ($\sim$30 km) of the interpolated satellite data elements.

4. Conclusions

The microwave sea ice emissivities at the various SMMR frequencies in the Antarctic region have been evaluated, and the results are in agreement with previous determinations of first year ice emissivities in the Arctic region. An analysis of brightness temperatures near the ice edge shows different sensitivities of the various SMMR channels to ice conditions near the marginal ice zone. It is observed that the 18 GHz data give the most reliable description of the ice edge conditions during the spring period because of less sensitivity to surface effects and higher resolution than the 6.6 and 10.7 GHz channels.

A time-dependent surface characteristics effect, observed during the expedition from October 22, 1981, to November 13, 1981, is found to coincide with a substantial change in the distribution of emissivities inferred from the region between the two periods. On November 13, 1981, the emissivity of consolidated first year ice is found to have a variability of as much as 20% at 37 GHz. Using multispectral analysis, it is demonstrated that an effective way to account for the variability of the emissivities in ice concentration calculations is to

adjust the emissivities until there is consistency in the ice concentrations determined from the various SMMR channels.

This study has helped identify some of the problems associated with the passive microwave remote sensing of sea ice in the southern ocean, especially during a period when a substantial change in the surface characteristics of the ice is observed. It also has shown the versatility of a multispectral sensor like the SMMR and the capability to handle the specific problem identified. Furthermore, it shows the importance of having surface observations as an aid in the interpretation of remotely inferred satellite geophysical data.

Acknowledgments. One of the authors (J.C.C.) is grateful to H. J. Zwally for some illuminating discussions during the course of this work. He also would like to thank Margot Osborne, Richard Johnson, and Ron Nieman from Computer Sciences Corporation for programing support. The authors are also grateful to Don Barnett from the Navy-NOAA Joint Ice Center and the Russian scientists for providing other satellite data, and to Sandra Smith from CRREL for compiling and organizing the sea ice data set of the U.S.-USSR Weddell Polynya Expedition. This work is partly supported by the NASA Oceans Program (J.C.C.). Funding for the expedition was provided by the Division of Polar Programs of the National Science Foundations; grant DPP 80-05765 funded the research of A. L. Gordon, and DPP 80-06922 funded the research of S. F. Ackley. ONR also supported the study of the Structure and Dielectric Properties of Sea Ice (S. F. Ackley). Lamont-Doherty Geological Observatory contribution number 3543.

REFERENCES

Ackley, S. F., and S. J. Smith, Weddell polynya expedition: Sea ice observations, CRRELL Special Report, Cold Reg. Res. and Eng. Lab., Hanover, N.H., 1982.

Ackley, S. F., S. J. Smith, and D. B. Clarke, Observations of pack ice properties during the U.S.-U.S.S.R. Weddell Polynya Expedition, *Antarctic J. U.S.*, *17*, 105–106, 1982.

Carsey, F., Arctic fall onset of sea ice, *J. Geophys. Res.*, *87*, 836–844, 1982.

Chang, A. T. C., and P. Gloersen, Microwave emission from dry and wet snow, in Operational Applications of Satellite Observations, edited by A. Rango, pp. 339–407, *NASA SP-361*, 1975.

Clarke, D. B., and S. F. Ackley, Physical, chemical, and biological properties of winter sea ice during the U.S.-U.S.S.R. Weddell Polynya Expedition, *Antarctic J. U.S.*, *17*, 107–109, 1982.

Comiso, J. C., Sea ice effective microwave emissivities from satellite passive microwave and infrared observations, *J. Geophys. Res.*, *88*, 686–704, 1983.

Comiso, J. C., and H. J. Zwally, Antarctic sea ice concentration inferred from Nimbus 5 ESMR and Landsat imagery, *J. Geophys. Res.*, *87*, 836–844, 1982.

Gloersen, P., and F. Barath, A scanning multichannel microwave radiometer for Nimbus 7 and Seasat, *IEEE Oceanic Eng.*, *OE2*, 172–178, 1977.

Gloersen, P., and J. K. Larabee, An optical model for the microwave properties of sea ice, *NASA TM 83865*, 1981.

Gloersen, P., D. J. Cavalieri, and H. V. Soule, Variations in the Nimbus-7 Scanning Multichannel Microwave Radiometer cold reference antenna signals and temperatures during two orbital periods, *NASA TM 81984*, 1980.

Gordon, A. L., and E. I. Sarukhanyan, American and Soviet expedition into the Southern Ocean sea ice in October and November 1981, *Eos Trans. AGU*, *63*, 2, 1982.

Gordon, A. L., and B. A. Huber, Thermohaline stratification below the Southern Ocean sea ice, *J. Geophys. Res.*, in press, 1983.

Gudmandsen, P., Remote sensing of sea ice, *ESA Bull.*, *22*, 8–13, 1980.

Hofer, R., and E. Schanda, Signature of snow in the 5 to 94 GHz range, *Radio Sci.*, *13*, 365–369, 1978.

Kunzi, K. F., S. Patil, and H. Rott, Snow-cover parameters retrieved from Nimbus-7 Scanning Multichannel Microwave Radiometer (SMMR) data, *IEEE Trans. Geosci. Rem. Sens.*, *GE-20*, 452–467, 1982.

Njoku, E. G., Antenna pattern correction procedures for the Scanning Multichannel Microwave Radiometer (SMMR), *Boundary Layer Meteorol.*, *18*, 79–98, 1980.

Njoku, E. G., J. M. Stacey, and F. Barath, The SEASAT Scanning Multichannel Microwave Radiometer (SMMR): Instrument description and performance, *IEEE J. Oceanic Eng.*, *OE5*, 100–115, 1980.

Ramseier, R. O., P. Gloersen, W. J. Campbell, and A. T. C. Chang, Mesoscale description for the principal Bering Sea ice experiment, *NASA TM 70648*, 1974.

Stiles, W. H., and F. T. Ulaby, The active and passive microwave response to snow parameter, 1, Wetness, *J. Geophys. Res.*, *85*, 1037–1044, 1980.

Svendsen, E., K. Kloster, B. Farrelly, O. M. Johannessen, J. A. Johannessen, W. J. Campbell, P. Gloersen, D. Cavalieri, and C. Matzler, Norwegian Remote Sensing Experiment: Evaluation of the Nimbus 7 Scanning Multichannel Microwave Radiometer for sea ice research, *J. Geophys. Res.*, *88*, 2755–2769, 1983.

Vant, M. R., R. B. Gray, R. O. Ramseier, and V. Makios, Dielectric properties of fresh sea ice at 10 and 35 GHz, *J. Appl. Phys.*, *45*, 4712–4717, 1974.

Wilheit, T. T., Atmospheric corrections to microwave radiometer data, *Boundary Layer Meteorol.*, *18*, 65–77, 1980.

Zwally, H. J., and P. Gloersen, Passive microwave images of the polar regions and research applications, *Polar Rec.*, *18*, 431–450, 1977.

Zwally, H. J., J. C. Comiso, C. L. Parkinson, W. J. Campbell, F. D. Carsey, and P. Gloersen, Antarctic sea ice 1973–1976 from satellite passive microwave observations, *NASA SP459*, 1983.

S. F. Ackley, Cold Regions Research and Engineering Laboratory, Hanover, NH 03755.

J. C. Comiso, Goddard Laboratory for Atmospheric Sciences, NASA Goddard Space Flight Center, Greenbelt, MD 20771.

A. L. Gordon, Lamont-Doherty Geological Observatory, Columbia University, Palisades, NY 10964.

(Received April 28, 1983;
revised August 22, 1983;
accepted September 6, 1983.)

JOURNAL OF GEOPHYSICAL RESEARCH, VOL. 89, NO. C2, PAGES 2087–2095, MARCH 20, 1984

Sea Ice Structure and Biological Activity in the Antarctic Marginal Ice Zone

D. B. CLARKE AND S. F. ACKLEY

U.S. Army Cold Regions Research and Engineering Laboratory

Ice cores obtained during October–November 1981 from Weddell Sea pack ice were analyzed for physical, chemical, and biological parameters. Frazil ice, which is associated with dynamic, turbulent conditions in the water column, predominated (70%). Both floe thickness and salinity indicate ice which is less than 1 year old. Chemical analyses, particularly with regard to the nutrients, revealed a complex picture. Phosphate values are scattered relative to the dilution curve. Nitrate and silicate values are lower than expected from simple scaling with salinity and suggest diatom growth within the ice. Nitrite values are higher in the ice than in adjacent waters. Frazil ice formation which probably concentrates algal cells from the water column into ice floes results in higher initial chlorophyll *a* concentrations in the ice than in adjacent waters. This mechanical concentration is further enhanced by subsequent reproduction within the ice. Ice core chlorophyll ranged from 0.09 to 3.8 mg/m^3, comparable to values previously reported for this area but significantly lower than values for Antarctic coastal fast ice. The dominance of frazil ice in the Weddell is one of the major differences between this area and others. Consequently, we believe that ice structural conditions significantly influence the biological communities in the ice.

INTRODUCTION

Sea ice cover in the southern ocean is important for several physical and biological reasons. At its maximum extent in September and October, ice covers approximately 20×10^6 km^2, while at its minimum in February it covers 3×10^6 km^2 [*Gordon*, 1981]. The difference between these two extremes, 17×10^6 km^2, represents an area larger than the Antarctic continent itself. In addition, ice cover of 85% or greater exists over a period of several months, thus effectively diminishing heat and gas exchange between the ocean and the atmosphere. Ice cover also acts as a filter, reducing the amount of sunlight available for photosynthesis in the underlying water column.

While the ice cover acts as a physical barrier to some processes beneath it, the ice itself provides a unique physical and chemical environment for other biological processes. The biological community associated with sea ice is, however, not yet fully understood and shows large-scale variability [*Ackley et al.*, 1979; *Garrison and Buck*, 1984; *Sullivan and Palmisano*, 1981; *Buynitsky*, 1977; *Hoshiai*, 1977]. This variability may depend on local ice growth conditions and the thermodynamic and dynamic history of the ice cover.

In this paper we present results obtained on the 1981 Weddell Polynya Expedition [*Gordon and Sarukhanyan*, 1982] on sea ice properties. We then infer relationships between ice structure and biological properties and compare these results to studies on sea ice from other regions of the Antarctic.

Sampling of ice floes during the joint U.S.-U.S.S.R. Weddell Polynya Expedition (WEPOLEX) was carried out in the pack ice of the Weddell Sea between 59°21′ and 62°00′S latitude and 0°–5°E longitude between October 22 and November 13, 1981 (Figure 1). Samples taken with a CRREL 7.6-cm ice coring auger totaled 27 cores obtained at 11 sampling stations. Each core was analyzed at nominal 10-cm intervals for the following parameters: salinity, ice structure, nutrients (phosphate, silicate, nitrate, and nitrite), in vivo fluorescence, chlorophyll *a*, phaeopigment, and diatom species enumeration. Studies of bacteria and oxygen isotopes were also made on a limited data set. Figure 2 shows the flow diagram followed in sampling the ice cores while on board ship. Analyses were performed going from left to right in the figure, allowing those that destroyed the sample to be performed last. Physical analysis of ice type and structure was done by using a thin section of the ice and observing its optical behavior between crossed polarizers. Samples were then melted and immediately analyzed for nutrients by using a Technicon Autoanalyzer (following the methods of *Gordon et al.* [1976]). Meltwater salinity was obtained with a Beckman salinometer, and in vivo fluorescence and chlorophyll *a* were determined by using a Turner Designs model 10 fluorometer. Chlorophyll *a* samples were filtered through Gelman type A/E filters, and the filters were frozen until analysis within several days of collection. Diatom enumeration was done, by using a Zeiss inverted light microscope, and species identifications were made by using a Hitachi S-500 Scanning Electron Microscope (SEM). Water column samples were obtained by *Gordon and Huber* [1984] using a CTD Rosette.

Paper number 3C1764.

RESULTS

Physical Properties

Ice cores were taken from the end of October to mid-November, which corresponds to the austral late winter-early spring, as indicated by freezing conditions in the early portion of the cruise and surface melting in the later portions. Pack ice is initially observed (by satellite) in this region during mid-June. We estimate from previous observations of ice drift velocities [*Ackley*, 1981] and modeling studies [*Hibler and Ackley*, 1983] that the ice in this region at the time of sampling was probably not formed before the previous June.

Table 1 shows the primary physical properties of the ice cores. The lengths of the cores varied between 32 and 162 cm with an average value of around 75 cm [*Clarke and Ackley*, 1982]. Snow cover ranged from 10 to 30 cm, the average being 20 cm. We attempted to sample level portions of ice floes away from ridges and other deformational features, but

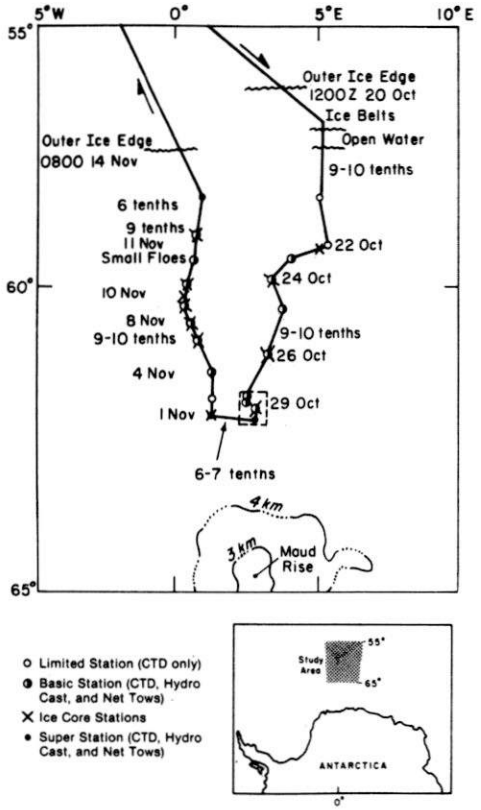

Fig. 1. Cruise track of the NES *Mikhail Somov* during the U.S.-U.S.S.R. Weddell Polynya Expedition, October-November 1981, and the relationship of the study area to Antarctica.

we were limited to sampling relatively localized areas in the region where the ship could abut a suitable ice floe. These average thicknesses are in accordance with previous estimates of Antarctic sea ice in the ice edge region where thicknesses of less than 1 m are believed to be typical [*Hibler and Ackley*, 1983]. Average salinities (Table 1) were similar to values previously found in the Arctic and Antarctic for end-of-winter conditions [*Gow et al.* 1982; *Ackley et al.*, 1979; *Weeks and Ackley*, 1982]. Higher salinity values, exceeding 4‰, were found in the top layers of the ice cores, indicating no significant brine drainage had yet occurred (Figure 3). Salinities lower than 4‰ were usually associated with high temperatures and spring-summer conditions [*Gow et al.*, 1982]. Both the average salinities and the salinity profiles therefore indicate end-of-winter conditions for the ice pack at the time of sampling.

Structurally, the ice was divided into three categories: congelation ice, frazil ice, and snow ice. *Weeks and Ackley* [1982] describe in detail the formation processes for these types of ice. In brief, frazil ice is associated with dynamic, turbulent conditions in the water column where small (~1 mm) ice crystals form, usually at high growth rates (>1 cm/hour). These crystals are advected downstream by wind-induced circulation in the water column and pile up into substantial thicknesses of ice in short time periods. *Bauer and Martin* [1983] indicate that ice thicknesses exceeding 50 cm can form from these frazil ice accumulations in periods on the order of a few hours. In contrast, congelation ice is composed of larger, columnar-grained crystals (~1 cm) resulting from the slow removal of heat from the water under an existing ice sheet. After a few centimeters of ice form, the low thermal conductivity of the ice limits the heat transfer and prevents growth rates greater than ~1 mm/hour, a rate which continues to decrease as the ice thickens. Congelation ice therefore forms more slowly and requires periods on the order of several weeks to achieve the thicknesses observed here. We found, as shown in Table 1, that the ice cores usually consisted of frazil ice, averaging 70% of the thickness, indicating that dynamic effects (the wind-induced circulation in leads and polynyas) and relatively rapid growth accounted for most of the ice formation process. These results were in general agreement with a previous structural survey in the perennial ice cover in the western Weddell Sea (along 40°W longitude) [*Ackley et al.*, 1980; *Gow et al.*, 1982] where the floes were found on the average

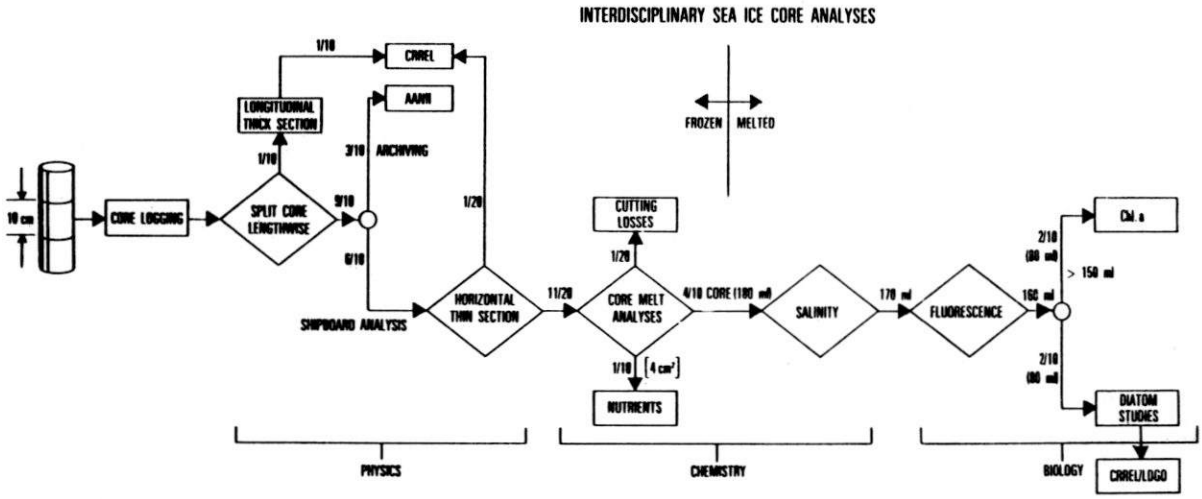

Fig. 2. Flow diagram indicating, from left to right, the successive core divisions and analyses performed on each 10 cm core sample. Fractions (e.g., 1/10) or quantities (e.g., 170 ml) refer to portions of solid core or meltwater used in the various steps. AANII (Arctic and Antarctic Research Institute, Leningrad), CRREL (Cold Regions Research and Engineering Laboratory), and LDGO (Lamont Doherty Geological Observatory) refer to the institutions where the designated samples are archived.

TABLE 1. Positions and Averaged Data for Ice Cores

Core Number	Date, 1981	Position	Thickness T, m	Salinity, ‰	Chlorophyll a (mg/m^3) Average Concentration	Chlorophyll a (mg/m^3) Maximum Concentration	Frazil, %
1-22/0	Oct. 22	59°21.5'S 5°13.2'E	0.60	5.0 ± 1.3	0.58	0.78	100
2-22/0	Oct. 22	59°21.5'S 5°13.2'E	1.17	6.5 ± 2.2	0.72	1.32	100
3-24/0	Oct. 24	59°53.7'S 3°24.9'E	0.60	5.3 ± 2.4	1.19	1.19	100
4-24/0	Oct. 24	59°53.7'S 3°24.9'E	0.57	4.5 ± 1.0	1.19	1.19	100
5-26/0	Oct. 26	61°10.7'S 3°03.9'E	1.52	4.8 ± 1.2	1.27	2.85	82
6-26/0	Oct. 26	61°10.7'S 3°03.9'E	1.62	4.7 ± 1.3	0.66	0.97	85
7-29/0	Oct. 29	62°00.2'S 2°25.9'E	0.32	10.7 ± 3.3	1.42	1.42	50
8-29/0	Oct. 29	62°00.2'S 2°25.9'E	0.60	6.6 ± 3.3	0.15	0.15	78
9-1/N	Nov. 1	62°11.2'S 2°53.8'E	0.81	6.2 ± 2.8	1.00	1.95	71
10-1/N	Nov. 1	62°11.2'S 2°53.8'E	0.67	4.7 ± 1.2	1.12	1.62	?
11-1/N	Nov. 1	62°11.2'S 2°53.8'E	0.64	4.2 ± 1.1	2.52	3.84	87
12-4/N	Nov. 4	62°12.4'S 1°03.5'E	0.69	4.9 ± 1.4	0.35	0.45	55
13-4/N	Nov. 4	62°12.4'S 1°03.5'E	0.68	6.4 ± 2.4	0.63	1.28	60
14-4/N	Nov. 4	62°12.4'S 1°03.5'E	0.68	4.1 ± 0.7	0.20	0.35	41
16-8/N	Nov. 8	60°57.7'S 0°43.5'E	0.68	4.0 ± 0.9	0.33	0.46	24
17-8/N	Nov. 8	60°57.7'S 0°43.5'E	0.68	4.9 ± 2.2	0.16	0.24	34
20-10/N	Nov. 10	60°39.7'S 0°37.1'E	0.78	5.3 ± 0.76	1.90	3.41	81
22-10/N	Nov. 10	60°17.0'S 0°15.3'E	0.54	5.1 ± 1.7	0.24	0.24	100
24-11/N	Nov. 11	60°05.1'S 0° .2'E	0.69	4.9 ± 2	0.28	0.35	57
26-13/N	Nov. 13	59°09.1'E 0°45.6'E	0.54	4.9 ± 1.3	0.43	0.43	15

to be composed of about 50% frazil ice. The higher wind regime and consequent increase in ice dynamics at the ice edge region could possibly account for the proportionately higher frazil ice percentages observed in the present study. Snow ice is formed when seawater floods the snow cover on a floe and subsequently freezes. This type of ice, while not as prevalent in this region as the other ice types, has some interesting biological properties which we discuss later.

The apparent rapid growth process of the majority of the ice cover is important for the distribution and structure of the biological and chemical regimes of the pack ice. One effect of rapid ice growth is the manner in which algal cells are incorporated into the ice cover. *Ackley* [1982] and *Garrison et al.* [1984] hypothesize that frazil ice can incorporate cells by two mechanical effects, either by nucleation of a frazil ice crystal or by scavenging (incidental incorporation) of cells as a frazil crystal floats up through the water column. The result is that frazil formation can initially concentrate algal material at higher levels in the ice than in the water column. In contrast, congelation ice formation may reject algal cells in the initial growth period much as salt is rejected during ice growth. However, the bottom ice layer in congelation ice, for example, the fast ice at McMurdo Sound, provides a unique growth habitat in the late season for certain species of well-adapted algae. *Sullivan and Palmisano* [1981, 1982] and *Palmisano and Sullivan* [1982] have detailed the structure of these communities. The results we show here, because of the dominance of frazil ice, provide some contrast to previous work as to how the composition and density of the community may relate to ice structure.

Chemical Properties

Twenty of the ice cores have been analyzed for nutrients (silicate, SiO_4; phosphate, PO_4; nitrate, NO_3; and nitrite, NO_2). (See, for example, Figure 3.) Comparison of the ice samples with surface water samples taken with the CTD rosette show that salinity and nutrient concentrations are higher in the surface waters and are reduced in the ice samples with one notable exception which we discuss below. In retrospect, we realize that ammonia (NH_3) measurements would have been extremely useful in understanding the nitrogen cycle. Unfortunately, laboratory conditions on the ship presented difficulties in obtaining these measurements, and at the time we did not realize the importance these measurements might have.

Figures 4–7 compare the nutrient values to the salinities of

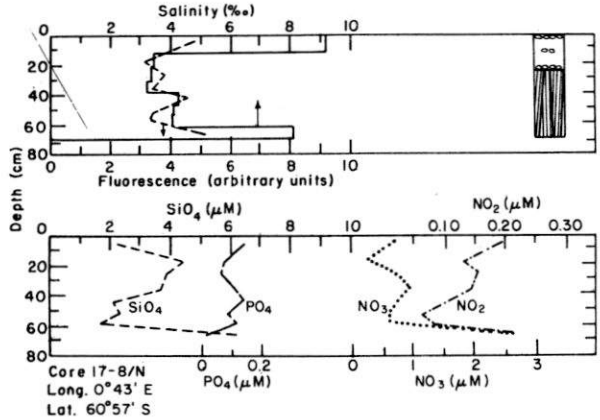

Fig. 3. A typical core profile (17-8/N) showing salinity, fluorescence, nutrients (silicate, phosphate, nitrate, and nitrite), and structure versus depth. In the structural cartoon, circles indicate frazil ice structure, and vertical lines show congelation or columnar ice structure.

the ice cores along with curves based on expected values from surface water diluted to the salinity of the ice samples. While the data generally show a large degree of scatter from any linear trend, some features are evident. Figure 4 shows the phosphate values, which are scattered but are of similar magnitude to the dilution curve. *Garrison and Buck* [1984] found that phosphate in their ice cores approximated the dilution curve. Also plotted on Figure 5 along with the silicate values is the least squares line that best fits the data. With regard to the dilution curve, all of the silicate values fall below it indicating that silicate is depleted in the ice cores relative to surface waters. *Garrison and Buck* [1984] found that while silicate in young thin ice followed the dilution curve, it was generally found in lower concentrations in older ice cores.

The plots of nitrate (Figure 6) and nitrite (Figure 7) also show that neither of these nutrients scales directly with salinity. The nitrate plot shows that nearly all of the data points fall significantly below the dilution curve, while the nitrite plot shows the opposite, with all of the data points above the dilution curve. In fact, nitrite concentrations are the exception mentioned earlier showing higher values in the ice than in the surface waters.

Linear correlations between depth, salinity, fluorescence, phosphate, silicate, nitrate, nitrite, chlorophyll *a*, and phaeopigments were computed. The results, as a correlation coefficient matrix, are shown in Table 2. When we examine both ice types together (frazil and congelation), the only significant correlation is between silicate and salinity. The correlation coefficient of 0.78 gives an F value in analysis of variance of 81, which with the 50 degrees of freedom is significant at the 1% level [*Panofsky and Brier*, 1965]. We have previously noted this linear relationship when examining silicate and salinity in Figure 5.

In summary, there are three points that can be made with regard to the nutrients in our ice cores:

1. With the exception of silicate, there is poor correlation between the nutrients and salinity.

2. Silicate and nitrate concentrations are generally depleted relative to the dilution curve (nearly all values fall below the lines).

3. Nitrite values are enriched relative to the dilution curve (all values are above the line) and actually exceed surface water values.

Biological Properties

Chlorophyll *a* concentrations in the surface layers of the ice cores ranged from 0.13 to 1.42 mg/m^3. Samples for chlorophyll *a* analysis were not taken at discrete depth intervals but rather were integrated over several depths. Chlorophyll *a* concentrations ranged from 0.09 to 3.8 mg/m^3 in the cores; generally higher values are found deeper in the ice than in the ice surface layers. No definite trend was found between chlorophyll *a* concentration and ice thickness. There was considerable variation in values from cores taken in close proximity to each other. Chlorophyll *a* concentrations were significantly higher in the ice cores (~1 mg/m^3) than in the adjacent surface waters (<0.1 mg/m^3).

No significant relationship was found between chlorophyll *a* and any other parameter when all ice samples were grouped. However, if the ice samples were segregated into frazil and congelation ice, some parameters were apparently correlated. For the frazil ice, the correlation coefficient matrix is shown in Table 3. While the relationship between silicate and salinity still exists (0.69), the correlation has decreased slightly. However, we now see some correlation between chlorophyll *a* and depth (0.62), between phaeopigment and depth (0.74) and between chlorophyll *a* and phaeopigment (0.63) (Table 3). All these high values exceed the F test for significance at the 1% level with 30 degrees of freedom. Since most of the surface samples are of frazil ice, this finding reflects what we mentioned earlier, that the surface samples are relatively lower in chlorophyll *a* than samples at depth. However, the weakness of the correlation implies that there is no continuing increase with depth but only a relative increase compared to surface ice layer values.

A similar correlation coefficient matrix was calculated for the congelation samples comprising a smaller number of data points which, unlike the frazil ice samples, are not randomly distributed over depth. We found low correlation, but feel this has little significance due to the paucity of data points. However, we have inferred from the observed correlation that the frazil ice at depth has slightly higher amounts of chlorophyll *a* than the frazil ice in the surface layers. Because this correlation breaks down when all ice samples are included, we also infer that frazil ice at depth has higher

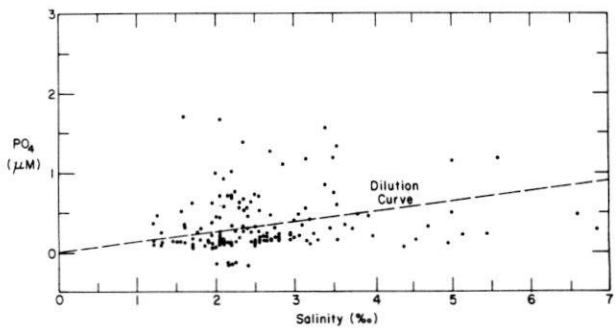

Fig. 4. Phosphate values plotted against salinity for all samples. The dilution curve shows the expected values if the decrease of phosphate is related solely to the reduced salinities in the ice (2.5–3.7‰) from values found in adjacent surface waters (34‰).

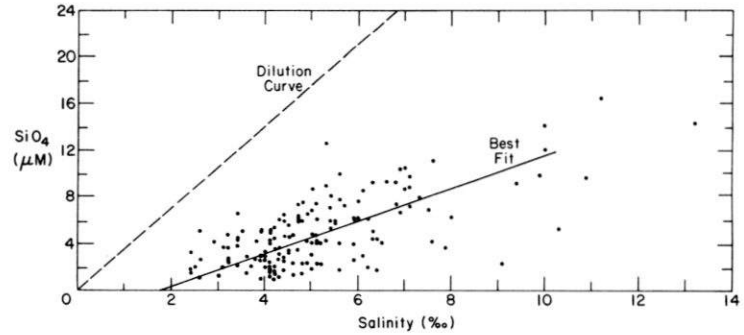

Fig. 5. Silicate values plotted against salinity for all samples. The dilution curve shows the expected values if the decrease of silicate is related solely to the reduced salinities in the ice (2.5–13.7‰) from values found in adjacent surface waters (34‰).

chlorophyll *a* than congelation ice at depth. This inference is confirmed by averaging the chlorophyll *a* values by ice type which gives 0.46 mg/m^3 for surface frazil ice, 1.36 mg/m^3 for frazil ice at depth, and 0.38 mg/m^3 for congelation ice at depth.

Salinities in the ice cores range from 2.4 to 13.7‰ with the average salinity for each core listed in Table 1. In general, surface salinities, those within the upper 15 cm, are highest in any individual ice core.

Samples analyzed from two ice cores and a chunk of ice obtained at the same station illustrate the variability in physical and biological properties. A yellow-brown ice chunk (10-N/K), found near a ridge, is composed of snow ice (seawater-infiltrated snow). Its chlorophyll *a* concentration is 43.2 mg/m^3. One of the ice cores, 22-10/N (Figure 8), is entirely frazil ice and its chlorophyll *a* concentration is 0.23 mg/m^3. The second core taken at this location, 23-10/N (Figure 9), while almost the same length as the first, nevertheless has 16 cm of congelation ice at the bottom overlain by frazil ice. Since chlorophyll was not measured in the second core, we can only compare the diatom concentrations present in both cores. Significant differences exist in the total full cell concentration between these two cores (3.4×10^5 cells/l in 22-10/N and 9.0×10^6 cells/l in 23-10/N). Owing to the visible coloration of 10-N/K, as well as its high chlorophyll concentration, we assume that it has a significantly greater cell concentration than either of the ice cores. The diatom species composition varies among these three samples. The diatom assemblage in the ice chunk is nearly monospecific (85% *Tropidoneis* species), whereas several species are codominant in the ice cores, their relative abundances changing with depth.

The cell count information for these cores was also compared with that from ice obtained in the western Weddell Sea during a different season. Figure 10 shows the salinity and structural profile for a core (51-G-4) obtained during February 1980 (at the end of the summer season). These two cores (23-10/N and 51-G-4) have dissimilar physical structure, varying in thickness (50 cm versus 191 cm length), composition (depth and position of frazil and congelation ice sequences), and salinity profiles. In biological content (Figures 11 and 12), they are somewhat similar in that the highest concentration of diatoms (greater by an order of magnitude) is seen near the bottom in both cores. These values reach 2.5×10^6 cells/l in core 23-10/N and 1.8×10^8 cells/l in core 51-G-4 (also highly colored). At the surface there are only 2.1×10^5 cells/l in core 23-10/N, while at the surface of 51-G-4 the number of full cells/liter is even lower (6.2×10^4 cells/l).

The difference in diatom concentration between these two cores is 2 orders of magnitude. This may in part be explained by the longer history (1 year or older) of 51-G-4 which survived the summer melt and was not sampled until the end of summer. The nutrient data of *Garrison and Buck* [1984] suggests that continuing diatom growth may have occurred during the spring-summer season since silicate is depleted relative to the dilution curve, thus accounting for the higher

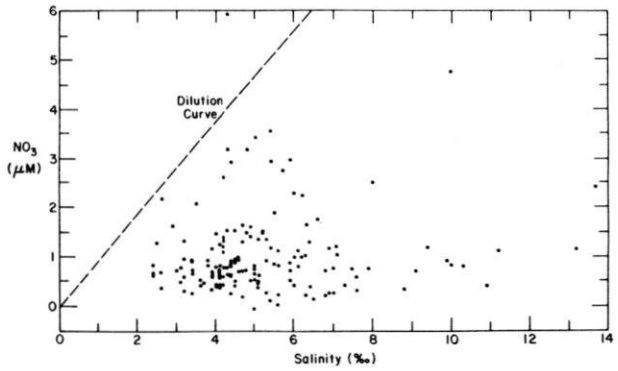

Fig. 6. Nitrate values plotted against salinity for all samples. The dilution curve shows the expected values if the decrease of nitrate is related solely to the reduced salinities in the ice (2.5–13.7‰) from values found in adjacent surface waters (34‰).

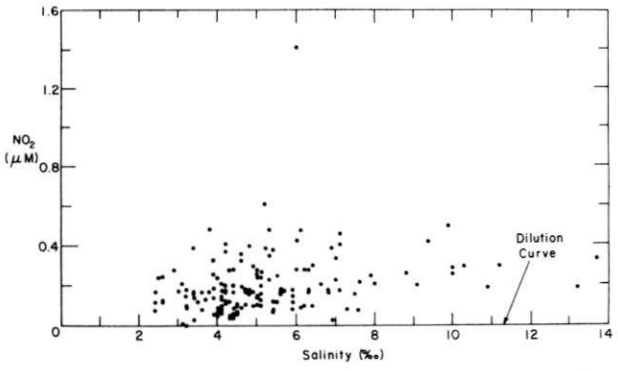

Fig. 7. Nitrite values plotted against salinity for all samples. Dilution curve follows zero line as nitrite had low values in surface water.

TABLE 2. Correlation Coefficient Matrix

	Depth	Salinity	Fluorescence	Phosphate	Silicate	Nitrite	Nitrate	Chlorophyll *a*	Phaeopigments
Depth	1.0	−0.31	0.23	0.19	−0.17	0.09	0.37	0.33	0.07
Salinity		1.0	0.20	0.18	0.78	0.16	0.06	−0.06	0.38
Fluorescence			1.0	0.16	0.25	−0.06	0.06	0.35	0.29
Phosphate				1.0	0.22	0.07	0.25	0.11	0.02
Silicate					1.0	0.16	0.21	−0.06	0.44
Nitrite						1.0	0.27	0	0.03
Nitrate							1.0	0.02	0.25
Chlorophyll *a*								1.0	0.27
Phaeopigments									1.0

Data averaged at depth interval corresponding to chlorophyll *a* and phaeopigment values.

biomass in this core. However, it appears that conditions at depth in both ice cores are generally more favorable than in the surface layer for diatom viability, irrespective of ice type, age, or season.

DISCUSSION

Physical, Chemical, and Biological Interactions

While the physical properties of the ice cores are often similar, the chemical and biological properties show greater disparities. In this section we will examine the variability of the ice in regard to how it is formed, its subsequent history, and how this affects the biological regime. Half of the ice cores taken at the same sampling station are nearly identical in length, ice type, and structure (i.e., layering of frazil and congelation ice). In the other half, however, the sequence of frazil and congelation ice is different, and the total length may vary by 20–30 cm. Even cores taken close to each other with similar physical structure may have differences in their chemical and biological properties. There is no discernible pattern to the salinity and nutrient concentrations in the cores as indicated by the weak correlations of these components with each other and with the physical properties. This variability is also seen in the chlorophyll *a* and phaeopigment values for the cores. A threefold difference in chlorophyll *a* concentration may exist between two cores from the same station with similar length and structure.

We believe that this variability in chlorophyll *a*, phaeopigments, and nutrient concentrations is caused by the formation conditions and subsequent history of ice floes. Frazil ice can form relatively quickly. In high wind and low temperature conditions, a 50- to 60-cm floe may form within a matter of several hours to a day or two. As it forms, it is incorporating the chemical and biological components of the water column from which it is derived. The rate of formation governs both how much brine is initially incorporated into the ice and how much biological material it will contain. Another factor that will influence the type and amount of biological material initially incorporated is the possible presence of a diatom bloom at the time of formation. Diatom blooms reported in the literature are noted for their patchiness [*El-Sayed*, 1971], and therefore ice floes formed within several kilometers of each other can have considerable differences in biological concentration and species composition. Ice formed later in the season in open leads or small polynyas will be formed from an entirely different water column and can be physically different from older ice. The "floe" that we sample is therefore an aggregate of several formation processes occurring at different times, over different water columns, and at different rates. Once a floe has formed, it is also subject to continuing change (e.g., temperature fluctuations within the ice, brine migration, and possibly deformation). Light penetration, a critical factor in regulating diatom growth, is drastically affected by the amount of snow cover on the floes [*Bunt and Lee*, 1970; *Sullivan and Palmisano*, 1981; *Grainger*, 1977] which varies with the age of each component of the floe.

All of these factors then must be taken into account when comparing cores from the same floe, as well as from different sampling locations. Much of the pack ice in the Antarctic is seasonal, a year old or less. In the Weddell Sea, off the Antarctic Peninsula, we also find multi-year floes. Multi-year floes have survived seasonal melting and refreezing and have considerably different physical, chemical, and biological features than 1-year floes. In turn, the seasonal ice differs from thin ice [*Ackley et al.*, 1979; *Garrison and Buck*, 1984]. D. L. Garrison (personal communication, 1983), however, finds evidence that after a certain amount of time drifting ice may reach an equilibrium state so that all the ice below the

TABLE 3. Structure-Frazil Ice Correlation Coefficient Matrix

	Depth	Salinity	Fluorescence	Phosphate	Silicate	Nitrite	Nitrate	Chlorophyll *a*	Phaeopigments
Depth	1.0	−0.26	0.40	0.28	−0.10	0.18	0.24	0.62	0.74
Salinity		1.0	0.06	0.28	0.69	0.21	0.08	−0.16	−0.08
Fluorescence			1.0	0.14	0.06	−0.11	−0.05	0.55	0.54
Phosphate				1.0	0.27	0.04	0.36	0.08	0.31
Silicate					1.0	0.17	0.09	−0.16	0
Nitrite						1.0	0.38	0	0.11
Nitrate							1.0	0.16	0.40
Chlorophyll *a*								1.0	0.63
Phaeopigments									1.0

Data averaged at depth interval corresponding to chlorophyll *a* and phaeopigment values.

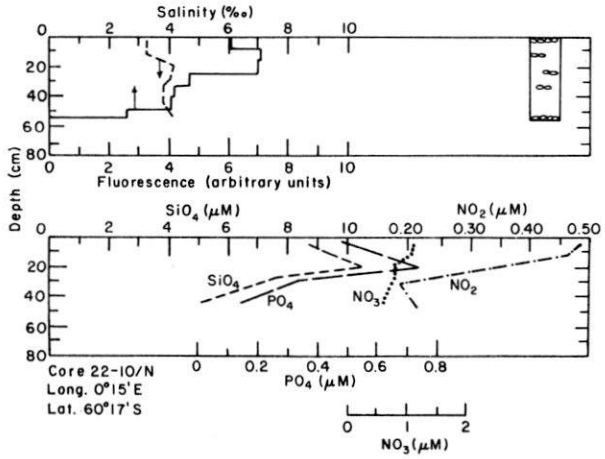

Fig. 8. Core profile of 22-10/N showing salinity, fluorescence, nutrients (silicate, phosphate, nitrate, nitrite), and structure versus depth.

2-m depth will have similar community characteristics. This equilibrium state is probably reached only by the end of a summer season.

The differences in physical properties of the frazil and congelation ice may affect the biological community. The mechanical incorporation of cells into frazil ice would initially create higher concentrations in frazil than in congelation ice. Subsequent growth in the ice might change these initial concentrations if one ice type provided a more suitable environment than the other. We found lower concentrations of biological material in congelation ice than in frazil ice at the same depths during the late winter–early spring. However, these differences in concentration are smaller than those between snow-ice and ice cores and between cores of similar structure from different locations (Table 1). We found that the maximum peak of full diatom cells per liter occurred near, but not at, the bottom in both frazil and congelation ice and penetrated as far as 50 cm up into the core. This distribution differs from that of the bottom, under-ice communities described by *Bunt* [1963], *Hoshiai* [1977], and *Sullivan and Palmisano* [1981]. The under-ice community described by these authors has its chlorophyll *a* maximum at the bottom and never extends farther than 20 cm up into the core. (The ice type found at these other sites is predominantly congelation ice.) We believe that the biological community in congelation ice may be considerably enhanced by passive water exchange in the lower ice levels thus allowing nutrients to be continually cycled from the underlying water or flushed down from the upper ice layers. The continuing water exchange in congelation ice may replenish nutrients and therefore not limit the biological growth.

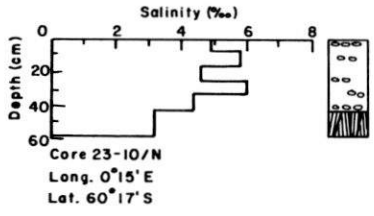

Fig. 9. Core profile of 23-10/N showing salinity and structure versus depth.

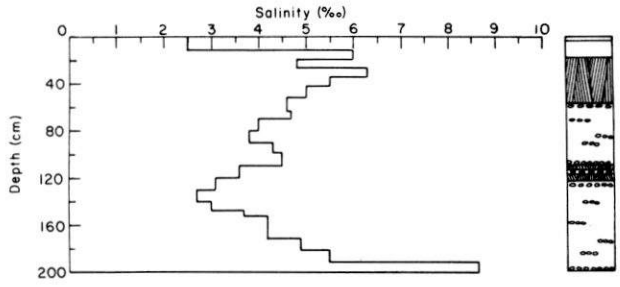

Fig. 10. Core profile of 51-G-4 showing salinity and structure versus depth.

Another observation [*Weeks and Ackley*, 1982] that indicates the favorable environment of congelation ice for biological activity is the presence of macroscopic (centimeter size) brine channels in end of summer congelation ice, features not present in frazil ice. Water exchange between the upper and lower layers of the ice during brine expulsion in spring is therefore inhibited in frazil ice and relatively enhanced in congelation ice. There is also a significant difference between the chlorophyll *a* concentrations in the Weddell Sea and those from McMurdo Sound and Syowa Station (Table 4). In the present study as well as those of *Ackley et al.* [1979] and *Garrison and Buck* [1984], the peak values of chlorophyll *a* in Weddell Sea samples, ranged from 3.8 to 26.8 mg/m^3 while the range from the studies of *Bunt* [1963], *Hoshiai* [1977], and *Sullivan and Palmisano* [1981] was from 248 to 2100 mg/m^3. In our snow-ice samples (ice chunks) the highest chlorophyll *a* concentration was 43.2 mg/m^3, while *Meguro* [1962] and *Burkholder and Mandelli* [1965] reported 407–670 mg/m^3 for this ice type in other locations. Therefore, differences in formation conditions influencing ice structure (snow ice, frazil ice, congelation ice) and growth history apparently can affect biological development. There may also be widespread regional differences as evidenced by the values we obtained compared to those of other studies of similar ice types.

CONCLUSIONS

There is a predominance (70%) of frazil ice in the section of the Weddell Sea ice we examined which indicates dynamic activity and leads to mechanical incorporation of biological material. Nutrient and salinity concentrations are generally lower than in adjacent surface water. *Garrison and Buck* [1984] found silicate depletion at the end of the summer and inferred that this depletion was the result of diatom growth. Our silicate data concurs with theirs and substantiates this inference. In addition, low nitrate concentration also indi-

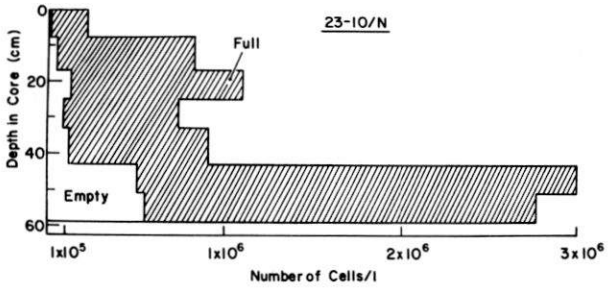

Fig. 11. Core profile of 23-10/N showing number of empty and full diatom cells per liter versus depth.

TABLE 4. Chlorophyll *a* Concentrations by Ice Type and Region

	Maximum Concentration of Chlorophyll *a* (mg/m^3)	Predominant Ice Type	Location
This study	3.8	frazil	Weddell, pack ice
Ackley et al. [1979]	4.54	frazil	Weddell, pack ice
Garrison and Buck	27.7	frazil	Weddell, pack ice
Meguro [1962]	670.0	snow ice	Syowa Station
Burkholder and Mandelli (1965)	407.2	snow ice	Palmer Peninsula
Bunt [1963]	248.0	congelation	McMurdo, fast ice
Hoshiai [1977]	1000.0	congelation	Syowa Station, fast ice
Sullivan and Palmisano [1981]	2100.0	congelation	McMurdo, fast ice

cates diatom utilization. Enhanced nitrite values are possibly the result of ammonia being nitrified by bacteria. *Sullivan and Palmisano* [1981] reported concentrations of up to 6×10^9 cells/l of live bacteria in sea ice from McMurdo. *Marra et al.* [1982] who examined samples from our Weddell Sea cores found concentrations of 10^9 cells/l bacteria. This inference is at best circumstantial without accompanying ammonia measurements, but it is supported by the active, thriving microbial communities found in both our samples and those from McMurdo. Phosphate values do not appear to reflect diatom growth, but we believe this may be the result of cell lysis during the preparation for nutrient analysis. Chlorophyll *a* concentrations are significantly higher in the ice than in the surrounding waters. Within the drifting pack ice, small differences in biological concentrations are found between frazil and congelation ice. Site-to-site variability (in both time and space) and the rate of ice formation may, however, override these small-scale structural controls when both ice types are present.

Chlorophyll *a* values, measured in drifting ice both at the beginning of the spring (our study) and the end of summer [*Garrison and Buck*, 1984], are lower by 2 orders of magnitude relative to the concentrations in McMurdo fast ice (congelation ice) from this same time period reported by *Sullivan and Palmisano* [1981]. This contrast suggests that frazil ice structure may actually inhibit the development of the large-scale bloom that occurs at the bottom of the McMurdo congelation ice. Although diatoms were present throughout the length of our cores, the numbers of cells are one to four orders of magnitude higher near (but not at) the bottom than near the surface of the ice. In the congelation ice cores the differences between the surface and the bottom layers were even more marked [*Sullivan and Palmisano*, 1981]. While our knowledge of the processes involved is limited and several factors may contribute to diatom blooms, we believe that near-bottom and bottom ice productivity is partially controlled by ice structure. Concurrent with increased light levels, passive nutrient exchange may be necessary to support massive ice blooms. This exchange would be enhanced by the columnar structure and brine channels in congelation ice. Since Weddell Sea ice is predominantly frazil, this mechanism does not exist to facilitate such blooms and therefore productivity would be lower. The high productivity reported at McMurdo Sound and Syowa Station occurs in somewhat protected near-shore environments, which account for only 1% of the Antarctic ice cover, and therefore the values reported here from the drifting pack of the Weddell Sea may be more representative of general conditions. More detailed seasonal field studies and laboratory work are necessary to further define the differences or similarities between the different ice types and their biological constituents.

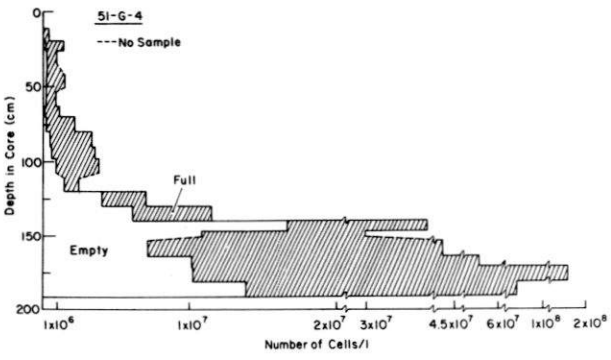

Fig. 12. Core profile of 51-G-4 showing number of empty and full diatom cells per liter versus depth.

Acknowledgments. We wish to thank David Boardman, Lamont-Doherty Geological Observatory; Joe Jennings, Oregon State University; Greta Fryxell and Kurt Buck, Texas A&M University; Sandra Smith, U.S. Army Cold Regions Research and Engineering Laboratory (CRREL); and Alexander Samoshkin, Arctic and Antarctic Research Institute (USSR) for their technical assistance. We would also like to thank the anonymous reviewer who clarified our explanation of the nitrogen cycle in sea ice. This research was supported by the National Science Foundation grant DPP 80-06922 to CRREL.

REFERENCES

Ackley, S. F., Sea-ice atmosphere interactions in the Weddell Sea using drifting buoys, in *Sea Level, Ice, and Climatic Change*, pp. 177–191, *Publ. 131*, International Association of Hydrological Sciences, Belgium, 1981.

Ackley, S. F., Ice scavenging and nucleation: Two mechanisms for incorporation of algae into newly forming sea ice, *Eos Trans. AGU, 63*(3), 54, 1982.

Ackley, S. F., K. R. Buck, and S. Taguchi, Standing crop of algae in the sea ice of the Weddell region, *Deep Sea Res., 26*A, 269–281, 1979.

Ackley, S. F., A. J. Gow, K. R. Buck, and K. M. Golden, Sea ice studies in the Weddell Sea aboard USCGC *Polar Sea, Antarct. J. U.S., 15*(5), 84–86, 1980.

Bauer, J., and S. L. Martin, A model of grease ice growth in leads, *J. Geophys. Res., 88*(5), 2917–2925, 1983.

Bunt, J. S., Diatoms of Antarctic sea ice as agents of primary production, *Nature, 199*, 1255–1257, 1963.

Bunt, J. S., and C. C. Lee, Seasonal primary production in Antarctic sea ice at McMurdo Sound in 1967, *J. Mar. Res., 1*(28), 304–320, 1970.

Burkholder, P. R., and E. F. Mandelli, Productivity of microalgae in Antarctic sea ice, *Science, 149*, 872–874, 1965.

Buynitsky, V. Kh., Organic life in sea ice, in *Polar Oceans*, edited

by M. J. Dunbar, pp. 301–306, Arctic Institute of North America, Calgary, Alberta, Canada, 1977.
Clarke, D. B., and S. F. Ackley, Physical, chemical and biological properties of winter sea ice in the Weddell Sea, *Antarct. J. U.S.*, *17*(5), 107–109, 1982.
El-Sayed, S. Z., Observations on a phytoplankton bloom in the Weddell Sea, *Antarct. Res. Ser.*, *17*, 301–302, 1971.
Garrison, D. L. and K. R. Buck, Sea ice algae in the Weddell Sea, I, Biomass, distribution and the physical environment, *Deep Sea Res.*, in press, 1984.
Garrison, D. L., S. F. Ackley, and K. R. Buck, A physical mechanism for establishing algal populations in frazil rock, *Nature*, in press, 1984.
Gordon, A. L., Seasonality of southern ocean sea ice, *J. Geophys. Res.*, *86*(5), 4193–4197, 1981.
Gordon, A. L., and B. A. Huber, In prep. Thermohaline stratification below the southern ocean sea ice, *J. Geophys. Res.*, *89*, 641, 1984.
Gordon, A. L., and B. A. Huber, WEPOLEX CTD and hydrographic data report, Lamont-Doherty Geol. Observ., Palisades, New York, 1984.
Gordon, A. L., and E. I. Sarukhanyan, American and Soviet expedition into the southern ocean sea ice in October and November 1981, *Eos Trans. AGU*, *63*, 2, 1982.
Gordon, A. L., C. T. A. Chen, and W. F. Metcalf, Winter mixed layer entrainment of Weddell deep water, *J. Geophys. Res.*, *89*, 637–640, 1984.
Gordon, L. I., C. N. Dahm, W. H. Dickinson, P. K. Park, and C. R. Stanley, A precision oceanographic nutrient data acquisition system, in *Proceedings of the UNOLS Working Conference on Oceanographic Data Systems*, Woods Hole Oceanographic Institute, 1975.
Gow, A. J., S. F. Ackley, W. F. Weeks, and J. W. Govoni, Physical and structural characteristics of Antarctic sea ice, *Ann. Glaciol.*, *3*, 113–117, 1982.
Grainger, E. H., The annual nutrient cycle in sea ice, in *Polar Oceans*, edited by M. J. Dunbar, pp. 285–299, Arctic Institute of North America, Calgary, Alberta, Canada, 1977.
Hibler, W. D., and S. F. Ackley, Numerical simulation of Weddell Sea pack ice, *J. Geophys. Res.*, *88*(5), 2873–2887, 1983.
Hoshiai, T., Seasonal change of ice communities in the sea ice near Syowa Station, Antarctica, in *Polar Oceans*, edited by M. J. Dunbar, pp. 307–317, Arctic Institute of North America, Location, 1977.
Marra, J., L. H. Burckle, and H. W. Ducklow, Sea ice and water column plankton distributions in the Weddell Sea in late winter, *Antarct. J. U.S.*, *17*, 111–112, 1982.
Meguro, H., Plankton ice in the Antarctic Ocean, *Antarct. Rec.*, *14*, 72–79, 1962.
Palmisano, A. C., and C. W. Sullivan, Physiology of sea ice diatoms, I, Response of three polar diatoms to a simulated summer-winter transition, *J. Phycol.*, *18*, 489–498, 1982.
Panofsky, H. A., and G. W. Brier, Analysis of the relationship between two variates, *in Some Application of Statistics to Meteorology*, pp. 89–93, Penn State University, University Park, Pa., 1965.
Sullivan, C. W., and A. C. Palmisano, Sea-ice microbial communities in McMurdo Sound, *Antarct. J. U.S.*, *16*(5), 126–127, 1981.
Sullivan, C. W., and A. C. Palmisano, Antarctic sea ice microbial communities, *Eos Trans. AGU*, *64*, 47, 1982.
Weeks, W. F., and S. F. Ackley, The growth, structure, and properties of sea ice, *CRREL Monogr. 82-1*, U.S. Army Cold Regions Res. and Eng. Lab., Hanover, N. H., 1982.

S. F. Ackley and D. B. Clarke, Cold Regions Research and Engineering Laboratory, U. S. Army Corps of Engineers, Hanover, NH 03755.

(Received June 13, 1983;
revised October 17, 1983;
accepted November 3, 1983.)

Observations of pack ice properties in the Weddell Sea

S. F. ACKLEY *and* S. J. SMITH

U.S. Army Cold Regions Research and Engineering Laboratory
Hanover, New Hampshire 03755

D. B. CLARKE*

Lamont-Doherty Geological Observatory
of Columbia University
Palisades, New York 10964

Among the programs undertaken during the U.S.-U.S.S.R. Weddell Polynya expedition (WEPOLEX-81) (Gordon, *Antarctic Journal*, this issue) was observation of ice as the ship was under way. These observations culminated in a daily map of ice conditions and a narrative observation log (Ackley and Smith 1982).

A section of the map prepared by the Soviet scientists who participated in the program is shown in figure 1. The ship's track as it left the ice is represented by the solid arrow line moving north and northwest. Locations of ice sampling stations taken along this line are given in Clarke and Ackley (*Antarctic Journal*, this issue).

The narrative log included information about ice concentration, ridging, amounts of thin ice and open water, and unusual ice features. As indicated in figure 1 and confirmed by the log, a transition in ice characteristics occurred between 60°20′ and 58°20′S latitude. In the southernmost regions the pack was characterized by fields of ice ("breccia") consisting mostly of medium-size floes (100–500 meters in diameter) and larger floes. Farther north, nearer the ice edge, the floes became smaller (20 meters or less in diameter) and surprisingly uniform. These northern observations coincided with observations of noticeable wave and swell penetration into the ice. Wave action apparently caused the breakup of the ice into smaller pieces. North of the area shown, ice of small floe size continued to be observed in lesser concentrations (6 tenths or less) for approximatey an additional 70 nautical miles.

The photographs in figure 2, taken at 0648 on 12 November and 0610 on 13 November, show the contrast in floe sizes between these two times. These characteristics also were observed on the inbound track at similar distances from the outer pack ice edge (first ice sighting).

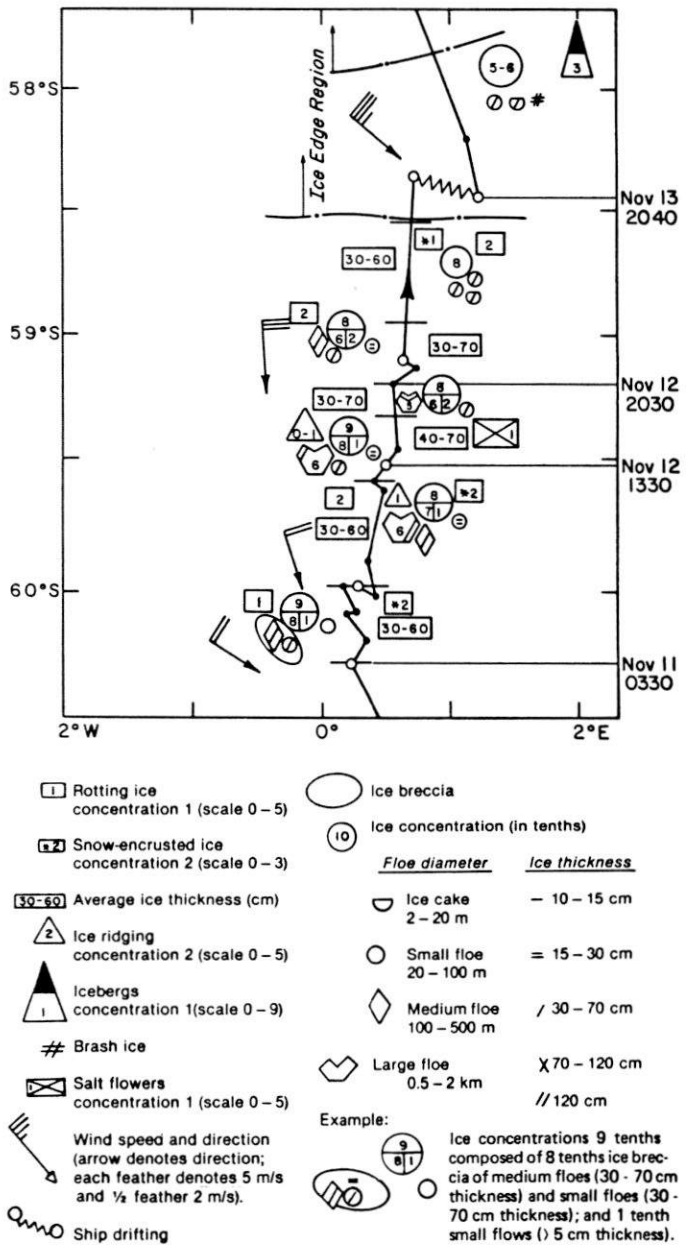

Figure 1. Ship's track showing sea ice conditions. Symbols are explained in the table.

*Present address: U.S. Army Cold Regions Research and Engineering Laboratory, Hanover, New Hampshire 03755.

1982 REVIEW

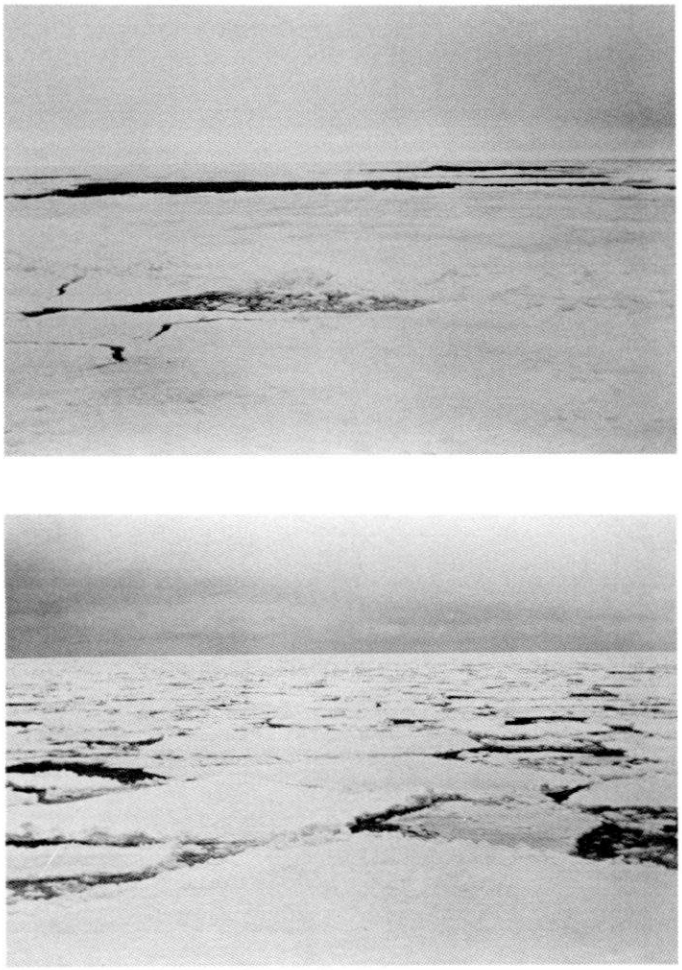

Figure 2. Photographs of sea ice conditions on 12 and 13 November 1981.

On the basis of these observations, we divide the pack ice zone into three relatively distinct regions:

- *Ice edge region (within 0 to 60 nautical miles of the northern limit of pack ice).* This area is characterized by uniformly small floes (less than 30 meters in diameter), ice of less than 10 tenths concentration, and continuous wave propagation. Frontal structure in the ocean might also be associated with these ice properties, but these ice changes should be closely correlated with conductivity-temperative-depth (CTD) and expendable bathythermograph (XBT) observations to determine the extent of this relationship. Increases in biological activity (birds, mammals, zooplankton, and phytoplankton) also were apparent in this region. Ship navigation was unimpeded, and it was easy to maintain speeds in excess of 5 knots.
- *Ice edge–pack ice transition zone (within 60 to 160 nautical miles of the outer limit of pack ice).* The boundary between the ice edge region and the transition zone is not well defined. We traversed regions of continuous small floes (9 to 10 tenths concentration) coinciding with noticeable swell propagation. As the swell became severely attenuated and discontinuous in the southern regions, the floe sizes ranged from about 30 meters in diameter at the outer edge into a jumble of very large and some smaller floes. Similar features were apparent on the inbound track. We traversed nearly 100 nautical miles of pack (160 to 60 nautical miles from the outer ice edge) from our first observations of swell motion in the ice until we encountered the "ice edge region." Ship navigation in this transition region was fairly easy, with only occasional difficulty encountered in crossing some of the larger floes. Figure 1 essentially brackets this region.
- *Deep pack (at distances greater than 160 nautical miles from the outer limit).* This region had ice concentrations usually in excess of 9 tenths (most commonly 10 tenths concentration). Narrow, parallel leads oriented according to the prevailing stress were the only open-water areas. Floes usually exceeded several kilometers in diameter. Ship navigation was exceedingly difficult, except where broad leads happened to coincide with the ship's course. These conditions were encountered between 150 and 180 nautical miles from the first (or last) ice sighting on both the inbound and outbound legs (south of the track shown in figure 1).

In most satellite microwave images, the ice edge-pack ice transition zone (60–160 nautical miles) appears as an area of lesser concentration. Our observations did not confirm this. We usually found ice concentrations of 9 to 10 tenths. We believe that this discrepancy arises from a change in the microwave signal; this change is caused by the infiltration of seawater into the snow/ice interface as a result of wave action breaking the floes and water surging into this porous layer. This process changes the surface emission characteristics of the ice at microwave frequencies. A comparison of the images received on board with our observations indicates that the Soviet meteorological satellites ("Meteor"), which use visible and infrared imagers, depicted the ice concentration in this region more accurately (that is, obtained higher values). Future work will include using our 300 photographs of ice conditions and the ice observation log (Ackley and Smith 1982) to correlate observed ice concentrations with those obtained from U.S. satellite mapping.

Also unexpected was our observation that noticeable swell propagation occurred at great distances from the outer pack limit. On both the inbound and outbound legs, we measured swell amplitudes of 0.25 meter or greater at distances greater than 120 nautical miles from the outer limit. This limit previously was thought to be about 60 nautical miles (100 kilometers) for the highly concentrated ice observed here (Wadhams 1980). A feature contributing to the deep pack propagation of swell in this region is the long wavelength (greater than 200 meters) and high amplitude (5–7 meters) of swell incident on the ice edge, characteristic of the long-fetch, high-wind regime of the southern ocean.

A complete report covering the entire cruise period and including interpretations of the ice map, the narrative log, sea level photographs, and satellite photographs is available from the authors.

We wish to thank Captain F. A. Pesyakov and the crew of the *Somov* for their support, and Edgar Andreas, Ivan Chuguy, and

Ed Lysakov for their technical assistance. We also acknowledge the support of the other members of the Soviet science and meteorological support group, E. I. Sarukhanyan, chief scientist. This research was supported by National Science Foundation grants DPP 80-06922 (to the U.S. Army Cold Regions Research and Engineering Laboratory) and DPP 80-08011 (to the Lamont-Doherty Geological Observatory).

References

Ackley, S. F., and Smith, S. J. 1982. *Weddell Polynya Expedition ice map interpretation and daily ice observation log* (USACRREL Tech. Note IR777). Hanover, N.H.: U.S. Army Cold Regions Research and Engineering Laboratory.

Clarke, D. B., and Ackley, S. F. 1982. Physical, chemical, and biological properties of winter sea ice in the Weddell Sea. *Antarctic Journal of the U.S.*, 17(5).

Gordon, A. L. 1982. The U.S.-U.S.S.R. Weddell Polynya Expedition. *Antarctic Journal of the U.S.*, 17(5).

Wadhams, P. 1980. Ice characteristics in the seasonal sea ice zone. *Cold Regions Science and Technology*, 2, 38–87.

Physical, chemical, and biological properties of winter sea ice in the Weddell Sea

D. B. CLARKE*

Lamont-Doherty Geological Observatory
of Columbia University
Palisades, New York 10964

S. F. ACKLEY

U.S. Army Cold Regions Research and Engineering Laboratory
Hanover, New Hampshire 03755

To investigate the physical, chemical, and biological regimes of drifting ice, an ice floe sampling program was carried out from the *Mikhail Somov* during the U.S.-U.S.S.R. Weddell Polynya expedition (WEPOLEX-81) (Gordon, *Antarctic Journal*, this issue). Sea ice algae is often an important constituent of the pack ice (Ackley, Buck, and Taguchi 1979; Buck and Garrison 1982; Buinitsky 1977; Garrison and Buck 1982; Hoshiai 1977; Sullivan and Palmisano 1982). At present, the ecology of the ice algae and its contribution to the overall productivity are poorly understood because the data set is limited. For example, the ice samples that we obtained comprise the first winter data set from antarctic drifting ice. We attempted to perform the most integrated data analysis possible because of the unique nature of these samples.

A total of 27 ice cores and 13 surface ice samples were taken at 11 sampling stations located between 59°21'S and 62°00'S (see Gordon, *Antarctic Journal*, this issue, for ice station locations). The ice cores were obtained using a Cold Regions Research and Engineering Laboratory ice auger as well as a Soviet coring device. The cores were analyzed for the following physical, chemical, and biological parameters: (1) ice structure, (2) salinity, (3) nutrients (silicate, phosphate, nitrite, and nitrate), (4) fluorescence, (5) chlorophyll *a*, (6) phaeo-pigment, (7) diatom species enumeration, and (8) bacteria. Figure 1 shows how the cores were subdivided to provide samples for each analysis.

Twenty of the cores have been analyzed so far—either on

*Present address: U.S. Army Cold Regions Research and Engineering Laboratory, Hanover, New Hampshire 03755.

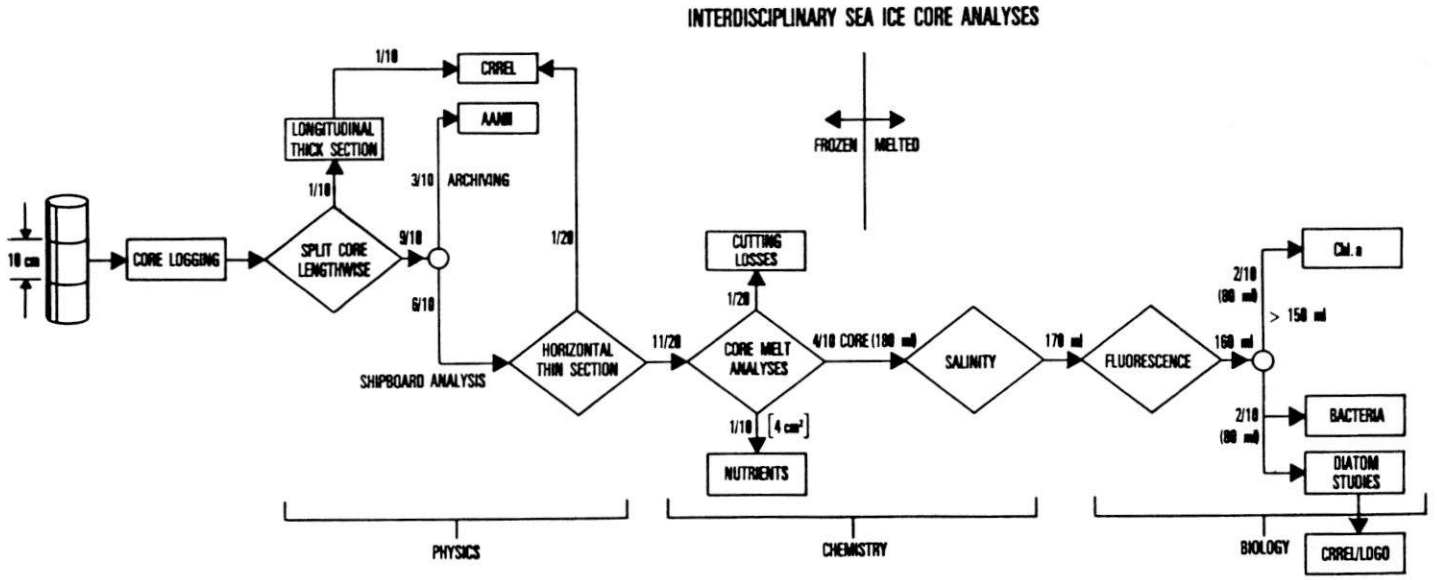

Figure 1. From left to right, this figure indicates the successive core divisions and analyses performed on each 10-centimeter ice core sample. Fractions (e.g., one-tenth) or quantities (e.g., 170 ml) refer to portions of solid core or meltwater used in the various steps. AANII (Arctic and Antarctic Research Institute, Leningrad), CRREL (Cold Regions Research and Engineering Laboratory), and LDGO (Lamont-Doherty Geological Observatory) refer to the institutions where the designated samples are archived.

Positions and averaged data for ice cores

Core number	Date	Position	Thickness (meters)	Average salinity (‰)	Average chlorophyll *a* (mg/m³)*	Percentage of frazil ice
1-22/O	22 Oct 81	59°21.5'S 5°13.2'E	.60	5.0 ± 1.3	.58	100
2-22/O	22 Oct 81	59°21.5'S 5°13.2'E	1.17	6.5 ± 2.2	.72	100
3-24/O	24 Oct 81	59°53.7'S 3°24.9'E	.60	5.3 ± 2.4	1.19	
4-24/O	24 Oct 81	59°53.7'S 3°24.9'E	.57	4.5 ± 1.0		100
5-26/O	26 Oct 81	61°10.7'S 3°03.9'E	1.52		1.27	82
6-26/O	26 Oct 81	61°10.7'S 3°03.9'E	.62	4.7 ± 1.3	.66	85
7-29/O	29 Oct 81	62°00.2'S 2°25.9'E	.32	10.7 ± 3.3	1.42	50
8-29/O	29 Oct 81	62°00.2'S 2°25.9'E	.60	6.6 ± 3	.15	78
9-1 N	1 Nov 81	62°11.2'S 2°53.8'E	.81	6.2 ± 2.8	1.00	71
10-1/N	1 Nov 81	62°11.2'S 2°53.8'E	.67	4.7 ± 1.2	1.12	?
11-1/N	1 Nov 81	62°11.2'S 2°53.8'E	.64	4.2 ± 1.1	2.52	87
12-4/N	4 Nov 81	62°12.4'S 1°03.5'E	.69	4.9 ± 1.4	.35	55
13-4/N	4 Nov 81	62°12.4'S 1°03.5'E	.68	6.4 ± 2.4	.63	60
14-4/N	4 Nov 81	62°12.4'S 1°03.5'E	.68	4.1 ± 0.71	.20	41
16-8/N	8 Nov 81	60°57.7'S 0°43.5'E	.68	4.0 ± 0.9	.33	24
17-8/N	8 Nov 81	60°57.7'S 0°43.5'E	.68	4.9 ± 2.2	.16	34
20-10/N	10 Nov 81	60°39.7'S 0°37.1'E	.78	5.3 ± 0.76	1.90	81
22-10/N	10 Nov 81	60°17.0'S 0°15.3'E	.54	5.1 ± 1.7	.24	100
24-11/N	11 Nov 81	60°05.1'S 0°14.2'E	.69	4.9 ± 2	.28	57
26-13/N	13 Nov 81	59°09.1'S 0°45.6'E	.54	4.9 ± 1.3	.43	15

* mg/m³ = milligrams per cubic meter.

board ship or in the shore labs (see table). The cores measured between 29 and 159 centimeters, with an average length of 75 centimeters. The primary physical feature is the dominance (70 percent) of frazil ice structure as opposed to congelation ice. This substantiates previous work in the western Weddell Sea, which also indicated that frazil ice structure is more predominant in the Antarctic than in the Arctic (Ackley et al. 1980). The dominance of frazil ice structure indicates the importance of dynamic activity—winds, ice deformation, and ocean convection—in the formation of the ice cover.

The salinity range in the cores is 2.4 to 13.7‰, with the higher salinities usually within the upper 15 centimeters (figure 2) (page 109). Chemical analysis of the nutrients in the ice cores indicates that they do not follow a dilution curve. Standard seawater ratios—for example, between phosphate and nitrate and between nitrate and nitrite—are not conserved within the ice with regard to the nutrients. A comparison of the ice core surface samples with samples from the adjacent surface waters, which were obtained from conductivity-temperature-depth rosette samples (Gordon and Huber, *Antarctic Journal*, this volume), shows several interesting differences. Silicate, phosphate, and nitrate are found in higher concentrations in the adjacent surface water than in the ice cores. Nitrite levels, however, showed the opposite trend: they are two to five times higher in the surface layer (0–20 centimeters) of the ice cores than in the adjacent surface water.

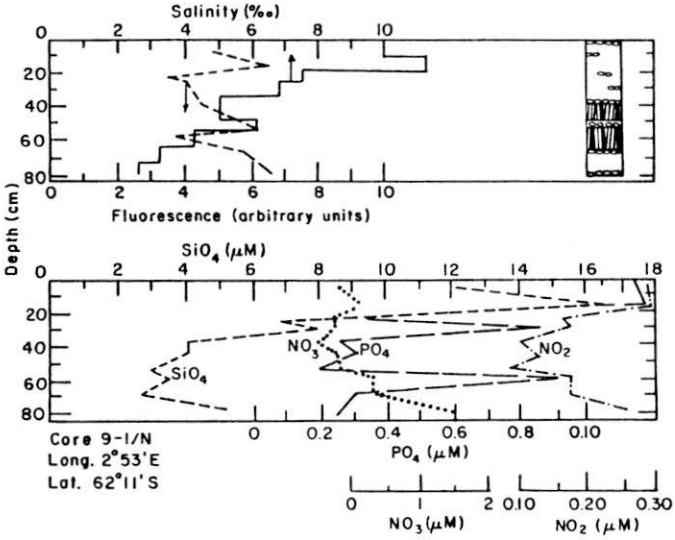

Figure 2. A typical core profile (core 9-1/N) showing salinity (solid line), fluorescence (dashed line), nutrients (in micromolars; SiO_4, silicate; NO_2, nitrite; NO_3, nitrate; PO_4, phosphate), and structure versus depth. In upper profile, arrows indicate which scale should be used. In the structural cartoon, circles indicate frazil ice structure and vertical lines show congelation or columnar ice structure.

Chlorophyll *a*, a measure of the viable biological material, followed a pattern similar to that of nitrite. Chlorophyll *a* occurred in higher concentrations (1.415 milligrams per cubic meter), both in the surface layer of the ice cores and throughout the core, than in the adjacent surface water (0.1 milligram per cubic meter). The values of phaeo-pigment (degradation products of chlorophyll) in the cores range from 0.04 to 4.02 milligrams per cubic meter but do not appear to follow any pattern within the cores.

Figure 2 shows that, as was previously found (Ackley et al. 1979), there is a general trend for meltwater fluorescence, which is correlated with total biological material, to scale with salinity within individual cores. Comparing the salinity and fluorescence values for all cores combined, however, these two parameters do not seem to scale when different cores are grouped.

Marra, Burckle, and Ducklow (*Antarctic Journal*, this issue) have shown that diatoms are present at all sample levels in the ice cores, but in varying concentration and condition. Most of the valves in the surface layers are whole, whereas those in the middle and lower portions of the cores are fragmented. This indicates that active growth is occurring in the surface layers. Further confirmation of this comes from K. R. Buck (personal communication), who has identified isogametes from two pennate species in cores 22-10/N, 24-11/N, and 26-13/N. The presence of these isogametes, which are formed as part of the sexual cycle, substantiates our belief that the diatoms are reproducing in the surface layers of ice cores.

With the remaining seven cores we will be able to sample for each parameter at 10-centimeter intervals, rather than integrate several levels as we did for chlorophyll *a* and diatom species in the shipboard analysis. In addition to this refinement in sampling technique, we anticipate using a multivariate analysis of all the parameters rather than a simple comparison of two parameters.

We wish to thank Captain F. A. Pesyakov and the crew of the *Mikhail Somov* for their support, as well as our colleagues Edgar Andreas, David Boardman, Kurt Buck, Joe Jennings, David Woodroffe, and Alexander Samoshkin for their technical assistance. We also acknowledge the support of the other members of the Soviet science and meteorological support group, E. I. Sarukhanyan, chief scientist. This research was supported by National Science Foundation grants DPP 80-06922 (to the U.S. Army Cold Regions Research and Engineering Laboratory) and DPP 80-08011 (to Lamont-Doherty Geological Observatory).

References

Ackley, S. F., Buck, K. R., and Taguchi, S. 1979. Standing crop of algae in the sea ice of the Weddell region. *Deep Sea Research*, 26A, 269–281.

Ackley, S. F., Gow, A. J., Buck, K. R., and Golden, K. M. 1980. Sea ice studies in the Weddell Sea aboard USCGC *Polar Sea*. *Antarctic Journal of the U.S.*, 15(5), 84–86.

Buck, K. R. Personal communication, 1982.

Buck, K. R., and Garrison, D. L. 1982. Sea-ice algae in the Weddell Sea. II. Population comparisons between sea-ice and water column. *EOS, Transactions of the American Geophysical Union*, 63(3), 47.

Buinitsky, V. Kh. 1977. Organic life in sea ice. In M. T. Dunbar (Ed.), *Polar oceans*. Toronto: McGill University Press.

Garrison, D. L., and Buck, K. R. 1982. Sea-ice algae in the Weddell Sea. I. Biomass, distribution and the physical environment. *EOS, Transactions of the American Geophysical Union*, 63(3), 47.

Gordon, A. L. 1982. The U.S.-U.S.S.R. Weddell Polynya Expedition. *Antarctic Journal of the U.S.*, 17(5).

Gordon, A. L., and Huber, B. A. 1982. Physical oceanography during WEPOLEX-81. *Antarctic Journal of the U.S.*, 17(5).

Hoshiai, T. 1977. Seasonal change in ice communities in the sea ice near Syowa Station, Antarctica. In M. J. Dunbar (Ed.), *Polar oceans*. Toronto: McGill University Press.

Marra, J., Burckle, L. H., and Ducklow, H. W. 1982. Sea-ice and water column plankton distributions in the Weddell Sea in late winter. *Antarctic Journal of the U.S.*, 17(5).

Sullivan, C. W., and Palmisano, A. C. 1982. Antarctic sea ice microbial communities. *EOS, Transactions of the American Geophysical Union*, 63(3), 47.

Elemental compositions and concentrations of microspherules in snow and pack ice from the Weddell Sea

MOTOI KUMAI, S. F. ACKLEY *and* D. B. CLARKE

U.S. Army Cold Regions Research and Engineering Laboratory
Hanover, New Hampshire 03755

Microspherules in snow and ice-fog crystals have been studied by electron microscopy. Microspherules, which are collected by snow through nucleation and scavenging processes in the atmosphere, are of terrestrial and extraterrestrial origin and were either precipitated with snow or by dry fall-out. They were generally found in percent of the snow crystals sampled at various remote areas in the Northern Hemisphere, but they were not found during an examination of 93 snow crystals sampled at the South Pole (Kumai 1976). King and Wagstaff (1980), however, observed andesitic microspherules and iron microspherules in firn from the South Pole in the layer estimated to have been deposited in 1833. The elemental compositions of microspherules in snow crystals from Antarctica have not yet been reported.

This paper presents the results of an investigation of microspherules found is snow and pack ice from the Weddell Sea, Antarctica, collected during the U.S.-U.S.S.R. Weddell Polynya Expedition, 1981 (Gordon 1982; Clarke and Ackley 1982) by Ackley and Clarke. Elemental composition, size, and concentration of microspherules were determined using a scanning electron microscope (SEM) and energy dispersive x-ray analysis (EDXA). In this report, we show typical textures of microspherules and compare these with those found in snow and ice-fog crystals sampled from the Northern Hemisphere.

Temperatures in the Weddell Sea ranged from +2 to −14°C, and the pack ice was covered with a layer of snow 10–30 centimeters in depth during October-November 1981. Snow samples from the pack-ice surface and an ice core sampled using a 7.6 centimeter diameter ice coring auger were collected in the Weddell Sea, (60°17'S 0°15'E); see Gordon 1982 for other sampling locations.

For SEM examination of microspherules, a snow sample and a snow-ice sample (10-N/K; Clarke and Ackley 1982) of 20 grams each were obtained from the surface of the pack ice. A sea-ice core (with the snowcover removed) 54 centimeters in length (core 22–10/N; Clarke and Ackley 1982) was also prepared for SEM examination to compare with the snow and snow-ice samples. The samples were melted and filtered through a polycarbonate membrane filter having a pore diameter of 1.0 micrometer. They were then rinsed with distilled water to remove any salt. Microspherules remained on the filters, and were coated with gold-palladium (60:40) vapor to a thickness of about 100 Å in a vacuum chamber and were subsequently examined under the SEM. The limit of detection for elemental analysis was determined using standard clay minerals and was found to be 0.1 percent for sodium and potassium and 0.01 percent for iron. Elemental composition of microspherules were measured using the EDXA by area or spot analysis at an accelerating voltage of 20 kilovolts.

In this study, 23 microspherules were found in the snow sample from the Weddell Sea and 6 from the snow-ice sample. The mass of a snow crystal ranges from 10^{-6} to 10^{-4} grams, and the mean mass is 3.8×10^{-5} grams in snowfalls at temperatures from −4 to −10°C (Kumai and Higuchi 1952). From this estimate the number of snow crystals in the 20 gram snow sample from the Weddell Sea is calculated at about 5.3×10^{5} crystals. The concentration of microspherules in the snow samples from the Weddell Sea are therefore calculated to be approximately 10^{-3} percent. In the Northern Hemisphere, the concentration of microspherules in snow crystals ranged from 1 to 2 percent (table 1). Thus, the concentration of microspherules in the snow sample from the Weddell Sea is three orders of magnitude smaller than that of the Northern Hemisphere. This indicates that the concentration of microspherules in the atomsphere of the Southern Hemisphere may be three orders of magnitude less than that of the Northern Hemisphere. On the other hand, three microspherules were found in 20 grams of ice core from the Weddell Sea. Thus the concentration of microspherules in the ice core was half the value for the snow-ice sample and approximately ⅛ that of the snow sample. This indicates that the concentration of microspherules in the samples was increased with the number of snow crystals in the samples.

Elemental compositions of the nine microspherules found in the snow ice and pack-ice samples were examined by SEM and EDXA, and the results are shown in table 2. There were two iron, two titanium, and five silicon rich microspherules, and their

Table 1. Concentrations of microspherules found in snow and ice-fog crystals from various locations

Year	Location	Ratio of microspherules to snow crystals	Percent of microspherule	Observer
Snow Crystals				
1956	Mt. Tokachi, Hokkaido	2 out of 202	1	Kumai
1959	Houghton, Michigan	5 out of 271	1.8	Kumai
1960	Site 2, Greenland	7 out of 356	2.0	Kumai
1976	South Pole	0 out of 93	0	Kumai
	Total	14 out of 922	1.5	Kumai
Ice-fog crystals				
1962–1963	Fairbanks, Alaska	4 out of 542	0.7	Kumai
1964	Eielson, Alaska	5 out of 116	4.3	Kumai
	Total	9 out of 658	1.3	Kumai
Snow crystals				
1981	Weddell Sea	23 out of 20 grams[a]	$\sim 10^{-3}$	This paper
Snow ice[b]				
1981	Weddell Sea	6 out of 20 grams	$\sim 10^{-3}$	This paper
Pack ice				
1981	Weddell Sea	3 out of 20 grams	$\sim 10^{-4}$	This paper

[a] We estimate 5.3×10^5 snow crystals in 20 grams of "typical" snow.

[b] This sample was taken from snow infiltrated with sea water and then frozen.

Table 2. Energy dispersive X-ray analysis (percentage of weight) of microspherules found in snow-ice and pack-ice samples from the Weddell Sea

Element	Microspherule Specimen Number								
	1799 (snow ice)	1899 (pack ice)	1665 (snow ice)	1896 (pack ice)	1851 (snow ice)	1819 (snow ice)	1865 (snow ice)	1693 (snow ice)	1888 (pack ice)
Sodium	1.0	1.0	2.1	4.7	—[b]	10.8	1.3	1.1	1.0
Magnesium	2.0	1.0	8.3	5.2	0.9	15.9	—	2.9	4.0
Aluminum	4.0	3.1	10.4	10.8	22.6	15.9	32.9	27.0	32.5
Silicon	5.0	7.3	23.6	10.8	69.6	57.5	50.6	46.0	40.0
Phosphorus	—	—	—	—	—	—	—	—	—
Sulfur	—	—	—	—	—	—	—	—	—
Chloride	5.0	—	—	8.4	—	—	—	—	4.0
Potassium	—	—	—	4.7	6.9	—	6.9	8.6	7.5
Calcium	3.0	—	—	4.7	—	—	1.9	4.0	—
Titanium	—	—	55.5	37.6	—	—	1.9	2.9	—
Chromium	—	—	—	—	—	—	—	—	—
Manganese	—	—	—	—	—	—	1.9	—	—
Iron	80.0	83.3	—	6.1	—	—	3.2	4.6	7.0
Cobalt	—	—	—	—	—	—	—	—	—
Nickel	—	—	—	—	—	—	—	—	—
Copper	—	4.2	—	7.0	—	—	—	2.9	4.0
Lead	—	—	—	—	—	—	—	—	—
Total	100.0	99.9	99.9	100.0	100.0	100.1	100.0	100.0	100.0
Diameter[a]	4.9	12.4	8.4	9.2	12.3	7.4	7.4	2.4	8.5

[a] In micrometers.

[b] Dashes denote "zero."

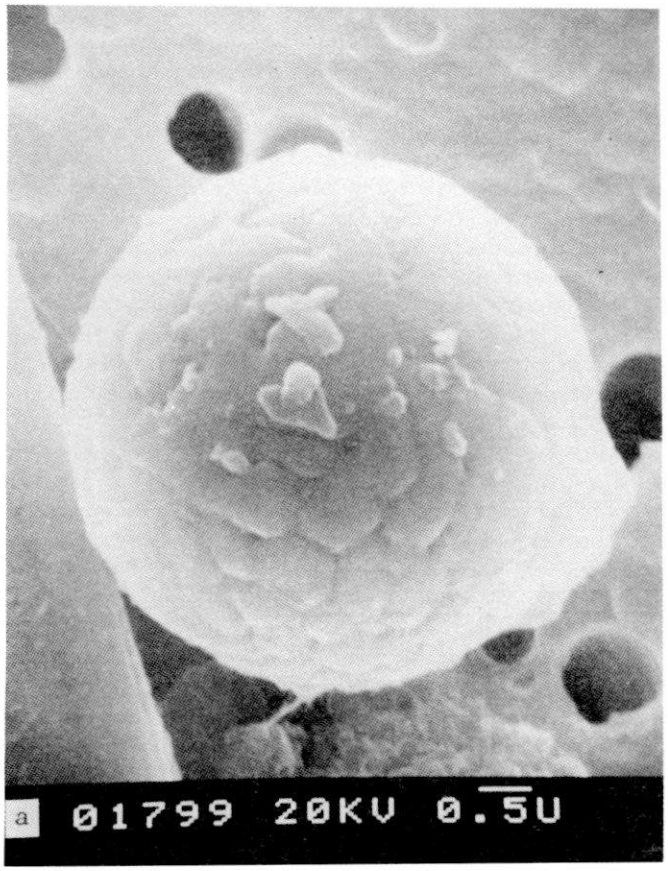

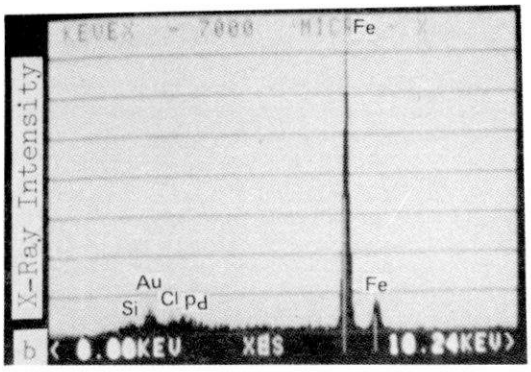

Figure 1. Iron-rich microspherule (a); the elemental analysis by energy dispersing X-ray(b) indicates that the microspherule is possibly a product of atmospheric ablation of a sporadic meteoroid. The specimen is coated with gold and palladium.

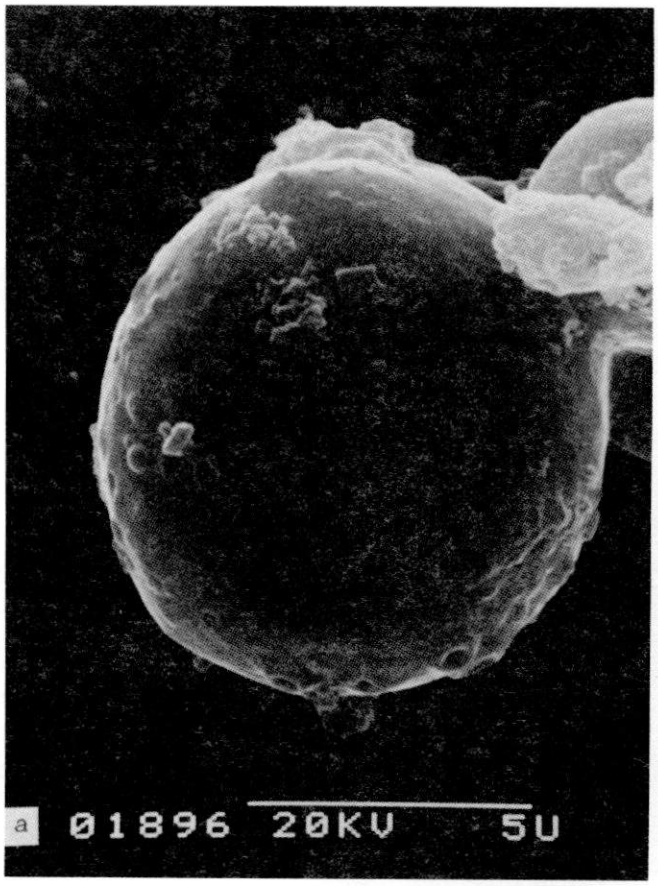

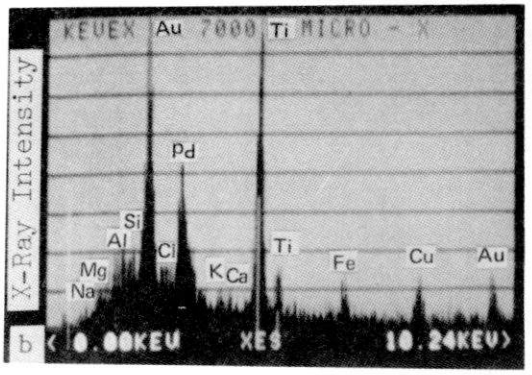

Figure 2. Titanium-rich microspherule (a) and the elemental analysis by energy dispersing X-ray(b) indicates that the microspherule is possibly a fly ash. The specimen is coated with gold and palladium.

diameters ranged from 2.4 to 12.4 micrometers. The iron microspherules were 80 and 83 percent iron with minor elements such as silicon, chlorine, aluminum, calcium, magnesium, and sodium comprising less than 7 percent, as shown in figure 1 and table 2. These iron-rich microspherules were different in elemental composition, morphology, and size range from those formed by solidification of iron spattered during a welding operation (McCrone, Brown, and Stewart 1980) and also from fly ash from coal burning electric power plants (Kumai 1977). However, these iron-rich microspherules from the Weddell Sea (figure 1) are quite similar in crystalline structure, morphology, and size range to those found in the ice core from the South Pole by King and Waggstaff (1980) which are considered to be of extraterrestrial origin. According to King and Wagstaff these microspherules are possibly a product of ablation in the atmosphere of a sporadic meteoroid.

The two titanium-rich microspherules were 37 and 55 percent titanium with minor elements such as silicon, aluminum, mag-

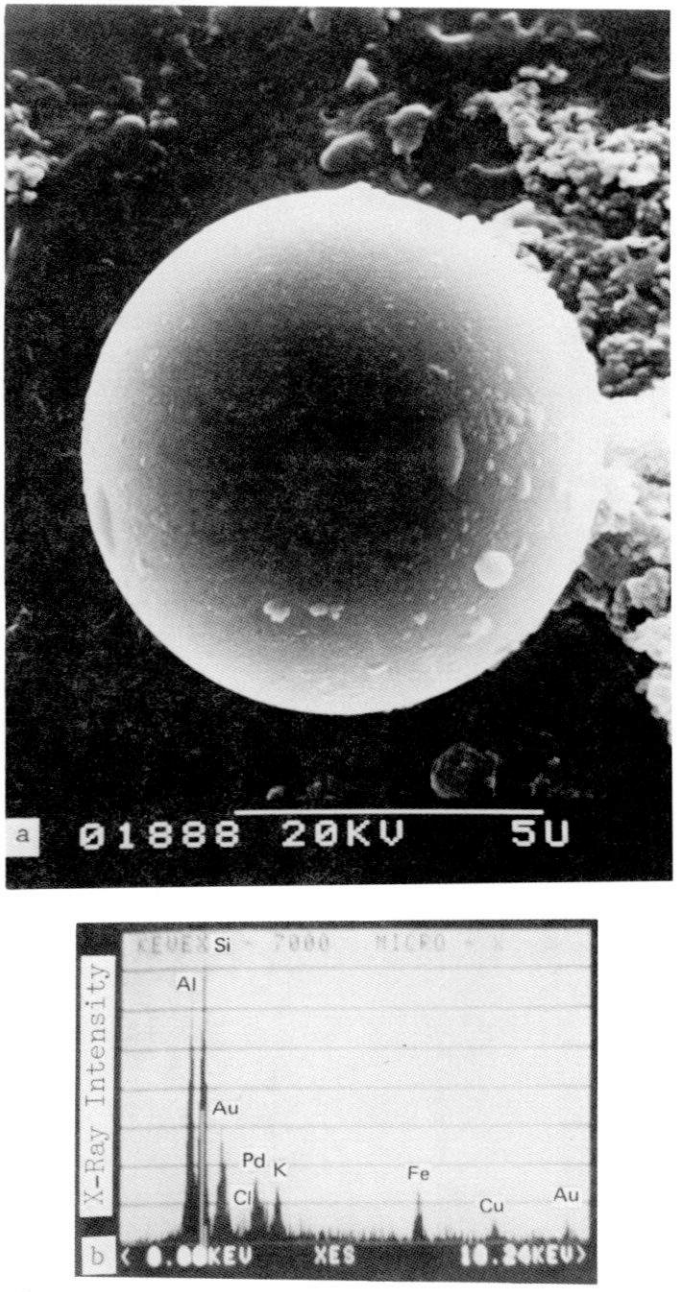

Figure 3. Silicon rich microspherule (a), and the elemental analysis by energy dispersing X-ray(b) indicates that the microspherule is possibly fly ash. The specimen is coated with gold and palladium.

nesium, chloride, potassium, calcium, iron, and copper. Many submicron particles were observed on the surface of the microspherules (figure 2). The titanium-rich microspherules (figure 2) are quite similar in elemental compositions, morphology, and size range to microspherules found in fly ash from electric power plants using coal (Kumai 1977).

Four silicon-rich microspherules were 40 to 70 percent silicon with minor elements of aluminum, magnesium, sodium, potassium, calcium, titanium, chlorine, iron, manganese, and copper. The microspherules were 2 to 12 micrometers in diameter, and many submicron particles were found on the surface (figure 3). These silicon-rich microspherules (figure 3) are more similar in morphology, elemental composition, and size range to microspherules in fly ash from coal burning electric power plants than those from volcanic ash.

In this investigation, only a few microspherules were found in approximately 100,000 snow crystals formed in the atmosphere over the Weddell Sea in comparison to one in about 100 snow crystals from various remote areas in the Northern Hemisphere. This indicates that the concentration of microsherules in the Antarctic may be three orders of magnitude smaller than the concentration found in the Northern Hemisphere (table 1 and Kumai 1976). Silicon- and titanium-rich microspherules from the Weddell Sea were similar to those found in fly ash of terrestrial origin. The iron rich microspherules from the Weddell Sea were tentatively identified to be of extraterrestrial origin.

This research was supported by National Science Foundation grant DPP 80-06922 and Department of the Army Project 4A161102AT2401/A/106.

References

Clark, D. B., and S. F. Ackley. 1982. Physical, chemical, and biological properties of winter sea ice in the Weddell Sea. *Antarctic Journal of the U.S.*, 17(5), 107–109.

Gordon, A. L. 1982. The U.S.-U.S.S.R. Weddell Polynya Expedition. *Antarctic Journal of the U.S.*, 17(5), 96–98.

King, E. A., and J. Wagstaff. 1980. Search for cometary dust in the Antarctic ice. *Antarctic Journal of the U.S.*, 15(5), 78–79.

Kumai, M. 1976. Identification of nuclei and concentrations of chemical species in snow crystals sampled at the South Pole. *Journal of the Atmospheric Sciences*, 33, 833–841.

Kumai, M. 1977. Elemental analysis of ice crystal nuclei and aerosols. In A. F. Rody, and T. C. O'Connor (Eds.), *Atmospheric aerosols and nuclei* Galway, Ireland: Galway University Press.

Kumai, M. and K. Higuchi. 1952. Measurement of mass and number of falling snow crystals in the atmosphere. *Journal of the Meteorological Society of Japan*, 30(11), 345–355.

McCrone, W. C., J. A. Brown, and I. M. Stewart. 1980. *The particle atlas, Vol. 6.* Ann Arbor, Mich.: Ann Arbor Science Publishers.

Relative abundance of diatoms in Weddell Sea pack ice

D. B. CLARKE *and* S. F. ACKLEY

U.S. Army Cold Regions Research and Engineering Laboratory
Hanover, New Hampshire 03755

In previous studies of algal communities in antarctic sea ice, it has been shown that pennate diatoms are generally numerically dominant to centric forms (Burkholder and Mandelli 1965; Fukushima and Meguro 1966; Richardson and Whitaker 1979). Ackley, Buck, and Taguchi (1979), Bunt and Wood (1963), and Watanabe (1982) are the only authors to have found centric species "in abundance" in sea ice. These comprised five genera and six species and were found in both frazil (fine-grained, equiaxial) and congelation (coarse grained, columnar) ice. Among the pennates, five genera and fourteen species have been reported in abundance in both ice types.

We sampled sea ice in the Weddell Sea during the October –November 1981 joint U.S.-U.S.S.R. (WEPOLEX) Expedition (Gordon and Sarukhanyan 1982). (See *Antarctic Journal*, 17 (5) 1982, Weddell Polynya expedition chapter, for cruise report of the expedition). We recovered both ice cores [drilled with a 7.6-centimeter U.S. Army Cold Regions Research and Engineering Laboratory (CRREL) ice coring auger] and chunks of snow ice

Ice sample depth, location, ice type, and percentage of each abundant species

Core number	Depth interval (in centimeters)	Latitude	Longitude	Abundant species	Percentage of total	Ice type
3–24/O	55–63	59°53.7'S	3°24.9'E	*Nitzschia prolongatoides*[a]	89	Frazil
4–24/O	33–49	59°53.7'	3°24.9'	*Nitzschia prolongatoides*[a]	85	Frazil
9–1/N	17–36	62°11.20'	2°53.8'	*Nitzschia subcurvata*	39	
				Nitzschia turgiduloides[a]	24	Frazil
				Nitzschia prolongatoides[a]	14	
14–4/N	44–58	62°12.4'	1°03.5'	*Nitzschia prolongatoides*[a]	35	
				Nitzschia cylindrus[a]	28	Congelation
				Chaetoceros dichaeta[a, b]	10	
17–8/N	23–53	60°57.7'	0°43.5'	*Nitzschia prolongatoides*[a]	54	Congelation
				Nitzschia closterium	31	
22–10/N	0–54	60°17.0'	0°15.3'	*Nitzschia closterium*	52	Frazil
				Tropidoneis glacialis[a]	28	
23–10/N	0–59	60°17.0'	0°15.3'	*Tropidoneis glacialis*[a]	24	
				Nitzschia cylindrus[a]	21	Frazil/
				Nitzschia prolongatoides[a]	21	congelation
				Nitzschia closterium	18	
24–11/N	32–69	60°05.1'	0°14.2'	*Nitzschia cylindrus*[a]	36	Frazil/
				Navicula species[a]	15	congelation
				Nitzschia closterium	10	
26–13/N	0–54	59°09.1'	0°45.6'	*Nitzschia closterium*	48	Frazil/
				Navicula species[a]	12	congelation
Ice chunk 10–N/K		60°17.0'	0°15.3'	*Tropidoneis glacialis*[a]	94	Snow ice

[a] Not previously reported as being abundant.

[b] Centric form, all other species listed are pennate forms.

floating in the water cleared by the ship or at the bases of ridges. These samples were taken between 59°09.1′ and 62°12.4′S latitude and 0°14.2 and 3°24.9′E longitude. Diatoms from several cores (table) were examined under a scanning electron microscope (SEM) and an inverted light microscope to determine the species composition and relative abundances (see Clarke and Ackley in preparation for additional information on ecology and relationships to sea-ice structure). Diatoms were found throughout the length of the cores, the average length being 75 centimeters (Ackley, Clarke, and Smith 1982) while snow cover on the cores ranged from 10 to 30 centimeters with an average of 20 centimeters (Clarke and Ackley in preparation).

As in previous studies, we found that the pennate forms were dominant. The centric to pennate ratio ranged from 1-to-6 to 1-to-34 with an average of 1-to-16. *Chaetoceros dichaeta* Ehrenberg was the only centric species which was "abundant" (we have defined "abundant" as greater than 10 percent of the sample composition) in our samples, and it has not previously been reported as abundant. Of the pennate species that we found in abundance, three have been found in abundance by other authors. These are *Nitzschia closterium* (Ehrenberg) W. Smith and *Nitzschia cylindrus* (Grunow) Hasle found by Ackley et al. (1979) and *Nitzschia subcurvata* Hasle found by Buck and Garrison (in preparation). In our samples, we also found *Nitzschia prolongatoides* Hasle, *Nitzschia turgiduloides* Hasle, *Tropidoneis glacialis* Heiden, and an unidentified *Navicula* species to be numerically significant. The table lists the dominant species in each sample and their relative abundances. As indicated by the footnote in the table, five of these species have not previously been found in abundance in antarctic sea ice.

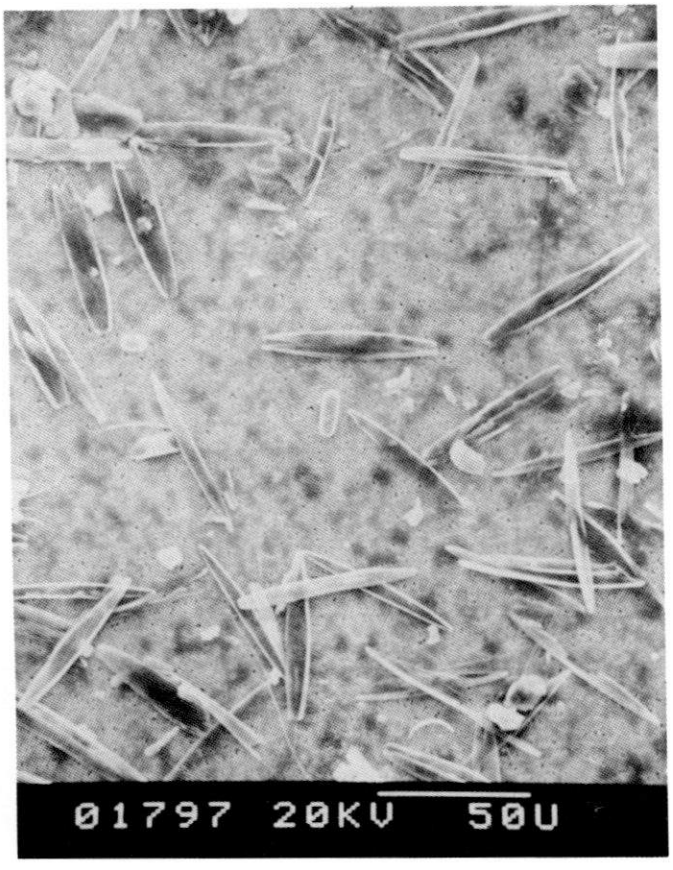

Scanning electron microscope photo of ice chunk 10-N/K showing typical assemblage: *Chaetoceros dichaeta*, *Nitzschia closterium*, *Nitzschia curta*, *Rhizosolenia alata*, and *Tropidoneis glacialis*. (Bar-line represents 5 micrometers.)

The figure, an SEM micrograph from ice chunk 10-N/K, shows a typical assemblage dominated by a single pennate, *T. glacialis*. The other pennates present are *N. closterium* and *Nitzschia curta* (Van Heurck) Hasle. The centrics are *Ch. dichaeta* and *Rhizosolenia alata* Brightwell.

There are several possible reasons for the variable species compositions in these samples. To start with, the incorporation mechanisms which exist in frazil and congelation ice are different. Frazil ice formation tends to concentrate algal cells through scavenging and/or nucleation (Ackley 1982; Garrison, Ackley, and Buck in preparation), while congelation ice formation tends to reject material. As the ice forms over a period of several hours to several weeks, the water mass below it—and hence its biological components—may change slightly. Lastly, when the light intensity increases in the spring, the diatoms generally begin to reproduce within the ice. The total cell volume and the species composition then is in part dependent on the amount of snow cover overlying the ice floe since it limits light penetration. For these samples, representing an end-of-winter population, it appears that ice-formation processes and water-column composition have the greatest impact on diatom composition and abundance in sea ice. This is described more completely in Clarke and Ackley (in preparation).

We wish to thank Motoi Kumai for the excellent SEM micrographs which aided our species identifications. We would also like to thank our American and Soviet colleagues and the crew of the NES *Mikhail Somov*. This research was supported by the National Science Foundation grant DPP 80-06922.

References

Ackley, S. F., K. R. Buck, and S. Taguchi. 1979. Standing crop of algae in the sea ice of the Weddell region. *Deep-Sea Research*, 26A, 269–281.

Ackley, S. F. 1982. Ice scavenging and nucleation: Two mechanisms for incorporation of algae into newly forming sea ice. *EOS, Transactions, American Geophysical Union*, 63(3), 47.

Ackley, S. F., D. B. Clarke, and S. J. Smith. 1982. *Weddell Polynya Expedition preliminary data report: Physical, chemical and biological properties of ice cores*. (CRREL Technical Note) Hanover, N.H.: U.S. Army Cold Regions Research and Engineering Laboratory.

Buck, K. R., and D. L. Garrison. In preparation. Protists from the water column at the Weddell Sea ice edge. *Deep-Sea Research*.

Bunt, J. S., and E. J. F. Wood. 1963. Microalgae and antarctic sea ice. *Nature*, 199, 1254–1255.

Burkholder, P. R., and E. F. Mandelli. 1965. Productivity of microalgae in antarctic sea ice. *Science*, 149(3686), 872–874.

Clarke, D. B., and S. F. Ackley. In preparation. Sea ice structure and biological activity in the Antarctic marginal ice zone. *Journal of Geophysical Research*.

Fukushima, H., and H. Meguro. 1966. The plankton ice as basic factor of the primary production in the Antarctic Ocean. *Antarctic Record*, 27, 99–101.

Garrison, D. L., S. F. Ackley, and K. R. Buck. In preparation. Frazil ice formation: An unusual physical mechanism for establishing ice algae communities. *Nature*.

Gordon, A. L., and E. I. Sarukhanyan. 1982. American and Soviet expedition into the Southern Ocean sea ice in October and November 1981. *EOS, Transactions, American Geophysical Union*, 63(1), 2.

Richardson, M. G., and T. M. Whitaker. 1979. An antarctic fast-ice food chain: Observations on the interaction of the amphipod *Pontogoneia antarctica* Chevereux with ice-associated microalgae. *British Antarctic Survey Bulletin*, 47, 107–115.

Watanabe, K. 1982. Centric diatom communities found in the antarctic sea ice. *Antarctic Record* 74, 119–126.

SECTION 5: ATMOSPHERE

JOURNAL OF GEOPHYSICAL RESEARCH, VOL. 89, NO. C1, PAGES 649–661, JANUARY 20, 1984

Atmospheric Boundary-Layer Modification, Drag Coefficient, and Surface Heat Flux in the Antarctic Marginal Ice Zone

EDGAR L. ANDREAS, WALTER B. TUCKER III, AND STEPHEN F. ACKLEY

U.S. Army Cold Regions Research and Engineering Laboratory

During a traverse of the Antarctic marginal ice zone (MIZ) near the Greenwich Meridian in October 1981, we launched a series of radiosondes along a 150-km track starting at the ice edge. Since the wind was from the north, off the ocean, these radiosonde profiles showed profound modification of the atmospheric boundary layer (ABL) as the increasing surface roughness decelerated the flow. The primary manifestation of this modification was a lifting of the inversion layer with increasing distance from the ice edge by the induced vertical velocity. But there was also a cooling of the stably stratified mixed layer below the inversion and a consequent flux of sensible heat to the surface that averaged over 200 W/m^2. The magnitude of this flux suggests that atmospheric heat transport plays a significant role in the destruction of ice in the Antarctic MIZ. Using the rising of the inversion and ABL similarity theory, we estimated the change in the neutral stability drag coefficient, C_D, across the MIZ. C_D increased from its open ocean value, 1.2×10^{-3}, at the ice edge to 4.0×10^{-3} at 80–90% ice concentration. We present an equation for this dependence of drag on ice concentration that should be useful for modeling the surface stress in marginal ice zones.

1. INTRODUCTION

The juxtaposition of ice and water in polar seas can have dramatic effects on the atmospheric boundary layer (ABL). Since *Vowinckel and Taylor* [1965] and *Badgley* [1966] first predicted the magnitude of the turbulent heat flux from open water to the atmosphere in winter, the emphasis has been primarily on convectively driven boundary-layer modification. *Miyake* [1965] and *Andreas et al.* [1979] studied the growth of the internal boundary layer that develops when very cold air blows over the relatively warm water in Arctic leads. *Orvig* [1974] discussed the feedback between the turbulent heat fluxes and ABL modification over large polynyas. *Streten* [1975] and *Walter* [1980] both looked at the roll clouds that can develop when cold air blows off the ice of the Bering Sea and out onto the open ocean. And *Salo et al.* [1980] studied mixed-layer growth and the surface heat flux for the same Bering Sea wind regime using radiosondes launched from a ship steaming downwind from the ice edge.

The ABL can also respond to a change in surface roughness, however. Although marked changes in roughness may not be as obvious over the polar seas as they are over land or at coastlines [*Panofsky and Petersen*, 1972; *Beljaars*, 1982], the ice edge, especially, can present a significant roughness change. The drag coefficient—which is a measure of the surface roughness—is very similar for the ocean [*Large and Pond*, 1981] and for smooth sea ice [*Banke et al.*, 1980]. But based on measurements by *Smith et al.* [1970] in the Gulf of St. Lawrence, by *Macklin* [1983] and *Pease et al.* [1983] in the Bering Sea, and by *Banke et al.* [1976, 1980] in the Beaufort Sea and in Robeson Channel, and on theoretical work by *Arya* [1975], a picture is emerging of how strongly the drag coefficient depends on surface topography. In the marginal ice zone (MIZ) [*Wadhams*, 1981], where the ice is broken and dispersed by wave activity, the drag coefficient is likely larger than anywhere else over the ocean, since the surface is essentially a continuous field of step functions: ice to water, then back up to ice. The drag coefficient here may thus be as much as 3 times larger than over the ocean; this corresponds to a 2 order of magnitude difference in the roughness length, z_0. An atmospheric flow crossing the ice edge consequently encounters a change not only in surface temperature but also in surface roughness. The roughness change alone is large enough to cause modifications in the ABL [*Taylor*, 1969; *Peterson*, 1969; *Panofsky and Petersen*, 1972; *Vager and Nadezhina*, 1975].

In October 1981 during the U.S.-U.S.S.R. Weddell Polynya Expedition [*Gordon and Sarukhanyan*, 1982] we traversed the Antarctic MIZ on the Soviet icebreaker *Mikhail Somov*. The wind was from the northwest, had been steady in direction for the 12 hours before we encountered the ice edge, and remained steady during the measurements we report here (Figure 1). We launched a radiosonde at the ice edge and four others over a 150-km track as the *Mikhail Somov* steamed southeast. These soundings (Figure 2) and our shipboard meteorological data provide the first comprehensive look at how the surface roughness and temperature change in the MIZ can affect the ABL during on-ice winds.

With the on-ice winds, the atmospheric flow felt an increase in surface roughness at the ice edge and consequently slowed [e.g., *Taylor*, 1969; *Vager and Nadezhina*, 1975]. By virtue of two-dimensional continuity,

$$\partial U/\partial x + \partial W/\partial z = 0 \tag{1}$$

where U is the mean horizontal wind velocity and so defines the x axis, W is the mean vertical velocity, and z is positive upward, there must thus have been a positive vertical velocity over the ice. In other words, the entire ABL should have risen downwind from the roughness change. This lifting is obvious in Figure 2, where the potential temperature profiles above the inversion remain virtually unchanged in form from sounding to sounding but rise with distance downwind from the ice edge. We have used this rising of the ABL to estimate the change in drag coefficient across the MIZ and thus found that for 80% ice cover the drag coefficient was 4.0×10^{-3}, more than 3 times its value over the ocean and twice its value over close, rough sea ice.

We have also estimated the surface sensible heat flux in the

Paper number 3C1716.

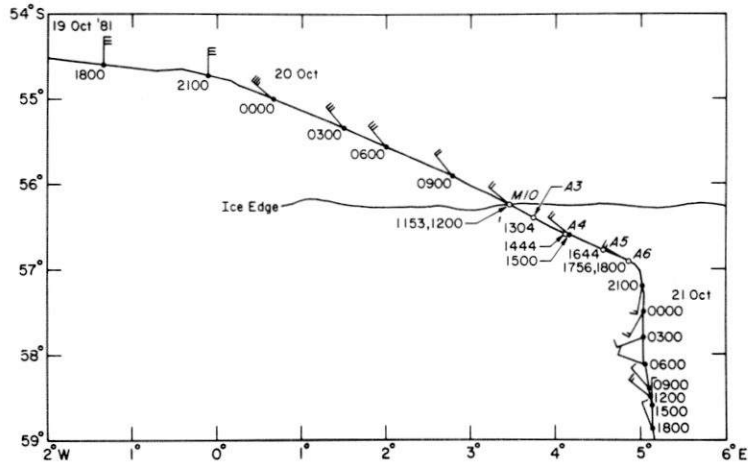

Fig. 1. The cruise track. The flags show observations of the surface wind vector, which were made every 3 hours as indicated; long barbs represent 5 m/s, short ones represent 2 m/s. The open circles show locations of the upper-air soundings with the time noted.

MIZ, basically by computing the change in integrated heat content between our soundings. This heat flux is toward the surface—relatively warm air from the ocean encountered a colder surface—and much larger than expected on the basis of a simple flux-gradient estimate of the flux. The reason for this large heat flux is the enchanced turbulent mixing resulting from the roughness change and the possible existence of secondary flows.

2. Observations

Table 1 summarizes the upper-air soundings that we made while crossing the MIZ. In the table the fetch is the actual distance the wind blew over the ice, not the distance perpendicular to the ice edge. The ice concentration, c, is the fraction of ice cover estimated from our visual observations [*Ackley and Smith*, 1983]; T_s, the surface temperature measured by a towed thermistor; T_{11}, a point value (no averaging) of the air temperature at a height of 11 m measured by a sensor on the bow; U_{21}, the wind speed 21 m above the surface measured on the ship's mast; and ϕ, the relative humidity determined from wet and dry bulb thermometers mounted on the bow.

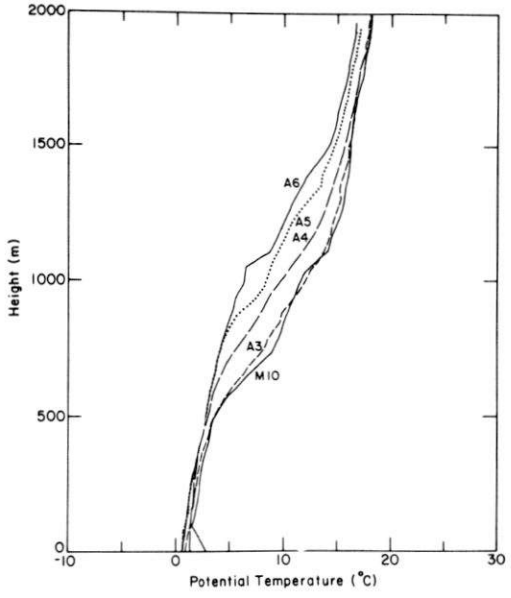

Fig. 2. Potential temperature profiles from the five soundings.

We used two different radiosonde systems for the soundings. The M10 sounding was made with a MicroCORA system manufactured by Vaisala of Helsinki, Finland. We made the other four soundings with an Airsonde system manufactured by A.I.R. of Boulder, Colorado. Both systems measure pressure, temperature, and humidity. The MicroCORA, in addition, measures the wind profile by using the Omega navaid signals to track the radiosonde [*Beukers*, 1979]. Thus, we had upper-air winds right at the ice edge, an advantage that *Salo et al.* [1980] did not have when they tried calculating the advective heat transport across the Bering Sea ice edge.

Andreas and Richter [1982] evaluated the performance of the two radiosonde systems that we used on the *Mikhail Somov* and found that they made comparable measurements of pressure and temperature. The interchangeability of temperature and pressure sensors between different sondes—more important than the absolute accuracy in our subsequent analysis—was pretty much as the manufacturers specify, ± 0.2°C for temperature and ± 1 mbar for pressure [*Call and Morris*, 1980]. The accuracy of the Omega-derived winds in this part of the Antarctic is, nominally, 1 m/s [*Olson*, 1979]. Although both radiosonde systems measure humidity, we have largely ignored the upper-air humidity profiles in what follows because they were inconsistent.

As is evident from the wind flags in Figure 1, the wind direction during our radiosonde transect and for the 12 hours preceding it was very steady. Figure 3 shows that at the ice edge at noon on October 20 the geostrophic wind was from 300° and that there was very little Ekman turning of the wind vector: only 11° between the surface and 2000 m. Figure 4, which shows the pressure contours derived from the radiosonde soundings, confirms that conditions were nearly stationary and that the flow was essentially two dimensional. This evidence of the two-dimensional nature of the flow will be the justification for some of our subsequent analysis.

Although pressure analysis fields for the southern ocean in the area of our transect are sometimes untrustworthy because of the sparsity of reporting stations, sea level pressure charts

TABLE 1. Summary of the Marginal ice Zone Upper-Air Soundings, October 20, 1981

Sounding	Time*	Latitude, °S	Longitude, °E	Fetch, km	c	T_s, °C	T_{11}, °C	U_{21}, m/s	ϕ, %
M10	1153	56.2	3.3	0	0.10†	−1.3	0.8	10.0	91
A3	1304	56.4	3.7	35	0.10	−1.4	−1.3	9.5	90
A4	1444	56.6	4.1	76	0.15	−1.4	−0.9	9.0	88
A5	1644	56.8	4.6	120	0.30	−1.6	−1.7	8.5	93
A6	1756	56.9	4.9	150	0.80	−1.7	−1.6	8.0	98

*Since we were near the 0° meridian, all times are Greenwich Mean Time (GMT) and local time.

†Although we specify c as 0.1 for this sounding, that value is really not appropriate for the radiosonde profile. We made this sounding virtually at the ice edge; with on-ice winds the air mass was, thus, representative of open ocean conditions, i.e., of $c = 0$.

obtained from the National Climate Center do let us interpret these shipboard observations in a synoptic context. During our radiosonde transect a low pressure center passed to our south. At 0000 GMT on October 20 the low was centered at 58°S, 2°W, and the geostrophic wind at our position was from the northwest, consistent with our surface observations early that day (Figure 1). The charts suggest that by 1200 GMT on October 20 the low had moved to 63°S, 7°E, and had deepened from 975 to 968 mbar, though the pressure gradient remained unchanged at our location. The indicated geostrophic wind also swung almost westerly, a shift refuted by our surface observations and noon radiosonde (Figure 3). During the next 12 hours the low moved to 66°S, 17°E, and deepened further to 959 mbar. Because it was now more distant from us, however, the local pressure gradient decreased and the geostrophic wind became southwesterly, thus explaining the shift in surface winds that we observed between 1800 and 2100 GMT (Figure 1). In summary, our position north of the low explains the directional consistency of the surface winds and the unchanging pressure field (Figure 4) during our 6 hour radiosonde transect.

Many have associated convective cloud formation with ABL modification over water [e.g., *Lenschow*, 1973; *Vowinckel and Orvig*, 1973; *Streten*, 1975; *Walter*, 1980]. But, as is evident from the potential temperature profiles in Figure 2, we did not have convective conditions: The ABL was stably stratified during our transect. Cloud conditions consequently did not change during the time of our observations. We were under a complete cover of low stratiform clouds during our radiosonde transect, for the 36 hours preceding it, and for 6 hours after it ended.

Ackley and Smith [1983] described in detail the ice conditions during our transect on October 20. In brief, we saw the first small chunks of ice at 1115 GMT and crossed very diffuse plumes of small broken floes until the M10 ice edge sounding at 1153, when ice concentration was judged to be 10%. We continued alternately to cross open water and low concentration streaks of brash ice and small broken floes until the A3 sounding 17 km from the edge. Now the plumes and bands became more concentrated and contained some older ice with evidence of ridging; but there was still a lot of open water. Figure 5 shows typical ice conditions in this region. Ice concentration for the A4 radiosonde 38 km from the ice edge was 15%, and the floe size was approximately 5 m. Between the A4 and A5 soundings we evidently crossed a more stable ice edge; by the time of the A5 sounding at 1644, 60 km into the ice, the concentration was 30%, the floes were older and sometimes ridged, and some were snow covered. The banding of the floes continued as we penetrated the MIZ; at 1717, 66 km from the edge, we crossed an extensive band of 5 m floes, and the ice coverage had increased to 40–60%. For the A6 sounding at 1756 we were 74 km from the ice edge and in first-year ice of 80% concentration; floe diameters were 8–10 m; and there was brash ice between floes. By 1815, 76 km from the edge, the ice concentration was 90%, a value typical of the interior pack; but the floes were still only about 10 m in diameter. Compare this description of the Antarctic MIZ with ones of the MIZ in Denmark Strait [*Kozo and Tucker*, 1974] and in the Bering Sea [*Bauer and Martin*, 1980].

In Figure 6 we have contoured the potential temperature data shown in the profiles in Figure 2. We also plot in the figure and list in Table 2 the inversion height, Z_i, the potential temperature at Z_i, θ_i, the height of the top of the inversion layer, Z_{it} (where the temperature profiles in Figure 7 bend back to a negative slope), and the potential temperature there, θ_{it}.

Figure 6 contains a fairly complete picture of what modification of the ABL involved. The Z_{it} level rose with distance downwind but remained essentially coincident with the 14°C potential temperature surface. The Z_i level also rose but, in contrast to Z_{it}, crossed isentropic surfaces: The inversion base was being eroded by mixing processes. Nevertheless, the slope of the inversion layer, $(\theta_{it} - \theta_i)/(Z_{it} - Z_i)$, remained constant at 0.017°C/m from the ice edge to 150 km. That is, above the inversion base the structure of the air mass did not change

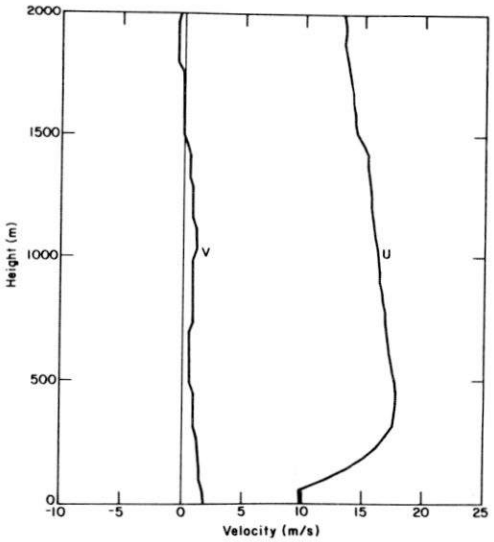

Fig. 3. Wind components from the M10 sounding, referenced to 300°.

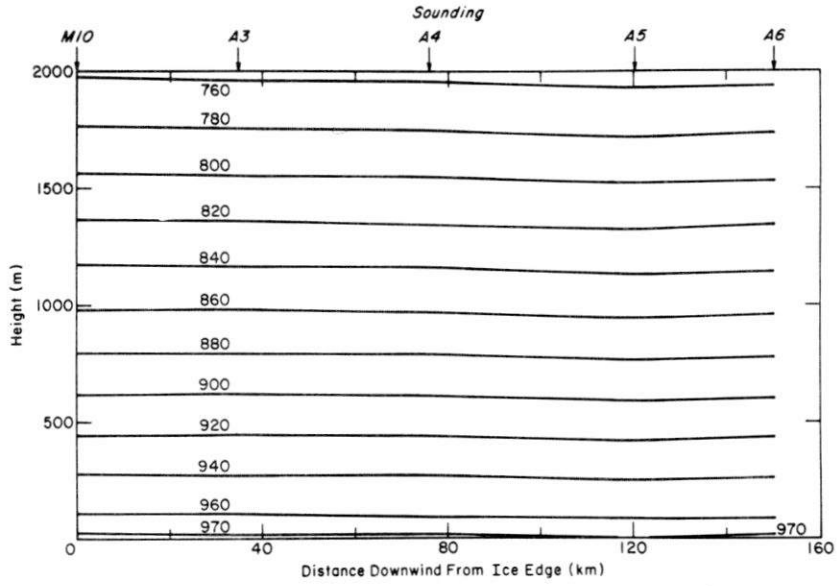

Fig. 4. The pressure contours in millibars along the ship track.

over the 150-km path; potential temperature is a conservative tracer.

Our interpretation of Figure 6 necessarily means that the entire air column rose in response to the increased surface roughness. From the entries in Table 2 we can approximate the vertical velocity: (1513–1113 m)/6 h $\approx$ 2 cm/s. As we explained, this vertical velocity was a consequence of mass continuity; as the horizontal flow was decelerated by the increased roughness of the ice, there must have been a compensating increase in vertical velocity. We can therefore also approximate the vertical velocity from (1) and the wind speeds listed in Table 1:

$$\Delta W \approx -\Delta z(\Delta U/\Delta x) \tag{2}$$

With $\Delta U = -2$ m/s, $\Delta x = 150$ km, and $\Delta z = 1500$ m, again $W \approx 2$ cm/s at Z_{it}. We conclude that our data are consistent and that our conceptual picture of the ABL modification is accurate.

3. Heat Flux Estimates

In encountering the ice edge, the ABL flow did not feel the large step change in surface temperature that can often occur over polar seas in winter when the surface changes from ice to water or vice versa [*Orvig*, 1974; *Andreas et al.*, 1979]. The

Fig. 5. Typical ice conditions between the A3 and A4 radiosonde ascents.

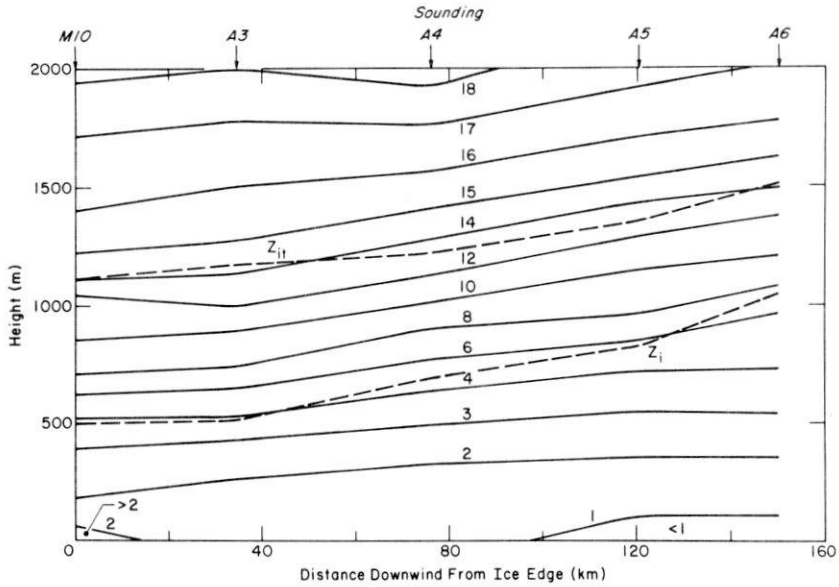

Fig. 6. Contours of potential temperature in °C along the ship track. Z_i indicates the height of the inversion, and Z_{it} shows the top of the inversion layer.

high percentage of open water clearly moderated the transition. The surface-layer air temperatures in Table 1 and the temperature profiles in Figure 7 do indicate, nonetheless, that the atmospheric mixed layer was being cooled by the new surface. In this section we estimate the turbulent heat flux at the surface in two ways.

3.1. *Flux-Gradient Method*

To get a first, quick estimate of the friction velocity, u_*, and the sensible (H_s) and latent (H_L) heat fluxes, we use the flux-gradient technique and the meteorological data listed in Table 1. We explain our procedure in Appendix A; the results are listed in Table 3, where L is the Obukhov length corrected for the moisture flux [*Busch*, 1973].

Except for u_*, the values inTable 3 are very scattered. This is, of course, not unexpected since surface-layer conditions were so nearly neutral, because we had only two profile levels with which to do the fitting, and because T_{11} was only a point measurement. It would be risky, in fact, trusting flux-gradient estimates in this region even if we had additional profile levels; the estimation technique is based on Monin-Obukhov similarity, which assumes horizontal homogeneity, a condition clearly violated in the MIZ. The heat flux values, especially, are thus merely suggestive.

The u_* values, however, should be more trustworthy since the surface-layer velocity profile typically has a much steeper slope than the temperature or humidity profiles and is, consequently, not as affected by stability conditions. *Andreas et al.* [1979] found that even over an extremely nonhomogeneous surface, flux-gradient values and eddy correlation measurements of u_* generally agreed within 10%.

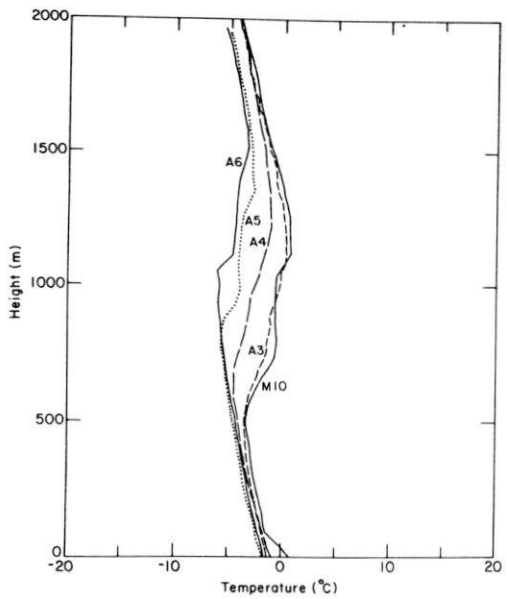

Fig. 7. Temperature profiles from the five soundings.

3.2. *Integral Method*

Because we have a series of temperature profiles, an obvious way to estimate the surface heat flux is to compute the heat transported through vertical planes perpendicular to the flow. From conservation of energy, in steady state conditions, the difference in flux through adjacent planes must be due to a surface source or sink. The appropriate integral equation,

TABLE 2. Parameters of the Inversion Layer

Sounding	Z_i, m	θ_i, °C	Z_{it}, m	θ_{it}, °C
M10	491	3.5	1113	14.1
A3	511	3.7	1169	14.3
A4	694	4.6	1219	13.4
A5	827	4.9	1351	13.4
A6	1050	6.4	1513	14.3

TABLE 3. Results of the Flux-Gradient Calculations

Sounding	u_*, m/s	H_s, W/m^2	H_L, W/m^2	L, m
M10	0.28	−25.1	−6.6	78
A3	0.31	−2.8	11.0	1300
A4	0.35	−11.2	15.4	360
A5	0.34	−0.1	14.0	−5000
A6	0.32	−3.5	1.9	810

which we derive in Appendix B, is

$$\rho_0 c_p \int_0^{Z_{it}(X_2)} U(X_2, z)\,[T'(X_2, z) - T_{it}'(X_2)]\,dz - \rho_0 c_p \int_0^{Z_{it}(X_1)} U(X_1, z)\,[T'(X_1, z) - T_{it}'(X_1)]\,dz + \tfrac{1}{2}\rho_0 c_p [T_{it}'(X_2) - T_{it}'(X_1)] \left[\int_0^{Z_{it}(X_1)} U(X_1, z)\,dz + \int_0^{Z_{it}(X_2)} U(X_2, z)\,dz\right] = (X_2 - X_1)\bar{H}_s \quad (3)$$

Here, ρ_0 is the air density at the surface; c_p, the specific heat of air at constant pressure; X_1 and X_2, locations of radiosonde profiles; $Z_{it}(X)$, the height of the top of the inversion layer at fetch X; U, the velocity profile; and $\bar{H}_s$, the average surface sensible heat flux between X_1 and X_2. In (3), T' is the temperature profile with the reference state T_0 subtracted;

$$T'(X, z) = T(X, z) - T_0(z) \quad (4)$$

where T is the measured temperature profile and

$$T_0(z) = T_s - (g/c_p)z \quad (5)$$

with g, the acceleration of gravity. T_{it}' is the value obtained from (4) corresponding to $T(Z_{it})$.

As we suggested, (3) is just a statement of conservation of energy. Consider a two-dimensional volume bounded by $x = X_1$ and $x = X_2$ and by $z = 0$ and $z = Z_{it}$. The first two integrals on the left-hand side reflect the heat transported out of and into the volume at its downwind and upwind faces, respectively. The third integral is the flux carried by the vertical velocity through the top of the volume if T_{it}' changes with fetch. In steady state conditions and with no internal sources or sinks, the heat energy content of the volume does not change, so these integral contributions must equal the total turbulent heat transfer through the bottom of the volume, $(X_2 - X_1)\bar{H}_s$.

From Figure 6 we showed that θ_{it} was virtually constant at 14°C. T_{it}' is therefore also independent of fetch because T' is another form of the potential temperature. Consequently, the third term on the left-hand side of (3) is essentially zero (the vertical velocity makes no contribution to the heat flux).

We use (3) to estimate the surface heat flux between any two of the soundings listed in Table 1. Although there are, of course, temperature profiles for all of these, we unfortunately have a velocity sounding only for M10. As we discussed, the velocity should decrease with distance into the MIZ; U_{21} in Table 1 shows this deceleration. Thus, in our computations, for the A3, A4, A5, and A6 soundings we used the M10 velocity profile multiplied by the rate of deceleration indicated by U_{21}. For example, we assumed that every level of the A5 velocity profile was 85% of the corresponding M10 velocity. This assumption may be an oversimplification since the structure of the velocity profile, as well as its overall magnitude, may change with fetch over the ice; but for the sake of continuing the calculations, it is necessary. Table 4 lists the values of the sensible heat flux between any two soundings computed using (3); a negative flux is downward (toward the surface), a positive flux is upward (away from the surface).

In the table we also show the uncertainty in the flux calculations due to the specified limits of interchangeability between radiosonde temperature sensors. In (3), the integration depends pretty much on the difference between $T'(X_1)$ and $T'(X_2)$. The uncertainty in this difference, ± 0.2°C, is present at every level of the integration; therefore, the uncertainty in the computed flux increases with Z_{it}. It decreases with distance between soundings, however, since the uncertainty in temperature is the same for each pair of soundings.

With these uncertainties established, we can check that our assumption of two dimensionality is valid by estimating the magnitude of the transfer perpendicular to x. Figure 3 shows that the transverse velocity was typically 1 m/s or less. From thermal wind considerations, the curvature of the longitudinal velocity profile suggests that the transverse temperature gradient was roughly 0.01°C/km. The heat carried across our track by the transverse flow consequently had a magnitude of roughly 20 W/m^2, well below the uncertainties in our flux estimates. We are, therefore, justified in ignoring three-dimensional effects.

The statistically significant fluxes in Table 4 are toward the surface from the atmosphere and 1–2 orders of magnitude larger than the sensible heat fluxes computed with flux-gradient techniques and shown in Table 3. We thus should discuss whether these fluxes are indeed real.

The question really is whether there is more than just the surface flux contributing to the heat lost by the air column. To be completely rigorous, we should have included a source (sink) term $S(x, z)$ in equation (B1). This would then have appeared on the left-hand side of (3) as

$$-\int_{X_1}^{X_2} dx \int_0^{Z_{it}(x)} S(x, z)\,dz$$

Possible sources (sinks) are ones that can increase (decrease) the temperature of the air column without contributing to the turbulent surface flux. Such processes include phase changes (a cloud forms or dissipates), radiative exchange between a cloud and the surface, and a divergence of the radiative flux.

If a stratiform cloud is 500 m thick, has a typical liquid water content of 0.3 g/m^3 [e.g., *Pruppacher and Klett*, 1978, chapter 2], moves at 15 m/s, and dissipates over a 150-km path, it acts as a heat sink of roughly 40 W/m^2. Not only is this value less than the uncertainty in our computed fluxes, as explained in section 2, we saw basically no change in the cloud cover as we penetrated the MIZ. Evidently, phase changes did not make a significant contribution to the fluxes tabulated in Table 4.

Fleagle and Businger [1980, p. 234] derived an equation for the net long-wave radiative exchange, E_n, between a cloud of temperature T_c and emissivity ε_c and a horizontal surface of temperature T_s and emissivity ε_s:

$$E_n = \frac{\varepsilon_c \varepsilon_s \sigma}{1 - (1 - \varepsilon_c)(1 - \varepsilon_s)} (T_c^4 - T_s^4) \quad (6)$$

where σ is the Stefan-Boltzmann constant. If we assume that

TABLE 4. Integral Results for the Average Surface Sensible Heat Flux in W/m² Between Any Two Soundings

Sounding/ Sounding	M10	A3	A4	A5
A3	10 ± 170 (35)			
A4	−240 ± 90 (76)	−450 ± 140 (41)		
A5	−300 ± 70 (120)	−430 ± 90 (85)	−410 ± 140 (44)	
A6	−230 ± 80 (150)	−300 ± 90 (115)	−220 ± 120 (74)	−75 ± 240 (30)

A negative flux is downward; a positive flux is upward. The numbers in parentheses are the distances between the soundings in kilometers.

the cloud base is at the inversion base, for our most extreme case, sounding A6, $T_c = -6.2°C$ and $T_s = -1.7°C$. Taking $\varepsilon_c = 0.95$ [*Paltridge and Platt*, 1976, chapter 8] and $\varepsilon_s = 0.97$ for a water and ice surface [*Kondratyev*, 1969, p. 43], we calculate $E_n = -18$ W/m². The cloud gains energy from the surface. But again, this value is below the uncertainty in our computed flux values: This kind of radiative transfer is not a significant source or sink.

Lastly, we consider the possibility that the ABL is cooling because of a radiative flux divergence. If such were the case, the temperature of the ABL would decrease with time, as we saw; but this lost heat, though contributing to the integrals in (3), would not contribute to the surface flux; it would be lost from the ABL. Measurements by *Suomi et al.* [1958] and calculations by *Sasamori* [1968] showed that in clear air the radiative flux divergence can lead to a cooling rate in the lower atmosphere that is typically 1°C/day. Remember, however, that according to our observations, radiative processes were not important above Z_i; we have shown that the temperature changes here were purely adiabatic. Also, because there was total cloud cover for our entire series of soundings, we suspect that the cooling rate was much less than this 1°C/day value. Nevertheless, if we suppose that below the inversion the air cooled by 0.25°C during the 6 hours between our first and last soundings, our computed average surface heat flux during that interval would be biased by only 45 W/m². Shorter intervals would, naturally, show smaller effects. Because this estimated contribution from radiative flux divergence is smaller than the uncertainty in any of our computed flux values, we can also ignore these effects.

We consequently conclude that the fluxes listed in Table 4 are indeed accurate estimates of the surface sensible heat flux, though they are significantly larger than those computed by flux-gradient techniques (Table 3). A large portion of the heat contributing to the flux values in Table 4 came from the top of the mixed layer and from the inversion base (Figure 7). Enhanced mechanical mixing associated with the increase in surface stress due to the roughness change must have been responsible for transporting this heat down to the surface. Because of the larger eddies involved in this exchange, the heat was likely delivered to the surface in intermittent bursts [*Haugen et al.*, 1971], possibly even by organized secondary flows, which are often associated with a change in surface conditions [*LeMone*, 1973; *Brown*, 1980, 1981]. Because such transfer processes are not adequately described by the eddy-diffusivity model on which the flux-gradient relations are based, and for the reasons already mentioned in section 2, the flux-gradient method badly underestimates the magnitude of the sensible heat flux, a fine example of the risks in using the flux-gradient equations in horizontally inhomogeneous conditions.

Because for every statistically significant entry in Table 4 the flux was to the surface, there must have been melting: There was no other way to dissipate this much heat. And the melting could have been rapid; a downward flux of 280 W/m² —typical of our values—can melt 8 cm of sea ice in a day.

The MIZ is, of course, a region of ice destruction. We saw evidence of melting as we crossed it during the radiosonde transect; but because we were always moving, we had no chance to make an independent estimate of the melting rate. Our suspicion is that ice destruction in the Antarctic MIZ is episodic. When the prevailing wind is northerly, carrying warm air in from the ocean, the melting can be at an almost catastrophic rate, as our results show. For southerly winds, which can drag the ice into warmer water, the melting might also be rapid [*McPhee*, 1983].

As a crude check of this indicated melting rate, 8 cm/day, let us compute a mass balance of the Weddell Sea. *Ackley* [1979] showed that 6×10^6 km² of sea ice with a typical thickness of 1 m is destroyed annually in the Weddell Sea sector of the ocean (from 60°W to 30°E) between October and March. In other words, over this 150-day period an average of 40 km³ of sea ice a day must be melted. Most of this melting occurs near the ice edge [*Hibler and Ackley*, 1983]. Suppose the melting zone between 60°W and 30°E is an 80-km-wide band (roughly 5000 km long) at the ice edge that moves south with the retreating pack. To destroy 40 km³ of sea ice per day in this band, the melting rate must average 10 cm/day, a value close to our estimated melting rate for on-ice winds, 8 cm/day. Clearly, the turbulent heat flux from the atmosphere contributes significantly to the destruction of ice in the Antarctic MIZ.

Gordon [1981] also considered this seasonal cycle of Antarctic sea ice. After estimating both the radiative and the turbulent components of the surface energy budget, he concluded that the sensible heat flux was the smallest term in the budget and that additional oceanic heat sources contributing, on the average, 30 W/m² over the entire southern ocean were thus necessary to explain the annual melting. However, his estimates of the turbulent fluxes were based on surface-layer parameterizations. Because for northerly winds such methods underestimate the sensible heat flux in the MIZ—since the entire ABL can contribute to the flux—*Gordon*'s [1981] value is really an upper bound on the oceanic heat flux. We were

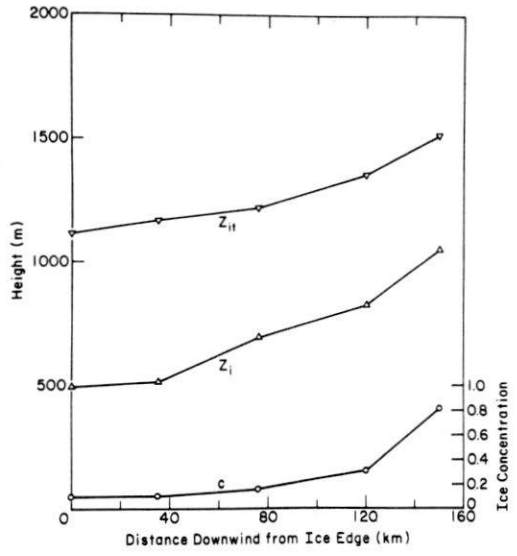

Fig. 8. The ice concentration, c, the inversion height, Z_i, and the height of the top of the inversion layer, Z_{it}, as a function of distance during the radiosonde transect.

thus not surprised to see that oceanographic data collected on our cruise suggested the oceanic flux during the winter is only 20–25 W/m^2 [*Gordon et al.*, this issue].

4. The Drag Coefficient

We have described how the inversion layer rose with distance over the MIZ and so with increasing ice concentration c (Figure 8). Since this lifting resulted from the flow deceleration due to the increased roughness and surface stress, it seems conceivable that we can estimate the drag coefficient in the MIZ from this rate of increase of Z_i.

Taylor [1969] and *Vager and Nadezhina* [1975] have made numerical studies of an ABL perturbed by a change in surface roughness; but an analytical framework specifically for the study of ABL modification does not exist. We, therefore, base our evaluation of the drag coefficient in the MIZ on ABL similarity theory such as that developed by *Zilitinkevich* [1972, 1975]. Admittedly, a fundamental assumption of the theory is horizontal homogeneity, which is certainly absent in the MIZ. But the precedent for our using such a procedure is well established; early analytic studies of horizontal nonhomogeneity in the atmospheric surface layer yielded useful results despite being based on relations derived for horizontally homogeneous conditions [see, e.g., *Calder*, 1949; *Sutton*, 1953, chapter 8; *Elliott*, 1958; *Philip*, 1959; *Panofsky and Townsend*, 1964; *Townsend*, 1965; *Taylor*, 1970].

Fortunately, for the scales with which we are concerned, the ABL over the MIZ seems to be in quasi-equilibrium with the surface, so similarity theory may be more valid than it at first appears. To see this, consider a horizontal length scale characterizing the rate at which the ABL responded to the new surface. Such a scale is $D_{\text{mod}} = Z_i/(\partial Z_i/\partial x)$, which is roughly (800 m)/(560 m/150 km) = 210 km. On the other hand, we form a distance scale representative of the turbulent processes in the ABL from the boundary-layer time scale, Z_i/u_*, and the mean wind speed, $\bar{U}$, $D_{\text{turb}} = \bar{U}Z_i/u_*$. This scale is interpreted simply as the distance an eddy is advected downwind while making one cycle of the boundary layer. From Table 3 and Figure 3, we approximate D_{turb} as (15 m/s)(800 m/0.32 m/s) = 38 km. Thus, the turbulence, which similarity theory models, has a much shorter distance scale than that characterizing the gross changes in the ABL. Evidently, in the MIZ the turbulence parameters can respond rapidly enough to be in quasi-equilibrium with the surface despite its obvious nonhomogeneity.

Zilitinkevich [1975] gave as a prediction for the height of a fully developed ABL in stable stratification

$$h_i = \alpha \frac{{u_*}^2}{|(g/\bar{T})(H_s f/\rho_0 c_p)|^{1/2}} \tag{7}$$

where α is a constant, which *Zilitinkevich* [1975] took as one, $\bar{T}$ is a temperature typical of the layer, and f is the Coriolis parameter.

Many have verified (7), though with different values of α; for example, *Businger and Arya* [1974] found $\alpha = 1.1$; *Brost and Wyngaard* [1978], $\alpha = 0.63$; and *Brown* [1981], $\alpha = 2.0$. *Businger and Arya* [1974] found that (7) is true for $u_*/|f|\,L > 20$; that is, for $L < 130$ m in our study. Because of the demonstrated inadequacy of Monin-Obukhov similarity in the MIZ, however, it is hard to know whether the Obukhov length L has any physical significance. But *Irwin and Binkowski* [1981] showed how L is related to the local gradient Richardson number, Ri, which we can easily compute from our data. Converting L to Ri using their method, we thus find that (7) is true for our data when $Ri > 0.1$, a criterion that all of our soundings meet for heights above 200 m. Equation (7) therefore seems applicable here. We will assume that h_i corresponds to the inversion height Z_i and use (7) to relate the expected increase in surface stress ${u_*}^2$ to the increase in Z_i.

The 10-m drag coefficient is defined as

$$C_D = (u_*/U_{10})^2 \tag{8}$$

where we obtained the 10-m wind speed, U_{10}, by interpolation of the U_{21} values in Table 1 using the u_* values in Table 3. Substituting (7) in (8) yields

$$C_D(x) \propto Z_i(x)U_{10}(x)^{-2}H_s(x)^{1/2} \tag{9}$$

We know fairly well the value of the drag coefficient for neutral stability at the ice edge, $C_D(x = 0) \equiv C_{D0}$; it was the open ocean value 1.2×10^{-3} [*Large and Pond*, 1981]. Making use of this reference point, we obtain from (9) the relative change in drag coefficient across the MIZ,

$$C_D(x)/C_{D0} = [Z_i(x)/Z_i(0)][U_{10}(0)/U_{10}(x)]^2[H_s(x)/H_s(0)]^{1/2} \tag{10}$$

Here, $Z_i(0)$ is the inversion height from the M10 sounding, a value that should represent the horizontally homogeneous conditions of the upwind ocean, and $U_{10}(0)$ and $H_s(0)$ are the wind speed and heat flux at the ice edge.

Excluding the values between the M10 and A3 soundings and the A5 and A6 soundings, which have the largest uncertainties, the $\bar{H}_s$ values in Table 4 are not incompatible with the assumption that the surface heat flux was constant during our radiosonde transect. Even if the flux changed across the MIZ, however, because the H_s ratio in (10) has a square-root dependence, the C_D ratio would respond only weakly. For example, if, as we would expect intuitively, H_s decreased across the MIZ, say, by 20%—a value typical of the variability in Table 4—the C_D ratio would be only a 10% overestimate. Because this uncertainty is well within the accuracy of other measure-

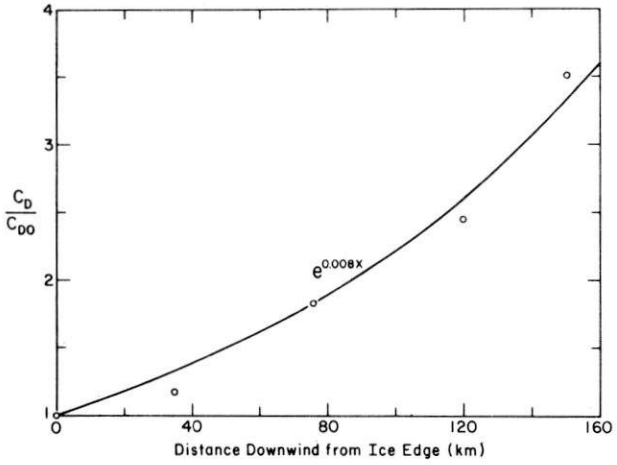

Fig. 9. The relative change in drag coefficient across the MIZ.

ments of the drag coefficient over sea ice, we henceforth ignore the heat flux term and rewrite (10) as

$$C_D(x)/C_{D0} = [Z_i(x)/Z_i(0)][U_{10}(0)/U_{10}(x)]^2 \qquad (11)$$

The beauty of (11) is that it involves only ratios of the measured quantities. Hence, uncertainty over the value of the constant in (7) does not affect it; and possible fetch-dependent stability effects or systematic errors in our determination of U_{10} are of minor consequence. C_D/C_{D0} is thus, in essence, the ratio of drag coefficients for neutral stability.

Figure 9 shows a plot of C_D/C_{D0} as a function of fetch for our data. The line, obtained from a least squares fitting of $\ln(C_D/C_{D0})$ versus X, is

$$C_D/C_{D0} = e^{0.008X} \qquad (12)$$

Remember that X is not the perpendicular distance into the MIZ; the equation

$$C_D/C_{D0} = e^{0.004d} \qquad (13)$$

with d in kilometers, describes the behavior of C_D/C_{D0} as a function of actual distance from the ice edge.

Figure 9 suggests that values of C_D in the MIZ can be more than 3 times larger than open ocean values: With $C_{D0} = 1.2 \times 10^{-3}$, C_D can be 4×10^{-3}. Such values are not without corroboration. *Macklin* [1983] reported an average C_D value of $3.09 \pm 0.49 \times 10^{-3}$ in the Bering Sea MIZ for close but heavily fractured and ridged ice. In 80–90% ice cover in the Gulf of St. Lawrence, *Smith et al.* [1970] found values of the drag coefficient in unstable conditions as large as 4.0×10^{-3}; these convert to C_D values for neutral stability of 3.5–3.8×10^{-3}. In contrast, the roughest ice that *Banke et al.* [1980] sampled in the close Arctic pack had a drag coefficient of 2×10^{-3}.

Equation (12) (or (13)) is not a very useful predictive tool, however, because the composition of the MIZ—its compactness and the distribution of ice types within it—can undergo significant temporal changes [*Bauer and Martin*, 1980]. The distance from the ice edge is thus not a meaningful model parameter. The ice concentration c is more useful. Equation (12) does help us smooth out some of the variability in our particular data set, however. In Figure 10 we plot our raw C_D/C_{D0} data and the corresponding points obtained from (12) versus c. The line, which we fitted by trial and error and intuition, is

$$C_D/C_{D0} = 1 + 2.4 \tanh (2.5\, c) \qquad 0 \le c \le 1 \qquad (14)$$

The values this predicts correspond well with the C_D values measured by *Smith et al.* [1970] in 80–90% ice concentration.

The tanh function increases monotonically with its argument; so (14) predicts that $C_D = 3.4\ C_{D0} (= 4.1 \times 10^{-3}$ if $C_{D0} = 1.2 \times 10^{-3})$ for total ice cover. Such a large value is incompatible with the measurements of *Banke et al.* [1980]; they showed that over close, smooth sea ice, C_D has virtually the same value that it has over the ocean, 1.1–1.2×10^{-3}. As the surface roughness of the interior pack increases, C_D also increases, but evidently not to values much larger than 2×10^{-3}. Consequently, we suggest with the dashed line in Figure 10 that C_D/C_{D0} must rapidly return to the smooth ice value—one—as the ice concentration increases from 80 to 100%. Wind tunnel studies summarized by *Rouse* [1965] showed essentially this same effect; the aerodynamic surface roughness goes through a mid-range maximum as the concentration of roughness elements increases from 0.0 to 1.0. For nearly complete ice cover, we therefore hypothesize that the relations parameterizing C_D as a function of surface roughness presented by *Banke et al.* [1980] replace (14).

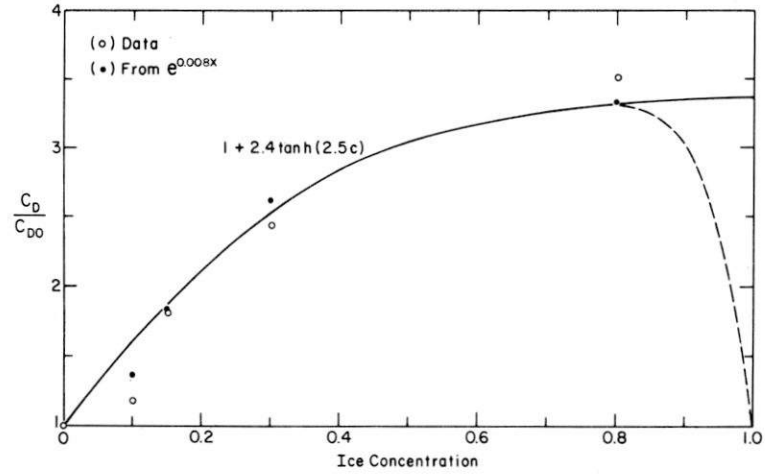

Fig. 10. Raw and smoothed C_D/C_{D0} ratios as a function of ice concentration. The dashed line suggests how we believe the ratio behaves for nearly complete ice cover.

Bauer and Martin [1980] speculated that the banding of ice common near ice edges [*Muench and Charnell*, 1977] is a result of the variation in drag coefficient across the MIZ. More recently, *Wadhams* [1983] suggested that the change in drag coefficient merely leads to divergence of the ice in the MIZ during off-ice winds; then other processes such as wave radiation pressure [*Wadhams*, 1983; *Martin et al.*, 1983] or the reduction in water drag caused by melting [*McPhee*, 1983] act to form and accelerate the bands. The ABL model of *Overland et al.* [1983] confirmed that changes in the drag coefficient across the MIZ can, indeed, lead to regions of divergence and convergence in the wind field during off-ice winds. Thus, by providing a functional expression for this variation in the drag coefficient—which by consensus is the initiating mechanism, at least—our results should be the impetus for more thorough studies of band formation.

5. Summary

The data that we have presented show a fairly complete picture of the modification of a stably stratified atmospheric boundary layer in response to an increase in surface roughness. The essential process in the modification was a deceleration of the flow because of the increased surface stress. The induced vertical velocity then lifted the entire ABL. The mixed layer below the inversion cooled by losing heat to the surface; but temperature changes above the inversion were purely adiabatic.

The cooling of the mixed layer and the eroding of the inversion base as the air mass crossed the MIZ necessitated substantial heat transfer to the surface, presumably by secondary flows. Our integral estimates of the flux of sensible heat to the surface yielded values that averaged over 200 W/m^2. Since there is seemingly no other way to dissipate this heat, there must be intense melting of the sea ice in the MIZ during episodes of northerly winds.

Our radiosonde observations of the height of the inversion let us make the first determination ever of the drag coefficient over the broken floes characteristic of the Antarctic MIZ. We found that C_D for neutral stability can be as large as 4.0×10^{-3} but depends strongly on ice concentration. We thus presented the first parameterization of the drag coefficient in terms of ice concentration (equation (14)), an important relation for use in modeling the surface stress in marginal ice zones.

6. Appendix A: The Flux-Gradient Technique

The flux-gradient technique for obtaining turbulent surface fluxes from the measured wind speed (U), potential temperature (θ), and specific humidity (Q) profiles is based on Monin-Obukhov similarity [*Businger et al.*, 1971]. The profile data are fitted with the models

$$U(z) = (u_*/k)[\ln (z/z_0) - \psi_m(z/L)] \tag{A1}$$

$$\theta(z) = T(z_s) + t_*[\ln (z/z_s) - \psi_h(z/L)] \tag{A2}$$

$$Q(z) = Q(z_s) + q_*[\ln (z/z_s) - \psi_h(z/L_Q)] \tag{A3}$$

where z is the height; z_0, the roughness length for velocity; z_s, the scalar roughness length; $T(z_s)$ and $Q(z_s)$, the surface temperature and humidity; and k, von Kármán's constant (0.4). The ψ are the semi-empirical Monin-Obukhov similarity functions, which are functions of the stability parameter $\zeta(=z/L$ or $z/L_Q)$.

For unstable conditions ($\zeta < 0$) [*Paulson*, 1970],

$$\psi_m(\zeta) = 2 \ln [(1 + x)/2] + \ln [(1 + x^2)/2] - 2 \arctan (x) + \pi/2 \tag{A4}$$

$$\psi_h(\zeta) = 2 \ln [(1 + x^2)/2] \tag{A5}$$

where

$$x = (1 + \beta_u\zeta)^{1/4} \tag{A6}$$

For stable conditions ($\zeta > 0$) [*Webb*, 1970],

$$\psi_m(\zeta) = \psi_h(\zeta) = -\beta_s\zeta \tag{A7}$$

In (A6) and (A7) we used the constants suggested by *Large and Pond* [1982], $\beta_u = 16$ and $\beta_s = 7$.

The u_*, t_*, and q_* in (A1) to (A3) are related to the surface stress (τ) and to the sensible (H_s) and latent (H_L) heat fluxes and thus link these to the measured profiles:

$$u_* = (\tau/\rho_0)^{1/2} \tag{A8}$$

$$t_* = -H_s/\rho_0 c_p u_* k \tag{A9}$$

$$q_* = -H_L/\rho_0 L_v u_* k \tag{A10}$$

Here ρ_0 is the surface air density, c_p is the specific heat of air at constant pressure, and L_v is the latent heat of vaporization (sublimation) of water (ice).

Finally, L and L_Q are the Obukhov lengths—stability parameters—

$$L_Q = \frac{1}{g}\left[\frac{1 + 0.61\,\bar{Q}}{0.61}\right]\frac{u_*^2}{k^2 q_*} \tag{A11}$$

$$L = \left\{\left[\frac{\bar{T}}{g}\frac{u_*^2}{k^2 t_*}\right]^{-1} + L_Q^{-1}\right\}^{-1} \tag{A12}$$

where g is the acceleration of gravity, $\bar{Q}$ is a representative humidity, and $\bar{T}$ is a representative temperature. Notice, in (A1) and (A2) we used L as the stability parameter for velocity and temperature, but in (A3) we used L_Q for humidity. *McBean* [1971] explained that unless a passive scalar, such as humidity, is highly correlated with temperature, L is not the proper scaling length [cf. *Dyer*, 1974]. A length scale based on the flux of the passive scalar alone, such as L_Q, is instead a more meaningful parameter.

For the flux-gradient estimates we discussed in section 3.1, we had only two levels for each of the variables U, θ, and Q, the surface and a reference height: 11 m for θ and Q, and 21 m for U (Table 1). For the surface values we set $z_0 = z_s$ and used $z_0 = 0.0001$ m over water (soundings M10 and A3) [*Large and Pond*, 1981], and $z_0 = 0.001$ m over ice (soundings A4, A5, and A6) [*Banke et al.*, 1980]. When there are just two levels, the profile equations are particularly simple:

$$u_* = \frac{kU_{21}}{\ln (21/z_0) - \psi_m(21/L)} \tag{A13}$$

$$t_* = \frac{\theta_{11} - T_s}{\ln (11/z_0) - \psi_h(11/L)} \tag{A14}$$

$$q_* = \frac{Q_{11} - Q_s}{\ln (11/z_0) - \psi_h(11/L_Q)} \tag{A15}$$

For Q_s in (A15) we used the specfic humidity of air in saturation with a water or ice surface at temperature T_s. For Q_{11} we used $\phi Q_{\text{sat}}(T_{11})$, where Q_{sat} is the saturation specific humidity at temperature T_{11} and ϕ is the relative humidity.

The flux-gradient estimation procedure is an iterative one.

We first assumed neutral stability, so $\psi_m = \psi_h = 0$ in (A13)–(A15). This yielded initial values of u_*, t_*, and q_*, which we then used to estimate L and L_Q. With these first estimates of L and L_Q we could begin accounting for the effects of stability by computing the ψ values to use in the model equations. New and better estimates of u_*, t_*, and q_* were the result. With these we, in turn, recomputed L and L_Q. The iteration continued until the relative changes in the u_*, t_*, and q_* values were all less than 1% between consecutive iterations, usually no more than two iterations.

7. Appendix B: The Heat-Flux Integral

The thermodynamic energy equation in two dimensions is

$$U(\partial T'/\partial x) + W(\partial T'/\partial z) = -\partial(\overline{wt})/\partial z \tag{B1}$$

where U is the average longitudinal velocity, W is the average vertical velocity, and w and t are the turbulent fluctuations in vertical velocity and temperature; $\overline{wt}$ is, thus, the Reynolds flux of temperature. T' is the deviation from a temperature reference state, T_0,

$$T'(z) = T(z) - T_0(z) \tag{B2}$$

where T is the measured temperature profile and

$$T_0(z) = T_s - (g/c_p)z \tag{B3}$$

Here T_s is the surface temperature; g, the acceleration of gravity; and c_p, the specific heat of air at constant pressure. We have discussed in section 2 why our assumption of two dimensionality is a good one in this study.

From T' in (B1) subtract the temperature at the top of the inversion layer, $T_{it}' = T'(Z_{it})$:

$$\partial[U(T' - T_{it}')]/\partial x + U(\partial T_{it}'/\partial x) + \partial[W(T' - T_{it}')]/\partial z = -\partial(\overline{wt})/\partial z \tag{B4}$$

Notice, to obtain this equation we have used two-dimensional continuity, equation (1), and the fact that T_{it}' depends only on x.

Let us integrate (B4) from the surface to the top of the inversion layer, Z_{it}. We get

$$\int_0^{Z_{it}} \{\partial[U(T' - T_{it}')]/\partial x\}\, dz + [\partial T_{it}'/\partial x] \int_0^{Z_{it}} U\, dz + [W(T' - T_{it}')]\Big|_0^{Z_{it}} = -\overline{wt}\Big|_0^{Z_{it}} \tag{B5}$$

The W term here is zero, since $W = 0$ at the surface and $T' - T_{it}' = 0$ at Z_{it} by definition. At Z_{it}, $\overline{wt}$ is also zero because there is no turbulent flux through the top of the inversion layer: The structure of the region does not change. The right side of (B5) is consequently just the surface flux, $\overline{wt}_0$. We can rewrite the first term in (B5) using Leibnitz's rule:

$$\int_0^{Z_{it}} \{\partial[U(T' - T_{it}')]/\partial x\}\, dz = \frac{\partial}{\partial x}\int_0^{Z_{it}} [U(T' - T_{it}')]\, dz - [U(T' - T_{it}')]\Big|_{Z_{it}} [\partial Z_{it}/\partial x] \tag{B6}$$

The last term in (B6), however, is again zero because $T' - T_{it}' = 0$ at Z_{it}. Substituting (B6), (B5) becomes

$$\frac{\partial}{\partial x}\int_0^{Z_{it}} [U(T' - T_{it}')]\, dz + [\partial T_{it}'/\partial x] \int_0^{Z_{it}} U\, dz = \overline{wt}_0 \tag{B7}$$

We now integrate (B7) over x between the soundings at X_1 and X_2:

$$\int_{X_1}^{X_2} d\left\{\int_0^{Z_{it}} [U(T' - T_{it}')]\, dz\right\} + \int_{X_1}^{X_2} dx\left\{[\partial T_{it}'/\partial x] \cdot \int_0^{Z_{it}} U\, dz\right\} = \int_{X_1}^{X_2} \overline{wt}_0\, dx \tag{B8}$$

The first term in (B8) integrates easily. Since $\partial T_{it}'/\partial x$ changes little with x, we can approximate the x integration in the second term by its average value. The term on the right-hand side of (B8) is simply the integrated surface flux; from it we define the average sensible heat flux, $\bar{H}_s$. Equation (B8) is thus

$$\begin{aligned}\rho_0 c_p \int_0^{Z_{it}(X_2)} U(X_2, z)[T'(X_2, z) - T_{it}'(X_2)]\, dz \\ - \rho_0 c_p \int_0^{Z_{it}(X_1)} U(X_1, z)[T'(X_1, z) - T_{it}'(X_1)]\, dz \\ + \tfrac{1}{2}\rho_0 c_p [T_{it}'(X_2) - T_{it}'(X_1)]\left[\int_0^{Z_{it}(X_1)} U(X_1, z)\, dz \right. \\ \left. + \int_0^{Z_{it}(X_2)} U(X_2, z)\, dz\right] \\ = (X_2 - X_1)\bar{H}_s\end{aligned} \tag{B9}$$

where ρ_0 is the air density at the surface. This is the equation we used to compute the average surface heat fluxes, $\bar{H}_s$, in section 3.2.

Acknowledgments. We would like to thank G. D. Ashton, M. G. McPhee, and B. A. Huber for reviewing this paper, S. L. Bowen for providing editorial assistance, and D. Harp for typing the manuscript. The National Science Foundation supported this research through grants DPP 80-06922 and DPP 81-20024. The National Oceanic and Atmospheric Administration, Office of Special Research and Programs, provided funds for the lease of the MicroCORA through the National Science Foundation, grant DPP 82-03489.

References

Ackley, S. F., Mass-balance aspects of Weddell Sea pack ice, *J. Glaciol., 24*, 391–405, 1979.

Ackley, S. F., and S. J. Smith, Reports of the U.S.-U.S.S.R. Weddell Polynya Expedition, October-November 1981, vol. 5, Sea ice observations, *Special Rep. 83-2*, p. 59, U.S. Army Cold Reg. Res. and Eng. Lab., Hanover, N. H., 1983.

Andreas, E. L., and W. A. Richter, An evaluation of Vaisala's MicroCORA Automatic Sounding System, *CRREL Rep. 82-28*, p. 17, U.S. Army Cold Reg. Res. and Eng. Lab., Hanover, N. H., 1982.

Andreas, E. L., C. A. Paulson, R. M. Williams, R. W. Lindsay, and J. A. Businger, The turbulent heat flux from Arctic leads, *Boundary Layer Meteorol., 17*, 57–91, 1979.

Arya, S. P. S., A drag partition theory for determining the large-scale roughness parameter and wind stress on the Arctic pack ice, *J. Geophys. Res., 80*, 3447–3454, 1975.

Badgley, F. I., Heat budget at the surface of the Arctic Ocean, in Proceedings of the Symposium on the Arctic Heat Budget and Atmospheric Circulation, edited by J. O. Fletcher, *Rep. RM-5233-NSF*, pp. 267–277, Rand Corp., Santa Monica, Calif., 1966.

Banke, E. G., S. D. Smith, and R. J. Anderson, Recent measurements of wind stress on Arctic sea ice, *J. Fish. Res. Bd. Canada, 33*, 2307–2317, 1976.

Banke, E. G., S. D. Smith, and R. J. Anderson, Drag coefficients at AIDJEX from sonic anemometer measurements, in *Sea Ice Processes and Models*, edited by R. S. Pritchard, pp. 430–442, University of Washington Press, Seattle, 1980.

Bauer, J., and S. Martin, Field observations of the Bering Sea ice edge properties during March 1979, *Mon. Weather Rev., 108*, 2045–2056, 1980.

Beljaars, A. C. M., The derivation of fluxes from profiles in perturbed areas, *Boundary Layer Meteorol., 24*, 35–55, 1982.

Beukers, J. M., The use of Loran and VLF navaids for windfinding, *Atmos. Technol., 10*, 3–13, 1979.

Brost, R. A., and J. C. Wyngaard, A model study of the stably stratified planetary boundary layer, *J. Atmos. Sci., 35*, 1427–1440, 1978.

Brown, R. A., Longitudinal instabilities and secondary flows in the planetary boundary layer: A review, *Rev. Geophys. Space Phys., 18*, 683–697, 1980.

Brown, R. A., Modeling the geostrophic drag coefficient for AIDJEX, *J. Geophys. Res., 86*, 1989–1994, 1981.

Busch, N. E., On the mechanics of atmospheric turbulence, in *Workshop on Micrometeorology*, edited by D. A. Haugen, pp. 1–65, American Meteorological Society, Boston, Mass., 1973.

Businger, J. A., and S. P. S. Arya, Height of the mixed layer in the stably stratified planetary boundary layer, in *Advances in Geophysics*, vol. 18A, edited by F. N. Frenkiel and R. E. Munn, pp. 73–92, Academic, New York, 1974.

Businger, J. A., J. C. Wyngaard, Y. Izumi, and E. F. Bradley, Flux-profile relationships in the atmospheric surface layer, *J. Atmos. Sci., 28*, 181–189, 1971.

Calder, K. L., Eddy diffusion and evaporation in flow over aerodynamically smooth and rough surfaces: A treatment based on laboratory laws of turbulent flow with special reference to conditions in the lower atmosphere, *Q. J. Mech. Appl. Math., 2*, 153–176, 1949.

Call, D. B., and A. L. Morris, The Airsonde System, in *The Boulder Low-Level Intercomparison Experiment*, edited by J. C. Kaimal, H. W. Baynton, and J. E. Gaynor, *Rep. 2*, pp. 108–116, NOAA/ERL Wave Propag. Lab., Boulder, Colo., 1980.

Dyer, A. J., A review of flux-profile relationships, *Boundary Layer Meteorol., 7*, 363–372, 1974.

Elliott, W. P., The growth of the atmospheric internal boundary layer, *Eos. Trans. AGU, 39*, 1048–1054, 1958.

Fleagle, R. G., and J. A. Businger, *An Introduction to Atmospheric Physics*, p. 432, Academic, New York, 1980.

Gordon, A. L., Seasonality of Southern Ocean sea ice, *J. Geophys. Res., 86*, 4193–4197, 1981.

Gordon, A. L., and E. I. Sarukhanyan, American and Soviet expedition into the Southern Ocean sea ice in October and November 1981, *Eos Trans. AGU, 63*, 2, 1982.

Gordon, A. L., C. T. A. Chen, and W. G. Metcalf, Winter mixed layer entrainment of Weddell Deep Water, *J. Geophys. Res.*, this issue.

Haugen, D. A., J. C. Kaimal, and E. F. Bradley, An experimental study of Reynolds stress and heat flux in the atmospheric surface layer, *Q. J. R. Meteorol. Soc., 97*, 168–180, 1971.

Hibler, W. D., III, and S. F. Ackley, Numerical simulation of the Weddell Sea pack ice, *J. Geophys. Res., 88*, 2873–2887, 1983.

Irwin, J. S., and F. S. Binkowski, Estimation of the Monin-Obukhov scaling length using on-site instrumentation, *Atmos. Environ., 15*, 1091–1094, 1981.

Kondratyev, K. Ya., *Radiation in the Atmosphere*, p. 912, Academic, New York, 1969.

Kozo, T. L., and W. B. Tucker, Sea ice bottomside features in the Denmark Strait, *J. Geophys. Res., 79*, 4505–4511, 1974.

Large, W. G., and S. Pond, Open ocean momentum flux measurements in moderate to strong winds, *J. Phys. Oceanogr., 11*, 324–336, 1981.

Large, W. G., and S. Pond, Sensible and latent heat flux measurements over the ocean, *J. Phys. Oceanogr., 12*, 464–482, 1982.

LeMone, M. A., The structure and dynamics of horizontal roll vortices in the planetary boundary layer, *J. Atmos. Sci., 30*, 1077–1091, 1973.

Lenschow, D. H., Two examples of planetary boundary layer modification over the Great Lakes, *J. Atmos. Sci., 30*, 568–581, 1973.

Macklin, S. A., Wind drag coefficient over first-year sea ice in the Bering Sea, *J. Geophys. Res., 88*, 2845–2852, 1983.

Martin, S., P. Kauffman, and C. Parkinson, The movement and decay of ice edge bands in the winter Bering Sea, *J. Geophys. Res., 88*, 2803–2812, 1983.

McBean, G. A., The variations of the statistics of wind, temperature and humidity fluctuations with stability, *Boundary Layer Meteorol., 1*, 438–457, 1971.

McPhee, M. G., Turbulent heat and momentum transfer in the oceanic boundary layer under melting pack ice, *J. Geophys. Res., 88*, 2827–2835, 1983.

Miyake, M., Transformation of the atmospheric boundary layer over inhomogeneous surfaces, technical report, p. 63, Department of Atmos. Sci., Univ. of Wash., Seattle, 1965.

Muench, R. D., and R. L. Charnell, Observations of medium-scale features along the seasonal ice edge in the Bering Sea, *J. Phys. Oceanogr., 7*, 602–606, 1977.

Olson, M. L., Global accuracy of Omega-derived winds, *Atmos. Technol., 10*, 14–23, 1979.

Orvig, S., The problem of transformation of the air mass over polynyas, in *Problems of the Arctic and the Antarctic*, vol. 43–44, edited by A. F. Treshnikov, pp. 202–207, Office of Polar Programs, National Science Foundation, Washington, D. C., 1974.

Overland, J. E., R. M. Reynolds, and C. H. Pease, A model of the atmospheric boundary layer over the marginal ice zone, *J. Geophys. Res., 88*, 2836–2840, 1983.

Paltridge, G. W., and C. M. R. Platt, *Radiative Processes in Meteorology and Climatology*, p. 318, Elsevier Scientific, New York, 1976.

Panofsky, H. A., and E. L. Petersen, Wind profiles and change of terrain roughness at Risø, *Q. J. R. Meteorol. Soc., 98*, 845–854, 1972.

Panofsky, H. A., and A. A. Townsend, Change of terrain roughness and the wind profile, *Q. J. R. Meteorol. Soc.*, 90, 147–155, 1964.

Paulson, C. A., The mathematical representation of wind speed and temperature profiles in the unstable atmospheric surface layer, *J. Appl. Meteorol., 9*, 857–861, 1970.

Pease, C. H., S. A. Salo, and J. E. Overland, Drag measurements for first-year sea ice over a shallow sea, *J. Geophys. Res., 88*, 2853–2862, 1983.

Peterson, E. W., Modification of mean flow and turbulent energy by a change in surface roughness under conditions of neutral stability, *Q. J. R. Meteorol. Soc., 95*, 561–575, 1969.

Philip, J. R., The theory of local advection, I, *J. Meteorol., 16*, 535–547, 1959.

Pruppacher, H. R., and J. D. Klett, *Microphysics of Clouds and Precipitation*, p. 714, D. Reidel, Hingham, Mass., 1978.

Rouse, H., Critical analysis of open-channel resistance, *J. Hydraul. Div., Am. Soc. Civ. Eng., 91*, 1–25, 1965.

Salo, S. A., C. H. Pease, and R. W. Lindsay, Physical environment of the eastern Bering Sea, *NOAA Tech. Mem. ERL PMEL-21*, p. 119, Pacific Mar. Environ. Lab., Seattle, Wash., 1980.

Sasamori, T., The radiative cooling calculation for application to general circulation experiments, *J. Appl. Meteorol., 7*, 721–729, 1968.

Smith, S. D., E. G. Banke, and O. M. Johannessen, Wind stress and turbulence in the Gulf of St. Lawrence, *J. Geophys. Res., 75*, 2803–2812, 1970.

Streten, N. A., Cloud cell size and pattern evolution in Arctic air advection over the North Pacific, *Arch. Meteorol. Geophys. Bioklimatol., A24*, 213–228, 1975.

Suomi, V. E., D. O. Staley, and P. M. Kuhn, A direct measurement of infrared radiation divergence to 160 mb, *Q. J. R. Meteorol. Soc., 84*, 134–141, 1958.

Sutton, O. G., 1953, *Micrometeorology*, p. 333, McGraw-Hill, New York, 1953.

Taylor, P. A., The planetary boundary layer above a change in surface roughness, *J. Atmos. Sci., 26*, 432–440, 1969.

Taylor, P. A., A model of airflow above changes in surface heat flux, temperature and roughness for neutral and unstable conditions, *Boundary Layer Meteorol., 1*, 18–39, 1970.

Townsend, A. A., Self-preserving flow inside a turbulent boundary layer, *J. Fluid Mech., 22*, 773–797, 1965.

Vager, B. G., and Ye. D. Nadezhina, The structure of the atmospheric boundary layer under horizontally inhomogeneous conditions, *Izv., Atmos. Oceanic Phys., 11*, 349–353, 1975.

Vowinckel, E., and S. Orvig, Synoptic energy budgets from the Beaufort Sea, in Energy Fluxes over Polar Surfaces, edited by S. Orvig, *WMO Tech. Note 129*, pp. 143–166, World Meteorol. Organ., Geneva, 1973.

Vowinckel, E., and B. Taylor, Energy balance of the Arctic, IV, Evaporation and sensible heat flux over the Arctic Ocean, *Arch. Meteorol. Geophys. Bioklimatol., B14*, 36–52, 1965.

Wadhams, P., The ice cover in the Greenland and Norwegian Seas, *Rev. Geophys. Space Phys.*, *19*, 345–393, 1981.
Wadhams, P., A mechanism for the formation of ice edge bands, *J. Geophys. Res.*, *88*, 2813–2818, 1983.
Walter, B. A., Wintertime observations of roll clouds over the Bering Sea, *Mon. Weather Rev.*, *108*, 2024–2031, 1980.
Webb, E. K., Profile relationships: The log-linear range, and extension to strong stability, *Q. J. R. Meteorol. Soc.*, *96*, 67–90, 1970.
Zilitinkevich, S. S., On the determination of the height of the Ekman boundary layer, *Boundary Layer Meteorol.*, *3*, 141–145, 1972.
Zilitinkevich, S. S., Resistance laws and prediction equations for the depth of the planetary boundary layer, *J. Atmos. Sci.*, *32*, 741–752, 1975.

S. F. Ackley, E. L. Andreas, and W. B. Tucker III, U.S. Army Cold Regions Research and Engineering Laboratory, Snow and Ice Branch, Hanover, NH 03755.

(Received April 14, 1983;
revised October 19, 1983;
accepted October 25, 1983.)

Ocean Engng, Vol. 11, No 3, pp. 227–237, 1984.
Printed in Great Britain.

0029–8018/84 $3.00 + .00
Pergamon Press Ltd.

A SIMPLE BOOM ASSEMBLY FOR THE SHIPBOARD DEPLOYMENT OF AIR–SEA INTERACTION INSTRUMENTS

EDGAR L. ANDREAS, JOHN H. RAND and STEPHEN F. ACKLEY
U.S. Army Cold Regions Research and Engineering Laboratory, Hanover, NH 03755, U.S.A.

Abstract—We have developed a simple boom for use in measuring meteorological variables from a ship. The main structural member of the boom, a triangular communications tower with rollers attached along its bottom side, is deployed horizontally from a long, flat deck, such as a helicopter deck, and will support a 100-kg payload at its outboard end. The boom is easy to deploy, requires minimal ship modifications, and provides ready access to the instruments mounted on it. And because it is designed for use with the ship crosswind, oceanographic work can go on at the same time as the air–sea interaction measurements.

We describe our use of the boom on the *Mikhail Somov* during a cruise into the Antarctic sea ice and present some representative measurements made with instruments mounted on it. Theory, experiment, and our data all imply that instruments deployed windward from a rear helicopter deck can reach air undisturbed by the ship. Such an instrument site has clear advantages over the more customary mast, bow, or buoy locations.

INTRODUCTION

BECAUSE a ship disturbs both the vector and scalar fields around it, measuring meteorological variables at sea is not a trivial problem. Seguin and Garstang (1971), Ching (1976), and Kahma and Leppäranta (1981), for example, all showed that the standard ship's anemometers they investigated—all mounted on forward masts—were typically in error by 10% when the ship was headed into the wind. For other ship orientations, the error was as high as 35% (Kahma and Leppäranta, 1981). Temperature and humidity measured on a forward mast were similarly subject to large errors (Seguin and Garstang, 1971). The uncertainties inherent in data from these mast-mounted instruments mean that bulk-aerodynamic estimates of the surface fluxes of momentum and of sensible and latent heat may be in error by 100% (Seguin and Garstang, 1971); in near-neutral conditions, it is therefore doubtful that even the correct signs of the scalar fluxes could be obtained from such sensors.

Placing the instruments on a bowsprit and heading the ship into the wind is one way of making more accurate measurements (Seguin and Garstang, 1971; Ching, 1976; Goerss and Duchon 1980; Kahma and Leppäranta, 1981). Mollo-Christensen (1979) suggested, on the basis of wind tunnel studies, that if the instruments are upwind a distance equal to the smaller of the ship beam or the forward freeboard, they will be disturbed little by the ship. Kahma and Leppäranta (1981) demonstrated that even if the ship is 30–40° from head-on into the mean wind, an anemometer mounted on a 10-m bowsprit will yield accurate values of wind speed.

Davidson *et al.* (1978) used yet a third location for measuring meteorological variables on a ship. They placed a portable, vertical mast forward on the main deck with sensors mounted well above the superstructure of the ship or instrumented a short, vertical mast right on the bow (see also Large and Pond, 1982). Although they evidently did not compare measurements at these locations with those at an obviously undisturbed location, i.e. on a buoy, because the turbulence parameters computed from their data agree well with theoretical expressions, their instruments seem to have suffered negligibly from flow distortion.

The general consensus, nevertheless, is that to assure undisturbed conditions, air–sea interaction instrumentation should be mounted on a buoy. If the buoy is well designed (Dorman and Pond, 1975), it should have little influence on the ambient conditions; and the effects of its motion on the measured velocity field will be small or can be corrected for (Pond, 1968; Dorman and Pond, 1975). Of course, buoy-mounted sensors are not

very accessible: cleaning and calibration checks are no longer routine as they are with the shipboard instruments. The buoy must also have a self-contained data recording system that then must be serviced, or it must remain somehow in communication with its tending ship—requirements that clearly limit ship operations. Therefore, although meteorological measurements on buoys may be the most representative, deploying, monitoring, and servicing the buoy create many problems that keeping the instruments on board ship obviates.

We will therefore describe here a simple shipboard instrument boom that we developed for a joint air–sea interaction and oceanographic cruise into the sea ice of the Weddell Sea in late 1981 (Gordon and Sarukhanyan, 1982). We deployed the boom from the rear, starboard corner of the helicopter deck of the Soviet icebreaker *Mikhail Somov* with the ship oriented crosswind. This use of the helicopter deck allowed much freer access to our instruments than with bow or mast locations, and the data that we obtained suggest that the instruments mounted on the boom were outside the boundary layer around the ship. Because the boom was intended for use with the ship crosswind, hydrographic or CTD work using winches on the starboard side of the ship could go on simultaneously with our measurement program. Such a method for carrying on diverse sampling programs simultaneously was of obvious benefit in minimizing station time.

DESCRIPTION OF THE BOOM

Our scientific objectives necessitated a boom that would let us turn the instruments mounted on it to follow the mean wind, would allow ready access to these instruments for calibration and cleaning, yet could extend far enough from the ship to reach undisturbed air. Practical considerations required that the boom break down for shipping, was easy to assemble, and could be put in place or retracted quickly.

The triangular communications towers (29 cm on a side) that are frequently used for mounting a vertical array of meteorological instruments have excellent strength even when used horizontally. We bolted five 3.05-m tower sections together, fastened cylindrical rollers at 3-m intervals on one side, fixed a counterweight at one end, and thus had a 15-m boom that we could easily roll on and off the helicopter deck of the *Somov* (Fig. 1).

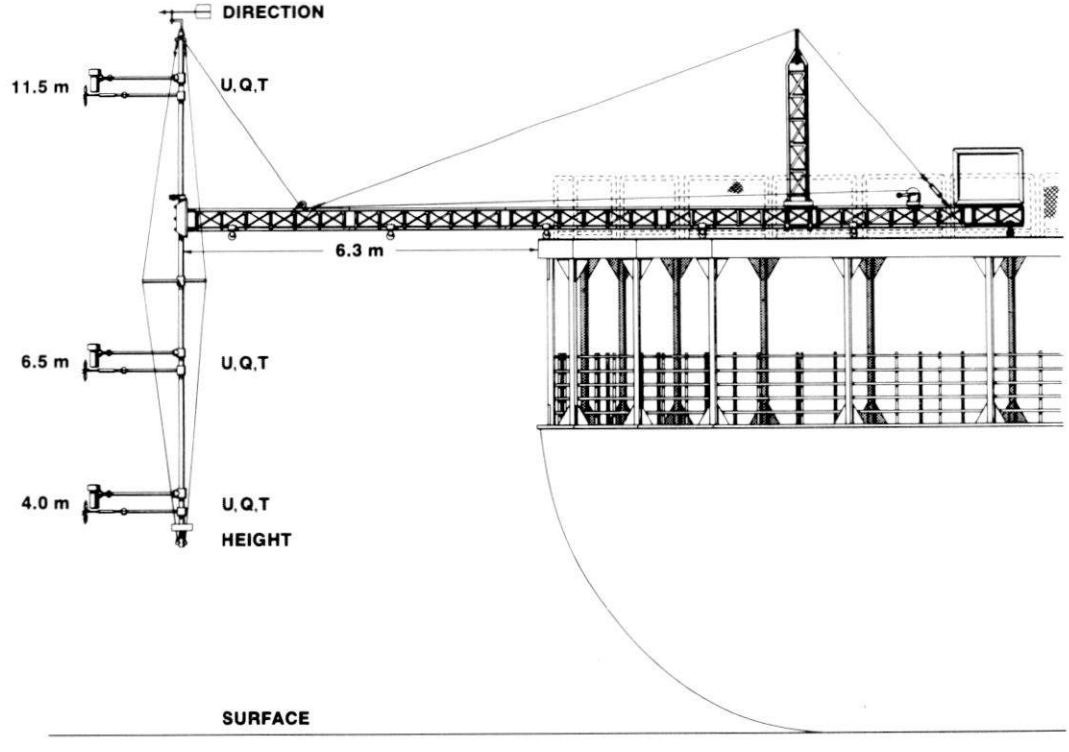

FIG. 1. The air–sea interaction boom as it was instrumented for our research on the *Mikhail Somov*. *U*, *T* and *Q* indicate locations of wind speed, temperature, and humidity measurements.

At the outboard end of the boom we fixed an 8.6-m-long, vertical mast to which we attached our sensors. This mast was mounted to the boom by a pivot assembly that allowed the mast two degrees of freedom: the mast could rotate about its axis, and it could tilt back into a horizontal position so the entire boom assembly could be pulled back on deck. The mast was made of two sections of 6-cm-diameter pipe of equal length. The lower section was aluminium, the upper steel, because we found that aluminium pipe was not strong enough to withstand the torque involved in raising and lowering the mast. A stud on the bottom mast section slid into the steel top section, and six set screws then held the two sections together. Three 0.5-cm steel guy wires, attached to the top and bottom of the mast and passing over the 50-cm arms of a midpoint spreader bar, gave this long, thin mast good stability.

We turned our mast instruments into the wind by pulling on one of two ropes that ran from the helicopter deck to the ends of a 70-cm torque arm (not shown in Fig. 1) that was fixed to the mast above the pivot assembly. Normally, such an arrangement would allow 180° of rotation, but because of the three mast guys, we had only 120°.

To provide for raising and lowering the mast, we ran a 0.5-cm steel cable from the upper end of the mast, through a pulley attached to the boom 2 m from the mast, to a small hand winch in front of the counterweight (Fig. 1). Our deployment routine was to mount our instruments on the mast with the mast horizontal and the entire boom assembly pulled back onto the helicopter deck. With the instruments in place, we then rolled the boom off the deck until we could lower the mast into its vertical position clear of any obstructions. With the mast vertical, we continued rolling the assembly out until the instruments were where we wanted them. Once the instruments were mounted on the mast, deploying and securing the boom took only about five minutes.

To give the boom better vertical stability, we ran a 0.5-cm steel guy wire from near the mast end of the boom to the counterweight end over a 2.9-m section of tower fixed to the boom 5 m from the counterweight end (Fig. 1). With the turnbuckle in this guy, we could raise the outboard end of the boom so that even when the mast was fully instrumented and 10 m off the ship, the horizontal boom was virtually straight. Two guys (not shown in Fig. 1) attached to the boom near its mast end and running to hand winches mounted on the helicopter deck on either side of the boom provided horizontal stability.

The counterweight was a plywood box that held ten 5-gallon gas cans, which we filled with water; the total mass of the counterweight was thus roughly 200 kg. Since the mass of the pivot assembly was about 20 kg, the boom was, therefore, capable of supporting an 80-kg instrument mast that extended 10 m from the edge of the helicopter deck.

Mollo-Christensen (1979) suggested that for a ship oriented crosswind, meteorological instruments must be a distance upwind greater than the freeboard of the ship to be clear of its disturbing effects. The main deck and the helicopter deck of the *Somov* are, respectively, 6 and 9 m above the surface. Because the rear of the *Somov* is relatively open under the helicopter deck, the appropriate free-board dimension is 6 m. Consequently, instruments outboard 10 m should have been well clear of ship effects if the wind was anywhere in the rear, starboard quadrant.

Before the cruise we assembled the boom on the roof of our laboratory and, with the mast loaded with everything but instrument cables (estimated total mass 66 kg), tested whether the assembly met our design criteria. It did. That is, when we rolled the assembly out until the mast was 10 m from the edge, everything remained impressively rigid and stable.

On the *Somov*, however, we could roll the mast out only 6.3 m (Fig. 1) because our instrument cables were a bit too short. Since all of our mast instruments were mounted on pipes that placed them an additional 1 m from the mast, they still were well beyond the 6-m limit for undisturbed flow set by the rear freeboard.

Figure 1 shows the boom as we instrumented it for our work on the *Somov*. We had sensors for measuring wind speed (U), temperature (T) and humdity (Q) at each of three levels, nominally 4.0, 6.5 and 11.5 m above the surface. Our wind speed sensors were propeller anemometers manufactured by the R.M. Young Company. The temperature

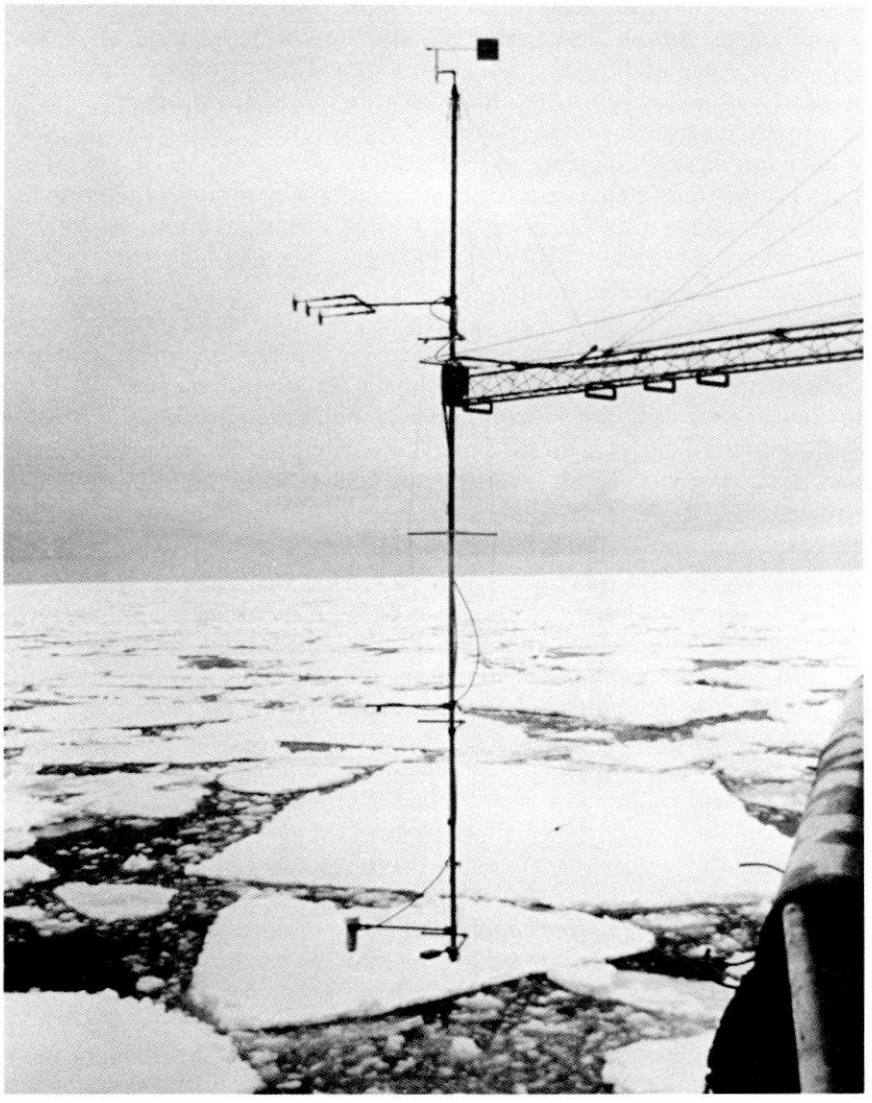

FIG. 2. The boom deployed from the *Somov* with our instruments in a configuration for checking the calibration of the anemometers: that is, all three anemometers at the same level.

and humidity sensors at each level were contained in the same aspirated radiation shield. These units were made by General Eastern; the temperature sensor was a platinum-resistance thermometer, and the humidity sensor was a cooled-mirror dew-point hygrometer. There was a wind vane at the top of the mast for use in aligning the sensors with the mean wind. At the bottom of the mast we mounted an acoustic ranging device (used in some Polaroid cameras), which gave us the actual height of the sensors above the surface and wave information.

We used tee adapters to mount the instruments to the mast. These slipped onto the mast and were held in place with set screws. At the base of each tee we welded a coupling that mated with a threaded, 2.6-cm galvanized pipe. Consequently, for mounting our sensors we had at our disposal the entire spectrum of galvanized pipe fittings found in any plumbing shop. The mast was thus very versatile (Fig. 2). With the sliding tees we could

place our sensors virtually anywhere along it. The entire mast could also be moved up or down with respect to the horizontal boom, the only constraints being that it had to be bottom-heavy, and that we could generate enough torque above the pivot assembly to crank the mast back to its horizontal position.

RESULTS AND DISCUSSION

Because of ship and buoy motions and the consequent difficulty in precisely aligning sensors, direct measurement of the Reynolds fluxes of momentum and heat over the ocean are very uncertain (e.g., Pond, 1968; Rayment and Readings, 1971). These fluxes can be obtained, however, from measurements of the vertical profiles of wind speed, temperature and humidity through Monin–Obukhov similarity (Businger *et al.*, 1971). Paulson (1967; see also Badgley *et al.*, 1972) demonstrated this technique with velocity, temperature, and humidity profiles obtained from a tethered buoy. And Bogorodskiy (1966) found good agreement between surface stress values computed from velocity profiles measured from a ship and on a nearby buoy.

During our Antarctic cruise on the *Somov* we made 21 sets of profile measurements between 25 October and 11 November 1981 using basically the boom configuration shown in Fig. 1 (Andreas, 1982). Figures 3 and 4 show two representative profile sets. The lines in these figures are the fits to the data obtained from Monin–Obukhov similarity theory: we describe the similarity functions and our procedure in the Appendix.

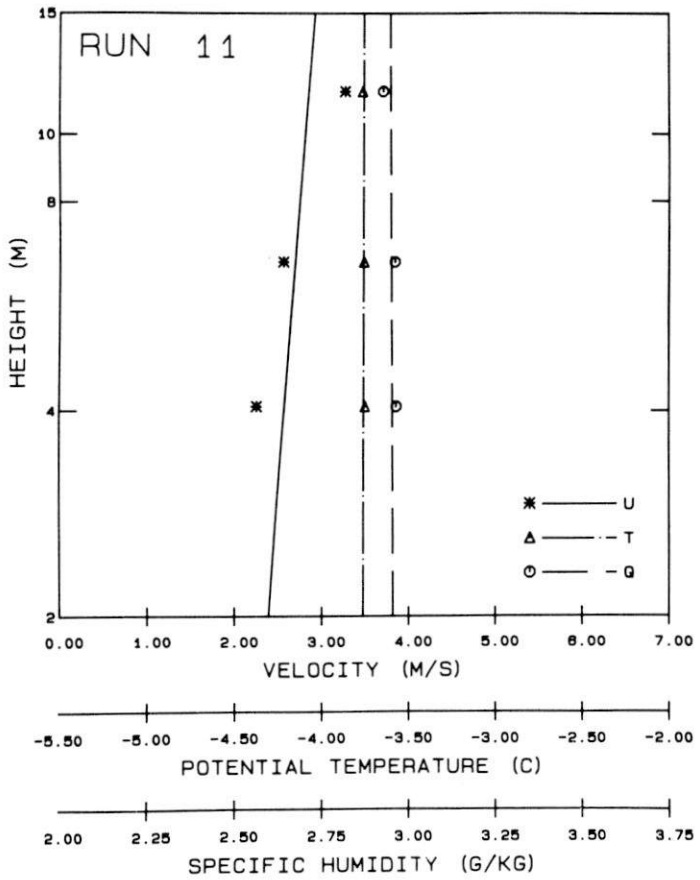

FIG. 3. The velocity, temperature and humidity profiles measured from the *Somov* at 2209 GMT (also local time) on 31 October 1981. The location was 62°5′S, 2°52′E, and the ship was at the downwind side of a 500-m-wide polynya.

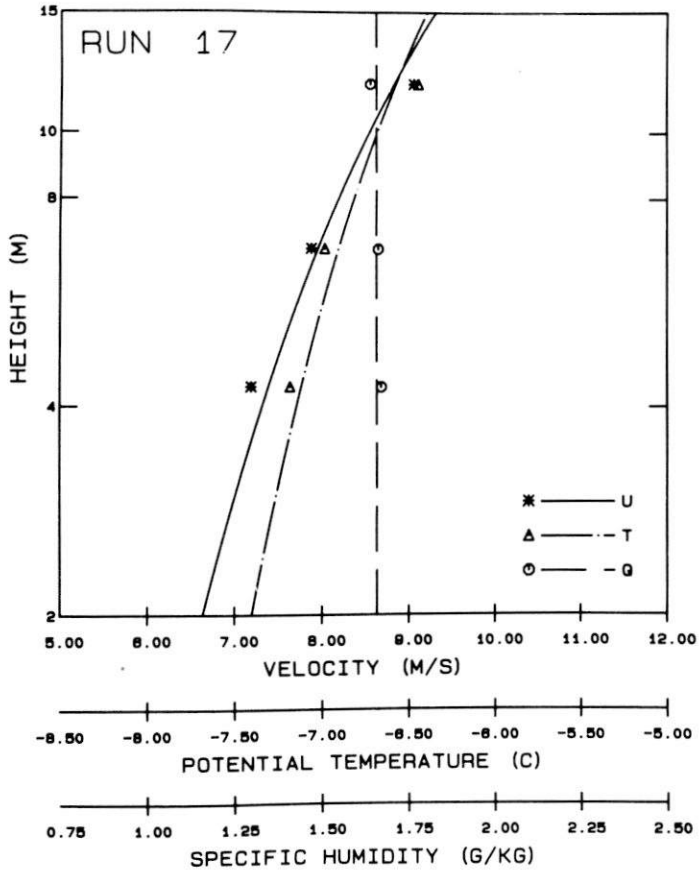

FIG. 4. The profiles measured from the *Somov* at 2139 GMT (also local time) on 6 November 1981. The location was 61°57′S, 1°13′E, and the ship was surrounded by small ice floes with freezing going on between them.

Table 1 contains the results of our Monin-Obukhov similarity analysis of the profiles in Figs 3 and 4. The friction velocity, u_*, and the sensible (H_S) and latent (H_L) heat flux values appear reasonable. During Run 11 (Fig. 3) we were at the downwind edge of a 500-m-wide polynya. The surface layer was virtually isothermal, so both the sensible and latent heat fluxes were very near zero. For Run 17 (Fig. 4) the surface was covered with small ice floes with ice forming between them. Our computations show a moderate flux of sensible heat from the relatively warm air to the colder ice. The air was dry enough, however, for the latent heat flux to be upward, away from the surface—its preferred direction over Antarctic sea ice (Andreas and Ackley, 1982).

TABLE 1. SURFACE FLUX VALUES COMPUTED FROM THE PROFILES SHOWN IN FIGS 3 AND 4. A POSITIVE FLUX IS UPWARD; A NEGATIVE ONE, DOWNWARD

Run	Surface conditions	u_* (ms^{-1})	H_S (Wm^{-2})	H_L (Wm^{-2})
11	polynya	0.10	−0.18	−0.17
17	small floes with ice forming	0.28	−39.2	0.48

Figure 3, especially, suggests that our instrument mast—extending out from the rear, starboard corner of the helicopter deck—was beyond the region affected by the ship. The potential temperature profile in this figure is vertical: the values at the three levels are within 0.01°C of each other. It is doubtful that, with the winds so light, we would ever have seen such a homogeneous surface layer if the ship were affecting the flow out at our instruments (cf. Stevenson, 1964). With the higher winds that we usually encountered, we thus feel confident that our instruments were sampling undisturbed air.

We made all of our measurements well within the Antarctic sea ice, where the wave environment was never very energetic, and, thus, have not tried deploying our boom on a severely rolling ship. On one occasion, however, long period swell was penetrating the ice so that the ship was rolling with a period of 13–14 sec. Although the instrument mast was consequently experiencing oscillations with a peak-to-peak amplitude of 1.5 m, the boom showed no signs of strain.

The highest winds in which we deployed the boom were roughly 20 m sec^{-1}. Again it showed no evidence of strain or instability, and, as usual, it took only two people to deploy it and three to retrieve it.

CONCLUSIONS

We have described a simple, relatively inexpensive, easy-to-handle boom that we have used to measure profiles and, thereby, the air–sea fluxes of momentum and heat from a ship within the Antarctic sea ice. As important as the design of the boom, however, is the idea of deploying it from a rear helicopter deck. A helicopter deck provides many advantages that the typical mast or bow locations do not. Mast-mounted instruments are often too far above the surface to be within the atmospheric surface layer—the constant flux layer, where Monin–Obukhov similarity applies. They also suffer frequently from flow distortion around the ship, regardless of its heading, and are relatively inaccessible. The bow is also usually higher than the helicopter deck, has a high, solid rail around it that makes it difficult to work from, and is often cluttered with windlasses, running lights, hawsers, and such. A helicopter deck, on the other hand, is large, flat, and wide open. And we have shown that with the ship oriented crosswind, instruments extended 6–10 m out into the wind at roughly a 45° angle to the ship's axis are as well exposed as bow-mounted instruments.

The boom could also be used for air–sea interaction measurements on other platforms. Air–sea flux measurements are sometimes made from oil or gas platforms or other permanent structures (Hicks and Dyer, 1970; Smith and Katsaros, 1981) that typically have helicopter decks or other large areas of open deck space. A boom like the one that we have described would be ideal for use on such structures.

Acknowledgements—We would like to thank Petr Bogorodskiy and Aleksandr Makshtas of the Arctic and Antarctic Research Institute, Leningrad, who were always willing to help us deploy the boom. W.B. Tucker III and D.E. Garfield reviewed the manuscript. This research was supported by the National Science Foundation through contract DPP-80-06922 and by the Department of the Army through Project 4A161102AT2403.

REFERENCES

Andreas, E.L. 1982. Atmospheric boundary layer measurements in the Weddell Sea. *Antarctic J. U.S.* **17**, 113–115.

Andreas, E.L. and Ackley, S.F. 1982. On the differences in ablation seasons of Arctic and Antarctic sea ice. *J. Atmos. Set.* **39**, 440–447.

Andreas, E.L., Paulson, C. A., Williams, R.M., Lindsay, R.W. and Businger, J.A. 1979. The turbulent heat flux from Arctic leads. *Boundary-Layer Meteorology* **17**, 59–91.

Badgley, F.I., Paulson, C.A. and Miyake, M. 1972. *Profiles of Wind, Temperature, and Humidity over the Arabian Sea*, 62 pp. University of Hawaii Press.

Bogorodskiy, M.M. 1966. A comparison of gradient observations of wind velocity by means of the Froude spear-buoy and a shipboard gradient installation. *Oceanology* **6**, 283–288.

Businger, J.A., Wyngaard, J.C., Izumi, Y. and Bradley, E.F. 1971. Flux-profile relationships in the atmospheric surface layer. *J. Atmos. Set.* **28**, 181–189.

Ching, J.K.S. 1976. Ship's influence on wind measurements determined from BOMEX mast and boom data. *J. app. Meteorology* **15**, 102–106.

Davidson, K.L., Houlihan, T.M., Fairall, C.W. and Schacher, G.E. 1978. Observation of the temperature structure function parameter, C_T^2, over the ocean. *Boundary-Layer Meteorology* **15**, 507–523.

DORMAN, C.E. and POND, S. 1975. A small buoy for meteorological measurements at sea. *Deep Sea Res.* **22**, 177–184.
GOERSS, J.S. and DUCHON, C.E. 1980. Effect of ship heating on dry-bulb temperature measurements in GATE. *J. Phys. Oceanogr.* **10**, 478–479.
GORDON, A.L. and SARUKHANYAN, E.I. 1982. American and Soviet expedition into the Southern Ocean sea ice in October and November 1981. *Trans. Am. geophys. Un.* **63**, 2.
HICKS, B.B. and DYER, A.J. 1970. Measurements of eddy-fluxes over the sea from an off-shore oil rig. *Q. Jl R. Met. Soc.* **96**, 523–528.
KAHMA, K.K. and LEPPÄRANTA, M. 1981. On errors in wind speed observations on R/V *Aranda*. *Geophysica* **17**, 155–165.
LARGE, W.G. and POND, S. 1982. Sensible and latent heat flux measurements over the ocean. *J. phys. Oceanogr.* **12**, 464–482.
MOLLO-CHRISTENSEN, E. 1979. Upwind distortion due to probe support in boundary-layer observation. *J. appl. Meteorology* **18**, 367–370.
PAULSON, C.A. 1967. Profiles of wind speed, temperature and humidity over the sea, 128 pp. Scientific Report (NTIS: PB-176 287), Department of Atmospheric Sciences, University of Washington, Seattle.
POND, S. 1968. Some effects of buoy motion on measurements of wind speed and stress. *J. geophys. Res.* **73**, 507–512.
RAYMENT, R. and READINGS, C.J. 1971. The importance of instrumental tilt on measurements of atmospheric turbulence. *Q. Jl R. Met. Soc.* **97**, 124–130.
SEGUIN, W.R. and GARSTANG, M. 1971. A comparison of meteorological sensors on the USCGSS *Discoverer* during the 1968 Barbados Experiment. *Bull. Am. met Soc.* **52**, 1071–1076.
SMITH, S.D. and KATSAROS, K.B. 1981. HEXOS—Humidity exchange over the sea, 133 pp. Report Series BI-R-81-17, Bedford Institute of Oceanography, Dartmouth, Nova Scotia.
STEVENSON, R.E. 1964. The influence of a ship on the surrounding air and water temperatures. *J. appl. Meteorology* **3**, 115–118.

APPENDIX

Andreas *et al.* (1979) described our technique for obtaining fluxes from measured wind speed (U), temperature (T) and specific humidity (Q) profiles using Monin–Obukhov similarity theory. Briefly, we iteratively fitted the profile data with the models

$$U(z) = (u_*/k)[\ln(z/z_0) - \psi_m(z/L)] \ , \tag{A1}$$

$$T(z) = T(z_s) + t_*[\ln(z/z_s) - \psi_h(z/L)] \ , \tag{A2}$$

$$Q(z) = Q(z_s) + q_* [\ln(z/z_s) - \psi_h(z/L_Q)] \ , \tag{A3}$$

where z is the height; z_0, the roughness length for velocity; z_s, the scalar roughness length; and k, von Kármán's constant (0.4). The ψ's are the semi-empirical Monin–Obukhov similarity functions, which are functions of the nondimensional stability parameters z/L and z/L_Q.

For unstable conditions, $\zeta < 0$,

$$\psi_m(\zeta) = 2 \ln [(1 + x)/2] + \ln[(1 + x^2)/2] - 2 \arctan (x) + \pi/2 \ , \tag{A4}$$

$$\psi_h(\zeta) = 2 \ln[(1 + x^2)/2] \ , \tag{A5}$$

where

$$x = (1 + \beta_u\zeta)^{1/4} \ . \tag{A6}$$

For stable conditions, $\zeta > 0$,

$$\psi_m(\zeta) = \psi_h(\zeta) = - \beta_s\zeta \ . \tag{A7}$$

The constants that we used in Equations (A6) and (A7) were $\beta_u = 16$ and $\beta_s = 7$ (Large and Pond, 1982).

The u_*, t_*, and q_* in Equations (A1) to (A3) are related to the momentum (τ) and sensible (H_s) and latent (H_L) heat fluxes and thereby link these fluxes to the measured profiles:

$$u_* = (\tau/\rho)^{1/2} \ , \tag{A8}$$

$$t_* = -H_s/\rho \ c_p \ u_* \ k \ , \tag{A9}$$

$$q_* = -H_L/\rho \ L_v \ u_* \ k \ . \tag{A10}$$

Here ρ is the air density, c_p is the specific heat of air at constant pressure, and L_v is the latent heat of vaporization (sublimation) of water (ice).

Finally, L and L_Q are stability parameters with the dimension of length—Obukhov lengths—

$$L_Q = \frac{1}{g}\left[\frac{1 + 0.61\,\bar{Q}}{0.61}\right]\frac{u_*^2}{k^2 q_*} \quad , \tag{A11}$$

$$L = \left\{\left[\frac{\bar{T}}{g}\,\frac{u_*^2}{k^2 t_*}\right]^{-1} + L_Q^{-1}\right\}^{-1} \quad , \tag{A12}$$

where g is the acceleration of gravity, $\bar{Q}$ is a representative humidity, and $\bar{T}$ is a representative temperature.

Heat and Moisture Advection over Antarctic Sea Ice

EDGAR L. ANDREAS

U.S. Army Cold Regions Research and Engineering Laboratory, Hanover, NH 03755

(Manuscript received 21 April 1984, in final form 18 December 1984)

ABSTRACT

Surface-level meteorological observations and upper-air soundings in the Weddell Sea provide the first *in situ* look at conditions over the deep Antarctic ice pack in the spring. The surface-level temperature and humidity were relatively high, and both were positively correlated with the northerly component of the 850 mb wind vector as far as 600 km from the ice edge. Since even at its maximum extent, at least 60% of the Antarctic ice pack is within 600 km of the open ocean, long-range atmospheric transport of heat and moisture from the ocean must play a key part in Antarctic sea ice heat and mass budgets. From one case study, the magnitude of the ocean's role is inferred: at this time of year the total turbulent surface heat loss can be 100 W m^{-2} greater under southerly winds than under northerly ones.

1. Introduction

Because Antarctic sea ice has an annual cycle that ranges between a coverage of about 20×10^6 km^2 at maximum extent and only 3×10^6 km^2 at minimum extent, the surface energy fluxes in the Southern Ocean undergo similar large changes (e.g., Gordon, 1981). Presumably then, Antarctic sea ice plays an important role in the climate of the Southern Hemisphere; therefore, many have tried to relate sea ice conditions to climatic variables or to the atmospheric circulation around Antarctica. These studies fall into three general categories: analyses seeking correlations between sea ice and atmospheric variables without regard to cause and effect; analyses presupposing that the ice affects atmospheric circulation; and, conversely, analyses assuming that the atmosphere forces the sea ice. The fourth possibility, a feedback-coupled ice-atmosphere system, has received little attention.

Fletcher (1969) initiated the correlation-type studies. Using the scant data available before the satellite era, he found a positive correlation between ice coverage in Scotia Bay and the intensity of the zonal wind at New Zealand. Streten and Pike (1980) continued this line of research on a five-year record (1972–77) of satellite-derived ice extent. They, too, found a correlation between the mean zonally averaged westerlies and the latitude of the zonally averaged ice edge, and increasing variability in the westerlies correlated with increasing variability in the average ice extent.

Schwerdtfeger and Kachelhoffer (1973), Ackley and Keliher (1976), and Ackley (1981) took the perspective that changes in the sea ice cover were generally forcing the atmosphere. Schwerdtfeger and Kachelhoffer (1973) supported this view by showing significant correlation between ice extent and the frequency of occurrence of cyclonic vortices: the latitude band of maximum cyclone frequency seemingly moved south with the retreating ice, and frequency maxima occurred in the Weddell and Ross Seas, which Streten and Pike (1980) identified as the regions of greatest variability in ice extent. Ackley (1981) reiterated the theme that variability in the ice extent corresponded broadly with regions of high variability in the zonal wind. In each of these studies, cyclogenesis driven by the release of baroclinic instability near the ice margin—where the meridional temperature gradient was supposed to be strongest—was the postulated mechanism for observed correlations between cyclones and ice extent.

Taking the opposite viewpoint, Gordon and Taylor (1975) proposed that atmospheric forcing through Ekman divergence (e.g., Neumann and Pierson, 1966) could explain the relationship between cyclones and ice extent. A curl in the wind stress—a cyclonic vortex—causes a general divergence in the oceanic mixed layer: the ice spreads open, new ice forms, and the ice field consequently expands. Ackley and Keliher (1976), however, described a sea ice model that predicts that ice of "normal" concentration will converge rather than diverge under a cyclonic vortex.

Although recognizing that Antarctic sea ice both responds to and forces the atmosphere, Cavalieri and Parkinson (1981) and Parkinson and Cavalieri (1982) presented some persuasive evidence for another atmospheric explanation of cyclone-ice correlations. Figure 7 in Cavalieri and Parkinson (1981), also Fig. 2–9 in Zwally *et al.* (1983), shows the Weddell Sea ice edge advancing under the southerly wind west of a persistent low-pressure center; in their Fig. 11, the ice edge retreats under a northerly wind east of another persistent low. Though suggesting alternatives,

their analysis left the actual physics of advance or retreat unclear. Does a northerly wind carry enough oceanic heat to melt ice, while a cold, southerly wind forms it, or does a northerly wind compact it, while a southerly wind distends it? That is, is the forcing predominantly thermodynamic or dynamic? Hibler and Ackley (1983) showed that the dominant forcing depends on the season. On the basis of a numerical sea ice model with rudimentary ice-atmosphere feedback they found that, except in the western Weddell Sea, the ice advance is primarily thermodynamic, while the retreat depends on ice advection and the presence of leads and so is largely dynamic.

This study provides some additional information on the thermodynamic control of ice extent using data collected in the eastern Weddell Sea in October and November 1981 during a cruise on the Soviet icebreaker *Mikhail Somov* (Gordon, 1982). Records of surface-layer temperature and humidity and of upper-air winds show that in the spring a northerly wind can carry oceanic heat and moisture long distances over the sea ice; similarly, a southerly wind off the Antarctic continent remains cold and relatively dry as it traverses the ice. The direction of the geostrophic wind, therefore, has an important thermodynamic role—as well as a likely dynamic one—in the heat and mass budgets of Antarctic sea ice.

2. Observations

The *Somov* crossed the Antarctic ice edge at 56°15′S about midday on 20 October 1981. We worked in the ice until 14 November, penetrating into the "deep pack" (Ackley *et al.*, 1982) as far as 62°28′S—over 600 km from the ice edge (Fig. 1).

During this time we measured upper-air wind profiles at 0000 and 1200 GMT (also local time) using a Väisälä MicroCORA radiosonde system with RS21-12CN sondes (Andreas and Richter, 1982). Andreas (1983) tabulated all of these upper-air data. The MicroCORA system uses the Omega navaid signals to track the sonde; our wind speed measurements were accurate to better than 1 m s^{-1} in this region of the Antarctic (Olson, 1979). The measured wind vector at 850 mb is used to represent the geostrophic flow; this level, generally 1000–1200 m, was always at or above the top of the atmospheric boundary layer (ABL).

These *in situ* measurements of the geostrophic flow are more reliable than winds estimated from the analysis fields for this data-poor area; Fig. 2 confirms this. The direction and speed of the measured 850 mb wind are compared in the figure with the geostrophic wind at the *Somov* estimated graphically from surface pressure charts. These charts were the 12-hourly Australian analysis fields provided by the National Climate Center, Asheville, North Carolina. Although the measured and estimated wind directions agree well, the estimated wind speed tends to overestimate the actual wind speed by about 50%. Hibler and Ackley (1983) also documented discrepancies between *in situ* measurements from the Weddell Sea and analysis field values; they inferred that these resulted because the Australian analysis ignores the presence of the sea ice (S. F. Ackley, personal communication, 1984).

The *Somov* cruise produced a high quality set of atmospheric surface-level temperature and humidity data. These humidity data, in particular, are the first accurate values ever measured over the deep Antarctic pack. Three identical General Eastern 1200MPS temperature and dew point monitoring systems were used for the measurements, each having its own aspirated radiation shield that houses both temperature and dew point sensors. The temperature sensor in each aspirator is a platinum resistance thermometer (PRT); the humidity sensor is a cooled-mirror dew point hygrometer, with a second PRT sensing the mirror temperature (the dew point). Both sensors have calibrations traceable to NBS standards. The calibration of each sensor was checked virtually every day; therefore, the accuracy of individual temperature and dew-point measurements was ±0.2°C at the temperatures that we encountered.

One temperature/humidity unit was mounted on a short boom on the bow of the *Somov;* the other two were set up side-by-side in a well exposed location on the (rear) helicopter deck; each was 11 m above the surface. Generally, all three instruments were in operation; the recorded observations were then the averages of the three temperature or dew point values. If one of the sensors was yielding spurious values, however, we could ignore it and still have two values for averaging. There was no evidence of systematic differences in either variable between the bow and helicopter deck locations.

Buck's (1981) method was used to convert dew point and temperature values to vapor pressures and standard methods were then applied to find specific and relative humidity. To make the temperature and humidity data compatible with the 12-hourly radiosonde data, 12-hourly averages at 0000 and 1200 GMT were computed by applying a triangular weighting function of 12-h base width to each data series.

3. Results

Figure 3 shows time series of ship distance south of the ice edge, the relative humidity (RH), the specific humidity (Q), the air temperature (T), and the northerly component of the measured 850 mb wind vector (V_N). The relative humidity was high—rarely did it fall below 75%. Andreas and Ackley (1982) had previously assumed—in the absence of

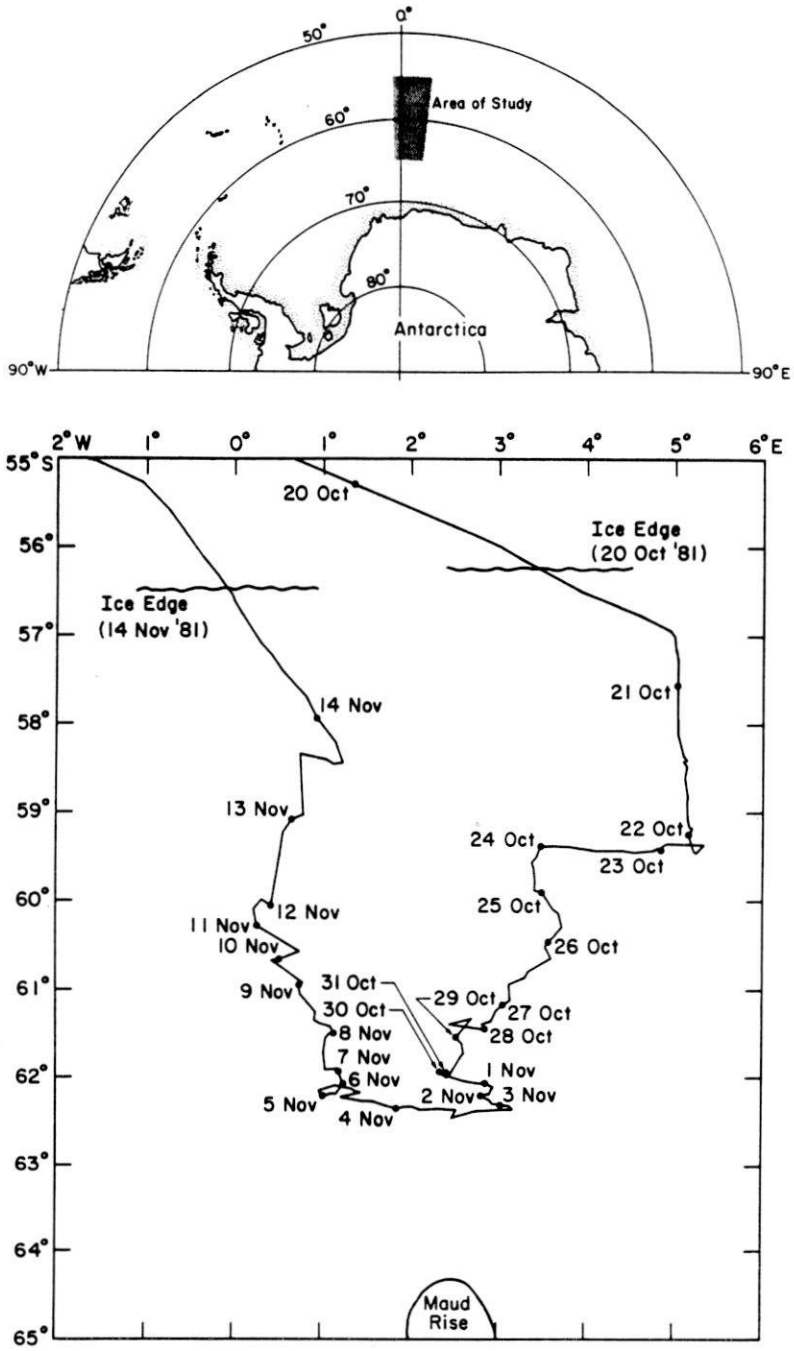

FIG. 1. Cruise track of the *Somov*. Dots mark the beginning of the indicated day.

reliable data—that the relative humidity in the Antarctic spring was approximately 60%. The air temperatures, though high by Arctic standards, seem compatible with the contour plots for this time of year as presented by Zwally *et al.* (1983). Their large contouring interval and monthly averaging, however, preclude a more meaningful comparison. No other *in situ* data are available for comparison.

Visual inspection of the time series suggests a source for the heat and moisture. Temperature and humidity are well correlated and each seems correlated with V_N; that is, a northerly wind—off the ocean—is relatively warm and moist; a southerly wind is cooler and drier. There is no suggestion, however, that the variables are correlated with distance from the ice edge. Wexler (1959) also observed the strong poleward

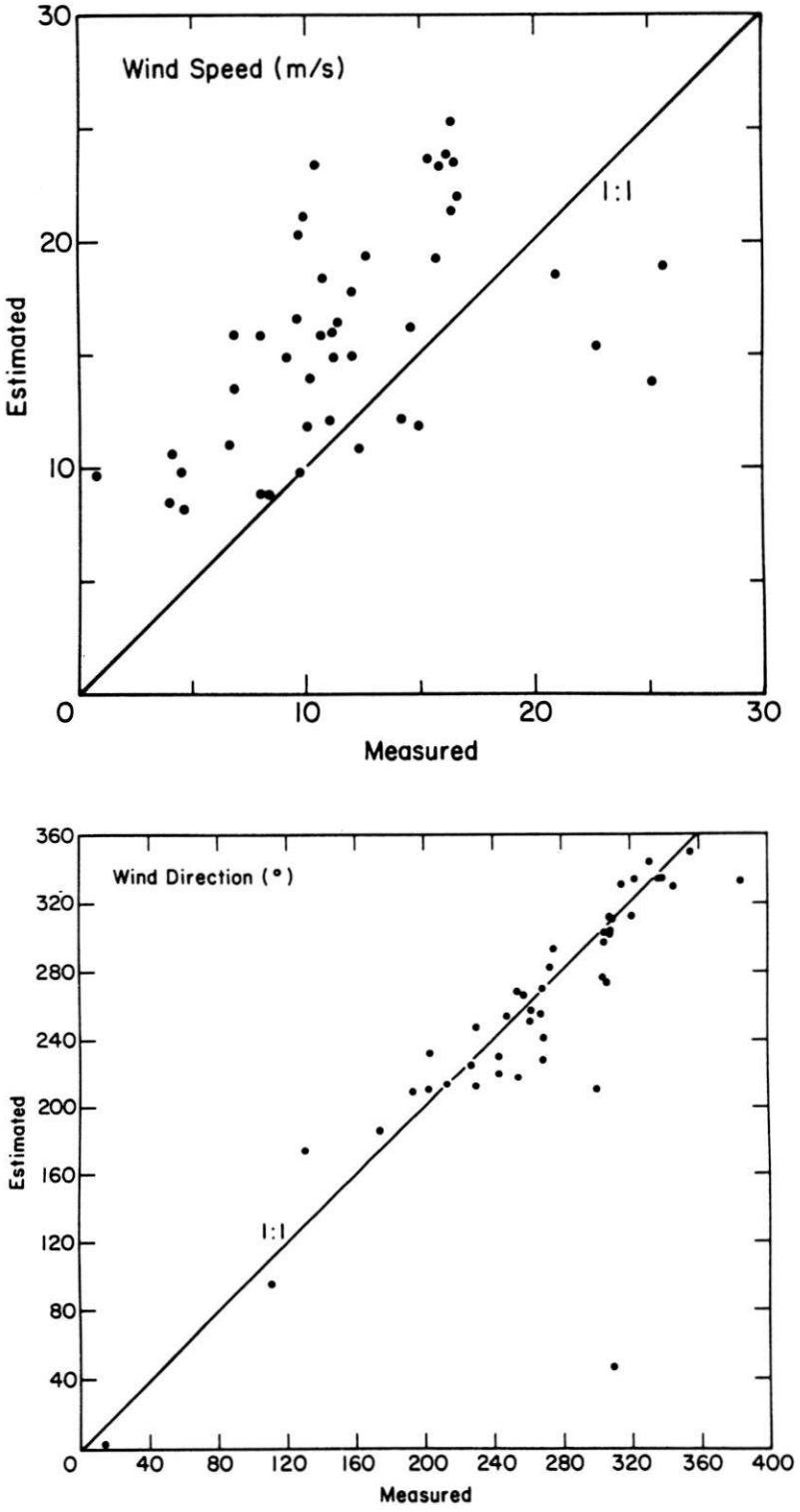

FIG. 2. Comparisons of the speed and direction of the measured 850 mb wind with estimates of the geostrophic wind obtained from surface pressure analysis fields.

advection of oceanic heat, even at the South Pole; but he found the heat there being carried higher in the troposphere rather than in the atmospheric boundary layer, as suggested here.

The cross-correlation functions of T, Q, and RH with V_N in Fig. 4 substantiate the foregoing intuitive analysis. Both T and Q are correlated with V_N with better than 99% confidence for lags from -1 day to

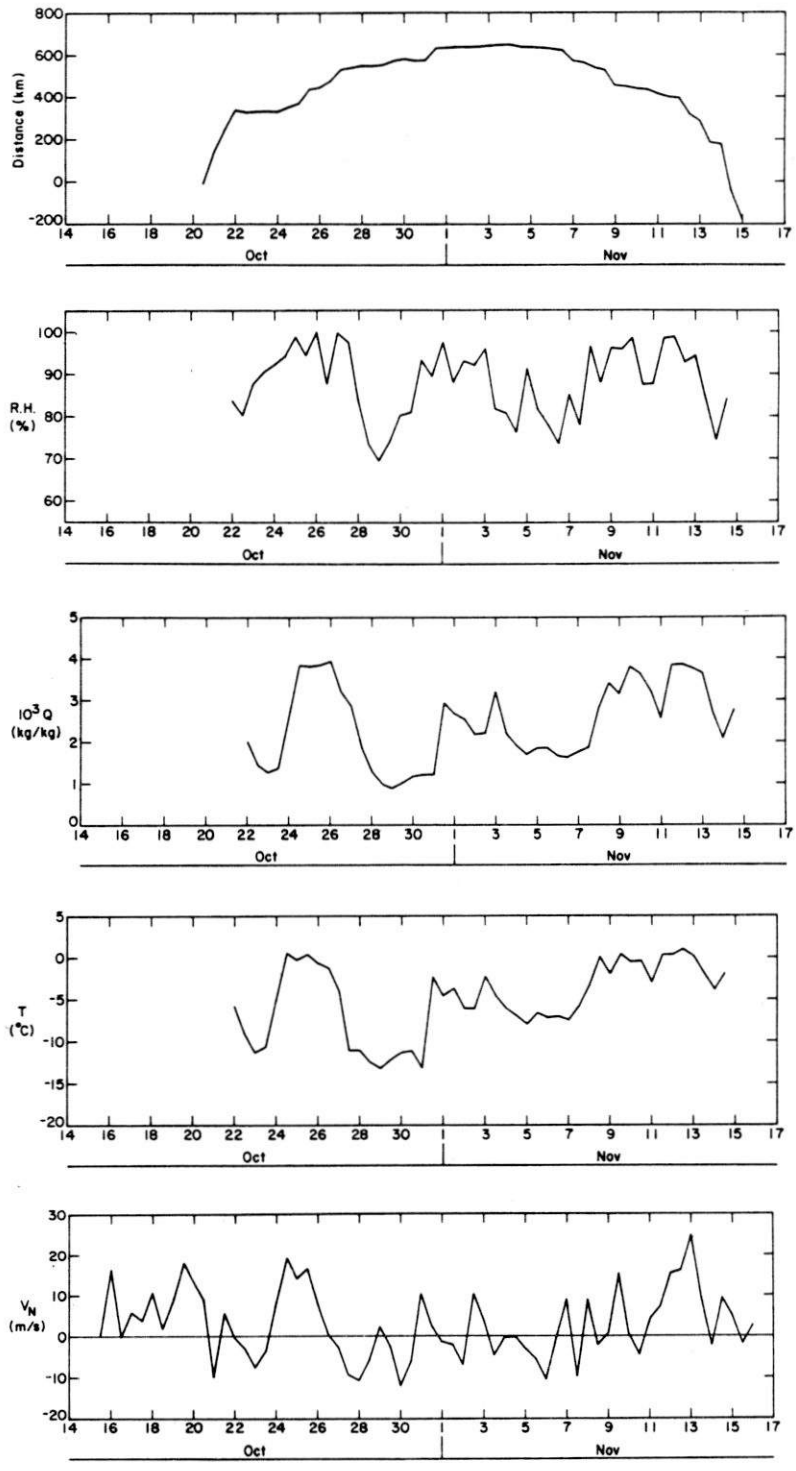

FIG. 3. Time series of the *Somov's* distance from the ice edge, the 12-h-averaged surface-level relative humidity, specific humidity, and temperature and individual radiosonde measurements of the northerly component of the 850 mb wind vector.

+½ day. Relative humidity is correlated with V_N with better than 99% confidence at zero lags.

The details of the cross-correlation functions imply that the open ocean was a source for the heat and moisture. The T–V_N and Q–V_N cross-correlations have main peaks at −½ day; that is, T and Q are best correlated with V_N when the wind time series measured at the *Somov* leads the local temperature

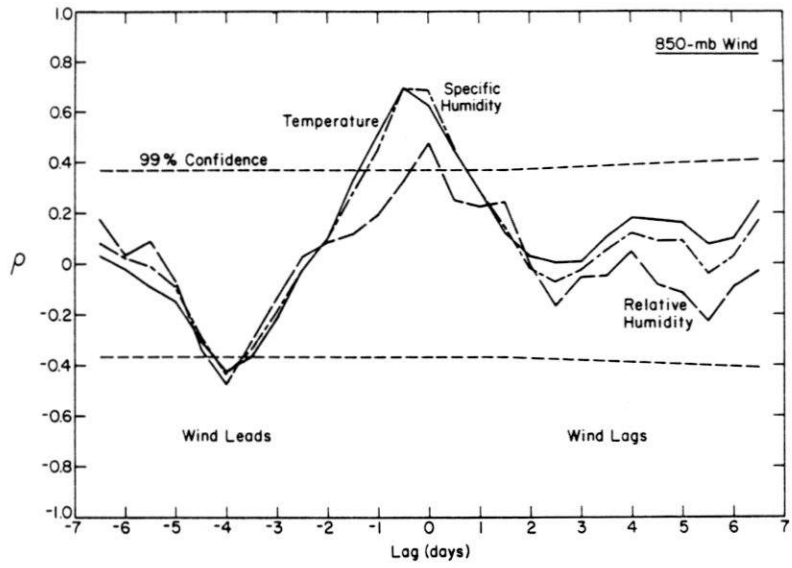

FIG. 4. Cross-correlation functions of temperature, specific humidity and relative humidity with V_N. Dashed lines delimit the 99% confidence interval.

and specific humidity time series by 12 hours. Note that an air mass moving at 10 m s^{-1} (typical of the 850 mb wind) can cover 430 km in 12 h, roughly our distance from the ice edge. The 12-h averaging of the scalar series effectively extends this distance to 650 km. Thus, the location of the maxima in the T–V_N and Q–V_N cross-correlations suggests that atmospheric transport of oceanic heat and moisture produced the high temperature and specific humidity events seen at the ship. The width of these main cross-correlation peaks, 1.5 days, is an indicator of the temporal variability within the ABL.

The RH–V_N cross-correlation is different than the T and Q cross-correlations: it has a lower main peak and significant correlation only at zero lags. Evidently, relative humidity behaves differently than specific humidity over sea ice. Specific humidity is a measure of how much water vapor the air holds and, therefore, has a strong temperature dependence. A warm air mass can hold much more water vapor than a cold air mass—hence the similarity between the T and Q time series and the T–V_N and Q–V_N cross-correlation functions. On the other hand, relative humidity, which is the ratio of actual water vapor content to potential water vapor content, is largely independent of temperature. Throughout most of the year, the deep Antarctic ice pack undergoes surface ablation. The ablation rate depends strongly on wind speed. An increase in the local wind speed will, thus, generally cause an increase in the relative humidity, regardless of wind direction. Consequently, the relative humidity should be high when $|V_N|$ is large (not just when V_N is large) and lower when $|V_N|$ is small. In other words, this effect tends to produce a good, positive correlation between RH and V_N when V_N is large and positive but a good, negative correlation when V_N is large and negative. It thus confounds the RH–V_N cross-correlation function at zero lags and explains why RH is not as well correlated with V_N as T and Q.

Another effect, however, is evidently strong enough to give the significant correlation between RH and V_N at zero lags. An oceanic air mass moving south across the sea ice would be cooled; its saturation vapor pressure would consequently decrease. Even without a change in its moisture content, its relative humidity would therefore increase. Conversely, a continental air mass moving north across the sea ice would warm, and its saturation vapor pressure would increase. With no change in its specific humidity, its relative humidity would decrease. Thus, simple physics leads to an inherent correlation between RH and V_N.

Recognizing these opposing effects of local wind speed changes and the meridional temperature gradient, we can infer what causes the significant main peak in the RH–V_N cross-correlation function. Long-range atmospheric transport of water vapor and the attendant effects of the meridional temperature gradient must have been responsible for the significant cross-correlation. The main cross-correlation peak is significant only at zero lags because the relative humidity also responds immediately to changes in the local surface wind. This effect, however, did not destroy the peak entirely because the strongest winds were northerly (V_N positive, see Fig. 3).

The significant negative peak at a lag of −4 days in all of the cross-correlation functions in Fig. 4 reflects the time scale of the atmospheric systems the *Somov* encountered. That is, a lag of −4 days correlates the low temperature and humidity associated with the southerly wind on the back side of a passing low with the positive V_N on its front side.

Since the 850-mb wind is not always available, the

foregoing analysis was redone using 12 hourly averages (again, triangular weighting function) of the northerly component of the surface wind measured on the *Somov* (V_{Ns}). With the fairly small turning angle over sea ice (Brown, 1981; Thorndike and Colony, 1982), V_{Ns}, not surprisingly, is well correlated with V_N. Figure 5 shows that a linear dependence on V_N would explain over 70% of the variance of V_{Ns}. The width of the cross-correlation peak, 1.5 days, again reflects the temporal variability of the atmospheric boundary layer.

The cross-correlation functions of T, Q, and RH with V_{Ns} in Fig. 6 look much like those in Fig. 4. Again, the T–V_{Ns} and Q–V_{Ns} correlations have main peaks at a lag of $-\frac{1}{2}$ day. Both correlation coefficients, however, are slighty higher here than in Fig. 4—probably a result of the enhanced V_{Ns} values resulting from clockwise turning of the wind profile under geostrophic winds predominantly from the northwest. The width of the T and Q peaks, 2–2½ days, is similar to the peak widths in Fig. 4 and, therefore, emphasizes the time scale of the temporal variability over Antarctic sea ice.

The cross-correlation function of relative humidity with V_{Ns} shown in Fig. 6 is strikingly similar to the RH–V_N function in Fig. 4. This similarity undercores the importance of local wind events on the relative humidity.

Although RH is significantly correlated with V_{Ns} at a lag of -4 days, this is not so for either T or Q. This is somewhat puzzling. Since V_N and V_{Ns} are uncorrelated at a lag of -4 days, it is not surprising that T and Q are uncorrelated with V_{Ns} there, although both were correlated there with V_N. I can suppose only that the RH–V_{Ns} correlation at -4 days is a combination of the very high V_{Ns}–V_N correlation at zero lags and the good (negative) RH–V_N correlation at -4 days.

4. Discussion

Though short, our time series imply that thermodynamic processes explain, in part, the observed correlations between Antarctic sea ice extent and atmospheric indices, at least in the spring. A northerly wind can carry oceanic heat deep into the pack, while a southerly wind can cool and dry the atmosphere over a large area of the pack ice. Thermodynamic processes at the ice surface are thus strongly coupled to the geostrophic wind direction. Freeze and thaw cycles or advance and retreat periods may thus be episodic, especially in the spring and fall when the energy budget of the ice is nearly balanced (Gordon, 1981). Andreas *et al.* (1984) also pointed out this probable episodic behavior of advance and retreat periods nearer the ice edge.

It is fairly easy to see that if the geostrophic wind has a long open ocean fetch, it is indeed oceanically derived heat and moisture that we are seeing 600 km into the ice. Admittedly, the concentration of Antarctic sea ice is low by Arctic standards; the open water could thus serve as a heat and moisture source under the right conditions. A northerly wind in initial equilibrium with the open ocean, however, does not present the right conditions. The open water percentage decreases poleward with distance from the ice edge (Zwally *et al.*, 1983); the surface must also cool with distance. An air mass crossing the ice edge and moving southward could in no way be warmed or

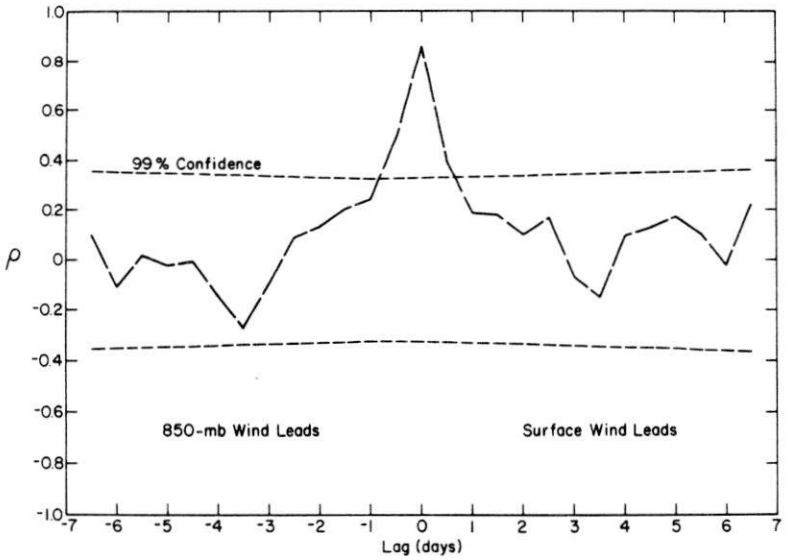

FIG. 5. Cross-correlation function of the 12-h-averaged northerly component of the surface wind vector with the northerly component of the 850 mb wind vector. Dashed lines delimit the 99% confidence limit.

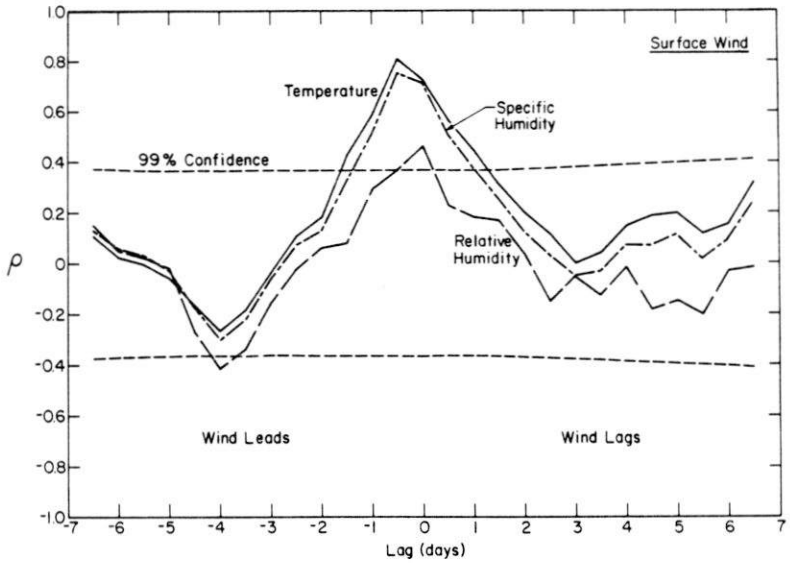

FIG. 6. As in Fig. 4, but for temperature, specific humidity and relative humidity with V_{N_1}. Dashed lines delimit the 99% confidence interval.

moistened above its oceanic equilibrium. It would, in fact, cool and dry if the meridional temperature gradient at the ice surface were strong enough. Our observations that the temperature and humidity remain surprisingly high under northerly winds, even 600 km from the ice edge, suggest that the temperature gradient is rather weak in the spring. Andreas *et al.* (1984) made the same observation in the Antarctic marginal ice zone; in their study the surface-layer air temperature under a northerly wind decreased only about 1°C along a 150 km path over sea ice of concentrations up to 80%. The many leads and polynyas evidently prevent the ice surface from being cooled much more than 10°C below freezing at this time of year, even under a southerly wind.

To appreciate the magnitude of the surface flux difference between northerly and southerly winds, let us look at the conditions from 25–31 October. The Fig. 3 time series show a southerly wind event from 27–31 October that produced the lowest temperatures and humidities we encountered during the cruise. In contrast, the 850 mb wind during the preceding two days had a strong northerly component, and both temperature and humidity were high. Let us put this event in a synoptic context and then compute representative turbulent surface fluxes during the event.

Although surface pressure analysis fields for the Southern Ocean are sometimes untrustworthy, let us, at least qualitatively, assess the synoptic conditions from 25–31 October 1981 (see Fig. 7). These maps are again the Australian analysis fields from the National Climate Center.

At noon on 25 October the *Somov* was just east of a deep low; the geostrophic wind was, thus, northerly and had a significant oceanic fetch. Figure 3 confirms the northerly wind and shows that temperature and humidity were both relatively high. During the next two days the low passed directly over us, so at noon on 27 October we were to its west; the geostrophic wind at the *Somov* was consequently from the south. The RH, Q, T, and V_N time series in Fig. 3 all show the consequences of the passage; the 850 mb wind swung to the south, and the temperature and humidity fell precipitously.

During the next two days another low pressure center moved into our area, but it stayed somewhat to the north; Fig. 7 shows the surface pressures at noon on 29 October. This northerly low produced a weak southeasterly wind at the *Somov;* V_N in Fig. 3 is thus near zero, but T, Q, and RH remain low. Evidently, the air mass was of continental rather than oceanic origin or had followed a very long path over sea ice. As the low moved to the southeast, the southerly winds behind it kept the temperature and humidity low at the *Somov* for another day (Fig. 3). Finally, yet another low approached from the west and—since it was at roughly the latitude of the *Somov*—brought northerly winds, higher temperatures, and moist air from the ocean to our region. Figure 7 shows the synoptic situation at noon on 31 October, while Fig. 3 reflects the sequence of changes associated with the approaching low that finally ended the low temperature event.

Estimates of the surface sensible and latent heat fluxes before, during, and after this event confirm the influence of the geostrophic wind direction on the surface energy budget. A simple flux-gradient iteration procedure (described by Andreas *et al.,* 1984) was used for these estimates; the data consisted of shipboard observations of wind speed and surface temperature, along with the temperature and specific humidity values shown in Fig. 3. Table 1 summarizes

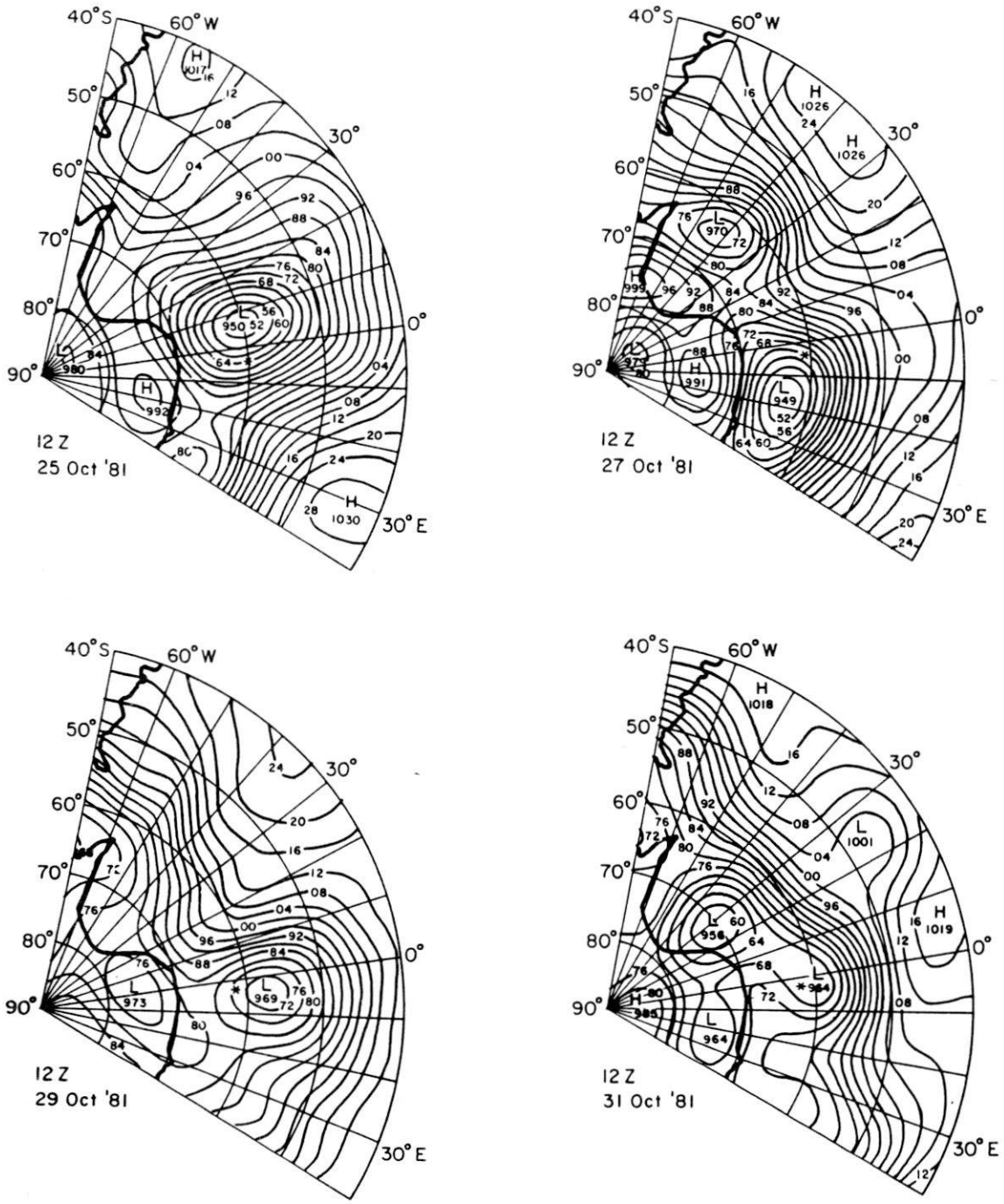

FIG. 7. Sea-level pressure fields during the low temperature event of 27–31 October 1981. The star near the 0° meridian shows location of the *Somov*.

the relevant observations and the associated fluxes for the four cases represented by the maps in Fig. 7.

The fluxes in Table 1 clearly depend on whether the air mass at our location was continental or oceanic but are unrelated to distance from the ice edge. Before the low temperature event on 25 October and after it on 31 October, the oceanic heat and moisture carried in on northerly winds kept the surface-layer air near thermal equilibrium with the surface. Sensible and latent heat losses from the surface were thus minimal—in fact, on 31 October, 630 km from the ice edge, the air was transferring heat to the surface. Since the net radiation budget was negative on both 25 and 31 October, there was likely some melting on these days. On 27 and 29 October, however, when the air mass was probably

TABLE 1. Data and results of a flux-gradient estimate of the turbulent sensible and latent heat fluxes (Time GMT).*

	25 Oct 1981 1200	27 Oct 1981 1200	29 Oct 1981 1200	31 Oct 1981 1200
Distance (km)	430	540	570	630
U (m s^{-1})	9.0	12.0	10.0	8.0
T (°C)	−0.2	−11.1	−12.1	−2.3
T_s (°C)	0.0	−3.5	−8.9	−3.6
Q (10^{-3} kg/kg)	3.85	1.53	1.02	2.94
Q_s (10^{-3} kg/kg)	3.96	2.97	1.83	2.94
u_* (m s^{-1})	0.31	0.45	0.36	0.24
H_s (W m^{-2})	2	169	58	−15
H_L (W m^{-2})	5	84	40	0
R_n (W m^{-2})	−45	−110	−140	−380

*U = the wind speed at a reference height of 21 m; T and Q = temperature and specific humidity at 11 m; T_s and Q_s = the temperature and specific humidity at the surface; u_* = the computed friction velocity; H_s and H_L = the computed sensible and latent heat fluxes; R_n = the measured net radiation (see Andreas and Makshtas, 1983). Positive fluxes indicate a transfer of heat from the surface to the atmosphere.

of continental origin, the turbulent surface heat losses were large. These losses overwhelmed the radiative fluxes on 27 October and probably fostered ice formation. Ackley and Smith (1983) observed extensive areas of grease ice on this day, substantiating this heat budget analysis. By 29 October the ice surface had cooled under the persistent cold winds; the turbulent heat losses consequently decreased though the winds were of similar strength. Adding a constant oceanic conductive heat flux C of 20–25 W m^{-2} (Gordon *et al.*, 1984) into the surface energy budget, we see that the ice was probably warming or melting on that day, even with the low temperatures (i.e., $R_n - C + H_s + H_L \approx -60$ W m^{-2}). However, the cold continental air kept this to a minimum, despite the large shortwave flux to the surface.

Although it is always dangerous to extrapolate from the specific to the general, these flux computations at least suggest an order of magnitude for the difference in the total turbulent surface flux between northerly and southerly winds. In the spring a southerly wind removes roughly 100 W m^{-2} more heat from the surface than a northerly wind. Or, expressed in another way, a northerly wind makes a −100 W m^{-2} difference in the surface energy budget. A flux to the surface, constant at 100 W m^{-2}, can melt 3 cm of ice per day.

The time series in Fig. 3 show no dramatic decrease in temperature or humidity as our distance from the ice edge increased from 200 to 600 km. Hence, a northerly wind off the ocean can influence the surface-layer temperature and humidity fields for distances of at least 600 km from the ice edge; i.e., even at maximum ice extent, marine air can reach roughly 60% of the Antarctic ice pack. At minimum ice extent, it can reach virtually the entire pack. Contrast this with conditions in the Arctic Ocean, which has only a very limited open ocean boundary.

5. Conclusions

The temperature and humidity time series presented herein are the first reliable, *in situ* measurements from the deep Antarctic ice pack during its near-maximum extent. Their main lessons are the temporal variability of both fields and the relatively mild conditions over the deep pack in the spring. The correlations of temperature and humidity with meridional wind imply an important thermodynamic contribution to previously observed relationships between sea ice extent and synoptic-scale atmospheric variables. They do not, however, rule out a concomitant dynamic contribution from the meridional wind stress. This may be as important as the thermodynamics in controlling ice extent, but the data are insufficient to investigate it.

The results also have implications for modeling both sea ice and the atmospheric boundary layer in the Antarctic. Monthly mean geostrophic winds (e.g., Parkinson and Washington, 1979) are not adequate for driving sea ice models. The day-to-day variability of the wind leads to episodic behavior in the surface energy budget. Atmospheric forcing fields updated daily (e.g., Hibler and Ackley, 1983) would seem to be a minimum requirement.

Because a northerly wind can still be losing heat 600 km from the ice edge, and because a southerly wind crossing the continental boundary immediately begins extracting heat and moisture from open water areas within the sea ice, the ABL over Antarctic sea ice is rarely in equilibrium with the surface. Modeling it will consequently be a large-scale boundary layer modification problem; one-dimensional models, which are successful in the Arctic, would be hard to defend here.

Acknowledgments. Stanislav Bobrov and Valerii Posazhenikov of the Arctic and Antarctic Research Institute, Leningrad, made all of the MicroCORA soundings; Brett Murphy helped with the computations; and William Bates drafted the figures. My colleagues, Steve Ackley and Tony Gow, offered helpful comments on an early draft of the manuscript; Mark Hardenberg provided editorial assistance. Two anonymous reviewers spent a lot of time with the manuscript and suggested many improvements. The National Science Foundation supported this research through Grants DPP 80-06922 and DPP 81-20024. The National Oceanic and Atmospheric Administration, Office of Special Research and Programs, provided funds for the lease of the MicroCORA through the National Science Foundation, Grant DPP 82-03489.

REFERENCES

Ackley, S. F., 1981: A review of sea-ice weather relationships in the Southern Hemisphere. *Sea Level, Ice, and Climate Change*, I. Allison, Ed., IAHS Publ. **131**, 127–159. [International

Association of Hydrological Sciences, 2000 Florida Ave. NW, Washington, DC 20009.]

——, and T. E. Keliher, 1976: Antarctic sea ice dynamics and its possible climatic effects. *AIDJEX Bull.*, **33,** 53–76. [Arctic Ice Dynamics Joint Experiment, Div. Marine Resources, University of Washington, Seattle, Wash. 98105.]

——, and S. J. Smith, 1983: Reports of the U.S.-U.S.S.R. Weddell Polynya Expedition, October–November 1981: Vol. 5, Sea ice observations. Special Rept. 83-2, U.S. Army Cold Regions Research and Engineering Laboratory, Hanover, N.H., 59 pp. [NTIS: AD-A130 140/7.]

——, —— and D. B. Clarke, 1982: Observations of pack ice properties in the Weddell Sea. *Antarct. J. U.S.*, **17,** 105–106.

Andreas, E. L., 1983: Reports of the U.S.-U.S.S.R. Weddell Polynya Expedition, October–November 1981: Vol. 6, Upper-air data. Special Rept. 83-13, U.S. Army Cold Regions Research and Engineering Laboratory, Hanover, N.H., 288 pp. [NTIS: AD-A134 871/3.]

——, and S. F. Ackley, 1982: On the differences in ablation seasons of Arctic and Antarctic sea ice. *J. Atmos. Sci.*, **39,** 440–447.

——, and W. A. Richter, 1982: An evaluation of Vaisala's MicroCORA Automatic Sounding System. CRREL Rept. 82-28, U.S. Army Cold Regions Research and Engineering Laboratory, Hanover, N.H., 17 pp. [NTIS: AD-B070 011/L.]

——, A. P. Makshtas, 1983: Reports of the U.S.-U.S.S.R. Weddell Polynya Expedition, October–November 1981: Vol. 7, Surface-level meteorological data. Special Rept. 83-14, U.S. Army Cold Regions Research and Engineering Laboratory, Hanover, N.H., 32 pp. [NTIS: AD-A134 476/1.]

——, W. B. Tucker III and S. F. Ackley, 1984: Atmospheric boundary-layer modification, drag coefficient, and surface heat flux in the Antarctic marginal ice zone. *J. Geophys. Res.*, **89,** 649–661.

Brown, R. A., 1981: Modeling the geostrophic drag coefficient for AIDJEX. *J. Geophys. Res.*, **86,** 1989–1994.

Buck, A. L., 1981: New equations for computing vapor pressure and enhancement factor. *J. Appl. Meteor.*, **20,** 1527–1532.

Cavalieri, D. J., and C. L. Parkinson, 1981: Large-scale variations in observed Antarctic sea ice extent and associated atmospheric circulation. *Mon. Wea. Rev.*, **109,** 2323–2336.

Fletcher, J. O., 1969: Ice extent on the Southern Ocean and its relation to world climate. RM-5793-NSF, Rand Corporation, 108 pp. [1700 Main St., Santa Monica, Calif. 90406.]

Gordon, A. L., 1981: Seasonality of Southern Ocean sea ice. *J. Geophys. Res.*, **86,** 4193–4197.

——, 1982: The U.S.-U.S.S.R. Weddell Polynya Expedition. *Antarctic J. U.S.*, **17,** 96–98.

——, and H. W. Taylor, 1975: Seasonal change of Antarctic sea ice cover. *Science*, 187, 346–347.

——, C.T.A. Chen and W. G. Metcalf, 1984: Winter mixed layer entrainment of Weddell Deep Water. *J. Geophys. Res.*, **89,** 637–640.

Hibler, W. D., III, and S. F. Ackley, 1983: Numerical simulation of the Weddell Sea pack ice. *J. Geophys. Res.*, **88,** 2873–2887.

Neumann, G., and W. J. Pierson, Jr., 1966: *Principles of Physical Oceanography.* Prentice-Hall, Englewood Cliffs, N.J., 545 pp.

Olson, M. L., 1979: Global accuracy of Omega-derived winds. *Atmos. Technology,* **10,** 14–23. [National Center for Atmospheric Research, P.O. Box 3000, Boulder, Colo. 80307.]

Parkinson, C. L., and W. M. Washington, 1979: A large-scale numerical model of sea ice. *J. Geophys. Res.*, **84,** 311–337.

——, and D. J. Cavalieri, 1982: Interannual sea-ice variations and sea-ice atmosphere interactions in the Southern Ocean, 1973–1975. *Ann. Glaciol.*, **3,** 249–254. [International Glaciological Society, Cambridge CB2 1ER, England.]

Schwerdtfeger, W., and St. Kachelhoffer, 1973: The frequency of cyclonic vortices over the Southern Ocean in relation to the extension of the pack ice belt. *Antarctic J. U.S.*, **8,** 234.

Streten, N. A., and D. J. Pike, 1980: Characteristics of the broadscale Antarctic sea ice extent and the associated atmospheric circulation 1972–1977. *Arch. Meteor. Geophys. Bioklim.*, **A29,** 279–299.

Thorndike, A. S., and R. Colony, 1982: Sea ice motion in response to geostrophic winds. *J. Geophys. Res.*, **87,** 5845–5852.

Wexler, H., 1959: Seasonal and other temperature changes in the Antarctic atmosphere. *Quart. J. Roy. Meteor. Soc.*, **85,** 196–208.

Zwally, H. J., J. C. Comiso, C. L. Parkinson, W. J. Campbell, F. D. Carsey and P. Gloersen, 1983: *Antarctic Sea Ice, 1973–1976: Satellite Passive-Microwave Observations.* NASA SP-459, National Aeronautics and Space Administration, Goddard Space Flight Center, Greenbelt, Md., 206 pp. [U.S. Government Printing Office, Washington, DC 20402.]

JOURNAL OF GEOPHYSICAL RESEARCH, VOL. 90, NO. C4, PAGES 7199–7212, JULY 20, 1985

Energy Exchange Over Antarctic Sea Ice in the Spring

EDGAR L. ANDREAS

U.S. Army Cold Regions Research and Engineering Laboratory, Hanover, New Hampshire

ALEKSANDR P. MAKSHTAS

Arctic and Antarctic Research Institute, Leningrad

In October and November of 1981, during the U.S.-USSR Weddell Polynya Expedition, we made the first measurements ever of the turbulent and radiative fluxes over the interior pack ice of the Southern Ocean. The daily averaged, surface-averaged sum of these fluxes—the so-called balance, which comprises the conductive, heat storage, and phase-change terms—was positive for all but one day during the cruise: the ablation season had begun. Variability in the sum of the turbulent fluxes produced most of the variability in the balance. And these turbulent fluxes generally correlated with the geostrophic wind—a northerly wind (in off the ocean) transferring heat to the surface, and a southerly wind removing it.

1. INTRODUCTION

Although there have been many air-sea-ice interaction studies over the interior of the Arctic ice pack [e.g., *Untersteiner and Badgley*, 1965; *Banke and Smith*, 1971, 1973; *Langleben*, 1972, 1974; *Thorpe et al.*, 1973; *Banke et al.*, 1976, 1980; *Borisenkov et al.*, 1977; *Leavitt et al.*, 1977; *Andreas and Paulson*, 1979; *Andreas et al.*, 1979, 1981], inaccessibility had precluded similar measurements over Antarctic sea ice. Instead, observations in the Antarctic were confined near shore. *Weller* [1968*a*, *b*] made one of the first Antarctic air-sea-ice interaction studies, collecting a full suite of radiation data and wind speed and temperature profiles for 5 months on the seasonal sea ice at Mawson. *Allison* [1973] and *Allison and Akerman* [1980] continued these micrometeorological observations at Mawson, and recently *Allison et al.* [1982] added oceanographic sampling and aircraft profiling of the atmospheric boundary layer. Data from Antarctic coastal sites may not, however, be representative of processes in the sea ice interior. For example, energetic katabatic winds can periodically scour coastal sea ice of its snow cover, thereby dramatically lowering its albedo [*Weller*, 1968*a*]. It is therefore essential to supplement these near-shore observations with ones from the interior pack.

The U.S.-USSR Weddell Polynya Expedition of October and November 1981 [*Gordon and Sarukhanyan*, 1982; *Gordon*, 1982] on the Soviet icebreaker *Mikhail Somov* was thus an important milestone in Antarctic research. Not only were we the first since the German Antarctic Expedition of 1911–1912 [*Brennecke*, 1921] and the Shackleton Expedition of 1914–1917 [*Wordie*, 1921] to visit the interior of the ice-covered Weddell Sea region, we report here the first micrometeorological measurements ever made over Antarctic sea ice at other than coastal sites.

The measurements that we will describe include 3-hourly observations of the wind speed, temperatures of the air and of the sea ice and water surfaces, humidity, incoming and reflected shortwave radiation, and net radiation. We also measured surface-layer profiles of wind speed, air temperature, and dew-point temperature at selected stations. Last, we made upper-air soundings every 12 hours. From these data we computed all but the storage, phase-change, and oceanic conduction terms of the surface energy budget for both sea ice and open water. The sum of these components, which we call the balance, was positive when spatially and temporally averaged. That is, the surface as a whole was gaining energy; spring had begun. During periods of cold southerly winds, however, the balance over open water areas was negative because the turbulent heat losses were still large enough to outweigh the shortwave flux.

Paper number 5C0085.
0148-0227/85/005C-0085$05.00

2. THE MEASUREMENTS

Because the original intention of our expedition was to make atmospheric, oceanographic, sea ice, and biological observations in the vicinity of the Weddell Polynya, which forms periodically near Maud Rise (65°S, 2°E) [*Gordon*, 1978; *Carsey*, 1980; *Martinson et al.*, 1981], the *Somov* entered the Antarctic ice pack near 56°S and 3°E on October 20, 1981. The polynya did not appear in 1981, unfortunately. We therefore collected all of our data in fairly complete ice cover (~90%) [*Ackley and Smith*, 1983; *Comiso et al.*, 1984] in what *Ackley et al.* [1982] defined as the "deep pack," regions more than 250 km from the ice edge. Figure 1 shows our cruise track.

2.1. *Time Series*

Our analysis will focus on the time series of 3-hourly observations that we made while within the limits of the pack ice. Figure 2 shows the locations of the sensors that produced these series. The air (T_a) and wet-bulb (T_w) temperatures were measured with thermistors mounted on a boom extending from the bow of the *Somov* 11 m above the surface. We obtained the relative humidity (f) from these using standard formulas. The wind speed (U) came from a propeller-vane mounted 21 m above the surface on a midship mast.

The accuracy of shipboard measurements of meteorological variables is always a question. *Romanov et al.* [1983] recently demonstrated in a wind tunnel that shipboard wind speed measurements are best made from a high mast, as ours were. They found that at this location the relative error in wind speed is less than 8% regardless of wind direction.

Our temperature sensors on the bow were potentially less well exposed, especially in a following wind; but we found no evidence of this. On occasion we mounted additional temperature and dew-point sensors on both the bow and the well-

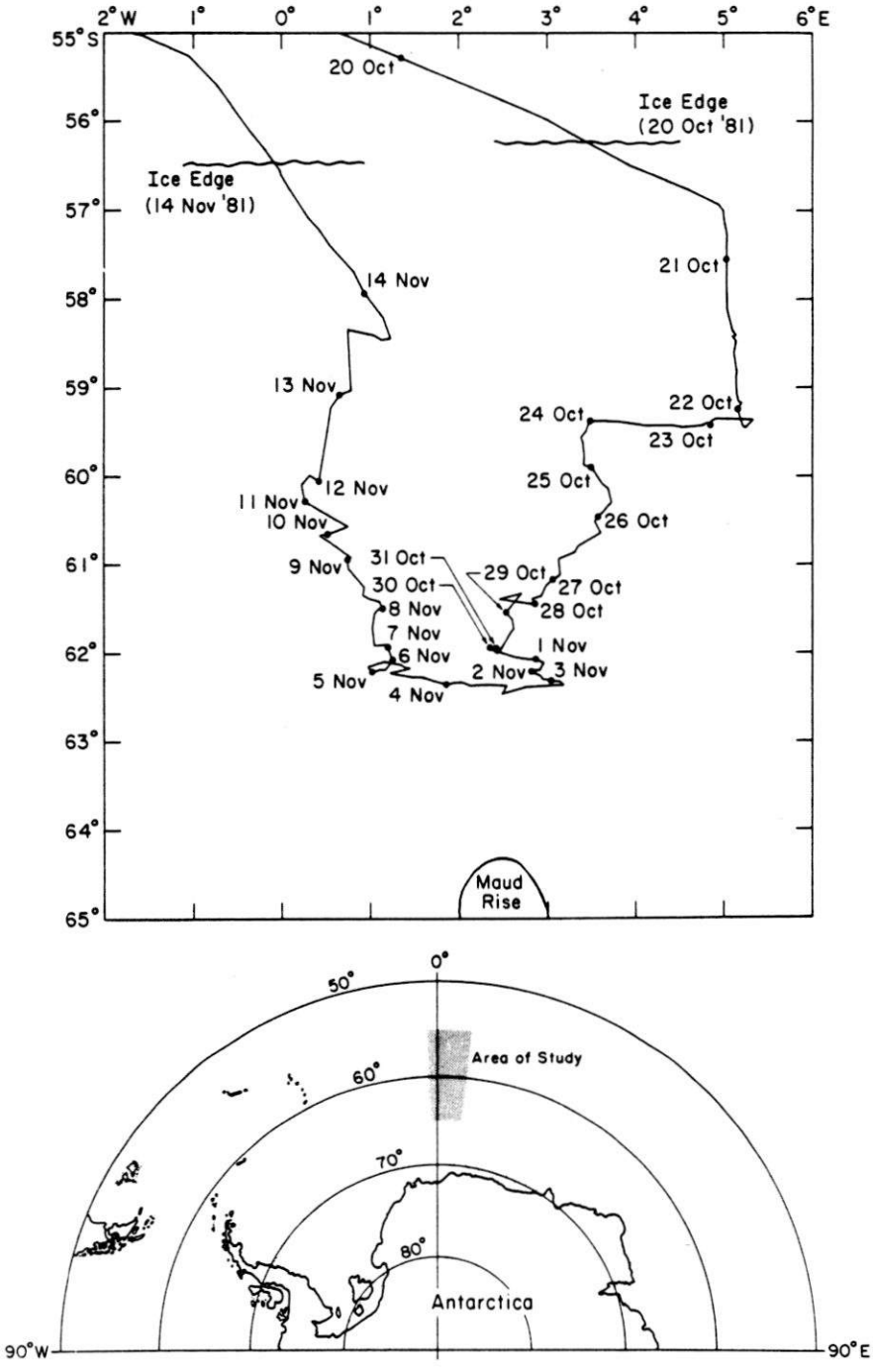

Fig. 1. The cruise track of the *Somov*. The dots mark the beginning of the indicated day.

exposed, rear helicopter deck [*Andreas*, 1985]. If the ship were affecting the temperature and moisture fields, windward and lee sensors would have read differently. These independent bow and helicopter-deck sensors, however, showed no systematic differences. *Goerss and Duchon* [1980] also found that the ship did not affect temperature sensors mounted on bow booms. We believe therefore that our temperature data are accurate to ± 1°C, and the relative humidity to ± 5%.

The surface temperature is a crucial parameter in any study of heat and moisture transfer across an interface. The oceanographers on the cruise provided us with the water surface temperature [*Huber et al.*, 1983]. Except on November 13, when it was -1.78°C, that temperature was always -1.84° or -1.85°C.

We measured the ice surface temperature (T_{ice}) with a thermistor protruding from a Styrofoam block. We lowered this assembly from the bow of the *Somov* onto sea ice yet undisturbed by the ship. The block rested flat on the ice or snow surface; the thermistor thus measured the temperature of a very thin surface layer. To make each observation representative, we sampled several floes ahead of the ship and then computed an average temperature. With this method we could

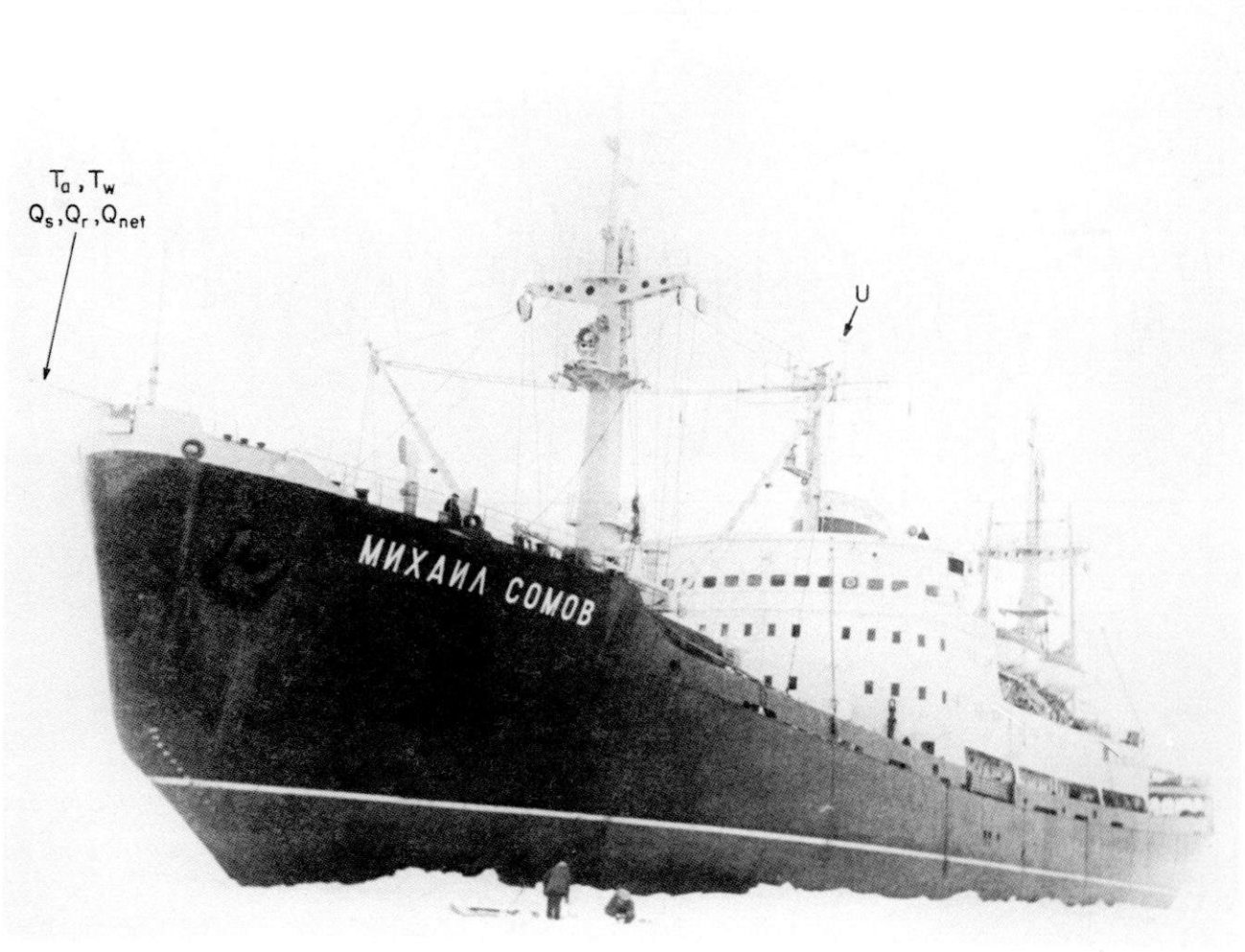

Fig. 2. Locations of sensors on the *Somov*.

make measurements whether the *Somov* was moving or stopped.

Figure 3 shows the series of our 3-hourly observations of wind speed, air and ice surface temperatures, and relative humidity. The wind speed averaged about 8 m/s but was highly variable. The temperature was relatively mild except for the dramatic event from October 27 to 31. The relative humidity was fairly high, 80–90%, and was moderately well correlated with the air temperature. *Andreas* [1985] elaborated on this correlation. The gap in the T_{ice} series around November 2 will appear in some of our subsequent heat flux series. The *Somov* spent this day on station in a small polynya; we were therefore unable to measure any ice surface temperatures.

The bow boom also had upward looking and downward looking pyranometers and a net radiometer for measuring, respectively, the global incoming shortwave radiation (Q_s), the reflected shortwave radiation (Q_r), and the net all-wave radiation (Q_{net}). The bow boom provided good exposure for the upward looking pyranometer; shadowing by the ship should have been minimal. Though hardly an ideal location, the bow boom is also clearly the best place for a shipboard measurement of Q_r and Q_{net}, since here the sensors have the least obstructed view of the surface. Nonetheless, we worry how the ship's hull may have affected these measurements. The measured albedo values (Q_r/Q_s) were typically 0.5–0.6 and thus seem somewhat low compared with the range 0.6–0.7 reported by *Predoehl and Spano* [1965] and by *Spano* [1965] over the Ross Sea and by *Weller* [1968*a*] on the shore-fast ice at Mawson. These lower values, however, might be more a consequence of the ubiquitous, though small, open water areas we encountered than of spurious absorption by the hull. The adverse effects of the hull on the Q_{net} measurement tended to cancel each other; the hull would have lowered Q_r but increased the emitted longwave radiation. In subsequent sections we discuss further how we handled inconsistencies in the Q_r and Q_{net} measurements.

Andreas and Makshtas [1983] discussed and tabulated all of the surface-level meteorological data that we have been describing.

2.2. *Profile Measurements*

We supplemented these time series with measurements of the surface-layer profiles of wind speed (U), temperature (T), and specific humidity (Q) when the *Somov* was on station. Our profiling instruments were mounted on a boom that extended from the rear, starboard corner of the helicopter deck at the

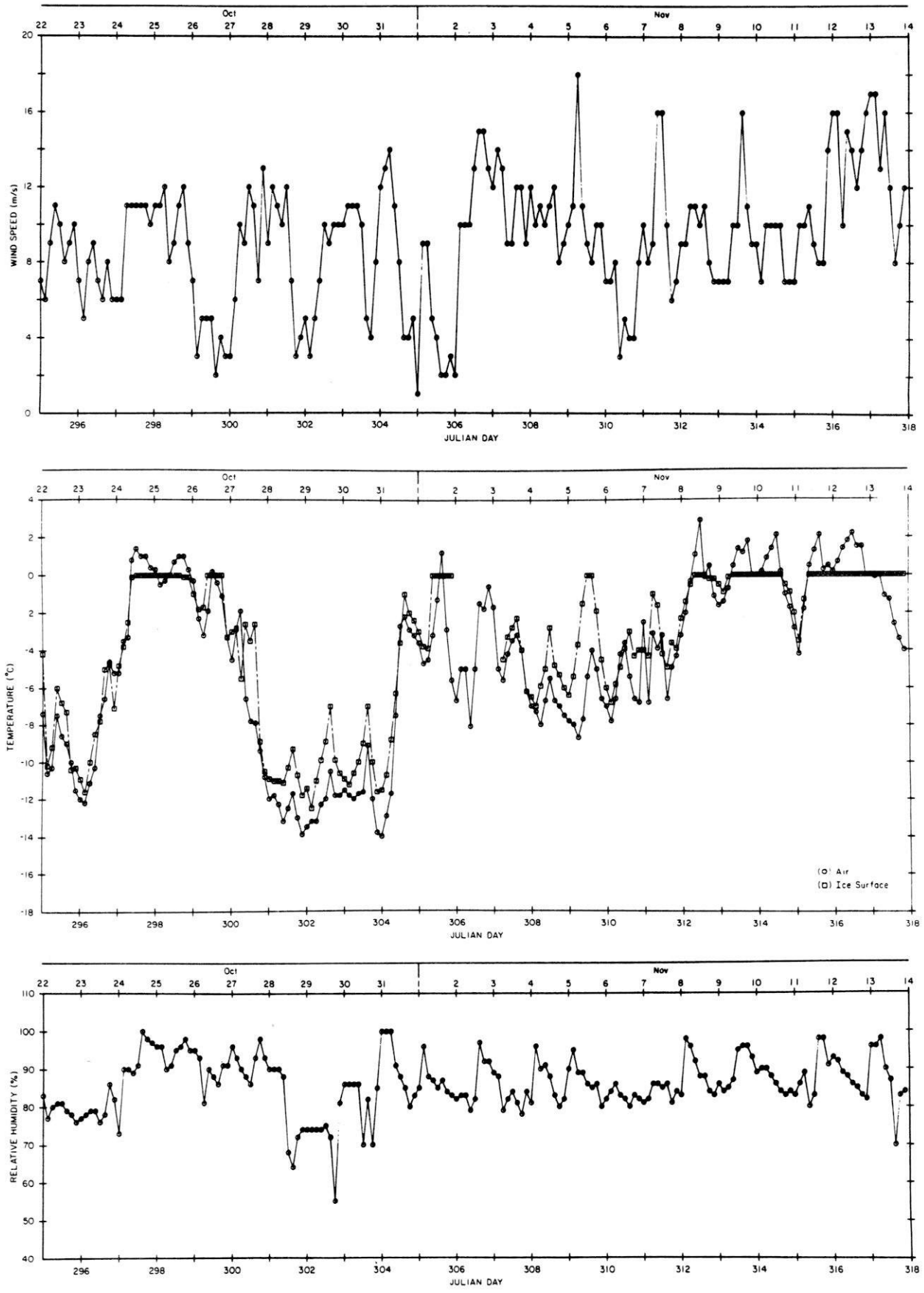

Fig. 3. Time series of the surface-level wind speed, air and ice surface temperatures, and relative humidity.

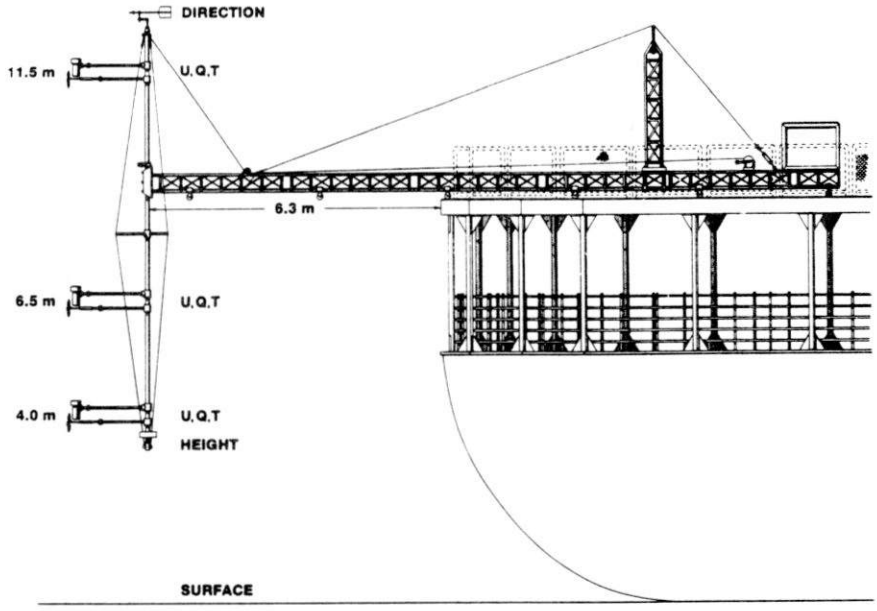

Fig. 4. The profiling boom deployed from the helicopter deck of the *Somov*. *U*, *T*, and *Q* indicate locations of the wind speed, temperature, and humidity sensors. An acoustic distance sensor at the base of the mast measured the height above the surface.

stern of the *Somov* (Figure 4). Because this was a multidisciplinary cruise, with physical, chemical, and biological oceanography programs, as well as air-sea-ice interaction research, we chose this location to minimize station time. All of the oceanographic sampling was done using starboard winches with the *Somov* oriented crosswind. With our boom on the helicopter deck, we could make simultaneous profile measurements in the undisturbed air skirting the rear of the *Somov*. *Andreas et al.* [1984*a*] described the boom assembly more completely and discussed empirical evidence, both ours and others', suggesting that the instruments on the boom were indeed sampling air unaffected by the ship. Just briefly, *Mollo-Christensen* [1979] recommended that, to sample undisturbed air, instruments must extend upwind a distance greater than the ship's freeboard, in this case about 6 m because the *Somov* is relatively open under the helicopter deck. Figure 4 shows that our instruments were about 8 m upwind from the hull.

The instruments on the boom were propeller anemometers for measuring wind speed, platinum resistance thermometers for temperature, and cooled-mirror dew-point hygrometers for humidity (dew point). R. M. Young manufactured the propeller anemometers; General Eastern, the temperature and dew-point sensors. We pointed the sensors into the wind during our runs by rotating the mast holding them, using the wind vane atop it for reference.

We feel that these were high-quality temperature and humidity measurements: the hygrometers measured a fundamental humidity variable; the calibration of both temperature and humidity sensors was very stable; and we intercalibrated instruments before and after each pair of profiling runs. The calibration of the propeller anemometers was even more stable, and we also intercalibrated these once late in the cruise [*Andreas et al.*, 1984*a*]. *Andreas and Makshtas* [1983] described the instruments on the profiling boom in more detail, discussed the data reduction, and tabulated all the profile data.

Table 1 lists the details of each set of profile observations and describes the upwind surface conditions. Figure 5 shows the measured profiles. Some of the temperature and humidity profiles reflect the complexity of the surface conditions described in Table 1. To simplify things, we divided the profile measurements into two groups, those made over a surface that was predominantly water (runs 1, 2, 11A, 11B, 12, 13, 14, and 21) and those made over ice (the rest). Despite the often broken-up nature of the surface, this division is meaningful because the internal boundary layer, a region of modification, existing in a flow encountering a surface step change from water to ice or vice versa is very shallow [*Rao*, 1975; *Andreas et al.*, 1979, 1981]. Thus because the lowest of our profiling instruments was at roughly 4 m, our instrument mast should have been sampling air that was in quasi-equilibrium with the surface [*Andreas*, 1982]. In other words, since the surface inhomogeneities may have been numerous but were generally small, the surface conditions would seem horizontally homogeneous to instruments far enough (order meters) above the surface. We thus used flux-gradient techniques [*Businger et al.*, 1971; *Dyer*, 1974] to obtain surface heat fluxes from both these profiles and the time series.

2.3. *Upper-Air Soundings*

We made routine upper-air soundings every day at 0000 and 1200 UT with a Vaisala MicroCORA automatic sounding system [*Andreas and Richter*, 1982]. The MicroCORA radiosonde measures profiles of pressure, temperature, humidity, and the wind vector. The upper-air wind information is especially important in understanding the surface energy exchange, as we will explain shortly. We believe the accuracy of these Omega-derived winds is as *Olson* [1979] estimated it for this region, ± 1 m/s. *Andreas* [1983] gave more details of the *Somov*'s upper-air program and tabulated all of the upper-air data collected during the expedition.

Figure 6 shows the time series of the wind vector at 850 mbar as measured from the *Somov*. We assume that this vector represents the geostrophic flow, since the 850-mbar level, gen-

TABLE 1. Chronological Listing of the Profiling Runs and a Summary of Upwind Surface Conditions

Run	Date (1981)	Time*	Duration, min	Surface Conditions
1	Oct. 25	2304	45	5 and 10-m floes for 100 m upwind—ice concentration 50%. Ice concentration 90%
2	Oct. 26	0056	45	for next 100 m. Continuous ice beyond 200 m.
3A	Oct. 26	2337	28	Small, broken floes and slush for 50 m upwind—ice concentration 70%. Broken floes
3B	Oct. 27	0006	29	with ice coverage 100% from 50 to 150 m upwind. Continuous, smooth first-year floe
4	Oct. 27	0055	45	beyond 150 m.
5	Oct. 28	2304	32	Small, broken floes for 200 m upwind. Continuous, smooth floe beyond 200 m.
6	Oct. 29	0026	36	Same as run 5.
7	Oct. 29	2134	46	Open water for 30 m upwind. Smooth, unbroken floe beyond.
8	Oct. 29	2255	45	Same as run 7.
9	Oct. 30	2221	32	20-m diameter floe under instrument mast. For more than 500 m upwind from this, small,
10	Oct. 30	2331	45	broken floes of 3–5 m predominated. Space between these filled with brash ice and slush giving an ice concentration of more than 90%.
11A	Oct. 31	2209	7	Open water for 500 m upwind.
11B	Oct. 31	2216	38	In a small polynya. Winds calm or sometimes across the helicopter deck from the port side
12	Oct. 31	2323	32	of the ship.
13	Nov. 2	1306	31	About 2 km of open water upwind.
14	Nov. 2	1420	33	Same as run 13.
15	Nov. 4	2256	48	Instrument mast over open water but only 2–3 m downwind from the edge of a large,
16	Nov. 5	0023	38	first-year floe. 20-m wide lead across this floe about 500 m upwind. Smooth ice beyond.
17	Nov. 6	2139	48	For 300 m upwind, a few scattered, small floes with ice forming between them. Open
18	Nov. 6	2258	43	water from 300 m to 1 km upwind. Continuous floe of first-year ice began at 1 km and continued upwind.
19	Nov. 11	0012	42	Open water under instrument mast and for 10 m upwind. For 75 m beyond this, thin (~25 cm)
20	Nov. 11	0115	22	pancake ice and slush. From here to 700 m, larger floes (~50 m) of thin ice with open water between. Floe of first-year ice continued from here upwind.
21	Nov. 11	2210	47	Open water with one or two larger floes (~50 m) for 300 m upwind. Beyond 300 m, thicker ice (~1 m), somewhat ridged, and containing a few open water areas—concentration 90%.

*UT and LT.

erally 1000–1200 m, was always at or near the top of the atmospheric boundary layer (ABL). In Figure 6 a vector above the 0-m/s line represents a northerly wind; thus most of the winds in the figure are northwesterly. Figure 6 does, however, show an event starting on October 24 that we will find significant later. Prior to October 24 the geostrophic wind was westerly. On October 24 it turned northerly and maintained this direction for 2 days. Then on October 27 it reversed and blew generally from the south until October 31. In other words, we experienced a strong northerly flow, in off the open ocean, that was followed quickly by a strong southerly flow, from the cold continent. We will discuss this week-long event more in our subsequent analysis.

3. ANALYSIS

3.1. *Turbulent Fluxes*

To obtain the sensible (H_s) and latent (H_L) heat fluxes from both the time series data and from the surface-layer profiles, we used the flux-gradient method. The appendix describes our procedure. Clearly, to estimate heat fluxes from the time series data, we had also to specify the surface conditions: $U(z_0) = 0$, $\Theta(z_0) = T_0$, and $Q(z_0) = Q_0$, where z_0 is the roughness length, Θ is the potential temperature, T_0 is the surface temperature, and Q_0 is the specific humidity of air in saturation with an ice or seawater surface at temperature T_0. (See *Buck* [1981] for equations relating saturation vapor pressure to temperature.) With profiles consisting of only the surface and one other level, the flux-gradient method is essentially a bulk-aerodynamic computation in which the bulk transfer coefficients for heat (C_H) and moisture (C_E) are specified:

$$H_s = C_H \rho c_p U_r (T_0 - \Theta_r) \quad (1)$$

$$H_L = C_E \rho L_v U_r (Q_0 - Q_r) \quad (2)$$

Here ρ is the air density; c_p, the specific heat of air; L_v, the latent heat of vaporization (sublimation) of water (ice); and U_r, Θ_r, and Q_r, the wind speed, potential temperature, and specific humidity at some reference height.

Although our surface-layer profiles had three levels above

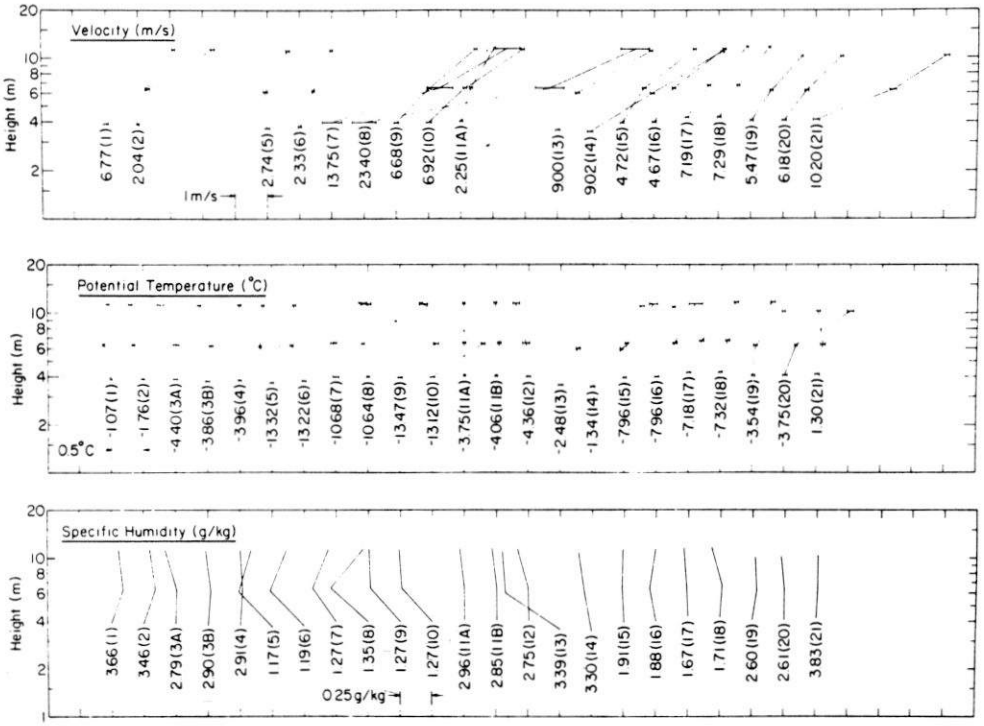

Fig. 5. Individual profiles of wind speed, potential temperature, and specific humidity. The number in parentheses under each profile is the run number (Table 1); the other number is the profile value at the lowest level.

the surface, we found that to compute H_s and H_L accurately, we ultimately had to include the surface conditions in these also. The flux-gradient method is thus here, too, tantamount to a bulk-aerodynamic computation. But with three levels above the surface, it is, in effect, a statistical procedure for determining U_r, Θ_r, and Q_r and thus should be better than relying on single-level measurements of these.

For both the time series data and the surface-layer profiles, we used $z_0 = 0.02$ cm when the surface was ice [*Banke et al.*, 1980] and $z_0 = 0.01$ cm when it was water [*Large and Pond*, 1981]. These values imply that for neutral stability the transfer coefficients are $C_D = C_H = C_E = 1.37 \times 10^{-3}$ over ice and $C_D = C_H = C_E = 1.21 \times 10^{-3}$ over water, where C_D is the drag coefficient.

We computed the turbulent fluxes over both water and ice from each set of 3-hourly observations of wind speed, temperature, and humidity by using the measured T_0 values for ice and water and by assuming U, T_a, and f were independent of the surface type. In other words, we assumed that the ABL was well mixed. This is reasonable in view of the ABL potential temperature profiles that *Andreas* [1983] showed and since the open water areas were seldom large enough to modify the wind and scalar fields appreciably at the heights where we measured U, T_a, and f.

Figure 7 shows the time series of computed sensible and latent heat fluxes over both ice and water. A positive value represents an upward flux, a flux from the surface to the air. In the figure we also plotted the fluxes computed from the profiling runs. In general, the two methods of flux computation are consistent.

At this time of year the fluxes over water are more variable and have more extreme values than those over ice. There is also a conspicuous difference in the magnitudes of the sensible and latent heat fluxes over water; this difference is much less over ice. In Figure 7, notice especially the large heat losses from open water on October 27–31. These were driven by the southerly wind event that we mentioned earlier. The open water was thus generally losing both sensible and latent heat

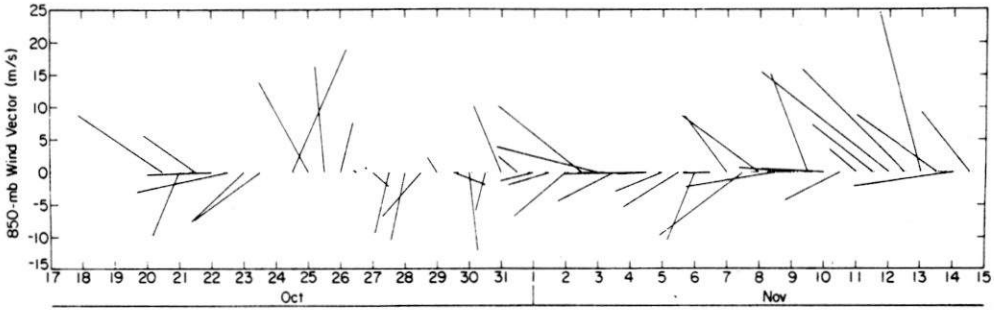

Fig. 6. Time series of the 850-mbar wind vector. Vectors above the 0-m/s line indicate northerly winds.

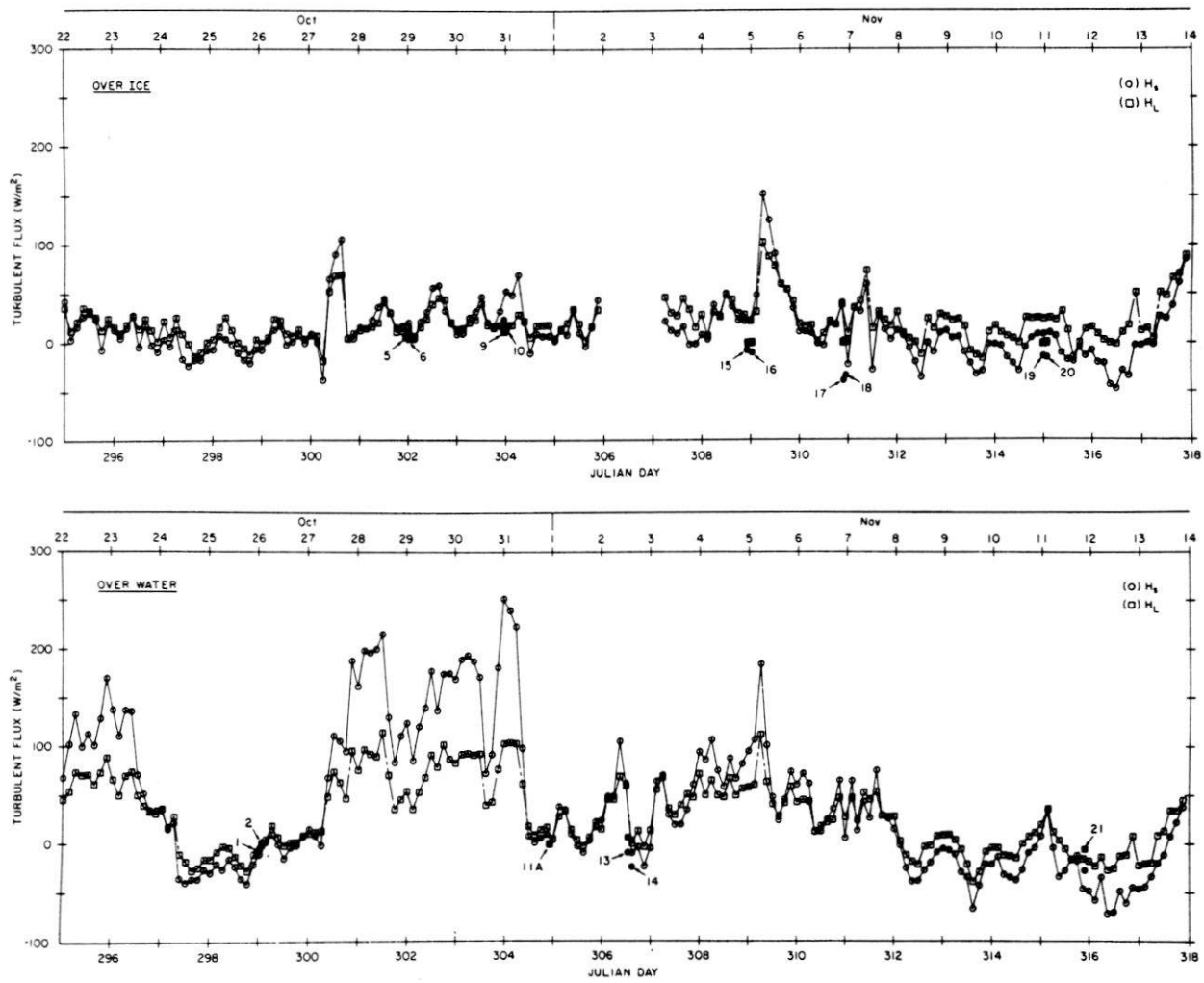

Fig. 7. Time series of sensible and latent heat fluxes over ice and over open water areas within the pack ice. The solid markers are profile measurements of the fluxes, with the run numbers indicated (Table 1).

to the air until late in the cruise. In contrast, the sensible heat flux over ice was as often negative as positive. The latent heat flux over ice, however, was rarely negative.

3.2. *Radiative Fluxes*

The net radiation at the ice or seawater surface is

$$Q_{\text{net}} = Q_s - Q_r + Q_{L\downarrow} - Q_{L\uparrow} \tag{3}$$

Our convention is that the shortwave fluxes and the incoming ($Q_{L\downarrow}$) and emitted ($Q_{L\uparrow}$) longwave fluxes are all positive. Hence, Q_{net} is positive if the surface is gaining energy. As with the turbulent fluxes, we evaluated each of the components in (3) over both ice and water.

Remember, we measured Q_{net}, Q_s, and Q_r at 3-hourly intervals. We assumed Q_s would be the same over both ice and water and computed Q_r over water using *Payne*'s [1972] tabulated sea surface albedo values. This computation required that we find the sun altitude A and the atmospheric transmittance,

$$\text{Tr} = Q_s r^2 / S_0 \sin^2 A \tag{4}$$

where r is the ratio of actual to mean earth-sun separation, and S_0 is the solar constant, 1353 W/m^2. With A and Tr, we selected an albedo value, α, generally 0.07, from Payne's table and computed

$$Q_r = \alpha Q_s \tag{5}$$

Over ice we took the measured Q_r value as the reflected shortwave radiation. But if the *Somov* was in open water when the radiation measurements were recorded, we computed Q_r from Q_s using a sea ice albedo of 0.64, a value representative of those reported by *Spano* [1965] and *Predoehl and Spano* [1965] for the Ross Sea in October and November.

We computed the emitted longwave radiation over both water and ice from the measured surface temperatures and observations of cloud cover:

$$Q_{L\uparrow} = (1 - 0.11c)\varepsilon\sigma T_0^4 \tag{6}$$

Here σ is the Stefan-Boltzmann constant (5.67032×10^{-8} W m^{-2} K^{-4}), T_0 is now the surface kelvin temperature, and ε is the surface emissivity, assumed to be 0.97 for both sea ice and seawater [*Zillman*, 1972; *Reed*, 1976; *Comiso*, 1983]. The factor in parentheses in (6) accounts for the effects of clouds [*Kondratyev*, 1969, p. 577], where c is the cloud cover in octas. On only rare occasions was c other than 8.

For the over-ice case, we thus had every term in (3) except

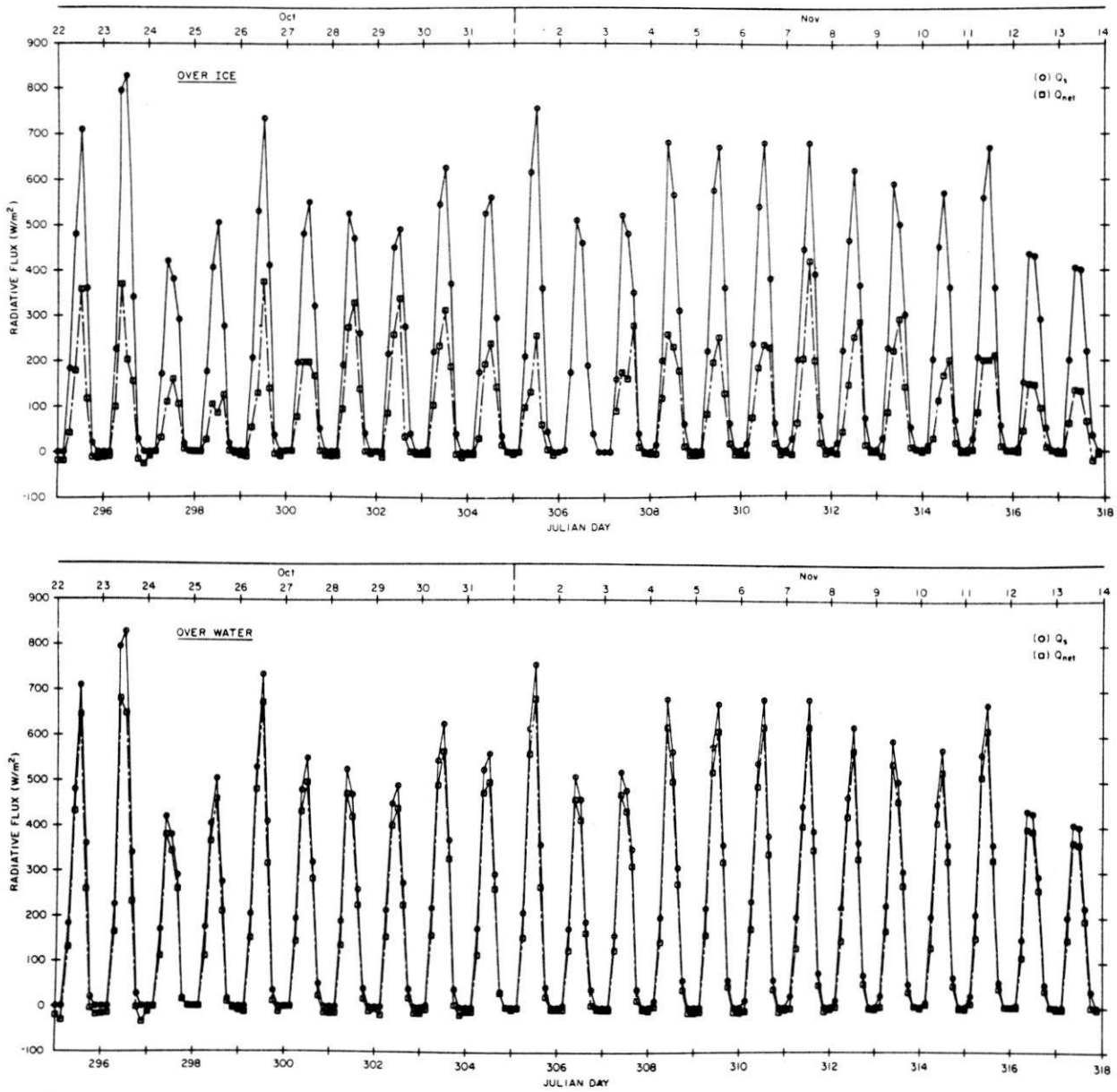

Fig. 8. Time series of the incoming shortwave flux and the net radiation balance over sea ice and over open water. Notice, Q_s is necessarily the same in both figures.

$Q_{L\downarrow}$; we therefore computed it from (3). As a consistency check, we compared this value with

$$Q_{L\downarrow}' = (1 - 0.11c)[0.601 + 5.95 \times 10^{-5} e_a \exp(1500/T_a)]\sigma T_a^4 \quad (7)$$

where T_a is the air temperature in kelvins, and e_a is the vapor pressure of the air in millibars. The term in square brackets in (7) is *Idso*'s [1981] atmospheric emissivity, modified to reflect the cleaner air in the Antarctic [*Idso*, 1980; *Andreas and Ackley*, 1982]. Generally, the values of $Q_{L\downarrow}$ computed from (3) and (7) agreed fairly well. But if the $Q_{L\downarrow}$ value computed from (3) was negative or larger than $Q_{L\uparrow}$, we used $Q_{L\downarrow}'$ instead and recomputed Q_{net} from (3) rather than using the spurious measured value. Since $Q_{L\downarrow}$ is independent of the surface type, we then assumed that the $Q_{L\downarrow}$ value we found over ice was the same as over water. Therefore we had all of the components to compute Q_{net} over water from (3).

If our radiation measurements happen to have been made over water, we simply used Q_{net} as the over-water value and went through the procedure described above to find $Q_{L\downarrow}$ and Q_{net} over ice.

Figure 8 compares Q_s and Q_{net} over water and over ice. (Remember, Q_s is the same in both figures.) The peak value of Q_s is fairly constant because the cloud cover was generally total; the maximum value on October 23 is the consequence of our one clearing episode. Because of the low albedo of open water, Q_s clearly dominates the net radiation budget over water. Over ice, on the other hand, Q_s is typically twice as large as Q_{net} during the day. At night, Q_{net} is negative over both surfaces but rarely has an absolute value larger than 20 W/m².

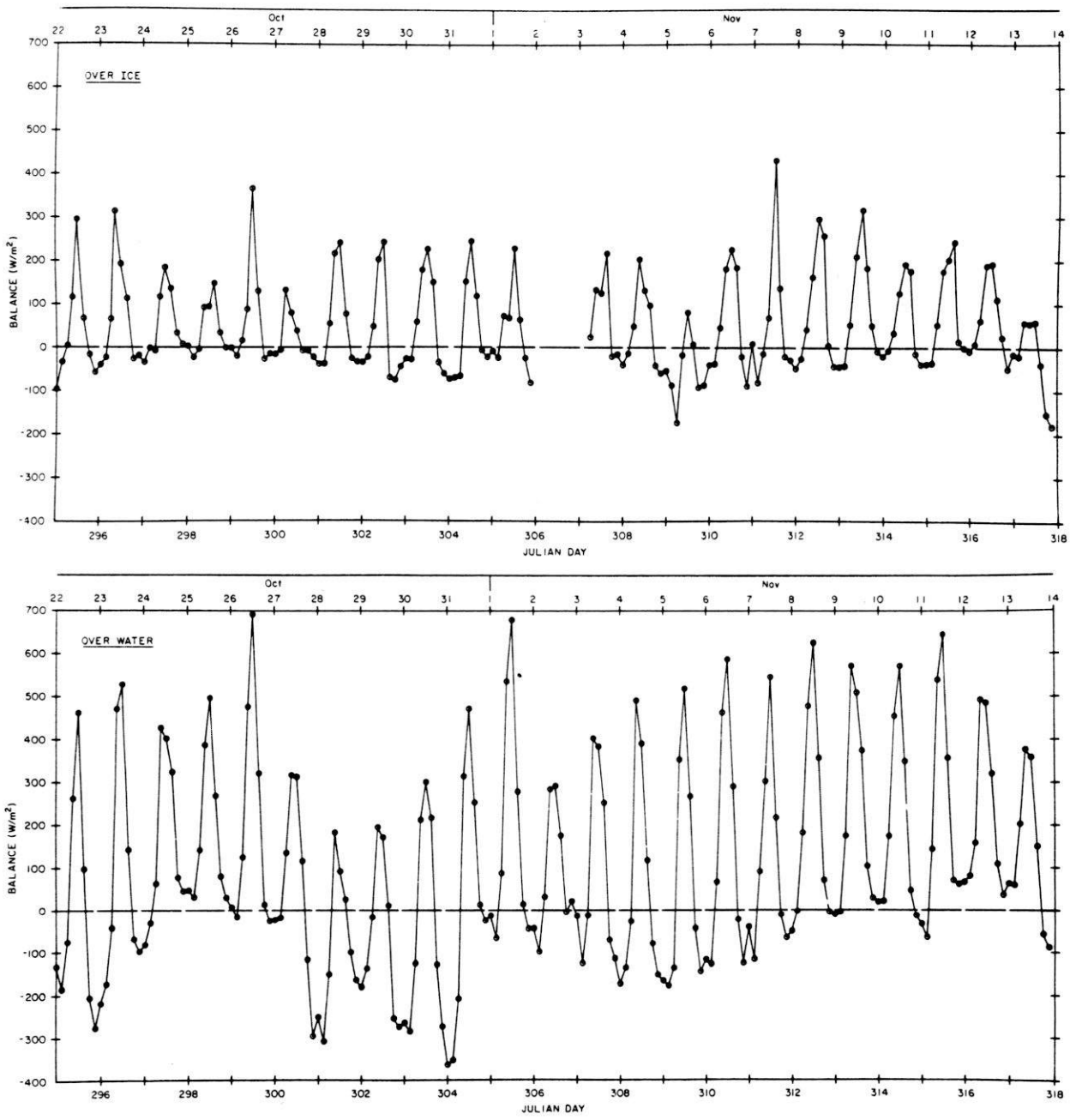

Fig. 9. Time series of B over sea ice and over open water areas within the ice cover.

3.3. *Surface Energy Balance*

From the radiative and turbulent flux components we computed the surface energy balance,

$$B = Q_s - Q_r + Q_{L\downarrow} - Q_{L\uparrow} - H_s - H_L \quad (8)$$

over both water and ice (Figure 9). With our sign conventions on the individual flux components, B is positive if the total flux is toward the surface (downward)—if the surface is gaining energy.

B is the sum of the terms in the surface energy budget that we have not measured—the phase-change term, the net-storage term, and the oceanic conductive flux term. *Gordon et al.* [1984] estimated that the conductive flux from the ocean to the surface during our cruise was 20–25 W/m^2; this term is small compared with the variability of B. In contrast, the phase-change and storage terms can be large. The heat storage capacity of sea ice is a strong function of its temperature and salinity. For the typical ice salinities (5‰) and thicknesses (0.8 m) that we encountered [*Clarke and Ackley*, 1984], a temperature increase in the ice of 1°C/d could be a heat sink of 100–500 W/m^2. Melting 6 cm of ice per day would require 200 W/m^2. Because these sink terms are comparable in magnitude to the variability in the balance shown in Figure 9, during the day, when the balance is large, the ice must have been warming and perhaps even melting.

To get a picture of how much the open water areas contribute to the various terms in the surface energy budget, we

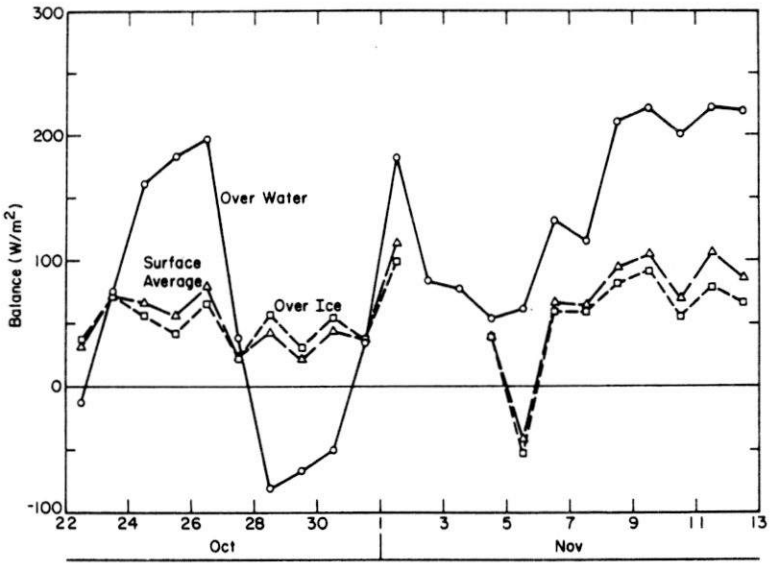

Fig. 10. Time series of daily averaged B values over sea ice, over open water, and averaged over the entire surface.

computed a surface average of each term by weighing it with the appropriate surface concentration. That is,

$$F = \gamma F_i + (1 - \gamma)F_w \tag{9}$$

where F_i is any over-ice flux component; F_w, the same flux over water; γ, the ice concentration; and F, thus the surface average of the particular flux. Except late in the cruise on November 11–13, when we found γ generally smaller, shipboard observations placed its value at 0.9 for virtually all observations in our analysis [*Ackley and Smith*, 1983].

To remove the diurnal variations and thus to make the data easier to assimilate, we also averaged the fluxes by days. Figure 10 shows the daily averaged values of the balance over ice, over water, and averaged over the entire surface. Although the balance over water has much larger variability than that over ice, because of the small open water fraction, the difference between the over-ice and surface-averaged values was seldom more than 15 W/m^2.

Figure 11 repeats the B series from Figure 10 but presents it in the context of the other daily-averaged fluxes. In this figure we reverse our sign convention for Q_s, $Q_{L\downarrow}$, and B to indicate that these are downward fluxes. In other words, in the figure a positive flux is a surface loss (upward); a negative flux is a surface gain (downward).

Since over ice $Q_{L\downarrow}$ and $Q_{L\uparrow}$ are nearly equal but opposite, and because Q_r is a mirror of Q_s, the variability in $H_s + H_L$ dictates the variability in B. $Q_s - Q_r$ sets its average value.

Over water much the same thing happens. Again $Q_{L\downarrow}$ and $Q_{L\uparrow}$ are nearly equal and opposite; $Q_s - Q_r$, which is much larger over water than over ice, sets the general level of B; and the variability in $H_s + H_L$ leads to the variability in B. For example, the large surface heat loss event (positive B) on October 28–30 corresponds with the very large turbulent losses during that period.

4. Discussion

It is interesting to compare our daily-averaged turbulent fluxes with the monthly-averaged values from *Maykut*'s [1978] numerical model of the central Arctic. Generally, the two studies show the same trends. In the spring Maykut's monthly-averaged sensible and latent heat fluxes are upward over both open water and ice 1 m thick or less. Our results usually concur, but with our shorter averaging time we see occasions when H_s can be downward over ice. Both H_s and H_L can be downward over water because the water temperature must remain around -1.8°C while the ice surface and the air can warm to 0°C. The total turbulent flux over water and over ice in the spring is another similarity between our results and *Maykut*'s [1978] Arctic model. Although there are no measurements from the interior Antarctic ice pack in winter, in the Arctic the turbulent loss from open water can total over 600 W/m^2 [*Maykut*, 1978; *Andreas et al.*, 1979], while the flux over 1-m-thick ice will be well under 100 W/m^2. In spring, on the other hand, both Maykut's model and our measurements show turbulent fluxes of similar magnitude over water and ice. Only under the cold, southerly winds during October 28–30 was the sensible heat loss from open water 100 W/m^2 more than the loss from the ice.

As Figure 10 shows, the surface-averaged, daily-averaged energy balance during our cruise was positive on all days except November 5, when the wind was high enough and the air temperature low enough to force large turbulent heat losses (Figure 11). That is, throughout our cruise the surface was gaining more energy than it was losing. Spring had begun. Since the balance comprises conductive, heat-storage, and phase-change terms, we expect the ice to have been warming and perhaps even melting during the cruise. Independent observations from the cruise qualitatively confirm our energy balance calculations. Although the log of ice observations [*Ackley and Smith*, 1983] mentions freezing in leads as late as November 3, S. F. Ackley (personal communication, 1983) saw no evidence of freezing at the ice underside in any of the 27 ice cores that he collected between October 22 and November 11. Measurements by *Gordon and Huber* [1984] also suggest that there was no freezing at the ice underside. They reported that the average oceanic mixed layer temperature during the expedition was slightly but significantly (0.035°C) above the freezing point.

With a positive balance term, the sea ice must eventually have warmed to its freezing point and begun melting. *Comiso*

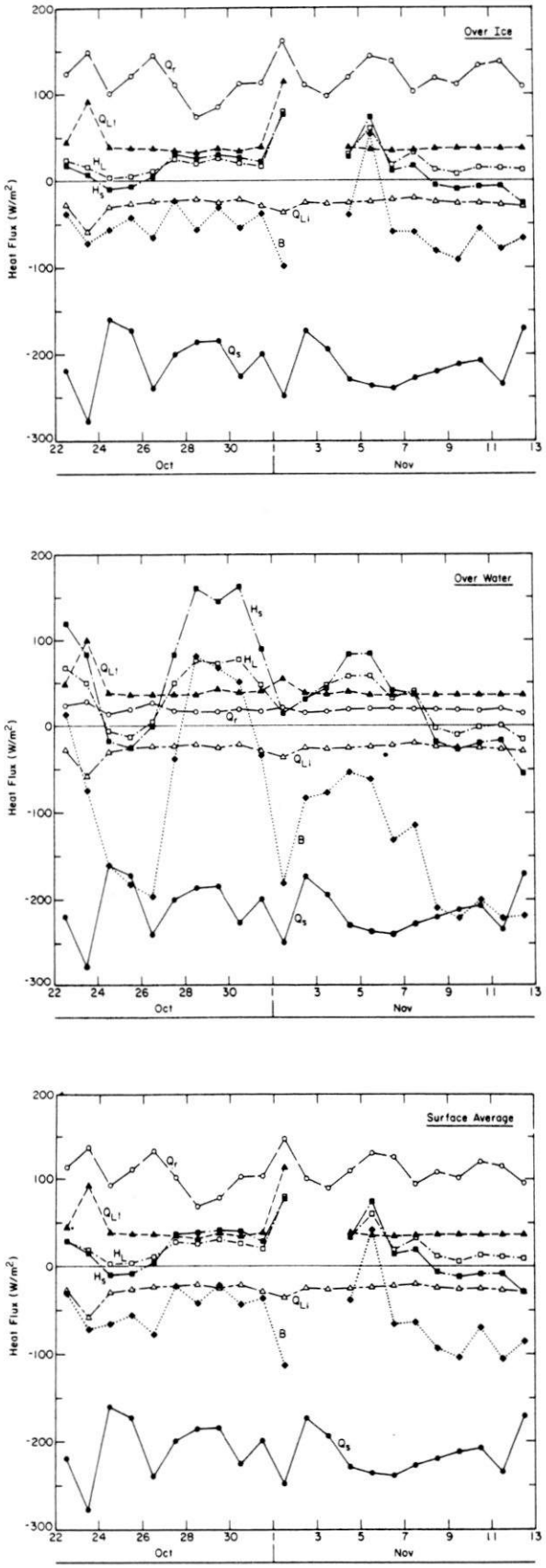

Fig. 11. Time series of the daily averaged components of the surface energy budget over sea ice, over open water, and averaged over the entire surface.

et al. [1984] bracketed the time when melting began. From satellite microwave emissivity values, they inferred increasing surface wetness in the vicinity of the *Somov* from November 1 to 13, with "widespread" melting by November 13. The Soviet ice log [*Ackley and Smith*, 1983] confirms the general time of this transition to melting with entries mentioning rotting ice from November 9 on. Our results are consistent with these observations. In Figure 10 the surface-averaged balance jumps from a negative value to a relatively high value on November 6 and remains at that level until the end of the record. The ice undoubtedly responded to this higher energy input.

Figures 3 and 6 put the transition to melting in a synoptic context. Both the air and ice temperatures rose dramatically on November 7 and hovered near 0°C until the end of the cruise (Figure 3). Thes higher temperatures were due to the predominantly northerly winds from November 7 on (Figure 6)—winds that brought in heat from the open ocean. Thus although the ice may have been warming, widespread melting probably did not begin until the geostrophic wind swung northerly, began carrying in large quantities of heat from the ocean, and thus pushed the balance term to over 70 W/m^2.

The large turbulent fluxes over open water on October 27–31 (Figure 7) were the consequence of a cold southerly wind, presumably from the Antarctic continent. These losses led to the smallest nonnegative surface-averaged balance terms of the cruise (Figure 10). We thus see again the importance of the geostrophic wind on the surface energy budget (also *Andreas* [1985]). Even 500–600 km from the ice edge, as we were from October 26 to November 8, a northerly wind carries enough oceanically derived heat to preclude large turbulent losses, even from open water.

This observation and the findings of *Andreas et al.* [1984*b*] imply a distinct difference between the processes that affect the surface energy budgets over sea ice in the Arctic Ocean and in the Southern Ocean. Because atmospheric advection can evidently carry heat from the ocean as far as 600 km over pack ice, more than half of the Antarctic seasonal sea ice is within the potential influence of the open ocean. The Arctic Ocean, in contrast, is surrounded by land and therefore is largely isolated from open ocean heat sources. Only in the narrow region between Greenland and Norway and in the Bering Sea is Arctic sea ice in proximity with the open ocean. Here, as in the Antarctic, heat advected from the ocean may play an important role in the annual sea ice retreat.

5. Conclusions

Using time series of wind speed, temperature, humidity, and radiation measured in the atmospheric surface layer, we have made the first in situ determination of the turbulent and radiative fluxes in the surface energy budget of the deep Antarctic ice pack. During our October–November cruise the sum of these fluxes, which we call the balance, was generally positive for both ice and open water. The surface was thus gaining more energy than it was losing. The ablation season had begun.

Incoming shortwave radiation dominates the surface energy budget for both ice and water at this time of year, despite almost complete cloud cover. That dominance is especially pronounced for open water because of its very small albedo; only in one case of persistent, cold southerly winds did the turbulent fluxes from open water outweigh the incoming shortwave term. The longwave radiation terms are of similar magnitudes for sea ice and open water and account for a fairly constant surface loss of 10–15 W/m^2.

Because the cloud cover was virtually constant, the variability in the sum of turbulent fluxes produced most of the variability in the balance terms for both water and ice. And this variability in the turbulent fluxes correlated with the direction of the geostrophic wind. Even 600 km from the ice edge, northerly winds (from the open ocean) were still losing heat to the relatively cooler ice and water surfaces. Cold southerly winds, on the other hand, removed heat from the ice and, especially, from the open water.

Modeling Antarctic sea ice will consequently be more complex than modeling sea ice in the central Arctic, which is virtually isolated from the open ocean. It will evidently be necessary to consider the entire atmospheric boundary layer in Antarctic models rather than just the atmospheric surface layer, as is the practice in the central Arctic. Models developed especially for the Arctic marginal ice zones, i.e., the Bering, Greenland, and Norwegian Seas, would be more applicable in the Antarctic.

6. Appendix: The Flux-Gradient Method

The flux-gradient method for obtaining fluxes from the measured wind speed (U), potential temperature (Θ), and specific humidity (Q) profiles is based on Monin-Obukhov similarity [*Businger et al.*, 1971]. The approach is to fit the profile data with the models

$$U(z) = (u_*/k)[\ln (z/z_0) - \psi_m(z/L)] \tag{A1}$$

$$\Theta(z) = \Theta(z_0) + t_*[\ln (z/z_0) - \psi_h(z/L)] \tag{A2}$$

$$Q(z) = Q(z_0) + q_*[\ln (z/z_0) - \psi_h(z/L_Q)] \tag{A3}$$

where z is the height; z_0, the surface roughness; k, von Karman's constant (0.4); $\Theta(z_0) = T_0$ and $Q(z_0) = Q_0$, the measured surface temperature and humidity; and the ψ's, the semi-empirical Monin-Obukhov similarity functions, which depend on the stability parameter ζ ($= z/L$ or z/L_Q).

For unstable conditions ($\zeta < 0$) [*Paulson*, 1970],

$$\psi_m(\zeta) = 2 \ln [(1 + x)/2] + \ln [(1 + x^2)/2] - 2 \arctan (x) + \pi/2 \tag{A4}$$

$$\psi_h(\zeta) = 2 \ln [(1 + x^2)/2] \tag{A5}$$

where

$$x = (1 - \beta_u\zeta)^{1/4} \tag{A6}$$

For stable conditions ($\zeta > 0$) [*Webb*, 1970],

$$\psi_m(\zeta) = \psi_h(\zeta) = -\beta_s\zeta \tag{A7}$$

In (A6) and (A7) we used the constants suggested by *Large and Pond* [1982], $\beta_u = 16$ and $\beta_s = 7$.

The u_*, t_*, and q_* in (A1)–(A3) are related to the surface stress (τ) and to the sensible (H_s) and latent (H_L) heat fluxes and thus link these to the measured profiles:

$$u_* = (\tau/\rho)^{1/2} \tag{A8}$$

$$t_* = -H_s/\rho c_p u_* k \tag{A9}$$

$$q_* = -H_L/\rho L_v u_* k \tag{A10}$$

Here ρ is the surface air density, c_p is the specific heat of air at constant pressure, and L_v is the latent heat of vaporization (sublimation) of water (ice).

Finally, L and L_Q are Obukhov lengths—stability parameters—

$$L_Q = g^{-1}[(1 + 0.61\bar{Q})/0.61](u_*^2/k^2q_*) \tag{A11}$$

$$L = \{[(\bar{T}/g)(u_*^2/k^2t_*)]^{-1} + L_Q^{-1}\}^{-1} \tag{A12}$$

where g is the acceleration of gravity, $\bar{Q}$ is a representative humidity, and $\bar{T}$ is a representative temperature. Notice, in (A1) and (A2) we use L as the stability parameter for velocity and temperature, but in (A3) we use L_Q for humidity. *McBean* [1971] explained that unless a passive scalar, such as humidity, is highly correlated with temperature, L is not the proper scaling length [c.f., *Dyer*, 1974]. A length scale based on the flux of the passive scalar alone, such as L_Q is for humidity, is instead a more meaningful parameter.

The flux-gradient procedure is an iterative one. We first assumed neutral stability; that is, $z/L = z/L_Q = 0$; thus $\psi_m = \psi_h = 0$. Fitting the profile data with least squares linear regression lines according to (A1)–(A3) then yielded initial values of u_*, t_*, and q_*, which we used, in turn, to estimate L and L_Q. With these first estimates of the Obukhov lengths we could begin accounting for the effects of stability in the model equations by computing the ψ values. Another least squares fit of the stability-corrected profile data resulted in new and better estimates of u_*, t_*, and q_*. We then recomputed L and L_Q. The iteration continued as such until for each profile the relative change in the sum of squared deviations between successive iterations was less than 0.1%, never more than four iterations.

Acknowledgments. We would like to thank P. V. Bogorodskii and S. F. Ackley for helping with the profile and radiation measurements; S. Bobrov and V. Posazhennikov, who made all of the MicroCORA soundings; W. B. Tucker III and M. Lepparanta for reviewing the manuscript; Bill Bates and Tom Vaughn for help with the drafting; and two anonymous reviewers, who suggested improvements in our presentation. The National Science Foundation supported this research through grants DDP 80-06922 and DPP 81-20024. The National Oceanic and Atmospheric Administration, Office of Special Research and Programs, provided funds for the lease of the MicroCORA through the National Science Foundation, grant DPP 82-03489.

References

Ackley, S. F., and S. J. Smith, Sea ice observations, Reports of the U.S.-U.S.S.R. Weddell Polynya Expedition, October–November 1981, vol. 5, *Spec. Rep. 83-2*, p. 59, U.S. Army Cold Reg. Res. and Eng. Lab., Hanover, N. H., 1983.

Ackley, S. F., S. J. Smith, and D. B. Clarke, Observations of pack ice properties in the Weddell Sea, *Antarct. J. U.S.*, *17*, 105–106, 1982.

Allison, I. F., A sample study of the energy fluxes preceding and accompanying the formation of Antarctic sea ice, *Energy Fluxes Over Polar Surfaces*, edited by S. Orvig, *Tech. Note 129*, pp. 115–132, World Meteorol. Organ., Geneva, 1973.

Allison, I. F., and G. J. Akerman, Sea ice and ocean energy balance studies at Mawson, Antarctica, in *Sea Ice Processes and Models*, edited by R. S. Pritchrd, pp. 347–359, University of Washington Press, Seattle, 1980.

Allison, I. F., C. M. Tivendale, G. J. Akerman, J. M. Tann, and R. H. Wills, Seasonal variations in the surface energy exchanges over Antarctic sea ice and coastal waters, *Ann. Glaciol.*, *3*, 12–16, 1982.

Andreas, E. L., Atmospheric boundary layer measurements in the Weddell Sea, *Antarct. J. U.S.*, *17*, 113–115, 1982.

Andreas, E. L., Upper-air data, Reports of the U.S.-U.S.S.R. Weddell Polynya Expedition, October–November 1981, vol. 6, *Spec. Rep. 83-13*, p. 288, U.S. Army Cold Reg. Res. and Eng. Lab., Hanover, N. H., 1983.

Andreas, E. L., Heat and moisture advection over Antarctic sea ice, *Mon. Weather Rev.*, in press, 1985.

Andreas, E. L., and S. F. Ackley, On the differences in ablation seasons of Arctic and Antarctic sea ice, *J. Atmos. Sci.*, *39*, 440–447, 1982.

Andreas, E. L., and A. P. Makshtas, Surface-level meteorological data, Reports of the U.S.-U.S.S.R. Weddell Polynya Expedition, October–November 1981, vol. 7, *Spec. Rep. 83-14*, p. 32, U.S. Army Cold Reg. Res. and Eng. Lab., Hanover, N. H., 1983.

Andreas, E. L., and C. A. Paulson, Velocity spectra and cospectra and

integral statistics over Arctic leads, *Q. J. R Meteorol. Soc.*, *105*, 1053–1070, 1979.

Andreas, E. L., and W. A. Richter, An evaluation of Vaisala's Micro-CORA automatic sounding system, *CRREL Rep. 82-28*, p. 17, U.S. Army Cold Reg. Res. and Eng. Lab., Hanover, N. H., 1982.

Andreas, E. L., C. A. Paulson, R. M. Williams, R. W. Lindsay and J. A. Businger, The turbulent heat flux from Arctic leads, *Boundary Layer Meteorol.*, *17*, 57–91, 1979.

Andreas, E. L., R. M. Williams, and C. A. Paulson, Observations of condensate profiles over Arctic leads with a hot-film anemometer, *Q. J. R. Meteorol. Soc.*, *107*, 437–460, 1981.

Andreas, E. L., J. H. Rand, and S. F. Ackley, A simple boom assembly for the shipboard deployment of air-sea interaction instruments, *Ocean Eng.*, *11*, 227–237, 1984*a*.

Andreas, E. L., W. B. Tucker III, and S. F. Ackley, Atmospheric boundary layer modification, drag coefficient, and surface heat flux in the Antarctic marginal ice zone, *J. Geophys. Res.*, *89*, 649–661, 1984*b*.

Banke, E. G., and S. D. Smith, Wind stress over ice and over water in the Beaufort Sea, *J. Geophys. Res.*, *76*, 7368–7374, 1971.

Banke, E. G., and S. D. Smith, Wind stress on Arctic sea ice, *J. Geophys. Res.*, *78*, 7871–7883, 1973.

Banke, E. G., S. D. Smith, and R. J. Anderson, Recent measurements of wind stress on Arctic sea ice, *J. Fish. Res. Board Can.*, *33*, 2307–2317, 1976.

Banke, E. G., S. D. Smith, and R. J. Anderson, Drag coefficients at AIDJEX from sonic anemometer measurements, in *Sea Ice Processes and Models*, edited by R. S. Pritchard, pp. 430–442, University of Washington Press, Seattle, 1980.

Borisenkov, E. P., A. P. Makshtas, and L. Yu. Preobrazhenskii, Experimental study of the effect of polynyas and leads on energy exchange between sea and atmosphere in high latitudes (in Russian), *Tr. Gl. Geofiz. Obs.*, *399*, 64–70, 1977.

Brennecke, W., Die ozeanographischen Arbeiten der deutschen antarktischen Expedition 1911–1912, *Arch. Dsch. Seewarte*, *39*(1), 216, 1921.

Buck, A. L., New equations for computing vapor pressure and enhancement factor, *J. Appl. Meteorol.*, *20*, 1527–1532, 1981.

Businger, J. A., J. C. Wyngaard, Y. Izumi, and E. F. Bradley, Flux-profile relationships in the atmospheric surface layer, *J. Atmos. Sci.*, *28*, 181–189, 1971.

Carsey, F. D., Microwave observations of the Weddell Polynya, *Mon. Weather Rev.*, *108*, 2032–2044, 1980.

Clarke, D. B., and S. F. Ackley, Sea ice structure and biological activity in the Antarctic marginal ice zone, *J. Geophys. Res.*, *89*, 2087–2095, 1984.

Comiso, J. C., Sea ice effective microwave emissivities from satellite passive microwave and infrared observations, *J. Geophys. Res.*, *88*, 7686–7704, 1983.

Comiso, J. C., S. F. Ackley, and A. L. Gordon, Antarctic sea ice microwave signatures and their correlation with in situ ice observations, *J. Geophys. Res.*, *89*, 662–672, 1984.

Dyer, A. J., A review of flux-profile relationships, *Boundary Layer Meteorol.*, *7*, 363–372, 1974.

Goerss, J. S., and C. E. Duchon, Effect of ship heating on dry-bulb temperature measurements in GATE, *J. Phys. Oceanogr.*, *10*, 478–479, 1980.

Gordon, A. L., Deep Antarctic convection west of Maud Rise, *J. Phys. Oceanogr.*, *8*, 600–612, 1978.

Gordon, A. L., The U.S.-U.S.S.R. Weddell Polynya Expedition, *Antarct. J. U.S.*, *17*, 96–98, 1982.

Gordon, A. L., and B. A. Huber, Thermohaline stratification below the southern ocean sea ice, *J. Geophys. Res.*, *89*, 641–648, 1984.

Gordon, A. L., and E. I. Sarukhanyan, American and Soviet expedition into the southern ocean sea ice in October and November 1981, *Eos Trans. AGU*, *63*, 2, 1982.

Gordon, A. L., C. T. A. Chen, and W. G. Metcalf, Winter mixed layer entrainment of Weddell deep water, *J. Geophys. Res.*, *89*, 637–640, 1984.

Huber, B. A., J. Jennings, C. T. Chen, J. Marra, S. E. Rennie, P. Mele, and A. L. Gordon, Hydrographic data, Reports of the U.S.-U.S.S.R. Weddell Polynya Expedition, October–November 1981, vol. 2, *Tech. Rep. L-DGO-83-1*, p. 99, Lamont-Doherty Geol. Observ., Palisades, N. Y., 1983.

Idso, S. B., On the apparent incompatibility of different atmospheric thermal radiation data sets, *Q. J. R. Meteorol. Soc.*, *106*, 375–376, 1980.

Idso, S. B., A set of equations for full spectrum and 8–14 μm and 10.5–12.5 μm thermal radiation from cloudless skies, *Water Resour. Res.*, *17*, 295–305, 1981.

Kondratyev, K. Ya., *Radiation in the Atmosphere*, p. 912, Academic, Orlando, Fla., 1969.

Langleben, M. P., A study of the roughness parameters of sea ice from wind profiles, *J. Geophys. Res.*, *77*, 5935–5944, 1972.

Langleben, M. P., On wind profiles over sea ice, *Geophys. Res. Lett.*, *1*, 82–85, 1974.

Large, W. G., and S. Pond, Open ocean momentum flux measurements in moderate to strong winds, *J. Phys. Oceanogr.*, *11*, 324–336, 1981.

Large, W. G., and S. Pond, Sensible and latent heat flux measurements over the ocean, *J. Phys. Oceanogr.*, *12*, 464–482, 1982.

Leavitt, E., D. Bell, M. Clarke, R. Anderson, and C. Paulson, Computation of air stress and sensible heat fluxes from surface layer profile data, AIDJEX, 1975, *AIDJEX Bull. 36*, pp. 157–174, Arct. Ice Dyn. Joint Exp., Div. of Mar. Resour., Univ. of Washington, Seattle, 1977.

Martinson, D. G., P. D. Killworth, and A. L. Gordon, A convective model for the Weddell Polynya, *J. Phys. Oceanogr.*, *11*, 466–488, 1981.

Maykut, G. A., Energy exchange over young sea ice in the Central Arctic, *J. Geophys. Res.*, *83*, 3646–3658, 1978.

McBean, G. A., The variations of the statistics of wind, temperature and humidity fluctuations with stability, *Boundary Layer Meteorol.*, *1*, 438–457, 1971.

Mollo-Christensen, E., Upwind distortion due to probe support in boundary-layer observation, *J. Appl. Meteorol.*, *18*, 367–370, 1979.

Olson, M. L., Global accuracy of Omega-derived winds, *Atmos. Technol.*, *10*, 14–23, 1979.

Paulson, C. A., The mathematical representation of wind speed and temperature profiles in the unstable atmospheric surface layer, *J. Appl. Meteorol.*, *9*, 857–861, 1970.

Payne, R. E., Albedo of the sea surface, *J. Atmos. Sci.*, *5*, 959–969, 1972.

Predoehl, M. C., and A. F. Spano, Airborne albedo measurements over the Ross Sea, October–November 1962, *Mon. Weather Rev.*, *93*, 687–696, 1965.

Rao, K. S., Effect of thermal stratification on the growth of the internal boundary layer, *Boundary Layer Meteorol.*, *8*, 227–234, 1975.

Reed, R. K., On estimation of net long-wave radiation from the oceans, *J. Geophys. Res.*, *81*, 5793–5794, 1976.

Romanov, Yu. A., I. B. Fedorova, M. S. Chervyakov, and G. I. Shapiro, An improvement in the accuracy of shipboard measurements of wind speed and direction based on aerodynamic tests of a ship model, *Oceanology*, *23*, 267–270, 1983.

Spano, A. F., Results of an airborne albedo program in Antarctica, 1963, *Mon. Weather Rev.*, *93*, 697–703, 1965.

Thorpe, M. R., E. G. Banke, and S. D. Smith, Eddy correlation measurements of evaporation and sensible heat flux over Arctic sea ice, *J. Geophys. Res.*, *78*, 3573–3584, 1973.

Untersteiner, N., and F. I. Badgley, The roughness parameter of sea ice, *J. Geophys. Res.*, *70*, 4573–4577, 1965.

Webb, E. K., Profile relationships: The log-linear range, and extension to strong stability, *Q. J. R. Meteorol. Soc.*, *96*, 67–90, 1970.

Weller, G. E., Heat-energy transfer through a four-layer system: Air, snow, sea ice, sea water, *J. Geophys. Res.*, *73*, 1209–1220, 1968*a*.

Weller, G. E., The heat budget and heat transfer processes in Antarctic plateau ice and sea ice, *ANARE Sci. Rep. 102*, p. 155, Aust. Natl. Antarct. Res. Exped., Dep. of External Aff., Melbourne, 1968*b*.

Wordie, J. M., Shackleton Antarctic Expedition, 1914–1917: The natural history of pack-ice as observed in the Weddell Sea, *Trans. R. Soc. Edinburgh*, *52*, 795–829, 1921.

Zillman, J. W., A study of some aspects of the radiation and heat budgets of the southern hemisphere ocean, *Meteorol. Study 26*, p. 562, Bur. of Meteorol., Dep. of the Inter., Canberra, Australia, 1972.

E. L. Andreas, Snow and Ice Branch, Department of the Army, Cold Regions Research and Engineering Laboratory, Corps of Engineers, Hanover, NH 03755.

A. P. Makshtas, Arctic and Antarctic Research Institute, Leningrad 191104, USSR.

(Received November 19, 1984;
accepted January 10, 1985.)

☆U.S. GOVERNMENT PRINTING OFFICE:1986—601-366

Atmospheric boundary layer measurements in the Weddell Sea

EDGAR L. ANDREAS

U.S. Army Cold Regions Research and Engineering Laboratory
Hanover, New Hampshire 03755

The atmospheric boundary layer component of the Weddell Polynya expedition (WEPOLEX-81) was one of the most intensive measurement programs ever carried out over floating ice in the Antarctic. Our research involved four distinct, yet complementary, sampling programs: upper-air soundings, surface-layer profiling, spectral measurements of surface-layer turbulence, and routine meteorological observations.

Two radiosonde systems for upper-air sampling were available on the *Mikhail Somov*. We used the MicroCORA automatic sounding system, manufactured by Vaisala of Helsinki, Finland, to make soundings of wind velocity, temperature, humidity, and pressure at 0000 and 1200 Greenwich mean time each day. Between 15 October and 16 November 1981 we collected 65 sets of such profiles, usually from the surface to an altitude of 20 kilometers. With an Airsonde system made by A.I.R., Inc., of Boulder, Colorado, we made closely spaced soundings of temperature, humidity, and pressure to roughly 5 kilometers in regions of special interest. We made 46 Airsonde soundings, including transects as the *Somov* entered the ice on 20 October and recrossed the marginal ice zone during the period 11–14 November. During both of these transects, the wind blew from the open ocean onto the ice, so modification of the planetary boundary layer was dramatic. On two occasions we attached both the MicroCORA and the A.I.R. radiosondes to the same helium-filled balloon and made simultaneous soundings to compare pressure, temperature, and humidity data obtained from the two systems (Andreas and Ackley in preparation).

The standard meteorological observations made on the *Somov* included recordings every 3 hours of wind speed and direction, air, water, and dew-point temperatures, ice conditions, and cloud cover. In addition, total Sun and sky radiation, reflected shortwave radiation, net all-wave radiation, and surface (ice) temperature were recorded every hour. With this data set we will estimate the surface energy budget at hourly intervals along the *Somov*'s track through the ice.

We collected 21 sets of surface-layer profiles of wind speed, temperature, and dew point with a boom deployed from the helicopter deck of the *Somov* (figure 1). Because the biological

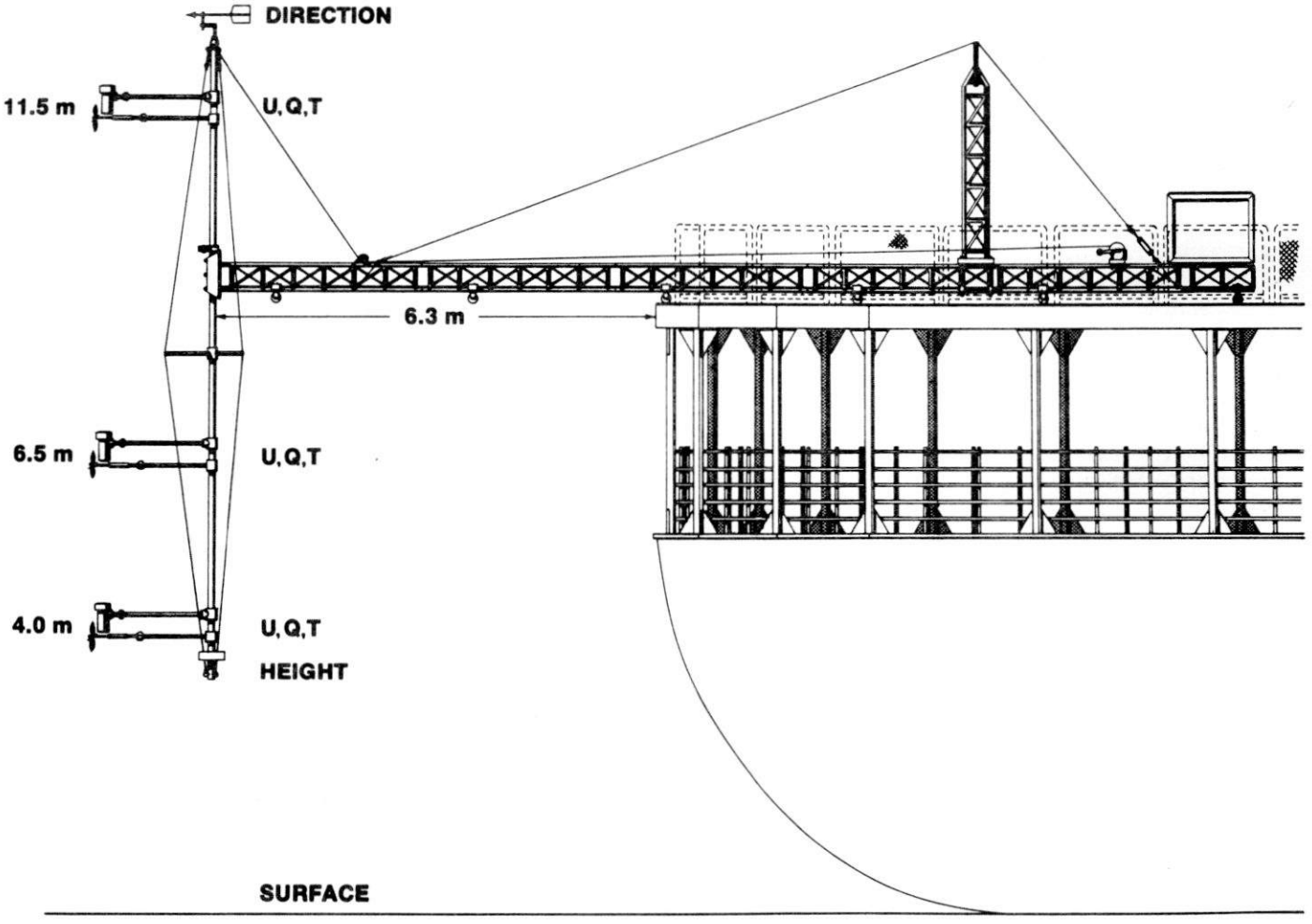

Figure 1. The profiling mast deployed from the helicopter deck. U, Q, and T indicate, respectively, the location of instruments for measuring wind speed, dew point, and temperature.

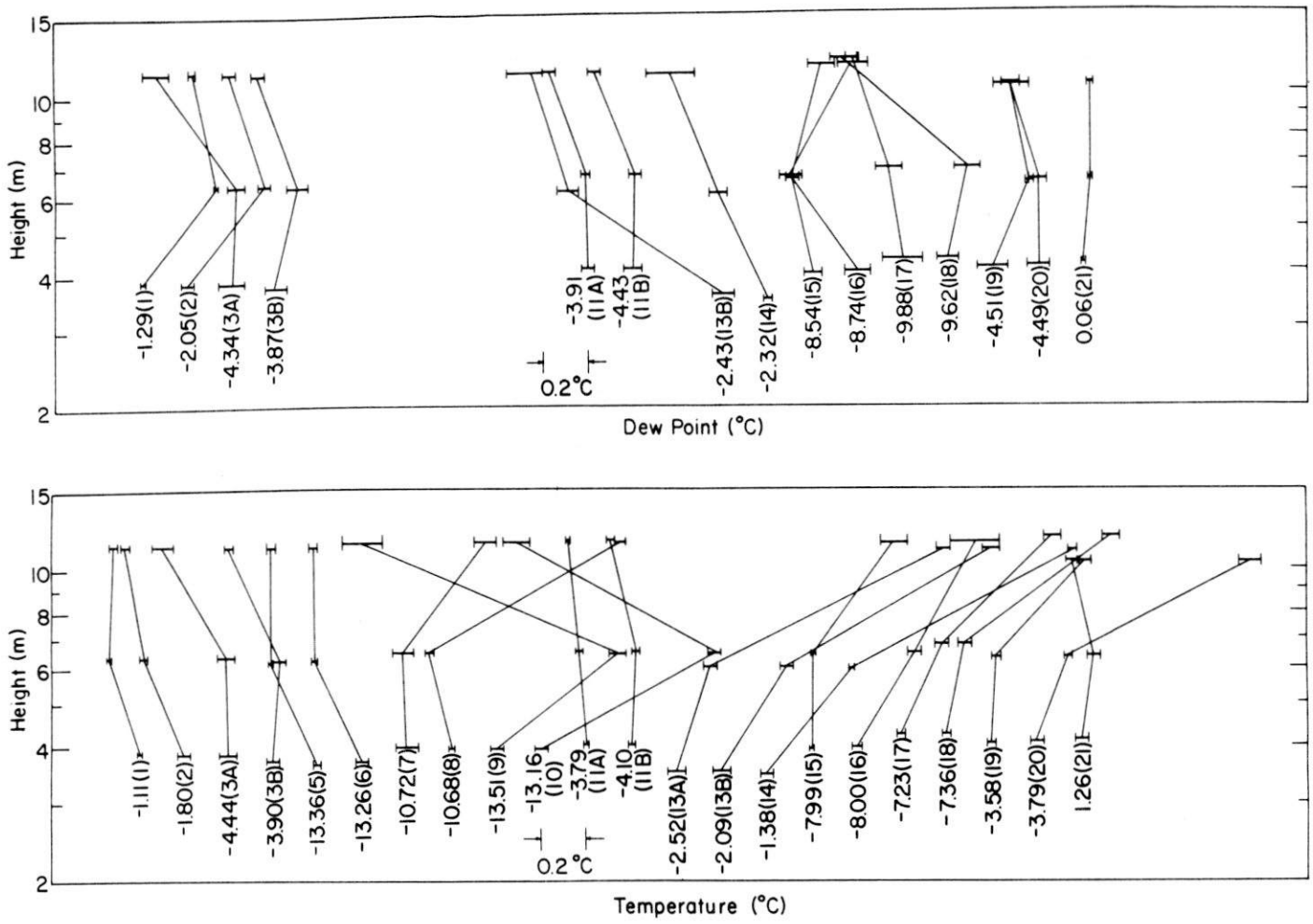

Figure 2. Some profiles of measured temperature (a) and dew point (b). The error bars indicate plus and minus one standard deviation. The numbers under the profiles indicate the measured value at the lowest level and the run number (in parentheses).

and physical oceanographers on the expedition used winches located on the starboard side of the *Somov* for their casts, they preferred to have the ship crosswind with the wind from starboard. Therefore we ran our boom out from the rear, starboard corner of the helicopter deck and then rotated our instrument mast into the wind. The ship thus did not disturb the airflow at our instruments very much, and all three measurement programs—boundary layer, biology, and physical oceanography—could go on simultaneously.

Our profiling mast was instrumented at three levels. Each level had a General Eastern 1200MPS system for measuring temperature and dew point and a Gill propeller anemometer, made by the R. M. Young Company, for measuring wind speed. A wind vane at the top of the mast was used for orienting the instruments into the wind.

Figure 2 shows some of the temperature and dew-point profiles we collected. These profiles are rather complex because we encountered a variety of surface conditions. Andreas (1982) and Andreas, Williams, and Paulson (1981) have shown that when an atmospheric flow encounters a change in surface moisture or temperature, an internal boundary layer—a region near the surface in which the flow is affected by the new surface—develops according to

$$h/z_T = 1.31\,(X/z_T)^{0.8},$$

where X is the fetch over the new surface, h is the maximum height at X that is affected by the new surface, and z_T is the scalar roughness length, that is, the height at which the extrapolated temperature or humidity profile equals the surface value of the variable. With z_T typically 0.025 centimeter over water and with the height of our highest profiling level about 11.5 meters, this equation shows that if the surface change was less than 120 meters upwind of our mast, the upper instruments were above the internal boundary layer and so were not influenced by the new surface. For longer fetches, all instrument levels were within the internal boundary layer.

Since we know this cutoff fetch, we can define three types of surface regimes and their corresponding profile runs:

- Ice—at least 90 percent ice cover upwind of the instrument mast: runs 3A, 3B, 7, 8, 9, 10, 15, 16;
- Open water—open water for at least 300 meters upwind: runs 11A, 11B, 13A, 13B, 14, 17, 18, 21; and
- Ice and water—roughly 50 percent ice cover for at least 100 meters upwind, at least 90 percent ice beyond: runs 1, 2, 5, 6, 19, 20.

Surface conditions generally control the shapes of the temperature and dew-point profiles. For example, although the

dew-point profiles for runs 11A, 11B, 13B, and 14 are consistent with our categorizing of them as "open water" runs, 11A and 11B show unstable temperature profiles while 13A, 13B, and 14 have very stable profiles. This is because for the former runs the air temperature was lower than the water temperature (about −1.9°C); for the latter runs it was nearly the same or higher (compare Andreas et al. 1979).

We wish to acknowledge the support of National Science Foundation grant DPP 80-06922. John Rand designed and built the surface-layer-profiling boom, and Stephen Ackley assisted with the measurements. Alexander Makshtas was responsible for the hourly meteorological observations. Ed Lysakov helped with Airsonde operations. Stanislav Bobrov and Valerii Posazhennikov of the *Somov* made the MicroCORA soundings.

References

Andreas, E. L. 1982. Sensible and latent heat fluxes and humidity profiles following a step change in surface moisture (USA CRREL Report 82–12). Hanover, N.H.: U.S. Army Cold Regions Research and Engineering Laboratory.

Andreas, E. L., and Ackley, S. F. In preparation. *A comparison of the pressure, temperature, and humidity data of two radiosonde systems.*

Andreas, E. L., Paulson, C. A., Williams, R. M., Lindsay, R. W., and Businger, J. A. 1979. The turbulent heat flux from Arctic leads. *Boundary-Layer Meteorology*, 17(1), 57–91.

Andreas, E. L., Williams, R. M., and Paulson, C. A. 1981. Observations of condensate profiles over Arctic leads with a hot-film anemometer. *Quarterly Journal of the Royal Meteorological Society*, 107(452), 437–460.